

Experimental and Finite Element Studies of Acetabular Cement Pressurisation and Socket Fixation in Total Hip Replacement

New, Andrew Michael Raymond

The copyright of this thesis rests with the author and no quotation from it or information derived from it may be published without the prior written consent of the author

For additional information about this publication click this link.

<http://qmro.qmul.ac.uk/jspui/handle/123456789/1804>

Information about this research object was correct at the time of download; we occasionally make corrections to records, please therefore check the published record when citing. For more information contact scholarlycommunications@qmul.ac.uk



IRC in Biomedical Materials
Queen Mary and Westfield College
UNIVERSITY OF LONDON



Unit for Joint Reconstruction
Institute of Orthopaedics
Robert Jones and Agnes Hunt Orthopaedic Hospital
OSWESTRY

Experimental and Finite Element Studies of Acetabular Cement Pressurisation and
Socket Fixation in Total Hip Replacement

by

Andrew Michael Raymond New, B.Eng., A.R.S.M.

Ph.D. Thesis, August 1997



Abstract

With time, the rate of symptomatic acetabular component loosening accelerates and overtakes that of the femoral component as the principal reason for the revision of total hip replacement. In the femur extensive study has shown that cement pressurisation and good preparation of the bone bed improves the survival rate, but acetabular fixation requires further investigation.

Production of cement pressure in the acetabulum is anatomically difficult. Pressurisation with conventional and novel designs of cement pressurisers has been compared to manual techniques and component insertion. The pressurisers increased peak and mean pressures and pressure duration. Finite element modelling of cup insertion showed that flanges and higher insertion rates increased cement penetration into cancellous bone. Per-operatively, one design of pressuriser produced cement pressures comparable to those found in the laboratory.

Structural finite element modelling of the natural hip indicated that the subchondral plate and the relatively dense cancellous bone supporting it distribute the joint contact force into the medial and lateral pelvic cortices. A perfectly bonded cemented polyethylene cup stiffened the acetabulum so that more load was transferred directly to the cortices at the acetabular rim, with consequent interface stress concentrations. However, complimentary experimental studies using a dynamic joint simulator and a servo-hydraulic materials testing machine suggested that perfect fixation between cement and bone at the rim was not possible, even under laboratory conditions. Debonding of the cement bone interface at the rim, where dense bone prevents cement interdigitation, allowed micromotion. Since the clinical mechanism of failure of the acetabular component appears to be progressive debonding, from rim to apex, of the cement-bone interface, these studies support the initiation of the failure mechanism by mechanical factors, which may then allow the ingress of wear debris. The experimental studies suggested that the use of pressurisers reduces the amount of micromotion and thus may improve the long term stability of the interface.

Acknowledgements

I would like to thank my supervisors Dr K.E. Tanner and Mr Martin Northmore-Ball for giving me the opportunity to escape London and work on an interesting and challenging project and for their continued advice and guidance. Bryan Pell, the legendary “Yodelling Cowboy” of Oswestry and Llandudno, has been an enthusiastic provider of technical assistance throughout. Mr Kevin Cheah has also been an eager contributor to much of the cement pressurisation work. Dr Chris Jackson has generously given up his own time to pass on the benefits of his experience. Jan Herman Kuiper has been an ever cheerful presence, always willing to give his help when asked.

I would also like to thank Professor Rik Huiskes of the University of Nijmegen, The Netherlands and Dr Michel Dalstra, now of The University of Aarhus, Denmark, for supplying the basic data for the structural finite element model of the pelvis. The development of this model was a significant part of Dr Dalstra's doctoral project at the University of Nijmegen in the period October 1988 to December 1993. Thanks also to Robert Scott of Johnson and Johnson Orthopaedics and Dr Frans Peter Bernoski of Westeinde Ziekenhuis, The Hague, The Netherlands for giving me the opportunity of being involved in testing their acetabular cement pressuriser. Mr Frank Sellers of DePuy International and Dr Neil Watkins of DePuy CMW have been most generous in providing additional financial support and supplies of bone cement and cement mixing equipment.

On a personal note, to name everyone who has made my time so far in the wilds of Shropshire a pleasure would mean a very long list. Thanks to my house-mate Richard Diamond, especially during the frustrations of the writing-up period, and Jason Roberts, whose perseverance in adversity helps to keep everything in perspective. Thanks to Margaret and Geoff Peach for their hospitality, boisterous Dutchmen too numerous to mention, Erica, Frank and last but not least, Dianne.

Trademarks

All trademarks throughout this thesis are acknowledged. In particular:-

ANSYS and FLOTRAN are registered trademarks of ANSYS Inc, Houston, Pennsylvania, U.S.A.

Boneloc is a registered trademark of Polymers Reconstructive A/S, Farum, Denmark.

CMW, DePuy, Ortron and Charnley are registered trademarks and Ogee is a trademark of DePuy International, Leeds, U.K.

Entran is a registered trademark of Entran Devices Inc, Fairfield, New Jersey, U.S.A.

MARC is a registered trademark of MARC Analysis Corporation, Palo Alto, California, U.S.A.

Microsoft, MS DOS and Windows are registered trademarks of Microsoft Corporation, Redmond, Washington, U.S.A.

Palacos is a registered trademark of Schering Plough, Mildenhall, Suffolk, U.K.

Pentium is a registered trademark of Intel Corporation, Santa Clara, California, U.S.A.

Simplex and Howmedica are registered trademarks of Howmedica, Park Royal, London, U.K.

Ultima is a registered trademark of Johnson and Johnson Orthopaedics, New Milton, Hampshire, U.K.

Contents

1. INTRODUCTION	10
2. REVIEW OF THE LITERATURE	13
2.1 THE HIP JOINT	13
2.1.1 <i>Functional Anatomy of the Pelvis and Acetabulum</i>	14
2.1.2 <i>Biological Materials</i>	17
2.1.2.1 Cortical Bone.....	19
2.1.2.2 Cancellous Bone	22
2.1.2.3 Factors Influencing Mechanical Properties	24
2.1.2.4 Dynamic Mechanical Properties	26
2.1.2.5 Density as a Predictor of Mechanical Properties	26
2.1.2.6 Fracture Properties of Bone.....	28
2.1.3 <i>Biomechanics of the Hip</i>	32
2.1.4 <i>Stresses in the Normal and Reconstructed Hip</i>	40
2.1.4.1 Stresses in the Implanted Pelvis	42
2.1.4.2 Factors Affecting the Mechanics of a Total Hip Replacement	44
2.2 HIP REPLACEMENT	46
2.2.1 <i>Reasons for Hip Replacement</i>	46
2.2.1.1 Osteoarthritis	46
2.2.1.2 Rheumatoid Arthritis	47
2.2.1.3 Avascular Necrosis	48
2.2.1.4 Ankylosing Spondylitis	48
2.2.1.5 Mechanical Derangement of the Joint.....	49
2.2.2 <i>Surgical Treatment</i>	49
2.3 DESIGN OF HIP REPLACEMENTS	50
2.3.1 <i>Cemented Implants</i>	51
2.3.2 <i>Uncemented Implants</i>	52
2.3.2.1 Primary Fixation	52
2.3.2.2 Porous Coatings	53
2.3.2.3 Bioactive Coatings	54
2.3.3 <i>Materials for Total Hip Replacement</i>	54
2.3.4 <i>Bone Cement</i>	56
2.3.4.1 Polymethylmethacrylate Cement	56
2.3.4.2 Alternatives to PMMA	58
2.4 FAILURE OF CEMENTED JOINT REPLACEMENT	60
2.4.1 <i>Causes of Aseptic Loosening</i>	64
2.4.1.1 Accumulated Damage	65
2.4.1.2 Implant Reaction and Wear	68

2.4.1.3 Bone Adaptation	69
2.5 ASPECTS OF FIXATION WITH ACRYLIC BONE CEMENT.....	71
2.5.1 <i>The Strength of the Bone-Cement Interface</i>	72
2.5.1.1 Variables Controlling Cement Penetration into Cancellous Bone.....	74
2.5.1.2 Pressures Required to Achieve Penetration.....	76
2.5.2 <i>Intra Operative Pressurisation of Bone Cement</i>	77
2.5.2.1 Side Effects of Cement Pressurisation	79
2.5.2.2 Alternative Techniques to Produce Cement Penetration.....	79
3. ACETABULAR CEMENT PRESSURISATION DURING TOTAL HIP REPLACEMENT. 81	
3.1 RATIONALE	81
3.2 LABORATORY STUDIES.....	82
3.2.1 <i>Introduction</i>	82
3.2.1.1 Machine Control.....	82
3.2.1.2 Manual Control.....	83
3.2.2 <i>Methods</i>	84
3.2.2.1 Machine Control.....	84
3.2.2.2 Manual Control.....	86
3.2.3 <i>Results</i>	87
3.2.3.1 Machine Control.....	87
3.2.3.2 Manual Control.....	90
3.2.4 <i>Discussion</i>	97
3.3 PER-OPERATIVE CEMENT PRESSURISATION MEASUREMENTS.....	101
3.3.1 <i>Design and Testing of the Instrumented Pressuriser</i>	101
3.3.1.1 Pressure Transducer and Data Acquisition System	101
3.3.1.2 Calibration and Testing.....	104
3.3.2 <i>Methods</i>	105
3.3.3 <i>Results</i>	107
3.3.4 <i>Discussion</i>	109
3.4 SUMMARY AND CONCLUSIONS	110
4. MODELLING OF CEMENT FLOW DURING ACETABULAR CUP INSERTION.....112	
4.1 PARAMETER DEFINITION	112
4.1.1 <i>The Rheological Behaviour of Acrylic Bone Cements by Oscillating Plate-on-Plate Rheometry</i>	112
4.1.1.1 Theory	112
4.1.1.2 Method.....	113
4.1.1.3 Results	114
4.1.2 <i>The Permeability of Cancellous Bone</i>	116
4.1.2.1 Method.....	117
4.1.2.2 Results	119

4.2 DEVELOPMENT OF MODELLING TECHNIQUE	119
4.2.1 Theory.....	119
4.2.2 Method.....	120
4.3 EXPERIMENTAL VALIDATION OF MODELLING TECHNIQUE	122
4.3.1 Acetabular Model.....	122
4.3.1.1 Experimental Methods	122
4.3.1.2 Finite Element Models.....	123
4.3.1.3 Results	125
4.3.2 Porous Material Model.....	133
4.3.2.1 Experimental Methods	133
4.3.2.2 Finite Element Model	134
4.3.2.3 Results	134
4.4 PARAMETRIC ANALYSIS OF CEMENT PENETRATION DURING ACETABULAR CUP INSERTION	135
4.4.1 Method.....	135
4.4.2 Results	136
4.5 DISCUSSION.....	138
4.6 SUMMARY	144
5. MECHANICAL ASPECTS OF ACETABULAR CUP FIXATION.....	146
5.1 INTRODUCTION.....	146
5.2 METHODS.....	146
5.2.1 The Basic Finite Element Mesh.....	146
5.2.2 Modifications	147
5.2.3 Applied Loads	149
5.2.4 Solution.....	150
5.2.5 Hoffman Failure Criterion for Cancellous Bone.....	150
5.3 ANALYSES.....	151
5.4 RESULTS.....	156
5.4.1 The Effect of Boundary Conditions on Pelvic Mechanics.....	156
5.4.2 Load Transfer in Normal and Reconstructed Acetabula.....	158
5.4.3 The Effect of Prosthesis Debonding on Acetabular Mechanics	161
5.5 DISCUSSION.....	170
5.6 CRITIQUE	176
5.7 SUMMARY AND CONCLUSIONS.....	178
6. STABILITY OF CEMENTED ACETABULAR CUPS UNDER DYNAMIC LOADING	180
6.1 DESIGN AND VALIDATION OF A NEW JOINT SIMULATOR.....	180
6.1.1 Description	180
6.1.2 Mechanical Design	182
6.1.3 Operation and Validation.....	183

6.1.3.1 Verification of Load Cycle	184
6.2 THE EFFECT OF CEMENTING TECHNIQUE ON ACETABULAR COMPONENT FIXATION	186
6.2.1 <i>Method</i>	186
6.2.1.1 Specimen Mounting	188
6.2.1.2 Transducer Calibration	190
6.3 MICROMOTION IN THE CEMENTED ACETABULAR RECONSTRUCTION.....	190
6.3.1 <i>Finite Element Models</i>	190
6.3.2 <i>Laboratory Experiments</i>	193
6.4 RESULTS.....	193
6.5 DISCUSSION.....	199
7. CONCLUSIONS.....	202
8. FUTURE WORK	206
9. REFERENCES.....	208
APPENDIX A SHEAR RATES IN OSCILLATING PLATE-ON-PLATE RHEOMETRY	223
APPENDIX B ERRORS IN IMAGE PROCESSING OF BONE MICROSTRUCTURES	224
APPENDIX C CALCULATION OF STRAIN RATE IN FLUID FLOW ANALYSIS.....	227
APPENDIX D PUBLICATIONS AND ABSTRACTS	231

List of Figures

FIGURE 2-1: CROSS-SECTIONAL ANATOMY OF THE HIP JOINT.	13
FIGURE 2-2: LIGAMENTS OF THE HIP JOINT.....	14
FIGURE 2-3: ANATOMY AND MUSCLE ATTACHMENTS OF THE INNOMINATE BONES:.....	15
FIGURE 2-4: CROSS SECTION OF THE ACETABULAR REGION OF THE INNOMINATE BONE.....	16
FIGURE 2-5: SCHEMATIC OF THE METAPHYSIS OF A TYPICAL LONG BONE.	18
FIGURE 2-6: TYPICAL STRESS-STRAIN CURVES FOR WET CORTICAL BONE.....	20
FIGURE 2-7: TYPICAL STRESS STRAIN CURVES FOR WET CANCELLOUS BONE.....	22
FIGURE 2-8: RELATIONSHIPS BETWEEN YOUNG’S MODULUS AND DENSITY FOR CANCELLOUS BONE.....	28
FIGURE 2-9: A SIMPLE MECHANICAL MODEL OF A TWO JOINT SYSTEM.	33
FIGURE 2-10: CHARNLEY’S ANALYSIS OF THE HIP JOINT.....	34
FIGURE 2-11: MAGNITUDE AND DIRECTION OF THE HIP JOINT RESULTANT FORCE.....	38
FIGURE 2-12: MAGNITUDE OF THE HIP JOINT RESULTANT FORCE FROM DIFFERENT AUTHORS.	39
FIGURE 2-13: DEFORMATION DURING <i>IN VITRO</i> LOADING OF THE ACETABULUM.....	42
FIGURE 2-14: FINITE ELEMENT PREDICTIONS OF VON MISES STRESS IN THE PELVIS.....	43
FIGURE 2-15: CLASSIFICATION OF OSTEOARTHRITIS.....	47
FIGURE 2-16: COMPARISON OF THE EFFECTS OF ARTHRITIC DISORDERS.	48
FIGURE 2-17: CLASSIFICATION OF HIP PROSTHESES ON THE BASIS OF FIXATION METHOD.	50
FIGURE 2-18: THE SURVIVORSHIP OF HIP REPLACEMENT COMPONENTS.	62
FIGURE 2-19: THERMAL NECROSIS DUE TO ACRYLIC BONE CEMENT.....	67
FIGURE 2-20: THE "WINDOWS" OF BONE RESPONSE TO MECHANICAL STIMULUS.....	70
FIGURE 2-21: CEMENT PENETRATION INTO CANCELLOUS BONE.....	76
FIGURE 2-22: APPROACHES TO CEMENT PRESSURISATION.....	77
FIGURE 2-23: CEMENT PRESSURE-TIME CURVES DURING ACETABULAR CUP INSERTION.....	78
FIGURE 3-1: SCHEMATIC OF THE BERNOSKI CEMENT PRESSURISER.	82
FIGURE 3-2: SCHEMATIC OF UJR 1.....	83
FIGURE 3-3: SCHEMATIC OF UJR 2.....	84
FIGURE 3-4: THE INSTRUMENTED MODEL ACETABULUM WITH THE BERNOSKI DEVICE.	85
FIGURE 3-5: PRESSURE MEASURED AT THE POLE OF THE ACETABULUM.	88
FIGURE 3-6: PRESSURE MEASURED AT THE RIM OF THE ACETABULUM.....	88
FIGURE 3-7: PEAK PRESSURES RECORDED.	89
FIGURE 3-8: MEAN PRESSURES RECORDED.....	89
FIGURE 3-9: PRESSURE RECORDING, UJR 1 PRESSURISER.	91
FIGURE 3-10: PRESSURE RECORDING, UJR 2 PRESSURISER.	91
FIGURE 3-11: PRESSURE RECORDING, EXETER PRESSURISER.....	91
FIGURE 3-12: PRESSURE RECORDING, BERNOSKI PRESSURISER.....	92
FIGURE 3-13: PRESSURE RECORDING, “OGEE” FLANGED CUP.....	92

FIGURE 3-14: PRESSURE RECORDING, FINGER PACKING.	92
FIGURE 3-15: PRESSURE RECORDING, HAND PRESSURISATION TECHNIQUE.	93
FIGURE 3-16: MEAN PRESSURE FOR VARIOUS CEMENTATION TECHNIQUES - CMW 1 CEMENT.	93
FIGURE 3-17: MEAN PRESSURE FOR VARIOUS CEMENTATION TECHNIQUES - CMW 3 CEMENT.	93
FIGURE 3-18: PEAK PRESSURE FOR VARIOUS CEMENTATION TECHNIQUES - CMW 1 CEMENT.	94
FIGURE 3-19: PEAK PRESSURE FOR VARIOUS CEMENTATION TECHNIQUES - CMW 3 CEMENT.	94
FIGURE 3-20: DETAIL OF PRESSURE TRANSDUCER MOUNTING IN THE INSTRUMENTED PRESSURISER.	101
FIGURE 3-21: FLOW DIAGRAM OF DATA ACQUISITION AND STORAGE SCHEME.	102
FIGURE 3-22: COMPONENTS OF THE INSTRUMENTATION.	103
FIGURE 3-23: THE INSTRUMENTED ACETABULAR CEMENT PRESSURISER AND RECORDING APPARATUS.	104
FIGURE 3-24: THE INSTRUMENTED PRESSURISER TESTED IN THE INSTRUMENTED ACETABULUM.	105
FIGURE 3-25: THE INSTRUMENTED PRESSURISER.	106
FIGURE 3-26: THE INSTRUMENTED CEMENT PRESSURISER IN USE.	107
FIGURE 3-27: REPRESENTATIVE PER-OPERATIVE PRESSURE RECORDING.	108
FIGURE 3-28: MEAN AND PEAK PER OPERATIVE CEMENT PRESSURES.	108
FIGURE 3-29: POST OPERATIVE RADIOGRAPH AFTER USE OF THE INSTRUMENTED PRESSURISER.	109
FIGURE 4-1: REAL PART OF COMPLEX VISCOSITY, η' , FOR COMMERCIAL ACRYLIC BONE CEMENTS.	114
FIGURE 4-2: TAN DELTA FOR COMMERCIAL ACRYLIC BONE CEMENTS.	115
FIGURE 4-3: STEPS IN EXTRACTING MORPHOLOGICAL PARAMETERS USING IMAGE TOOL.	118
FIGURE 4-4: PERMEABILITY OF CANCELLOUS BONE VS. APPARENT DRY DENSITY.	119
FIGURE 4-5: FLOW CHART SHOWING CEMENT FLOW MODELLING TECHNIQUE.	121
FIGURE 4-6: A SCALLOPED (LEFT) AND A TRIMMED FLANGED (RIGHT) ACETABULAR CUP.	122
FIGURE 4-7: INITIAL AXISYMMETRIC AND 3D MESHES OF BONE CEMENT FLOW DOMAINS.	124
FIGURE 4-8: CEMENT PRESSURE DISTRIBUTIONS DURING ACETABULAR CUP INSERTION.	126
FIGURE 4-9: EXPERIMENTALLY DETERMINED PRESSURE VS. TIME CURVES, REPEATED CUP INSERTION.	127
FIGURE 4-10: COMPARISON OF MEASURED AND PREDICTED PRESSURE VS. TIME CURVES.	128
FIGURE 4-11: COMPARISON OF PREDICTED AND MEASURED PRESSURES FOR CMW 1 CEMENT.	130
FIGURE 4-12: COMPARISON OF PREDICTED AND MEASURED PRESSURES FOR CMW 3 CEMENT.	131
FIGURE 4-13: STRAIN RATES DURING CUP INSERTION (s^{-1}).	132
FIGURE 4-14: SCHEMATIC OF THE POROUS DISK EXPERIMENT.	133
FIGURE 4-15: INITIAL FINITE ELEMENT MESH FOR THE POROUS DISK SIMULATION.	134
FIGURE 4-16: DEVELOPMENT OF THE MESH SHOWING THREE STAGES OF CEMENT PENETRATION.	134
FIGURE 4-17: PREDICTED PENETRATION PROFILE SUPERIMPOSED ON AN X-RAY OF THE POROUS DISK.	135
FIGURE 4-18: FINITE ELEMENT MESHES OF ACETABULA WITH UNFLANGED AND FLANGED CUPS.	136
FIGURE 4-19: PRESSURE DISTRIBUTIONS AT TWO CUP POSITIONS FOR 100 N INSERTION FORCE.	137
FIGURE 4-20: PREDICTED RELATIONSHIP BETWEEN CEMENT PENETRATION AND CEMENT VISCOSITY.	137
FIGURE 4-21: PREDICTED RELATIONSHIP BETWEEN CEMENT PENETRATION AND INSERTION FORCE.	138
FIGURE 4-22: PREDICTED RELATIONSHIP BETWEEN CEMENT PENETRATION AND BONE PERMEABILITY.	138

FIGURE 4-23: PERMEABILITY OF CANCELLOUS BONE VS. APPARENT WET DENSITY.	140
FIGURE 5-1: LATERAL (TOP) AND MEDIAL (BOTTOM) VIEWS OF THE FINITE ELEMENT MODEL.	148
FIGURE 5-2: YOUNG’S MODULUS DISTRIBUTION IN THE SUB-LUNATE CANCELLOUS BONE.	152
FIGURE 5-3: POSITIVE DIRECTION OF NORMAL, TWISTING AND TILTING SHEAR STRESS.	153
FIGURE 5-4: SECTIONS THROUGH THE NORMAL AND IMPLANTED ACETABULA.	154
FIGURE 5-5: LOCATIONS OF DEBONDING FOR THE ONE-, TWO- AND THREE LAYER DEBONDED MODELS.	155
FIGURE 5-6: FORCE DEFLECTION RELATIONSHIPS FOR CONTACT (GAP) ELEMENTS.	156
FIGURE 5-7: PELVIC DEFORMATION AND VON MISES STRESS IN THE SUB-LUNATE CANCELLOUS BONE.	157
FIGURE 5-8: PERI-ACETABULAR DISPLACEMENTS IN NORMAL AND RECONSTRUCTED ACETABULA.	158
FIGURE 5-9: DISTRIBUTION OF THE HOFFMAN CRITERION AND VON MISES STRESS.	159
FIGURE 5-10: EFFECT OF SACRIFICE OF THE SUBCHONDRAL PLATE ON INTERFACE STRESS.	160
FIGURE 5-11: MAXIMUM AND MINIMUM VALUES OF THE INTERFACE STRESS COMPONENTS.	161
FIGURE 5-12: TILTING AND TWISTING MICROMOTION AT THE ILIUM, ISCHIUM AND PUBIS.	161
FIGURE 5-13: TILTING AND TWISTING MICROMOTION AT THE ILIUM, PUBIS AND ISCHIUM.	163
FIGURE 5-14: THE EFFECT OF FRICTION ON MICROMOTION AT THE ILIUM.	163
FIGURE 5-15: EFFECT OF VARYING MODEL PARAMETERS ON THE RANGE OF MICROMOTION.	164
FIGURE 5-16: THE EFFECT OF DEBONDING AT THE CEMENT BONE INTERFACE ON INTERFACE STRESSES.	165
FIGURE 5-17: THE EFFECT OF DEBONDING AT THE CEMENT BONE INTERFACE ON INTERFACE STRESSES.	166
FIGURE 5-18: MAXIMUM INTERFACE STRESSES FOR THE BONDED AND DEBONDED MODELS.	167
FIGURE 5-19: VON MISES STRESS IN CORTICAL AND CANCELLOUS BONE FOR VARIOUS MODELS.	169
FIGURE 6-1: TWO VIEWS OF THE UNIT FOR JOINT RECONSTRUCTION JOINT SIMULATOR.	181
FIGURE 6-2: THE PRINCIPAL MECHANICAL COMPONENTS OF THE UJR JOINT SIMULATOR.	182
FIGURE 6-3: FUNCTIONAL DIAGRAM OF THE UJR JOINT SIMULATOR.	184
FIGURE 6-4: SIMULATED GAIT CYCLE: MAGNITUDE AND ORIENTATION OF THE HIP LOAD.	185
FIGURE 6-5: VIEW OF A MOUNTED SPECIMEN ALONG THE AXIS OF THE TESTING MACHINE ACTUATOR.	185
FIGURE 6-6: COMPARISON OF COMMAND AND OUTPUT SIGNALS OF THE UJR JOINT SIMULATOR.	186
FIGURE 6-7: THE PREPARED CALF ACETABULUM.	187
FIGURE 6-8: TYPICAL PRESSURE TIME TRACE FOR CEMENT PRESSURISATION IN GROUP 2.	188
FIGURE 6-9: POTTED ACETABULUM READY FOR TESTING.	189
FIGURE 6-10: A CALIBRATION CURVE FOR THE LVDT.	190
FIGURE 6-11: MESH AND MATERIAL PROPERTY DISTRIBUTION FOR THE FINITE ELEMENT MODELS.	192
FIGURE 6-12: MICROMOTION AT THE ILIUM FOR TWO CEMENTING TECHNIQUES.	193
FIGURE 6-13: RADIOGRAPHIC APPEARANCE CEMENT BONE INTERFACES.	194
FIGURE 6-14: COMPARISON OF MICROMOTION VARIATION BETWEEN 1 ST AND 5 TH EXPERIMENTAL RUN.	195
FIGURE 6-15: INITIAL RUN MICROMOTIONS FOR THE THREE CASES.	196
FIGURE 6-16: FINAL RUN MICROMOTIONS FOR THE THREE CASES.	196
FIGURE 6-17: MICROMOTION AS A FUNCTION OF LOAD AMPLITUDE.	197
FIGURE 6-18: CYCLIC MICROMOTION: FINITE ELEMENT AND EXPERIMENTAL RESULTS.	197

FIGURE 6-19: RANGE OF MICROMOTION: FINITE ELEMENT AND EXPERIMENTAL RESULTS.....	198
FIGURE 6-20: PREDICTED ARTEFACT DUE TO REMOTE MEASUREMENT OF INTERFACE MICROMOTION.....	199
FIGURE A-1: DIAGRAM AND NOMENCLATURE FOR OSCILLATING PARALLEL PLATE PROBLEM.	223
FIGURE A-2: SHEAR STRAIN RATES IN RHEOMETER TESTS AS A FUNCTION OF R (M).....	223
FIGURE B-1: COMPUTER GENERATED IMAGES OF PENETRABLE SPHERE MATERIAL.....	225
FIGURE B-2: SURFACE AREA TO VOLUME RATIO FOR THE COMPUTER GENERATED IMAGES.	226
FIGURE B-3: EXAMPLE OF THE BREAKDOWN OF THE OBJECT BOUNDARY MEASUREMENT.	226
FIGURE C-1: EIGHT NODE ISOPARAMETRIC BRICK ELEMENT.....	227
FIGURE C-2: FINITE ELEMENT MESH AND BOUNDARY CONDITIONS.....	229
FIGURE C-3: VARIATION IN STRAIN RATE ACROSS PIPE SECTION.....	229
FIGURE C-4: COMPARISON OF ANALYTICAL AND FINITE ELEMENT RESULTS.	230

List of Tables

TABLE 2-1: MUSCLES CROSSING THE HIP JOINT, GROUPED BY ACTION	15
TABLE 2-2: VALUES FOR THE MECHANICAL PROPERTIES OF CORTICAL BONE	21
TABLE 2-3: VALUES FOR THE MECHANICAL PROPERTIES OF CANCELLOUS BONE.	23
TABLE 2-4: LITERATURE VALUES FOR THE FRACTURE PROPERTIES OF CORTICAL BONE.	31
TABLE 2-5: THE MECHANICAL PROPERTIES OF SOME MATERIALS USED IN HIP JOINT PROSTHESES	55
TABLE 2-6: VALUES FOR THE MECHANICAL PROPERTIES OF ACRYLIC BONE CEMENTS.	59
TABLE 2-7: RADIOGRAPHIC EVIDENCE OF SOCKET CONDITION	61
TABLE 3-1: COMPARISONS SHOWING STATISTICALLY SIGNIFICANT DIFFERENCES AT THE $p = 0.05$ LEVEL.	95
TABLE 3-2: DETAILS OF PATIENTS FOR THE PER OPERATIVE CEMENT PRESSURE MEASUREMENTS.	106
TABLE 4-1: LINEAR RELATIONSHIPS FOR LOG (REAL PART OF COMPLEX VISCOSITY) VS. TIME.	115
TABLE 5-1: HIP JOINT FORCE AND MUSCLE FORCES FOR EIGHT LOAD CASES DURING GAIT.	149

1. Introduction

Modern total hip replacement provides a highly successful treatment for disabling disorders of the hip. Although the first attempts at artificial hip joints were described over 100 years ago by Gluck (1891), the modern hip replacement owes a great part of its success to the work of Sir John Charnley, who pioneered the fixation of hip prostheses to the living skeleton with self-polymerising acrylic bone cement, a technology he borrowed from dental surgery. Fundamentally, the philosophy of the cemented hip implant has changed little since then, indeed variants of the Charnley design remain amongst the most successful 30 years after they were first implanted. The performance of cementless implants, introduced after perceived problems with the material that initially gave the hip replacement its success, has not yet reached the standard set by cemented implants.

Multi-centre studies show the failure rate for well established designs of cemented implant to be around 10% after 10 years (Malchau *et al.*, 1993). However, 38,000 hip replacements were performed in the U.K. in 1995, 18% of which were revision operations (Biomaterials and Implants Research Advisory Group, 1996). Similar trends are seen throughout the world and the number of revisions are forecast to rise for the foreseeable future. Revisions are complicated, costly and, in general, less successful than the primary operation (Kershaw *et al.*, 1991). Further improvements to the long term performance of the primary hip are therefore essential.

Late failure in the absence of infection is generally referred to as “aseptic loosening”, more properly described as a process rather than an event (Huiskes, 1993) and characterised by the formation and progressive thickening of a continuous layer of fibrous tissue around the prosthesis, accompanied by bone resorption and ultimately gross migration of the prosthesis and clinical failure. A finding common to many long term reviews (Morscher, 1992) is the increased risk of early revision due to aseptic loosening for the younger patient. Other notable risk factors are higher than average body weight (Schurman *et al.*, 1989) and certain diagnoses, e.g. rheumatoid arthritis rather than osteoarthritis (Ahnfelt *et al.*, 1990; Malchau *et al.*, 1993).

Much clinical evidence points to an early mechanical initiation of failure. Recent work suggests that all prostheses migrate from “day one”, but it is those that show early, rapid migration that eventually require early revision (Freeman and Plante-Bordeneuve, 1994; Kärrholm *et al.*, 1994). Specialised radiographic techniques such as Röntgen stereophotogrammetric analysis (RSA) enable accurate measurements, in three dimensions, of the position of implants within the body and their movement with time. These studies provide evidence that the early migration of implants in bone is correlated with, and therefore may predict, early clinical failure.

Since the first long term clinical reviews (e.g. Charnley, 1979), loosening of the acetabular component of cemented hip arthroplasty has been recognised as a significant failure mode. The rate of acetabular loosening can be 2 to 3 times that of the femoral component (Schulte *et al.*, 1993). Wroblewski (1986) reported that in three major series, the incidence of acetabular loosening, as determined radiographically, was 22-25% after 10 years. Snorrason *et al.* (1993) have used RSA to evaluate several factors affecting the success of cemented acetabular components. They considered that early migration indicated an inferior bone cement interface and that the poor primary fixation that this implied indicated that the fate of the prosthesis might be revealed in the first post-operative months. Similarly, Carlsson and Gentz (1984) and Hodgkinson *et al.* (1988) found that even minor radiological defects in the cement bone interface appearing in the first post-operative year lead to 35-40% radiological loosening after ten years.

Improvements in cementing technique have led to a valuable increase in the survivorship of cemented hip replacements (Malchau and Herberts, 1996). Hodgkinson *et al.* (1993) reported an improvement in post-operative radiological appearance of the cement-bone interface with flanged compared to unflanged cups which was reflected in the radiological appearance at 10 years where 43% of flanged sockets showed no evidence of radiolucency as against 30% of the unflanged group.

Chapter 2 of this thesis provides an overview of current knowledge of total hip replacement. Having identified clinical evidence that mechanical events in the post-operative period and pressurisation of bone cement are both important determinants of the longevity of a hip replacement, the thesis goes on to attempt to investigate the relationship between these two. Chapter 3 proceeds from the assumption that cement

pressurisation is an effective means of achieving secure acetabular component fixation. Various methods of cement pressurisation are then compared using an instrumented model acetabulum, with the goal of identifying the most effective of current techniques, such as finger packing, component insertion and the use of various pressurisation tools. The *in vivo* measurement of cement pressures with an instrumented cement pressuriser are also presented. Chapter 4 describes the development and validation of a finite element modelling technique to predict the pressurisation and penetration of cement into cancellous bone, going on to describe a parametric study of the factors that affect the ultimate cement penetration and consequently the component fixation. Chapters 5 and 6 describe finite element models of the reconstructed hip. In the first an attempt is made to investigate the mechanics of the human hip under realistic loading. In the second, the results of finite element models are compared with experiment for a laboratory model of human acetabular reconstruction, a bovine calf acetabulum, loaded in a newly developed hip joint simulator, representing a first attempt to inter-relate the results of chapters 3, 4 and 5 and the relevant orthopaedic literature. Chapter 7 summarises the results and discusses their significance with regard to the clinical situation, while chapter 8 suggests progress for the work.

2. Review of the Literature

2.1 The Hip Joint

The hip (coxal) joint is the articulation of the pelvis and the femur, the long bone of the thigh. It is a synovial ball-and-socket joint, where the head of the femur is the ball and the acetabulum the socket (Figure 2-1). The hip joint is highly stable due to its physical configuration. In normal activity, muscle and gravitational forces transmitted across the joint tend to maintain the congruency of the joint surfaces. The ligaments and joint capsule (Figure 2-2) together serve to augment the stability of the joints, to help guide joint motion and to prevent excessive motion (Carlstedt and Nordin, 1989). The extended lip of fibrocartilage around the rim of the acetabulum, the acetabular labrum, serves to increase stability by acting as a skirt extending over the femoral head past the articular surface. At the extremes of motion of the hip the iliofemoral ligament limits extension, the pubofemoral ligament limits abduction and extension and the ischiofemoral ligament limits internal rotation. These functions are also assisted by the fibrous joint capsule. In a total hip replacement, it is important to note that the ligaments and joint capsule are sometimes resected, although a pseudo-capsule usually reforms. This capsule has a bearing on the stability (in the sense of resisting dislocation) of the replacement hip joint, which must now be achieved by careful implant design and surgical procedure.

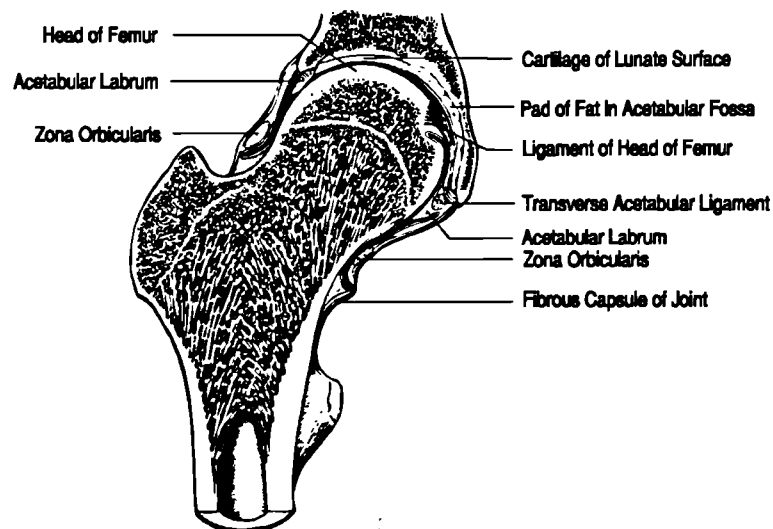


Figure 2-1: Cross-sectional anatomy of the hip joint.
(Adapted from Platzer, 1981)

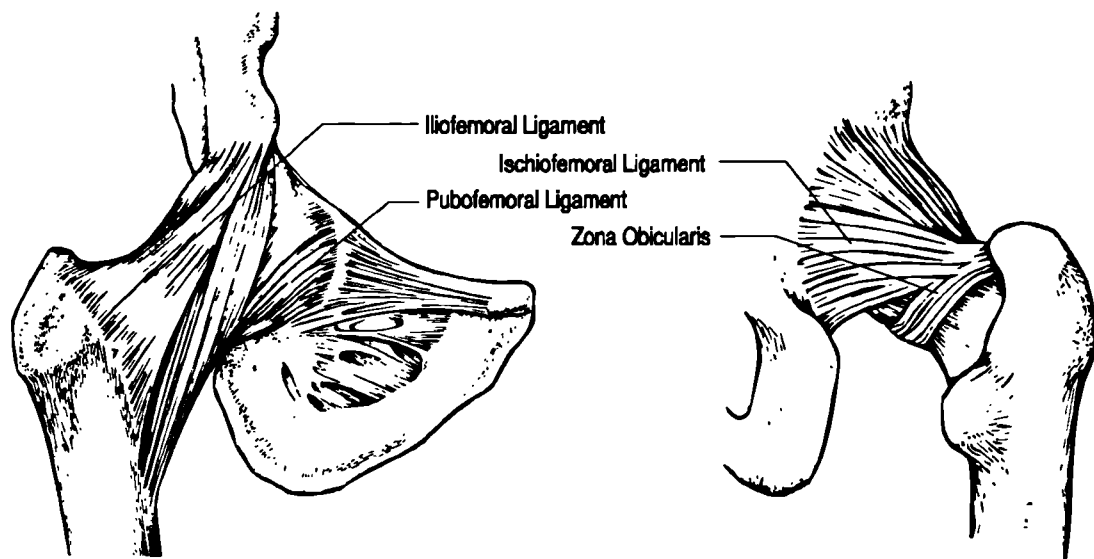


Figure 2-2: Ligaments of the hip joint
 (Adapted from Platzer, 1981)

2.1.1 Functional Anatomy of the Pelvis and Acetabulum

The pelvic girdle consists of the two innominate bones (Figure 2-3), each of which, in the mature adult, is a bony fusion of three separate smaller bones, the ilium, ischium and pubis. The area of the union of the three bones forms the acetabulum, the socket of the hip joint. The major function of the pelvic bones is to distribute the weight of the upper body, the major part of which is transmitted via the vertebral column, into the lower limbs and to provide attachments for the muscles that articulate the hip joints and some of the major muscles that maintain vertebral posture. The pelvis also has secondary roles in protecting and providing attachments for muscles supporting organs of the abdomen.

In fulfilling its major role, the pelvis transmits forces that can be several multiples of body weight. The pelvis has thus evolved into an efficient structure according with the sandwich principle, with a stiff, strong outer shell of cortical bone that bears the bulk of the loads and a low density "honeycomb" inner core of cancellous bone that serves as a spacer, a reservoir for haemopoietic tissue and to resist buckling. This is similar to engineering components highly loaded in bending and designed for minimum weight such as glider wings and helicopter rotor blades.

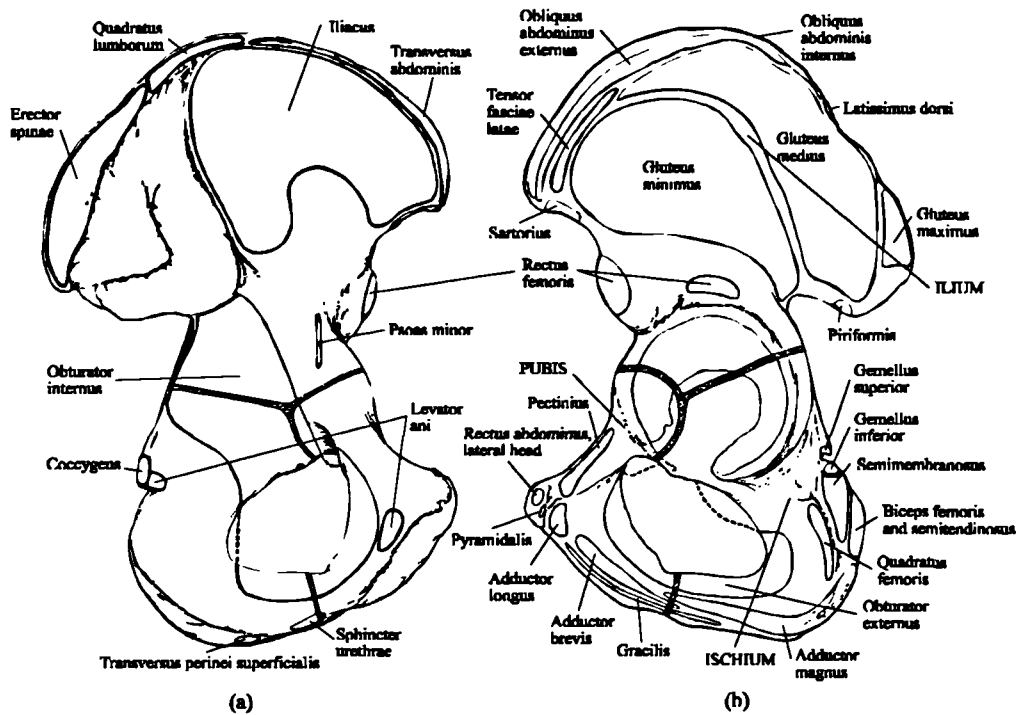


Figure 2-3: Anatomy and muscle attachments of the innominate bones:
 (a) medial view, (b) lateral view.
 (Adapted from Gray's Anatomy, 1980)

There are approximately 20 major muscles attached to the pelvis. The areas of muscle attachment are shown in Figure 2-2, while Table 2-1 gives the attachments and actions of the major muscles that cross the hip joint, grouped by principle active movement.

Table 2-1: Muscles crossing the hip joint, grouped by action
 (from Cunningham's Textbook of Anatomy, 1972)

Extension	Gluteus maximus Semimembranosus Semitendinosus Biceps femoris (long head) Adductor magnus (ischial fibres)	Abduction	Gluteus medius Gluteus minimus Tensor fasciae latae Obturator internus (in flexion) Piriformis (in flexion)
Flexion	Iliopsoas Rectus femoris Tensor fasciae latae Sartorius Adductor longus Adductor brevis Pectineus	External Rotation	Gluteus maximus Obturator internus Obturator externus Quadratus femoris Piriformis Sartorius Gemellus superior & inferior Adductor magnus Adductor longus Adductor brevis
Adduction	Adductor magnus Adductor longus Adductor brevis Gracilis Pectineus Gluteus maximus (lower fibres) Quadratus femoris	Internal Rotation	Anterior of gluteus medius Anterior of gluteus minimus Tensor fasciae latae Iliopsoas (initial stages)

The normal acetabulum is approximately hemispherical in shape, with a raised horseshoe shaped subchondral bone and articular cartilage layer extending around the postero-lateral rim and inwards towards the depth, framing a fovea which is filled with fatty tissue. Kurrat and Oberländer (1978) showed that the thickness of the articular cartilage in both the femoral head and acetabulum varies with position. The inner edge of the acetabular cartilage ends abruptly and frames the fovea as an unbroken line. The outer edge blends gradually into the acetabular labrum. As in all synovial joints, the principle function of the articular cartilage is to provide a low friction bearing surface (the coefficient of friction of animal joints can be as low as 0.001, Charnley, 1979). The low coefficient of friction means that effectively only compressive forces can be transmitted across joint surfaces. Below the cartilage and subchondral bone layer is cancellous bone in the depth of the acetabulum and the cortical bone of the pelvis at the rim. The macrostructure of the bone in the vicinity of the acetabulum has been studied by Rubenstein *et al.* (1982), who examined transverse cross sections, and Holm (1980) who used various cross-sections, to qualitatively elucidate the patterns of trabeculae. A representative section is shown in Figure 2-4.



Figure 2-4: Cross section of the acetabular region of the innominate bone. (Holm, 1980)

A significant point to note is that the trabeculae of the cancellous bone are thicker and more densely packed in the region swept, in normal activity, by the hip joint force vector, i.e. the dome of the acetabulum.

2.1.2 Biological Materials

Bone is the word used to describe both the rigid structural elements of the skeleton and the material from which these structures are made. One of the most important characteristics of bones as structures is that they can alter their structure in response to varying mechanical demands - they are "dynamically adaptable". Bone is constantly being "remodelled" by osteoclastic (resorption) and osteoblastic (deposition) cellular activity. This mechanism enables the bone to adapt to changes in load-bearing requirements and is discussed further in section 2.4.1(iii). Until recently, with the advent of "smart materials", no man-made materials shared this property.

Two general types of bone can be distinguished in the adult, on the basis of structure, properties and function. Cortical (or compact) bone forms the outer shell of most bones (Figure 2-5). On a microstructural level, it consists of sheets containing fibres of an ultrastructural collagen-hydroxyapatite composite arranged into densely packed concentric lamellar structures called osteons, bonded together by calcified organic material. The osteons are orientated approximately parallel to the principal load axis of long bones such as the femur. The microstructure of cortical bone is thus comparable to modern fibre reinforced composite materials. Characteristic macroscopic properties are a low porosity (5-30 %) (Carter and Spengler, 1978) and high stiffness and strength.

Cancellous bone is found at the ends of long bones such as the femur and throughout the core of others such as the pelvis and the vertebrae, and has a porosity between 30 and over 90% (Carter and Spengler, 1978), although the distinction between porous cortical bone and dense cancellous bone is fairly arbitrary.

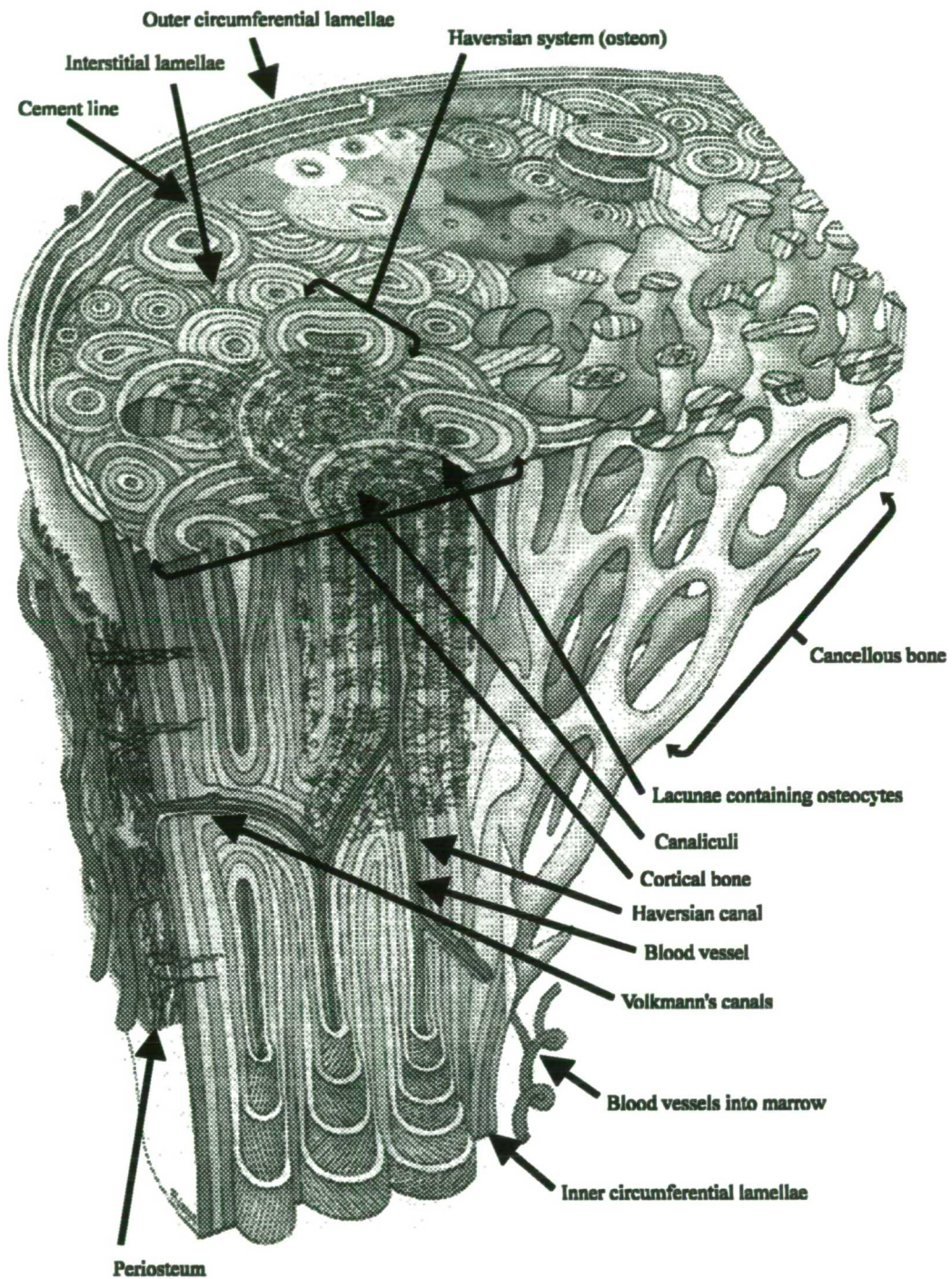


Figure 2-5: Schematic of the metaphysis of a typical long bone.
 (From Gray's Anatomy, 1980)

Cancellous bone has many properties characteristic of man-made cellular materials such as polymeric foams. The pore spaces of cancellous bone are filled with semi-fluid bone marrow. The cellular structure is made up of a three dimensional interconnecting lattice of rods (trabeculae) and plates, with the trabeculae tending to be orientated in the directions of maximum stress. It is interesting to note that cancellous bone is present close to joints, where efficient distribution of bearing loads

is required, and in elaborately shaped bones, such as the pelvis, where complex loading involving bending is present.

Subchondral bone, the bone found beneath the articular surfaces of synovial joints, is essentially very thin cortical bone (0.2-0.4mm), which merges with the cancellous bone on one side and the calcified zone of the articular cartilage on the other.

A huge body of literature exists on the mechanical properties of bone, using both direct (mechanically tested) and indirect (e.g. ultrasound velocity) methods. Several reviews have been published (Carter and Spengler, 1978; Currey, 1984; Goldstein, 1987; Natali and Meroi, 1989).

The most general description of bone is a heterogeneous, anisotropic material, with asymmetrical (different in tension and compression) properties. Viscoelastic deformation within the normal range of physiological loading has been proposed. Characteristics also depend on the type of bone (cortical vs. cancellous), age (Currey and Butler, 1975), anatomical source (summarised in Goldstein, 1987) and pathological state (Abendschein and Hyatt, 1970; Deligianni *et al.*, 1991). Experimental factors such as specimen storage conditions and preparation (Carter and Hayes, 1977b), testing environment (Brown and Ferguson, 1980) and specimen geometry (Choi *et al.*, 1990) have also been shown to be important in some cases.

The combination of these factors results in a large "data space" of mechanical properties and difficulty in comparing properties obtained by different authors. This is a reflection of the inherent variability of biological materials and also the lack of testing standards and protocols.

2.1.2.1 Cortical Bone

A typical stress-strain curve for cortical bone is shown in Figure 2-6. The Young's modulus in the longitudinal direction is typically twice that in the transverse direction. In the longitudinal direction, the ultimate tensile strength is approximately 3 times that in the transverse direction. Some workers have reported transverse tensile strengths as low as 10% of the longitudinal tensile strength (Dempster and Coleman, 1960). The difference in compressive strengths is much less, since in compression there is

reduced tendency to separate the fibre-like osteons by failure of the cement lines (Figure 2-5).

Dry bone tested in the longitudinal direction typically shows values of Young's modulus and ultimate strength in compression 35% and 65% higher than wet bone respectively (Dempster and Liddicoat, 1952). These discrepancies are less for the tangential and radial directions. This emphasises the importance of testing bone wet if experimental values are to be reliable indicators of *in vivo* properties. Table 2-1 gives some literature values for the mechanical properties of cortical bone.

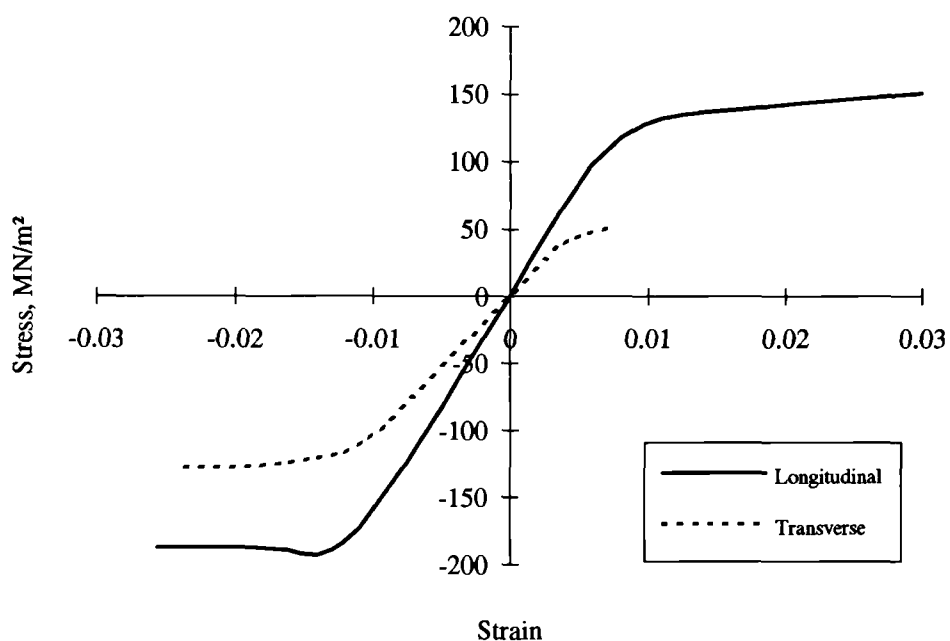


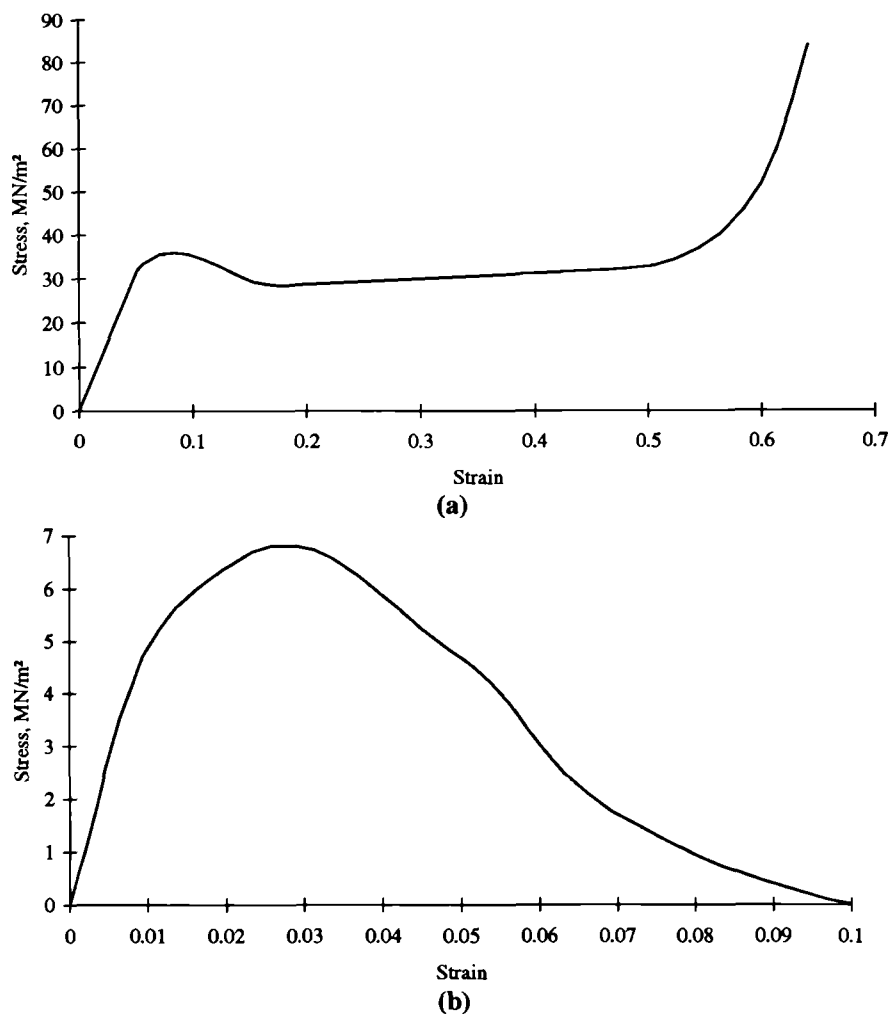
Figure 2-6: Typical stress-strain curves for wet cortical bone.
{Gibson and Ashby (1988), adapted from Reilly and Burstein (1975) and Currey (1984)}

Table 2-2: Values for the mechanical properties of cortical bone.

Authors	Materials	Methods	n	Strain-rate (s ⁻¹)	Ultimate Strength (MPa)	Young's modulus (GPa)
Bonfield and Li (1966)	Bovine	Tensile	10	3.3 x 10 ⁻⁴		26.5
Yamada (1970)	Human	Tensile	15-20		122	
		Comp.	15-20		167	
		Bend	15-20		168	
		Shear	15-20		82.4	
		Torsion			50	3.63
McElhaney et al (1970)	Human	Comp.	160		179	12.7
Evans (1973)	Human	Tensile	403		78.3	14.48
		Comp.	23		117.4	15.45
		Shear	229		70.6±10.5	
Bonfield and Datta (1974)	Bovine	Tensile	9	3x10 ⁻⁴		22.5-30 (mean 27.3)
Reilly and Bursstein (1975)	Bovine Human (long., trans.) Human (long., trans.)	Tensile	4			12
			12, 7			18.3, 14.1
		Comp.	4, 5			18.2, 11.7
Schaffler and Burr (1988)	Bovine	Tensile		0.01		22.1
				0.03		21.4
Currey (1988)	Bovine	Tensile	1			31.33
		Bend	7			18.49±2.84
Rice et al (1988)	Human	Comp.				17-20

2.1.2.2 Cancellous Bone

Typical stress-strain curves for cancellous bone are shown in Figure 2-7. The curves in tension and compression show marked differences. The initial portion of both curves shows approximately linear elastic behaviour, but the "yield" stress in compression is significantly higher. The initial portion of both curves corresponds to either elastic extension/compression, or bending of the trabeculae, depending on the load orientation with respect to the material's principal directions. In compression beyond the linear elastic region there is collapse of the cell walls, either by elastic or plastic buckling, depending on density and specimen conditions (Gibson, 1985). In tension this regime is accompanied by irreversible deformation and fracture of the trabeculae. Table 2-3 gives some literature values for the mechanical properties of cancellous bone.



**Figure 2-7: Typical stress strain curves for wet cancellous bone.
(a) Compressive and (b) tensile loading.
{Gibson and Ashby (1988), adapted from Carter *et al.* (1980)}**

Table 2-3: Values for the mechanical properties of cancellous bone.

Authors	Materials	Methods	n	Strain-rate (s ⁻¹)	Ultimate Strength (MPa)	Young's modulus (MPa)
Evans and King (1961)	Human-Fem. head	Comp.	19		7.61	581
	-Lat. Fem. cond.		13		5.05	571
	-Med. Fem. cond.		23		4.65	418
	-Greater troch.		1		1.35	81
	-Fem. neck		5		8.75	780
Galante <i>et al.</i> (1970)	Human	Comp.	72		2.06	
McElhaney <i>et al.</i> (1970)	Human	Comp.	288		4.1	152
Carter and Hayes (1977b)	Human	Comp.	100	0.001	4.2	56.6
				0.01	4.1	17.5
				0.1	5.8	81.5
				1	6.7	81.2
				10	9.13	83.7
Halawa <i>et al.</i> (1978)	Human	Shear	22	0.01-0.1	2-14	
Martens <i>et al.</i> (1983)	Human -x axis	Comp.	2-7		9.3	900
	-y axis				10.2	811
	-z axis				4.9	404
Keaveny <i>et al.</i> (1994b)	Bovine	Tensile	22		16.9	2630
		Comp.	22		23.6	2380

2.1.2.3 Factors Influencing Mechanical Properties

Cortical bone is anisotropic. The ratio of Young's modulus in the longitudinal and transverse directions for bovine femoral specimens is between 1.7 (wet specimens) and 2.3 (dry specimens) (Bonfield and Gryn timer, 1977). Cancellous bone exhibits anisotropy, mainly due to orientation of the trabecular structure (Hodgskinson and Currey, 1990). Dalstra (1993) suggests that for many purposes, such as F.E. analysis, pelvic cancellous bone can be adequately described as isotropic.

Wright and Hayes (1976) and Carter and Hayes (1977b) investigated the relationship of modulus of elasticity and ultimate strength with strain rate for cortical and cancellous bone. All the data showed similar trends, with both properties increasing approximately linearly with increasing strain rate in the region 10^{-4} to 10^3 s⁻¹. The presence of marrow was influential in increasing the strength of the cancellous bone only in tests at high strain rates, i.e. when the forces required to exude the marrow from the trabecular spaces became significant. Interestingly, energy absorption capacity, a measure of toughness, was found to show a peak centred around strain rate values between 10^{-2} and 10^{-1} s⁻¹. Dalstra (1993), in a finite element analysis of load transfer across the pelvic bone during walking, found peak strain rates of 4×10^{-1} s⁻¹ in cancellous bone and 10^{-1} s⁻¹ in cortical bone.

Burstein *et al.* (1976) examined the effect of ageing on the properties of cortical bone specimens from the femur and tibia. A consistent decrease in all measured properties of femoral bone with age was found with no significant differences between male and female bone. Tibial tissue showed no regular change. The most important change was identified as the decrease in ultimate strain which implies a reduced work of fracture and lower energy absorption capacity.

Deligianni *et al.* (1991) studied the mechanical behaviour of human trabecular bone obtained from the femoral heads of females with osteoarthritis, fractured neck of femur and from cadavers, using compression tests. They concluded that cadaveric and osteoporotic bone were mechanically equivalent, with the observed differences due to reduction in density due to osteoporosis. However, osteoarthritis caused some change in the structure of the bone and they quote Gryn timer *et al.* (1991) as finding more bone, but of lower mineral content in osteoarthritis.

Goldstein (1987) noted that testing conditions, in particular temperature, moisture content and previous storage conditions, contribute significantly to variation in materials properties data from different authors. The most reliable data will come from *in vitro* experiments that most closely simulate the *in vivo* conditions. Dempster and Liddicoat (1952) showed that dry bone has significantly different properties to wet and recent studies (Hodgkinson and Currey, 1992) have tested bone specimens in a water bath at 37°C. In conventional materials testing specimens are usually prepared with a geometry so that a uniform stress field is produced in the region of interest or "gauge length" and artefacts due to end constraints, e.g. testing machine grips etc., can be excluded. Due to the difficulties of testing biological materials, especially lack of material, the importance of specimen geometry has, in general, been neglected. A recent study by Keaveny *et al.* (1993) made the point that inter study comparisons of materials properties may not be valid when differing specimen geometries were used, since they found different values for Young's modulus and compressive strength during compression testing of different shaped specimens from the same source.

Røhl *et al.* (1991) tested cancellous bone specimens with their ends embedded in epoxy resin, in order to conduct non-destructive measurements of both tensile and compressive modulus on the same sample. This has similarities with the cancellous/cortical bone junction in that there are no unconstrained trabeculae exposed at the ends, although epoxy resin has a lower modulus than cortical bone. Strain was measured with an extensometer, which tends to eliminate end effects. They found no evidence for asymmetry of the Young's modulus and also no evidence of departure from non-linearity in the elastic regime as has been suggested by earlier studies utilising ω -embedded specimens, which suggests that this effect may be an artefact of the particular testing conditions employed.

Using careful specimen design to ensure a gauge length under uniform stress where specimen strain could be accurately measured and to avoid artefacts associated with cut specimen ends, Keaveny *et al.* (1994a, 1994b) found no difference between the tensile and compressive Young's modulus of cancellous bone, linear elastic behaviour until yield and lower average yield strain and yield strength for tensile than compressive loading. They also proposed an elegant explanation for the greater progressive reduction of tensile modulus than compressive modulus associated with

multiple loading cycles based on cracking of trabeculae both parallel and perpendicular to the load path, rather than yielding behaviour.

2.1.2.4 Dynamic Mechanical Properties

If the stresses during repeated loading are sufficiently high, fatigue failure of bone may result. The fatigue behaviour of devitalised cortical bone has been extensively studied. Carter and Hayes (1977a) showed that repeated loading of cortical bone caused a progressive loss of bone stiffness and strength, which was attributed to accumulation of microscopic damage such as microcracking and osteon debonding. The review by Currey (1984) suggests that the mechanisms of fatigue fracture are more similar to those of fibre reinforced materials than metals, involving accumulation of diffuse damage, rather than the growth of isolated critical flaws.

The behaviour of cancellous bone has not been so well studied. The reduction in bone stiffness with number of cycles for bovine cancellous bone tested at various cyclic stress amplitudes has been measured by Michel *et al.* (1993). Their results caused them to speculate that both damage accumulation and creep of trabeculae contributed to fatigue failure, with damage accumulation most significant for high stress levels and creep for low stress levels.

Normally, any fatigue damage accumulation will be compensated for by the processes of bone turnover and repair. Indeed the equilibrium between rate of damage accumulation and rate of bone repair has been used as to describe and predict the remodelling behaviour of bone (Prendergast and Taylor, 1994). Immediately after joint replacement, however, a necrotic zone of bone exists around the implant, which takes a significant period of time to revitalise. This region is especially prone to fatigue damage, since, initially at least, remodelling cannot repair the damage.

2.1.2.5 Density as a Predictor of Mechanical Properties

Many studies have investigated the correlation between density and mechanical properties. This is of major interest since bone density can be assessed clinically using techniques such as quantitative CT scanning. Knowledge of the relationship of bone strength to density, for example, enables assessment of fracture risk in osteoporotic

patients. The relationship is also useful in providing data for finite element models of bones and joints.

The theoretical background to the properties of cellular materials can be found in Gibson and Ashby (1988). For an idealised open cell foam a power law type relationship is predicted between elastic properties and density, e.g. for equiaxed cells:-

$$\frac{E^*}{E_s} = A \left(\frac{\rho^*}{\rho_s} \right)^2 \quad \text{Equation 2-1}$$

and for a stress oriented "parallel plate-like" structure:-

$$\frac{E_T^*}{E_s} = B \left(\frac{\rho^*}{\rho_s} \right)^3 \quad \text{Equation 2-2}$$

and:-

$$\frac{E_L^*}{E_s} = C \left(\frac{\rho^*}{\rho_s} \right) \quad \text{Equation 2-3}$$

depending on direction, where E = elastic modulus, ρ = density, superscript * refers to the properties of the foam, subscript s refers to the properties of the solid, subscript L refers to in-plane loading of the plates, subscript T refers to transverse loading of the plates and A, B and C are constants. Similar theoretically derived expressions are also available for strength.

Hodgkinson and Currey (1992) tested cubes of cancellous bone from various species (including human) and bones, giving a large density range. They found that density was an "extremely effective explanatory variable, accounting for 97% of the variance in mean (Young's) modulus". (The cubes were loaded in the three orthogonal directions, the mean modulus being the average of these three values). This indicates that the most important way that cancellous bone properties vary, even between species, is in amount of bone material present in a given volume.

For human bone the relationships between apparent density (measured on dry, defatted bone) and modulus were:-

$$\log E' = -2.43 + 1.96 \log D \quad \text{Equation 2-4}$$

$$\log E'' = -1.46 + 1.66 \log D \quad \text{Equation 2-5}$$

$$\log E''' = -4.10 + 2.47 \log D \quad \text{Equation 2-6}$$

where E = Young's modulus in compression (MPa), D = apparent density (kg m^{-3}), superscript ' refers to the mean Young's modulus for the three orthogonal directions, superscript '' refers to the highest Young's modulus for the three orthogonal directions and superscript ''' refers to the lowest Young's modulus for the three orthogonal directions.

These equations are plotted in Figure 2-8.

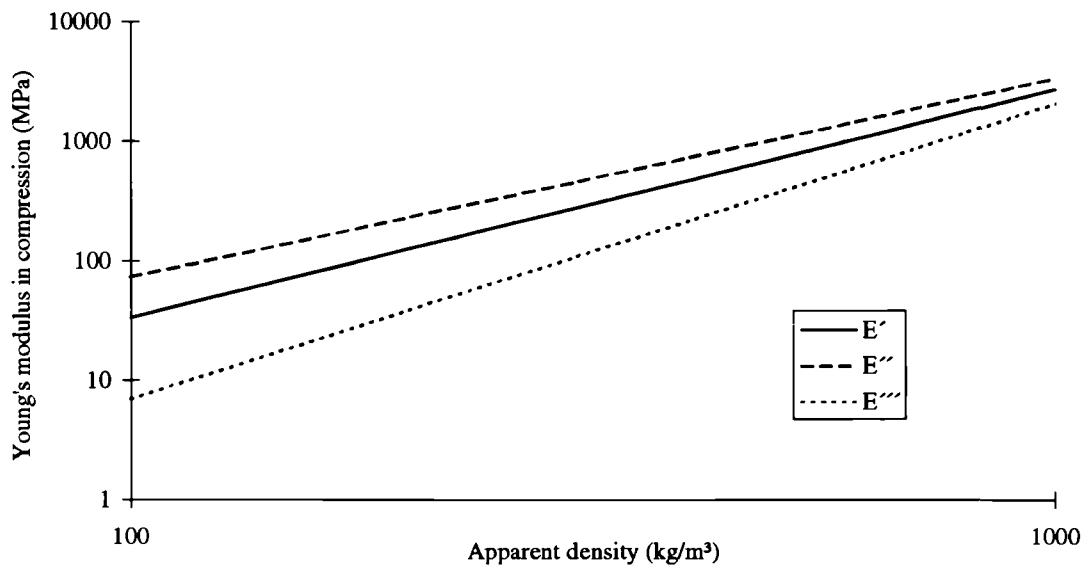


Figure 2-8: Relationships between Young's modulus and density for cancellous bone. (Equation 2-4 - Equation 2-6) (Hodgskinson and Currey, 1992)

2.1.2.6 Fracture Properties of Bone

One of the features of cortical bone testing is the large variation in ultimate strength properties found within groups of nominally identical specimens. Together with typical strains to failure of 0.5-3.5 % and limited deviations from linear elasticity, these characteristics establish cortical bone as a semi-brittle material. As such a material, fracture of cortical bone is controlled not only by the applied loads and microstructural features, but the size and distribution of intrinsic or applied defects. In conventional

strength of materials specimens the distribution of defects is more or less random, going some way to explain the large scatter found in this type of data.

Such a material is suitable for treatment by a linear elastic fracture mechanics (LEFM) approach, in which the concept of ultimate strength is replaced by that of resistance to fracture in terms of resistance to crack propagation or “fracture toughness”. Two parameters have been used to express fracture toughness. The first is derived from the stress intensity, K , at the tip of the crack. K is a measure of the driving force for crack growth, formed from the physical quantities σ and a which represent the nominal stress in the material and the crack length respectively. It is given by a relationship of the form:-

$$K = \sigma\sqrt{\pi a} \quad \text{Equation 2-7}$$

In analogy with the yield stress of a ductile material, crack propagation occurs when the value of K exceeds a critical value, the critical stress intensity factor K_c . K_c is in fact defined for three loading modes (mode I = opening mode, mode II = shearing mode, mode III = tearing mode) and also turns out to be a thickness dependent property, which reaches a constant minimum value when plane strain (large thickness) conditions are approached.

The second parameter is the critical strain energy release rate G_c . It is derived by considering the balance between the energy released by the extension of a crack in a loaded specimen and the energy required to extend the crack. As soon as the specimen load increases to the point when this process becomes energetically favourable, i.e. the energy released by crack extension is greater than that absorbed in creating the new surfaces, crack propagation occurs. In an ideal elastically isotropic solid the quantities K_c and G_c are related by:-

$$K_c^2 = \frac{E}{1-\nu^2} G_c \quad \text{Equation 2-8}$$

where E = Young’s modulus and ν = Poisson’s ratio.

In a typical fracture mechanics test specimens have a single well characterised crack or notch deliberately introduced to predetermine the location of the critical defect. The relationship between load at the onset of crack growth and crack length is then determined by loading the specimen. From these the fracture toughness can be calculated.

Early studies attempted to validate the application of fracture mechanics principles to bone. Bonfield and Datta (1976) sought to establish K_c as a materials property by using single edge notch specimens to investigate the dependence of fracture stress on crack length and the radius of curvature of the crack tip. The first requirement for the validity of LEFM, i.e. a linear elastic stress-strain curve, was closely approached. Fracture stress was found to be inversely proportional to the square root of crack length as predicted by Equation 2-7. The value of K_c derived was also found to be independent of the nominal crack tip radius, suggesting that on a microscopic level the cracks were propagating from similar flaws at the edge of the machined notch which closely approached the ideal atomically sharp crack. Tests with centre notched cylindrical specimens, in which a longitudinally oriented notch was loaded by hoop stresses generated by a shock wave, confirmed the applicability of Equation 2-8 (Bonfield and Datta, 1974) and also revealed the sensitivity of the measured K_c to strain rate and hence crack propagation velocity. Wright and Hayes (1977) and Bonfield *et al.* (1978) used compact tension (CT) specimens to again demonstrate the linear relationship between load at the onset of crack growth and crack length. The CT specimen has the advantage of stable rather than catastrophic crack propagation. Bonfield *et al.* also discovered that crack propagation velocity could be controlled by varying the speed of the cross head of the materials testing machine and used this to establish the existence of a critical crack velocity associated with a maximum in the fracture toughness of bone and coinciding with the transition from controlled to catastrophic crack propagation. Grooved CT specimens have also been used to evaluate the anisotropy of fracture characteristics, by forcing the crack to remain in the plane of the groove and the starter crack, rather than taking the line of least resistance in the osteon direction (Bonfield *et al.*, 1985).

The microstructural features of bone have a large effect on fracture toughness. Wright and Hayes (1977) demonstrated the significant effect of increased bone density increasing K_c and G_c . It has also been shown that a higher number of osteons and larger osteons inhibit crack propagation (Corondan and Haworth, 1986). Norman *et al.* (1995) suggested that, because of the effects of the microstructural variations of bone on the assumptions of LEFM theory, G_c would be a better defined indicator of fracture toughness, since it is a measure of global specimen behaviour rather than the local processes at the crack tip.

Table 2-4: Literature values for the fracture properties of cortical bone.

Authors	Bone source	Specimen type	Direction of crack propagation	K_c (MPam ^{1/2})	G_c (Jm ⁻²)	Comments
Melvin and Evans (1973)	Bovine femur	SEN ¹	Transverse	5.58	3135-5534	
Bonfield and Datta (1976)	Bovine tibia	SEN	Longitudinal	3.21	1388-2557	
Bonfield and Datta (1974)	Bovine femur	CNC ²	Transverse	2.2-4.6	780-1120	G_c calculated from K_c
Wright and Hayes (1977)	Bovine femur	CT ³	Longitudinal	0.23	4	High strain rate (7 s ⁻¹) G_c calculated from K_c
Bonfield <i>et al.</i> (1985)	Human tibia	Miniaturised CT	Longitudinal	3.6	820	G_c obtained independently (from compliance calibration)
Norman <i>et al.</i> (1995)	Human tibia	Miniaturised CT	Longitudinal	4.5 (25 yrs) 2.5 (90 yrs)	827 (2 mm thickness) 595 (2 mm thickness)	G_c obtained independently (from compliance calibration)

¹ Single edge notched

² Centre notched cylindrical

³ Compact tension

2.1.3 Biomechanics of the Hip

A full engineering analysis of the mechanics of a single joint system is an extremely complex task, since most joints, including the hip joint, possess a mechanically redundant set of load transmitting elements, i.e. the musculotendinous structures, ligaments, joint capsule and the joint surfaces themselves. Muscles, transmitting the forces they generate to the bones via tendons, can only produce tensile forces, so active movement of even a simple hinge joint in both directions requires at least two muscles. However, many synovial joints in the human body allow more degrees of freedom than a pure hinge and hence, for their control, require more muscles, many contributing to the control of more than one degree of freedom. In addition to the muscles, passive structures such as ligaments and the joint capsule can limit movement at the extremes of the range of movement of the joint; this results in redundancy. An example of a redundant two joint system is shown in Figure 2-9.

Mathematically, redundancy means that the available set of (in general six) equilibrium equations that can be written for a joint cannot be solved with a unique solution since the number of forces (variables) exceeds the number of equilibrium equations that can be written. In principle, an infinite number of solutions to these equations exist corresponding to an infinite number of combinations of forces in each of the load transmitting elements.

Further complications arise: muscles produce forces across joints by active contraction. As discussed by Thunnissen (1993), this force is dynamic and can vary with time, the length of the individual muscle and the muscle shortening velocity (i.e. a muscle is not a constant force actuator). In addition, antagonistic muscle activity is observed, in which both the muscle(s) which opposes a particular specified motion and the muscle(s) that produces it are active simultaneously. Muscles also frequently cross more than one joint (biarticular). Several techniques and combinations of techniques have been used to overcome these problems. Two general approaches have been used: (1) Reduction techniques, in which the number of variables is reduced so as to make exact solution of the equilibrium equations possible by making simplifying assumptions about the anatomy and function of the load transmitting elements. (2) Optimisation

techniques, where the full number of variables is included and the "best" of the possible solutions chosen by minimising some chosen performance criterion.

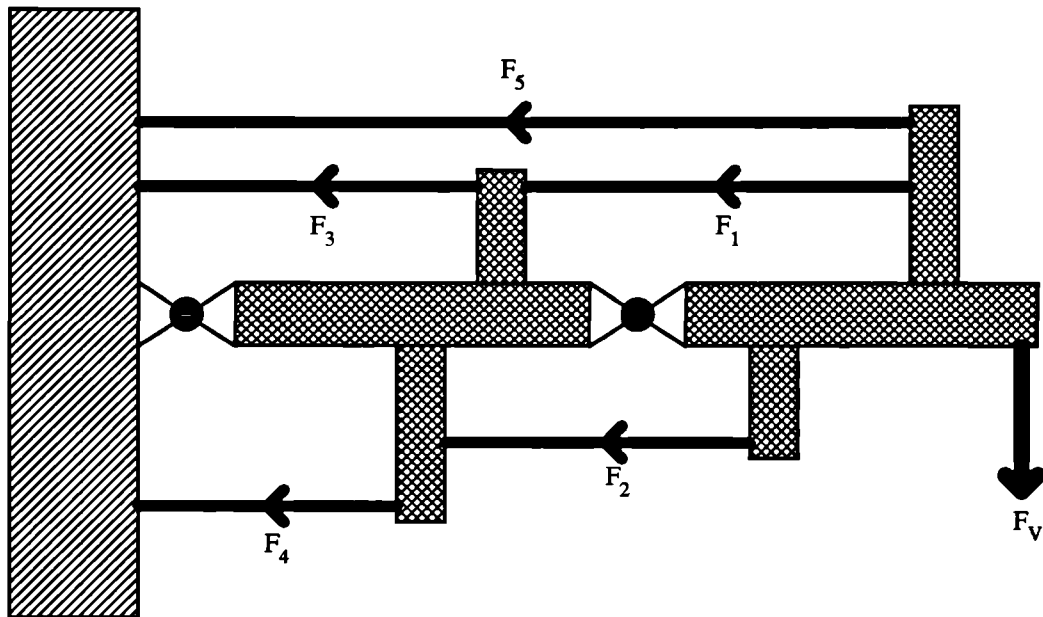


Figure 2-9: A simple mechanical model of a two joint system.
 F_V is the variable applied load. F_1 to F_4 represent monoarticular and F_5 a biarticular muscle.
 (Adapted from Thunnissen, 1993)

Probably the simplest analysis of hip joint biomechanics is presented by Charnley (1979), based on the early work of Pauwels. In this procedure the hip joint was analysed during one legged stance, considering only the moments about the hip joint, generated by the body weight acting through the centre of gravity and the abductor muscles (lumped into one equivalent abduction force). The force vectors were assumed to lie in the coronal plane passing through the centre of rotation of the hip joint. This situation was assumed to be representative of the slow walking of the elderly and/or infirm. By making these assumptions, the principal of moments of forces could then be applied to calculate the abductor muscle force and the triangle of forces to calculate the joint reaction force (Figure 2-10).

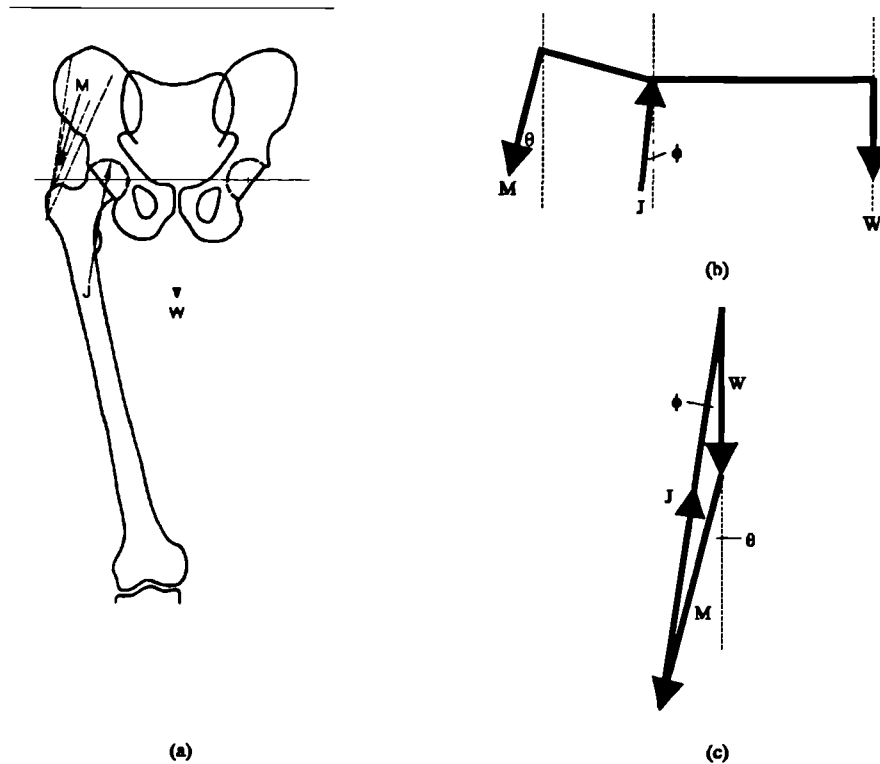


Figure 2-10: Charnley's analysis of the hip joint.

(a) Anatomical plane considered, (b) Moment equilibrium diagram, (c) Triangle of forces where M = muscle force, J = joint reaction force, W = body weight - weight of supporting leg

In their experimental study of one legged stance, McLeish and Charnley (1970) included the variation in the true position of the centre of gravity for various body attitudes in order to more accurately calculate the joint and muscle forces. A beam, simply supported on knife edges at one end and suspended by a load-indicating proving ring at the other, was used to identify the centre of gravity of a body whose weight was known. An X-ray was also taken, so the position of the centre of gravity could be related to the anatomy of the subject. Results when the pelvis was in slight elevation (considered the most relevant) were that muscle forces (normalised to body weight) varied from 1.0 to 1.8 and joint forces from 1.8 to 2.7 at 7° to 10° to the vertical. As the pelvis angle varied, the joint force varied from 1.2 to 1.8 at 2° for a more elevated pelvis (13° to 17° to the horizontal) and 2.9 to 3.1 at 15° to 20° for a sagging pelvis (-9° to -18° to the horizontal). As can be expected, considerable variation was seen between subjects since the pelvic rotation was not simply related to the positional shift of the centre of gravity. It was also noted that the shifts in pelvic angle produced a change in the angle of the femur to the vertical, resulting in greater variation of the direction of the joint force relative to the femur than its variation relative to the vertical. Due to their simplicity and relative ease of duplication *in vitro*, models of this

type have been used in the development of various tests for hips and hip prostheses, for example Tanner *et al.* (1988).

A more complex, pioneering, series of studies of various locomotor activities was presented by Paul and co-workers (summarised in Paul, 1976). An early form of modern gait analysis was used, in which ground reaction force, measured using a six degree-of-freedom force plate, was related to the positions of the lower limb by cinematic recording. The values of the force components at the hip were calculated from equilibrium equations, based on the forces and moments at the force plate and the accelerations of the components of the limb deduced by differentiation of the displacement of reference points with time (velocity) measured from the films. The reduction method, to make the equations exactly solvable, was then applied in the following way.

The friction at the joints was considered to be zero. This is reasonable in a healthy joint, given the extremely low coefficient of friction of the cartilaginous surfaces and short moment arm compared to most of the muscles. Only muscle groups whose action was likely to produce significant compression between the femur and acetabulum were considered. This led to elimination of the hip rotators (obturator internus and externus, gemellus superior and inferior, quadratus femoris and piriformis). The remaining muscles of the hip joint were grouped according to their action and anatomical positions into long flexors, short flexors, long extensors, short extensors, abductors and adductors, so that each muscle group could then be represented as a single "line of force". Representative muscles from each group were chosen for EMG measurements. Evidence from myographic studies was cited in order to justify elimination of antagonistic muscle action, so that the two flexor groups or the two extensor groups were considered active with either the abductors or adductors.

As a result, five equations (the sixth equation, for moments about the axis perpendicular to the ground, was excluded as the rotator muscles had been eliminated and it was not realistic to apportion rotation to other muscles) were formed with six unknowns (the three muscle group forces and the three components of the joint reaction force). The procedure then followed was to obtain solutions with first one flexor/extensor group and then the other and to assume that the true value of the calculated joint force components would lie between the two extremes.

The basic assumption of an optimisation technique is that the body selects the muscles to perform a particular action on the basis of some performance criterion, for example the minimisation of muscle stresses. Mathematically, the performance criteria are expressed as "cost functions" which are minimised. The advantage of this type of approach is that the relatively large anatomical and functional approximations and assumptions that need to be made in the reduction method can be avoided. The disadvantage is that the performance criteria do not have a well defined physiological basis and would be likely to vary according the activity being performed (e.g. walking or sprinting), so a complete description might require different performance criteria for different activities.

Crowninshield and Brand (1981) presented a model to predict muscle forces in the lower limb during locomotion, using a cost function based on a maximum endurance criterion that they suggested was applicable to prolonged and repetitive activities such as normal walking. The lower limb model incorporated 47 musculotendinous elements and five rigid bodies; hemi-pelvis, upper leg, lower leg, patella and foot. The hip joint was modelled with three components of intersegmental resultant moment, the knee with one component and the ankle with one component. Ligament function at the hip was assumed to be negligible, while at the knee and ankle was assumed to fully constrain varus/valgus and internal/external rotation. This effectively assumes that, during normal walking, the hip acts as a ball and socket joint and the knee and ankle as pure hinges.

The muscle forces during gait were predicted such that:-

$$\bar{M}_j^h = \sum_{i=1}^{31} \bar{r}_i^h \times \bar{f}_i \quad j = 1, 2, 3 \quad \text{Equation 2-9}$$

$$\bar{M}_3^k = \sum_{i=25}^{37} \bar{r}_i^k \times \bar{f}_i \quad \text{Equation 2-10}$$

$$\bar{M}_3^a = \sum_{i=36}^{47} \bar{r}_i^a \times \bar{f}_i \quad \text{Equation 2-11}$$

where superscripts *h*, *k* and *a* refer to the hip, knee and ankle respectively, *M* = intersegmental resultant moment, *r* = length of moment arm of muscle and *f* is the muscle force.

Simultaneously the cost function, Equation 2-12, was minimised.

$$u = \sum_{i=1}^{47} (f_i / A_i)^3 \quad \text{Equation 2-12}$$

where A_i is the cross sectional area of the muscle. The minimisation of the cost function represents maximising endurance by minimising muscle stress. The required joint moments of force M were obtained from gait kinetics.

Thunnissen (1993) presented a complete three dimensional model of the lower body, incorporating seven rigid bodies, the pelvis, left and right thighs, left and right lower legs and left and right feet. The hip, knee and ankle joints were all modelled as ball and socket joints. The principle feature of this model was a mathematically sophisticated treatment of muscle action. However, the forces predicted were significantly higher than the results of other authors, including those where direct measurements were taken (Bergmann *et al.*, 1993). The author suggested that the sophistication of the model made the muscle force predictions very dependent on the choice of certain parameters, such as the physiological cross section and force-length relationship of the muscles, which were not known with sufficient accuracy.

Probably the definitive measurements of hip joint force are those of Rydell (1966), Davy *et al.* (1988) and Bergmann *et al.* (1993), who derived their data from instrumented femoral prostheses. Rydell used two comparatively young patients and found forces varying from 1.59 to 3.3 times body weight in the stance phase of walking. There was a marked difference in maximum forces between the two patients. The measured hip joint resultant force from the study of Bergmann *et al.* for an active, healthy 82 year old male patient walking on a treadmill at 4 km h⁻¹ are reproduced in Figure 2-11.

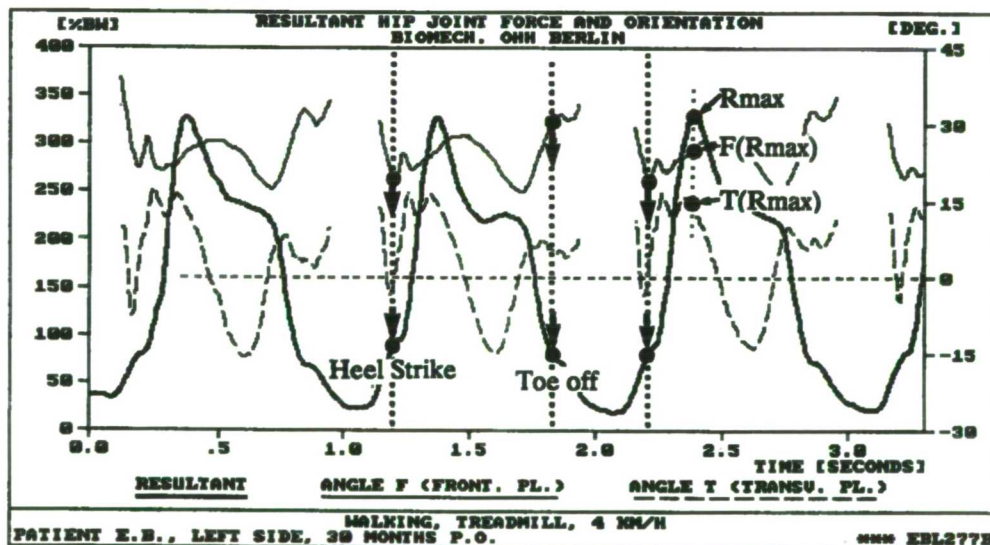
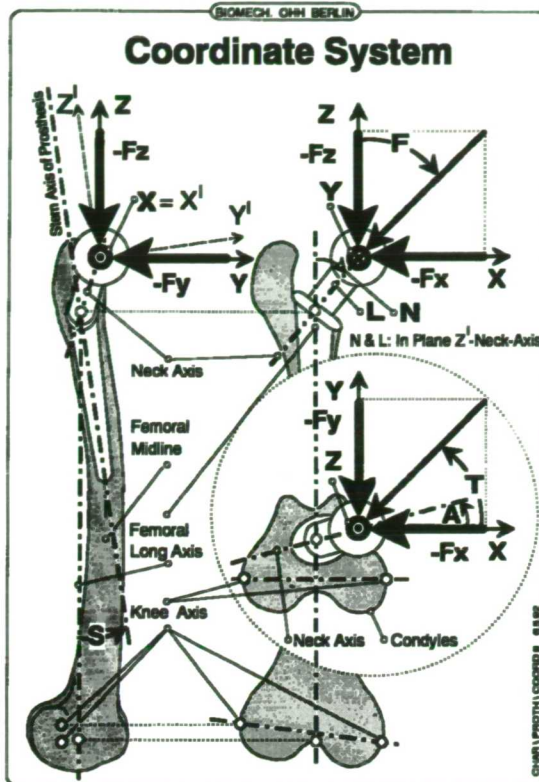


Figure 2-11: Magnitude and direction of the hip joint resultant force. (Bergmann *et al.*, 1993)

Some differences were noted between the measured joint forces and those that had been previously calculated (see above). In particular the second peak at toe-off was less pronounced in the measured data than that predicted by analytical models.

The peak hip joint force varied with speed of walking in an approximately linear manner, increasing from three times body weight at 1 km h⁻¹ to five times body weight at 8 km h⁻¹. Jogging at low speed increased the peak force by 15 to 30 % over walking

at the same speed. However, as the speed increased, the peak forces for walking and jogging appeared to converge. The highest forces measured were those that occurred when the patients stumbled, reaching almost nine times body weight. Figure 2-12 shows a comparison of the hip joint resultant forces predicted by Paul, Crowninshield and Brand and Thunnissen, compared with the measurements of Bergmann *et al.*

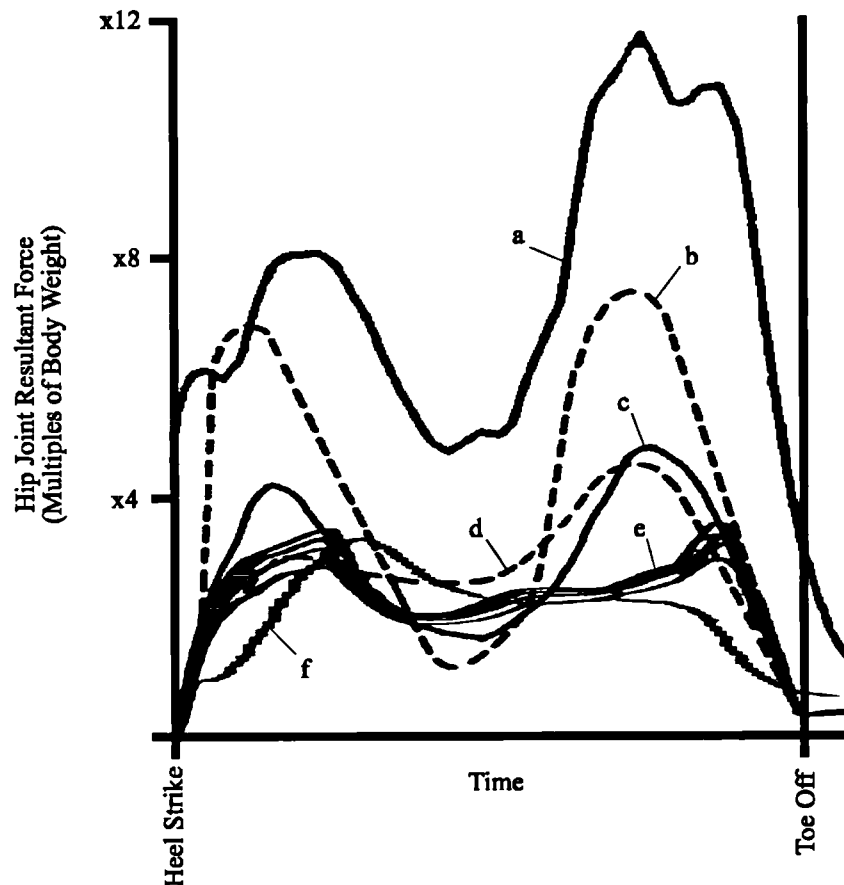


Figure 2-12: Magnitude of the hip joint resultant force from different authors.

Thunnissen (1993)

(a) prediction for walking @ 1.4 m s^{-1}

Paul (1976)

(b) prediction for walking @ 2.01 m s^{-1}

(c) prediction for walking @ 1.48 m s^{-1}

(d) prediction for walking @ 1.10 m s^{-1}

Crowninshield and Brand (1981)

(e) prediction for walking (based on a maximum endurance optimisation criterion)

Bergmann (1993)

(f) measured for walking @ 1.11 m s^{-1} (as Figure 2-11)

Bergmann quoted analytical models as showing "a more pronounced speed dependent increase in the peak forces than was measured." In Bergmann's results, the peak hip joint resultant force increased to approximately 4.5x body weight at a walking speed of 1.67 m s^{-1} (6 km h^{-1}). This may be a consequence of the rigid body assumption used in these models and suggested that impact forces at heel strike were damped by the structures of the lower leg before they reach the hip joint.

2.1.4 Stresses in the Normal and Reconstructed Hip

The hip joint forces are reacted by the pelvis. After joint replacement the stresses in the bone when compared to the non-implanted case give indications of the likely host response to the implant in relation to theories of adaptive bone remodelling and interface breakdown. Stresses in the implant and cement are important as, unlike bone, they have no capacity for self repair and hence are susceptible to fatigue failure. Similarly interface stresses between the prosthesis and bone are also important.

The stresses and strains in the pelvis generated by muscle and joint force loading have been studied using several techniques. These include strain gauging, photoelastic coating and interferometric studies of cadaveric pelvises, model studies and finite element analyses. Each method has associated advantages and disadvantages and all the techniques require some approximations to be made. However, they all share the requirements for the application of realistic boundary conditions and forces. A significant advantage of F.E. models is that they analyse the whole volumetric field. This is in contrast to strain gauge, photoelastic coating and interferometric studies which are essentially surface techniques. A disadvantage is that because F.E. models are very often simplified to accommodate restrictions in computing power, results can easily become unrepresentative. In the femur, geometrically simplified models have been applied to good effect, since the femur possesses an inherent symmetry and the normal loads are applied approximately parallel to its axis of symmetry. Simple 2D models can describe the femur reasonably well. The pelvis, however is a 3D structure with a low degree of symmetry. This means that 3D models are essential for accurate analyses. As compared to 3D models, 2D models of the pelvic bone tend to underestimate the structural stiffness of the acetabulum, since they cannot account for the out-of-plane components of the acetabular wall, and overestimate bone stresses (Huiskes, 1987). Axisymmetric models are restricted to representing the region close to the acetabulum and assume a complete acetabular rim, which tends to overestimate the structural stiffness of the acetabulum (Dalstra, 1993).

Probably the most detailed analysis of the pelvis to date is that of Dalstra (1993) who used a full three dimensional finite element analysis of the pelvis incorporating multiple muscle forces and realistic geometry and mechanical properties for the pelvic bone obtained from CT data.

Jacob *et al.* (1976) investigated the mechanical function of subchondral bone in an epoxy "sandwich" model ($E_{\text{subchondral bone}} = 7.9\text{-}11.8$ GPa, $E_{\text{cancellous bone}} = 0.8$ GPa). They conclude that the horseshoe of subchondral bone in the acetabulum transmits most of the load as membrane stresses from the point of load application to the acetabular rim and then into the cortical shell. Thus they suggest the cancellous bone is relatively lightly stressed in the physiological condition (compared with the FE results of Dalstra.)

Ries *et al.* (1989) performed a strain gauge study of intact human pelvis, loaded with a "joint reaction force" and an abductor muscle force to simulate single leg stance. The pattern showed vertical and lateral tensile stresses in the medial wall of the acetabulum, with the ilium in compression. Using a two dimensional contact finite element model, Rappoport *et al.* (1985) found high compression in the iliac and pubic regions of the acetabulum as it "squeezed" the femoral head.

Recently, concerns have been raised about the accuracy of the McLeish and Charnley single leg stance models which show high bending in the medio-lateral plane at the femoral diaphysis. These concerns are based on Wolff's law type considerations which might be expected to produce an oval cross section with the major axis aligned with the plane of bending whereas the cross section in reality is close to circular. The explanation offered is that muscles can act to apply compensatory bending moments. Recent finite element models that include the ilio-tibial tract (Taylor *et al.*, 1994) can be made to predict much less bending in the femur than those which do not. Concerns like this may be applicable to the pelvis.

Massin *et al.* (1993) used a more elaborate set-up, using cadaveric bones (Figure 2-13). Particular attention was paid to deformations in the region of the acetabulum. The model included representations of the gluteal muscles, iliopsoas, rectus abdominis and posterior lumbar muscles.

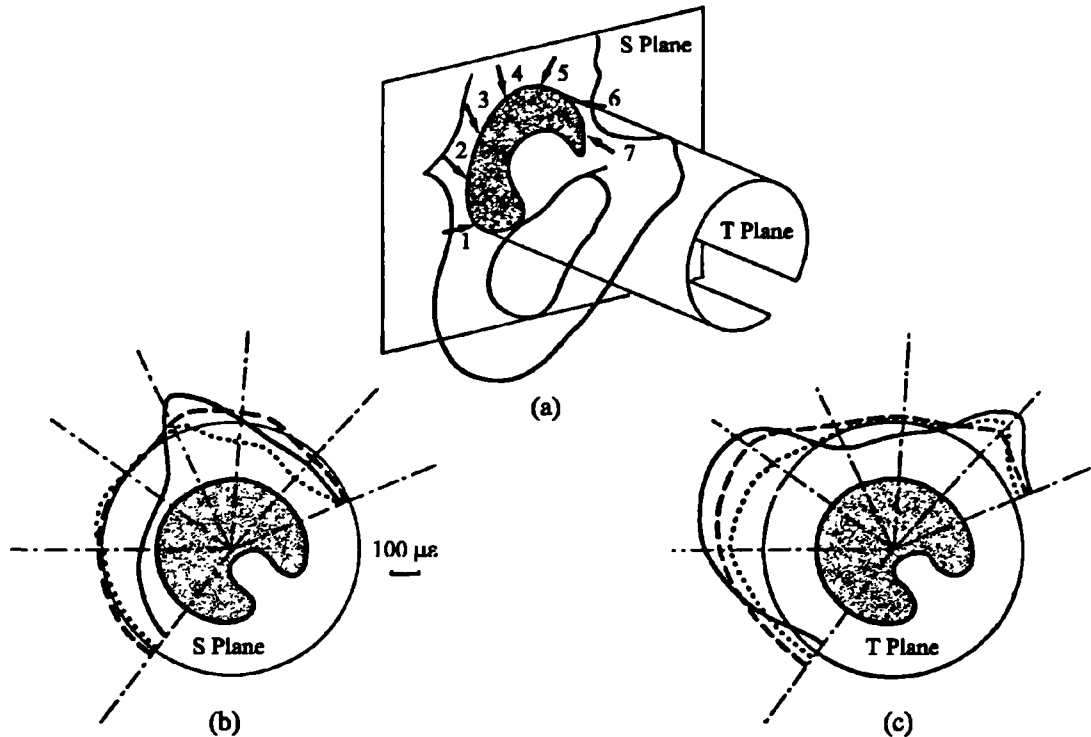


Figure 2-13: Deformation during *in vitro* loading of the acetabulum.
(Massin *et al.*, 1993)

Circles drawn around the acetabulum represent zero strain. Strains inside the circle are compressive, outside tensile. (b) shows tangential and (c) normal strain for
 — neutral, - - - - lateral and ····· medial rotation of the femur.

Yoshioka and Shiba (1981) used a stress freezing technique on 3D photoelastic models (epoxy resin) of the pelvis. They included four muscle forces (abductor, adductor, rectus femoris, gluteus maximus) and body weight. Slices cut from the model contained the "frozen-in" stresses. Conclusions were that the "horseshoe" is deformed so as to "close the beak" of the acetabulum, with the acetabulum stretched vertically and deformed into an oval shape.

2.1.4.1 Stresses in the Implanted Pelvis

Petty *et al.* (1980) performed experiments to determine the effects of details of socket implantation technique (depth of reaming, use of pilot hole, use of anchoring hole, methods of reinforcing weakened acetabula) on cadaveric hemi-pelves, instrumented with strain gauges on the medial acetabular wall, in simulated single leg stance. The normal pattern was established by applying the hip joint load with an Austin-Moore type prosthesis (diameter approximately equal to the femoral head). The strain pattern in the medial wall was hardly altered by the introduction of a prosthesis where the acetabular subchondral bone was preserved. This suggests that subchondral plate disruption is an important factor.

Selected results from Dalstra's finite element model are shown in Figure 2-14.

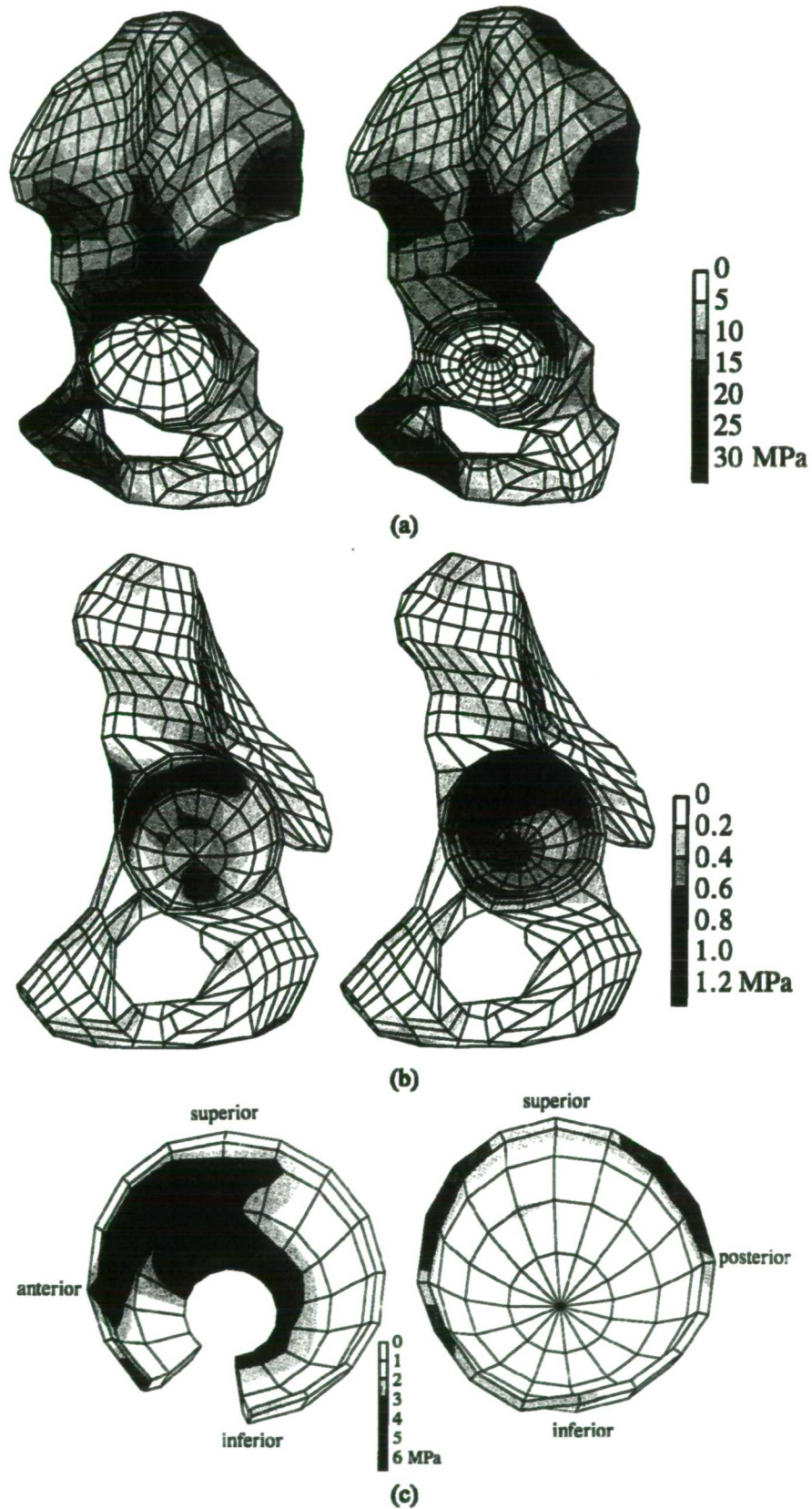


Figure 2-14: Finite element predictions of von Mises stress in the pelvis. Stresses in (a) the cortical shell, (b) the cancellous bone and (c) subchondral bone layer for a normal pelvic bone (left) and a pelvis implanted with a cemented PE cup (right), loaded in simulated one legged stance (Dalstra, 1993).

Dalstra found that load transfer into the acetabulum takes place in the antero-superior quadrant of the acetabulum with the principal stress transfer into the cortical shell directed at the sacroiliac joint along the superior acetabular rim, with a smaller portion towards the pubic symphysis. After reconstruction with a cemented polyethylene cup, the overall load transfer hardly changes. The largest differences are restricted to the immediate vicinity of the acetabulum, as might be expected in accordance with St Venant's principle. For the subchondral bone and trabecular bone in the acetabular region the changes are more substantial. In the intact case, the highest stresses are in the subchondral bone of the antero-superior quadrant. In the reconstructed case the loads are reduced considerably and are shifted towards the edges (in particular the posterior edge) with the deeper areas of the acetabulum becoming stress shielded. This suggests that fixation of acetabular components is critical around the rim. In the underlying trabecular bone, the situation is approximately reversed, with the trabecular bone stresses in the superior wall highest.

2.1.4.2 Factors Affecting the Mechanics of a Total Hip Replacement

Several finite element and experimental studies have looked at the effects of specific details of the prosthesis and surgical technique on the acetabulum, although few FE models have made use of 3D models because of the practical difficulties involved. Cup thickness and the diameter of the "femoral head" were shown by Charnley to be important. In a photoelastic model, for a given external diameter, a thick cup (small head) produced a much more uniform stress distribution and lower stresses in the surrounding acetabular bone (Charnley, 1979). This finding was confirmed by Dalstra (1993) who showed that increasing the polyethylene cup thickness reduced peak stresses in all surrounding materials (bone, polyethylene, bone cement). Oh (1983) looked at the effect of cement thickness and concentricity of cup placement on cement strains in a strain gauge model. All measured strains were less than 10% of the failure strain of the cement, even at applied loads of four times body weight. This result seems to match the clinical observation that full thickness fatigue cracks in the acetabular cement mantle are rarely found even at late revision (Richardson, 1995). Metal backed polyethylene acetabular cups were originally introduced to facilitate exchange of the polyethylene liner. Some finite element studies that used simplified plane 2D and

axisymmetric models also predicted that load would be more uniformly transferred with a metal backing. However, this type of cup has a much lower success rate than the conventional all polyethylene cemented cup (Ritter *et al.*, 1990). More sophisticated finite element studies reveal that metal backing causes fairly severe stress concentrations at the acetabular rim. The stresses at the implant-bone interface in these regions of stress concentration are three to four times higher for metal backed cups than non-backed cups (Dalstra, 1993).

The subchondral bone plate plays a vital role in transferring load to the cortical shell. Removal of this plate by aggressive reaming means load is transferred to the weak cancellous bone and the sandwich design of the pelvis compromised (Jacob *et al.*, 1976). Some studies have considered the effects of drilling anchoring holes through the subchondral plate. In an early study of the torsional strength of acetabular reconstruction Andersson *et al.* (1972) concluded that reaming the subchondral plate to produce an irregular surface played the major role, with drill holes being less significant and suffering the disadvantage of increasing the disruption to the acetabulum. In another experiment (Oh, 1983) using wooden blocks as model acetabula in which only the simulated anchoring holes contributed to torsional strength, the failure torque was 84-157 Nm, very comparable to the results of Andersson *et al.*

2.2 Hip Replacement

2.2.1 Reasons for Hip Replacement

Joint replacement is performed to relieve pain and/or reduced mobility at an affected joint. A variety of clinical conditions can lead to these problems, the most important being osteoarthritis, rheumatoid arthritis, trauma, avascular necrosis and ankylosing spondylitis.

2.2.1.1 Osteoarthritis

The most common reason for joint replacement is osteoarthritis. Osteoarthritis refers to any degenerative changes to a joint leading to pain, inflammation and loss of function. The terms osteoarthritis and osteoarthrosis are commonly interchanged, but osteoarthrosis is probably a better term for primary idiopathic osteoarthritis (Figure 2-15) as it implies "degeneration" rather than "inflammation". It has been estimated that 52% of the adult population of the U.K. have some form of osteoarthritis in one or more joints, with the frequency of incidence increasing with age. Prevalence in men and women is similar, but women tend to have more joints affected (Lawrence, 1977). Pathologically and radiologically, typical features of osteoarthritis are destruction of articular cartilage and reduction of joint space, osteosclerosis (an increase in bone density), osteophytosis (production of abnormal bony masses) and formation of fluid filled cysts.

Many possible biochemical and mechanical causes have been identified, but a general classification into primary and secondary osteoarthritis can be made (Figure 2-15). In secondary osteoarthritis, an identifiable cause of the disease can be established, whereas primary osteoarthritis does not have an easily determined aetiology and thus is described as idiopathic.

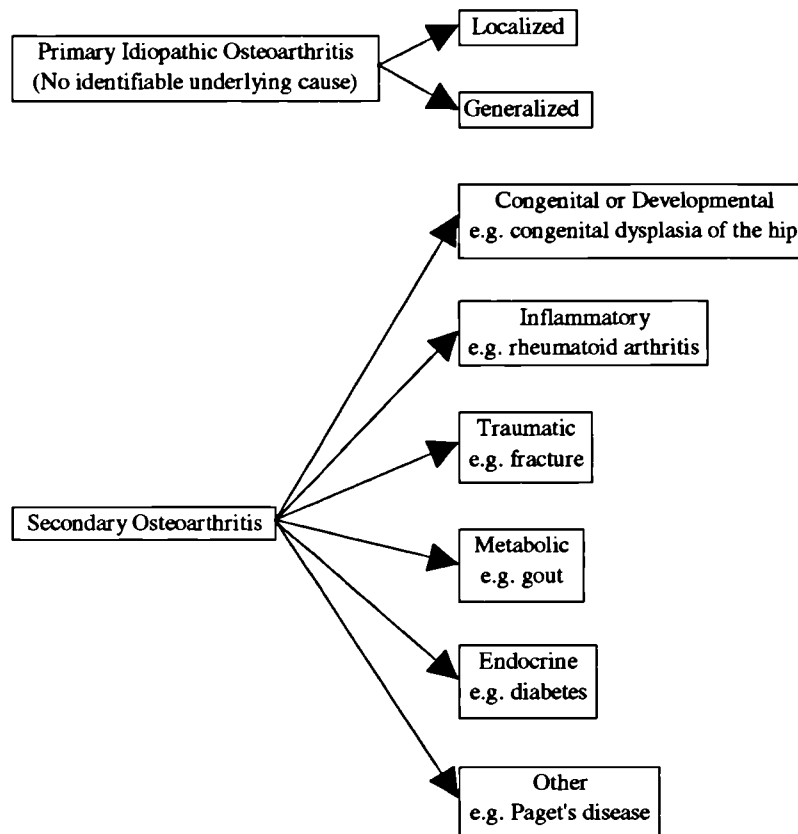


Figure 2-15: Classification of osteoarthritis.
(adapted from Grennan, 1984)

2.2.1.2 Rheumatoid Arthritis

Rheumatoid arthritis is an inflammatory disorder involving a complex immunological reaction centred on the synovial membrane to a, currently unknown, stimulus. The immunological reaction culminates in release of enzymes that can destroy cartilage and ultimately bone adjacent to the affected joint. The disease affects about 5% of women and 2% of men in the U.K., with onset commonly in the middle years. However, less than 25% of these will go on to develop severe symptoms and loss of function (Lawrence, 1977). The disease eventually "burns out", but after several months or years and often leaving permanent damage (secondary osteoarthritis). Juvenile rheumatoid arthritis or Still's disease affects children and teenagers, but in all but a very few patients resolves with no permanent damage.

A comparison of the typical destructive effects of rheumatoid arthritis and osteoarthritis is shown in Figure 2-16.

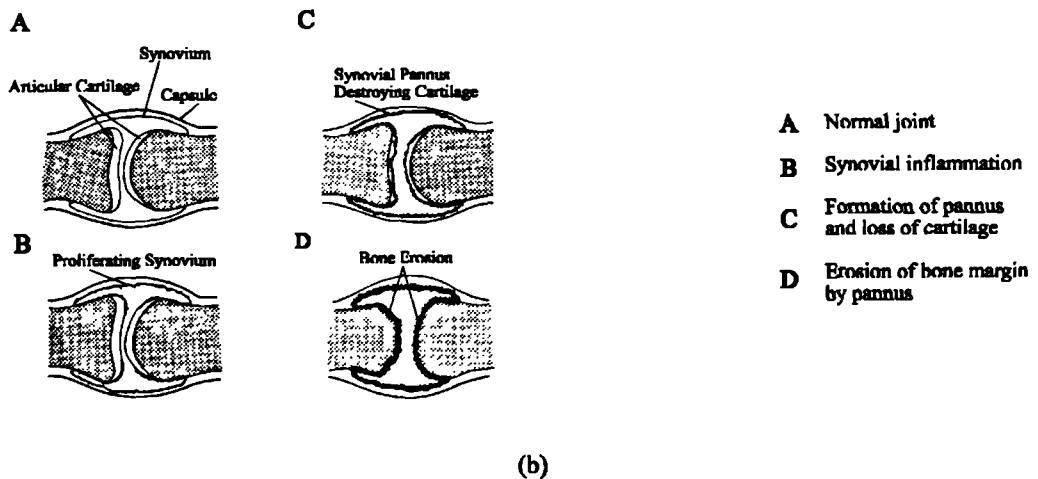
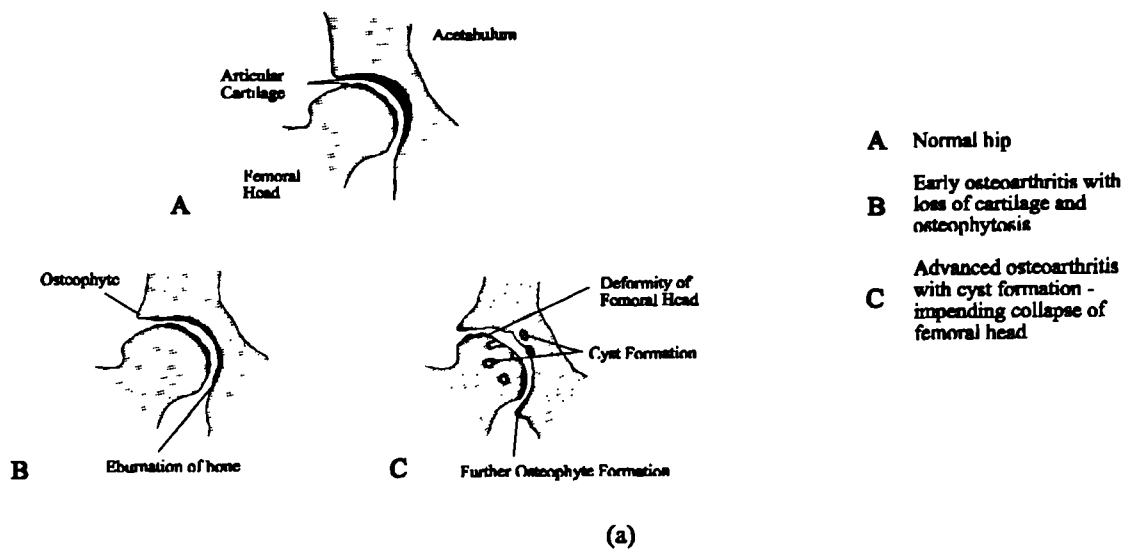


Figure 2-16: Comparison of the effects of arthritic disorders.
 (a) Osteoarthritis and (b) rheumatoid arthritis.
 (Adapted from Grennan, 1984)

2.2.1.3 Avascular Necrosis

Avascular necrosis is the deprivation of the blood supply to an area of bone, leading to collapse of the bone, commonly the femoral head. This may be due to traumatic damage to blood vessels, or precipitated by treatment with steroid drugs or by alcohol abuse.

2.2.1.4 Ankylosing Spondylitis

Ankylosing spondylitis is another inflammatory disorder, involving inflammation of the synovial membrane and the bone entheses (regions where ligaments and joint capsules

are attached to bones). In severe cases of the disease, calcification and ossification of the entheses can occur leading to loss of range of motion, sometimes complete. The principal affected joints are the sacro-iliac joints and those of the lumbar spine, often with the involvement of the hip and knee joints. Incidence of the disease with clinical significance are approximately 0.5% in men and 0.05% in women, with onset in the late teens and early twenties (Lawrence, 1977). Hip joint surgery is the most common orthopaedic procedure performed in severe cases of ankylosing spondylitis.

2.2.1.5 Mechanical Derangement of the Joint

Where the mechanics of the joint are altered secondary osteoarthritis can occur. This will typically be the result of intra-articular fractures, where part of the joint surface is displaced, after congenital dislocation or dysplasia of the hip, or childhood problems such as slipped upper femoral epiphysis and joint sepsis.

2.2.2 Surgical Treatment

Surgery for the above problems, when they affect the hip, usually follows attempts at a more conservative approach, e.g. physiotherapy, drug treatment etc. The principal procedures are (Northmore-Ball, 1992):

1. Osteotomy, where the shape of the femur or pelvis is altered to produce a desired effect by dividing and re-fixing the bone. The desired effect may be alteration in the mechanics of the joint, realignment of the joint surfaces etc.
2. Arthrodesis, where bony fusion of the joint is induced by excising the joint surfaces and fixing as a fracture.
3. Excision arthroplasty, where the bone ends with joint surfaces are removed, in the hope that a fibrous tissue bridge will form a "pseudo-joint" (Girdlestone arthroplasty).
4. Total hip arthroplasty, where the malfunctioning joint is completely replaced by an artificial implant.

The last has to a great extent superseded the others, except in cases where the known shortcomings of total hip replacement are currently unacceptable, such as very young

patients or where there is infection of the joint and even in these cases has become widely used. In some cases total hip arthroplasty is performed as a conversion procedure, for example to restore a greater degree of function than a previous operation allowed.

2.3 Design of Hip Replacements

A plethora of hip prostheses is available to replace the defective hip joint, although nearly all are based on a ball-on-stem for the femoral component and a cup for the acetabular component. One of the major reasons for all these designs is commercial pressure, but also reflected are the difficulties in evaluating the efficacy of a particular design using *in vitro* methods, or short term clinical trials. Short term clinical studies do not reliably predict long term performance of implants (Fowler *et al.*, 1988; Harris, 1992b). Long term studies establishing the success of an implant are only available for relatively few cases (e.g. the Charnley-type prosthesis, Schulte *et al.*, 1993). Due to the multitude of prostheses, classification has been attempted on the basis of major design principles, the most obvious of which is method of fixation (Figure 2-17).

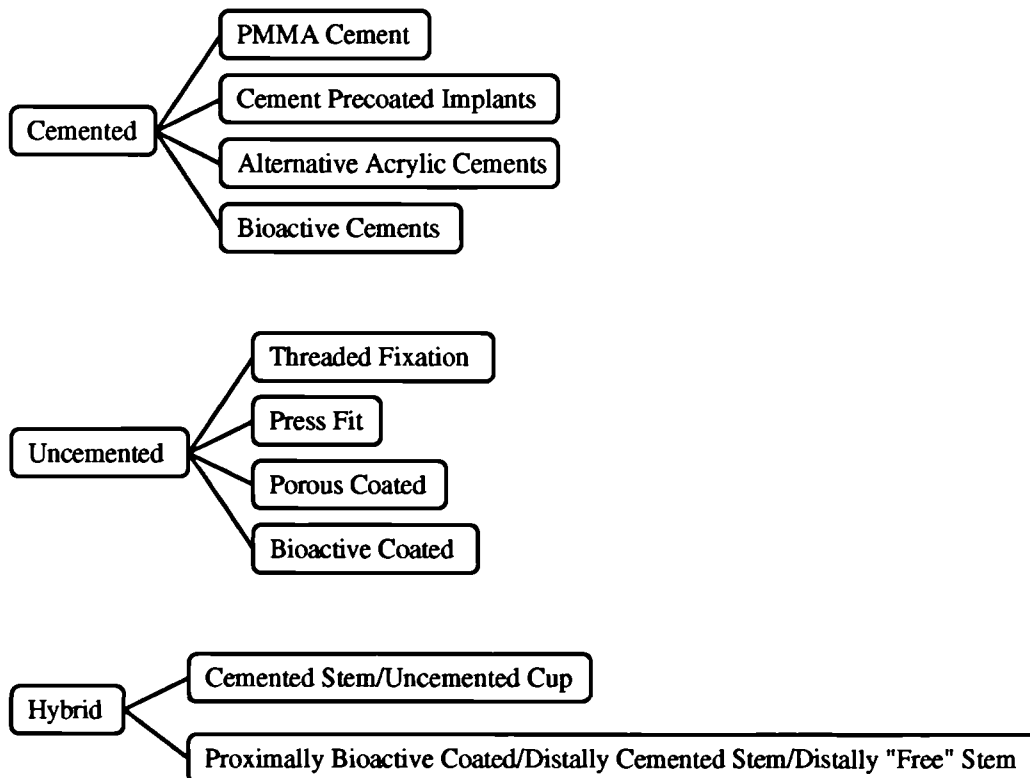


Figure 2-17: Classification of hip prostheses on the basis of fixation method.

The common aim of all fixation methods is to produce a strong, durable interface between the implant and bone. The loads transmitted across the bearing surfaces of the joint prosthesis are transmitted into the natural bone via the interface, which must be capable of performing this task for the maximum possible time, ideally the life of the patient. The integrity of the interface is under threat from both biological and mechanical processes, although it is difficult to make a true distinction between these. Aseptic loosening and its consequences, identified as the single most important cause of long term failure of hip replacements, is due to the breakdown of the original implant-bone interface and its replacement with a thick membrane of connective tissue. The mechanisms that have been proposed to lead to interface breakdown and aseptic loosening are discussed later.

2.3.1 Cemented Implants

Most hip prostheses are still fixed to the skeleton using polymethylmethacrylate (PMMA) cement. The original reason for using cement was as a grout to fill the irregular gap between the bone and the prosthesis and thus obtain a more uniform load transfer. Being of a low modulus (c. 3 GPa), the cement also functions as a compliant de-coupling layer between stiff (metallic) implants and bone.

PMMA itself has poor adhesive properties and relies for fixation almost entirely on the mechanical interlock that can be achieved with the porous cancellous bone and suitably prepared cortical bone and the geometric features of the prosthesis. For this reason it is essential to ensure intimate contact between both the cement and bone and the cement and implant over the maximum possible areas. Intimate bone contact effectively means intrusion of cement into the cancellous pore spaces or irregularities in cortical surfaces. Cement intrusion into cancellous bone results in a transition region of a bone-cement composite, rather than a flat interface between homogeneous cement on one side and bone on the other. The true bone-cement interface is only revealed on a finer scale, between individual trabeculae and cement.

In the initial period after implantation, if cement intrusion into a cancellous bone bed has been achieved, failure of the fixation occurs by failure of bone trabeculae. In the long term, the precise cause of fixation failure leading to aseptic loosening is not absolutely clear, although several theories exist.

Current cementing techniques seek to achieve mechanical interlock by careful preparation of the bone bed and pressurisation of cement.

2.3.2 Uncemented Implants

It has been theorised that the long term stability of an uncemented prosthesis depends on both the initial stability of the implant and the biological response of the host. Initially, all uncemented implants rely on a purely mechanical fixation to the bone. For the development of secondary, long term, stability uncemented implants rely on a favourable host bone response, the conditions for which must be achieved by the initial fixation. In general this will require some growth response and gap bridging by the bone, since with current surgical techniques, it is impossible to ensure perfect contact between bone and implant over the whole of the implant. The design features of uncemented implants can thus be classified into those designed to enhance primary stability and those designed to promote the required bone response, which take the form of various surface modifications and coatings. There seems to be a consensus that enhancement of osseointegration into uncemented prostheses is dependent on development of improved coating materials and techniques for their application, since recent studies evaluating osseointegration with uncemented implants have revealed bony apposition over only a small fraction of the coated area (Pereira *et al.*, 1995). The two most important classes of surface treatment are porous metal coatings and bioactive ceramics.

2.3.2.1 Primary Fixation

To provide the necessary primary stability, several techniques have been applied, including additional screws, pegs and interference fit (press fit). Threaded fixation produces initial stability by the mechanical interference between the screw thread and bone. The thread may be an integral part of the prosthesis or separate fixation screws. Threaded fasteners serve to "pre-stress" the bone and to provide resistance to shear forces at the prosthesis-bone interface. Pegs on acetabular components, such as found on the Freeman acetabular component, essentially provide similar resistance to shearing forces but do not pre-stress the bone.

Press fit prostheses rely for their stability on frictional forces developed at the interface between implant and bone and on the natural shape of the bone. The press fit was the original method of fixing implants to bone. Modern designs typically feature large stiff, space filling intramedullary stems in an effort to improve contact area.

Press fit insertion of oversized cups in the acetabulum has been used to obtain the initial stability needed for bony ingrowth (Kim *et al.*, 1995). However, press fitting has disadvantages. In the acetabulum, while equatorial press fit can be achieved, polar contact is often compromised, with gaps of greater than that thought to be the maximum for bone bridging (McKenzie *et al.*, 1994), even with impaction forces of 2 kN. Vigorously inserted oversized press fit cups can also cause acetabular fractures (Kim *et al.*, 1995).

2.3.2.2 Porous Coatings

Porous coatings on prostheses are meant to encourage bone ingrowth. Commonly they are produced by coating the prostheses with beads or mesh, usually titanium on a Ti-6Al-4V alloy base. The optimum pore size (in dogs) is 50 to 400 μm (Bobyne *et al.*, 1980). Retrieval studies have displayed ingrowth into the porous coating between 0 and 50-60 percent (Sumner *et al.*, 1993). Proposed reasons for failure of porous coated implants are:

- Bony ingrowth never achieved because of excessive micromotion. The bone adaptation to porous coated implants is thought to occur in two distinct phases (Galante, 1985), the first phase similar to primary fracture healing and the second involving remodelling of the primary tissue in response to mechanical stimuli. The first phase healing response appears to have a much greater influence on bone adaptation to porous coated implants than mechanical stimuli (Hollister *et al.*, 1995). Excessive micromotion at the interface leads to development of a fibrous tissue interface instead of bone ingrowth (Søballe *et al.*, 1992, section 2.4.1.1), so initially a stable press-fit or some means of supplementary fixation is required.
- ingrowth is achieved but not maintained
- coating problems such as fatigue failures of the coating/implant interface due to the difficulty of welding the dissimilar alloys of the coating and substrate and at the joints between beads and between the mesh wires.

2.3.2.3 Bioactive Coatings

The mineral component of bone is a hydrated calcium phosphate, hydroxyapatite ($\text{Ca}_{10}(\text{PO}_4)_6(\text{OH})_2$) with some carbonate substitutions. Animal studies have shown direct bone bonding to hydroxyapatite coated implants and thus clinical trials of HA coated prostheses in humans have been undertaken (Geesink *et al.*, 1987).

A direct chemical bond is formed between bone and a wide variety of calcium phosphate substances, as has been seen by electron microscopy (Luklinska and Bonfield, 1992) and mechanical testing (Geesink *et al.*, 1987). Additionally hydroxyapatite coatings encourage bone growth into features of the implant thus enabling a mechanical bond on the macroscopic scale as well as a chemical bond on the microscopic scale (Stephenson *et al.*, 1991). It has been found however that failure of the interface between implant and HA coating can occur (Cook *et al.*, 1991). The composition and structure (crystallinity and porosity) of the coating is important. Bauer *et al.* (1995) have shown that mixed HA/TCP (tri-calcium phosphate) coatings of various compositions were all osteoconductive, but coatings with TCP were less stable (greater reduction in coating thickness, more coating debris particles, less coating remaining). This was attributed to the different solubility characteristics under physiological conditions. The degree of coating stability required for optimal bone apposition and implant fixation is controversial and some authors suggest that coating dissolution is required for bioactivity. Also of concern is the rate of coating resorption with regard to mechanical loading. Overgaard *et al.* (1995) implanted plasma sprayed HA coated implants in dogs. Continuous loading resulted in significantly more resorption of the HA coating than in unloaded implants.

2.3.3 Materials for Total Hip Replacement

The most commonly used materials in hip replacements are the austenitic stainless steels, cobalt based and titanium based alloys, ultra high molecular weight polyethylene and, to a lesser extent, the engineering ceramics alumina and zirconia (for femoral heads and occasionally acetabular cups). The mechanical properties of implant materials (Table 2-5) are dependent on composition, processing route and, particularly for metallic implants, the shaping process used to form the final implant.

Table 2-5: The mechanical properties of some materials used in hip joint prostheses

Material	Composition	Young's modulus (GPa)	0.2% offset yield stress (MPa)	Ultimate strength (MPa)	Ultimate strain (%)	Fatigue strength (MPa)
ASTM F55/F138 (equivalent to AISI 316L) Stainless Steel	Fe Cr 17-20, Ni 13-16, Mo 2.25-3.5, Mn <2 C, Cu, P, Si, S	193	170 a 250 hf 310 cw 1200 cf	480 a 550 hf 655 cw 1300 cf	40 a 55 hf 28 cw 12 cf	240 a 310 cw
Ortron 90 (Trade name) Stainless Steel	Fe Cr 21.5, Ni 9, Mo 2.6, Mn 4, N 0.39, Nb 0.3 C, P, Si, S		479 a 928 cw	834 a 1035 cw	72 a 64 cw	459 a 640 cw
ASTM F75 Co-Cr-Mo	Co Cr 27-30, Mo 5-7 Mn, Si, Ni, Fe, C	195	450 ac 890 f	655 ac 1400 f	8 ac 28 f	310 ac 793 f
ASTM F90 Co-Cr	Co Cr 19-21, W 14-16, Ni 9-11 Fe, Mn, Si, C	210	310 a	860 a	30 a	485 f 825 pm, f
ASTM F67 C.P. titanium	Ti >99 Fe, O, C, N, H	100	485 af	550 af	15 af	240 af
ASTM F136 Ti-6Al-4V	Ti Al 5.5-6.5, V 3.5-4.5, Fe, O, C, N, H	105	795 a	860 af	10 af	520 f, a
UHMWPE (M. wt. 2x10 ⁶)		0.94-1.05	21-28	39	420-525	

a = annealed, hf = hot forged, cw = cold worked, cf = cold forged, ac = as cast, f = forged, af = as fabricated

2.3.4 Bone Cement

2.3.4.1 Polymethylmethacrylate Cement

PMMA bone cement is produced *in situ* by mixing together a liquid component, methyl methacrylate monomer with an activator, and a solid powder, polymethylmethacrylate with an initiator/catalyst. When the liquid and powder components are mixed, the activator reacts with the initiator to produce free-radicals, which initiate a free-radical addition polymerisation reaction. As the reaction proceeds, portions of the polymer chains at the surface of the powder particles become intermingled with and incorporated in the newly forming polymer chains in the liquid. Eventually, as the reaction completes, the mixture becomes a single solid mass. The mechanical properties of the cured cement are sensitive to such factors as preparation and testing method, preparation and testing temperature and conditions and method of specimen preparation. Thus it is essential for experimental results to include these conditions along with the mechanical data. If data are to be used for design or engineering analysis of prostheses, especially the results of extended tests, they need to be collected under conditions as close as possible to those experienced *in vivo*. If comparative data is all that is required, this necessity can be relaxed for convenience, providing a reasonably representative test is chosen.

PMMA cement is a brittle material with a low fracture toughness and hence its ultimate properties are controlled by the number, size and distribution of internal flaws, such as pores and second phase particles, which can serve as stress raisers and crack initiators. In general, pores are worse than second phase particles, especially in compression (Gordon, 1976). The mechanical properties and fracture behaviour of bone cement samples thus vary principally according to additives, mixing and handling techniques and are relatively insensitive to the variation in intrinsic mechanical properties that can be produced by differences due to polymer manufacture such as molecular weight variations. Modern mixing techniques such as vacuum mixing seek to reduce the porosity in cement introduced by hand mixing in air. The effects of preparation techniques on porosity have been assessed by Schreurs *et al.* (1988), who compared hand mixing, use of a pressurisation pistol, centrifugation and vacuum mixing. They showed that vacuum mixing is much the most efficient in

reducing the overall porosity, but the average pore size was not greatly affected by any of the methods. Askew *et al.* (1990) reported that vacuum mixing significantly increased bending strength and modulus for specimens conditioned in water at 37°C. However, this effect was cancelled by the addition of antibiotics, which reduced the bending strength and modulus of vacuum mixed specimens to that of air mixed specimens. This was probably due to the antibiotic particle inclusions and the additional porosity generated when the antibiotic leached out as the samples were conditioned. It is also possible, depending on the "mould" environment of the cement, that monomer boiling occurs during cementation of the implant (Huiskes, 1980) which could produce additional porosity. Gardner *et al.* (1992) studied the effects of incorporation of fluids into cement during implantation by measuring the compressive Young's modulus and yield stress of cylindrical specimens. The specimens were produced by hand mixing the cement with small quantities of blood, marrow fat, saline solution and hydrogen peroxide solution, the last two being common lavage fluids. It was found that all fluids lead to a significant reduction in compressive properties. Interestingly, the effects of hydrogen peroxide were significantly greater than the others. This may be due to a chemical effect on the cement polymerisation reaction (hydrogen peroxide can be a free radical generator like the benzoyl peroxide catalyst). Some mechanical properties of acrylic bone cements are summarised in Table 2-6. Being a viscoelastic material, the "static" mechanical properties of bone cement are dependent on strain rate. High strain rate tests emphasise the elastic contribution to the mechanical behaviour. The assignment of bone cement to the "brittle" class of materials is thus only strictly valid at high strain rates. Lee *et al.* (1977) have shown 50% increases in strength and elastic modulus at a strain rate of 1.8 s⁻¹ compared to "quasistatic" strain rates, but ultimate strain and energy absorbed to failure decreased. The dynamic mechanical properties of bone cement are even more sensitive to flaws than the static properties. Measures taken to reduce porosity (e.g. centrifugation) are effective in increasing fatigue life at physiological strain levels (Davies *et al.*, 1987). Some investigators suggest that fatigue failure of cement is more dependent on crack propagation than crack initiation and consequently that the average molecular weight is important in controlling fatigue strength (Wright and Robinson, 1982). Pal and Saha (1982) showed that surgical grade PMMA cement subject to 1% compressive strain showed stress relaxation of 24% in 8 hours. Creep

deformation under a constant compressive stress of 10.5 MPa produced 55-70 % creep strain in 24 hours.

Cement adheres very poorly to most materials, including metal implants. However, special surface treatment of the implant with silane coupling agents and subsequent coating with a thin layer of PMMA during manufacture has been used to promote the adherence of the *in situ* cement layer. The effect of bonding conditions at the prosthesis-cement interface is still a subject of discussion with regards to its role in transmitting stresses and as a source of wear debris. Harris (1992a) suggests that measures should be taken to promote firm bonding of the femoral stem to the cement, whereas Ling (1992) favours a smooth (unbonded) tapered stem to accommodate cement creep. Weightman *et al.* (1987) found little evidence for cement creep in tests of femoral prostheses fixed with PMMA (CMW) cement, but significant creep when using an acrylic formulation incorporating butyl methacrylate monomer. Verdonshot and Huiskes (1994) showed that under physiological conditions creep of PMMA cement (Simplex P) was possible and that a femoral prosthesis could subside without cement cracking. McKellop *et al.* (1994) showed with a finite element model that a debonded interface increased the stresses at the stem cement interface.

2.3.4.2 Alternatives to PMMA

Alternative acrylic cement formulations to PMMA exist, for example PEMA (polyethylmethacrylate) and PMMA/PBMA (polybutylmethacrylate) copolymers. These cements have improved resistance to fracture, but lower stiffness, strength and creep resistance (Weightman *et al.*, 1987). Typically these cements are also less exothermic on curing and the monomer is less toxic. Several bioactive cements are in development with the aim, as with hydroxyapatite coatings, of achieving direct bone bonding. The cured cements are either inorganic monoliths or polymer matrix composites with a bioactive reinforcing phase. An example of the former type is that formed by the reaction of CaO-SiO₂-P₂O₅-CaF₂ glass powder and ammonium phosphate solution to form initially calcium ammonium phosphate hydrate (CaNH₄PO₄·H₂O) which then further reacts to produce a hydroxyapatite-like material (Nishimura *et al.*, 1991). The polymer matrix composite materials may consist of an acrylic matrix reinforced with a similar glass powder (Kawanabe *et al.*, 1992).

Table 2-6: Values for the mechanical properties of acrylic bone cements.

Loading regime	Cement	Sample geometry Test conditions	Value	Comments	Authors
Tension	CMW	Waisted rectangular section specimens 3 x 5 x 32 mm gauge length Cross head displacement 10 mm/min	E = 1.72 GPa, UTS = 36 MPa, ϵ_f = 2.45 %		Weightman <i>et al.</i> (1987)
	Sulphix		E = 1.35 GPa, UTS = 43 MPa, ϵ_f = 4.65 %		
	PMMA/PBMA copolymer		E = 0.65 GPa, UTS = 19.3 MPa, ϵ_f = 26.2 %		
Tension	Simplex radio-opaque	Waisted cylindrical specimens, \varnothing 5 x 10mm gauge length 37°C wet environment	E = 2.4±2 (S.D.) GPa, UTS = 43±5 MPa E = 2.5±0.3 (S.D.) GPa, UTS = 34±10 MPa	Centrifuged Control	Burke <i>et al.</i> (1984)
Compression	CMW	Cylindrical specimens \varnothing 6.35 x 12.5 mm Cross head displacement 25 mm/min	E = 1.70 GPa, UCS = 113.2 MPa (room temp) E = 1.38 GPa, UCS = 91.1 MPa (37°C)		Weightman <i>et al.</i> (1987)
	Sulphix		E = 1.13 GPa, UCS = 92.1 MPa (room temp) E = 1.00 GPa, UCS = 78.3 MPa (37°C)		
	PMMA/PBMA copolymer		E = 0.83 GPa, UCS = 46.1 MPa (room temp) E = 0.58 GPa, UCS = 33.5 MPa (37°C)		
	Simplex		USS = 41 MPa		Lee <i>et al.</i> (1977)
	Simplex		G = 0.85 GPa, USS = 37 MPa		Lee <i>et al.</i> (1977)

E = Young's modulus, G = shear modulus, UTS = ultimate tensile strength, UCS = ultimate compressive strength, USS = ultimate shear strength, ϵ_f = strain at failure

2.4 Failure of Cemented Joint Replacement

The cemented total hip replacement, by the standards of any surgical procedure, is tremendously successful and has been called the "operation of the century". The incidence of early problems, such as fracture of the stem and deep infection, has been reduced to low levels by improvements in materials and aseptic techniques respectively. The infection rate at Wrightington Hospital, for example, dropped from 2.2% in the period 1963-1965 to 0.5% in the period 1989-1992, due to a combination of clean air systems and antibiotic prophylaxis (Howorth, 1993). The reasons for these problems are well understood and therefore they can be minimised. The remaining failures are longer term and more complex in origin and are generally referred to as "aseptic loosening". The process is characterised by the formation and progressive thickening of a continuous fibrous layer, bone resorption and ultimately migration of the prosthesis and clinical failure. Recent work suggests, however, that all prostheses migrate from "day one", but it is those that show early, rapid migration that eventually require early revision (Freeman and Plante-Bordeneuve, 1994; Kärrholm *et al.*, 1994).

One of the most comprehensive and hence valuable follow-up studies of clinical failure of cemented total hip arthroplasty is that reported by Ahnfelt *et al.* (1990) and Malchau *et al.* (1993) which records all re-operations after total hip replacement carried out in Sweden from 1979-1986, a total of more than 92,675 primary total hip replacements. The study used the survivorship analysis of Kaplan and Meier (1958) which seems to have become the *de facto* technique in recently reported follow-up studies. Principally evaluated were the influence of implant and patient related factors on revision rates. Clearly demonstrated was that aseptic loosening was the major reason for revision in all patient groups and that improvements in surgical technique, cementing technique and selective use of implants that had previously proved to be well designed had reduced the revision rate. Overall, a revision rate of approximately 10% after 10 years was reported. In general, an increased risk for revision due to aseptic loosening was shown for the younger patient. This has been a finding common to many long term reviews, as reported by Morscher (1992). Other notable risk factors for early loosening are higher than average body weight (Schurman *et al.*, 1989) and certain diagnoses, e.g. rheumatoid arthritis (Ahnfelt *et al.*, 1990; Malchau *et al.*, 1993).

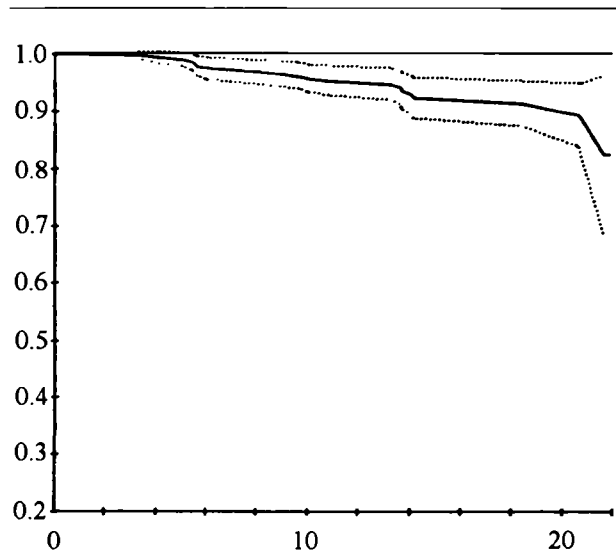
Since the first long term clinical reviews (e.g. Charnley, 1979), loosening of the acetabular component of cemented hip arthroplasty has been recognised as a significant failure mode. Charnley's study, which was the 12-15 year follow up of conventional Charnley cemented total hip replacements carried out between November 1962 and December 1965, cemented sockets were classified according to clinical result and radiographic appearance. Few of the original 396 were revised for aseptic loosening of the socket. Radiographic appearance was classified according to the following scheme: grade I represented perfect acceptance of cement with no demarcation of the radio-opaque bone cement from the bone of the acetabulum, grade II represented slight or moderate demarcation, grade III severe demarcation and grade IV migration. The incidence of each is shown in Table 2-7.

Table 2-7: Radiographic evidence of socket condition

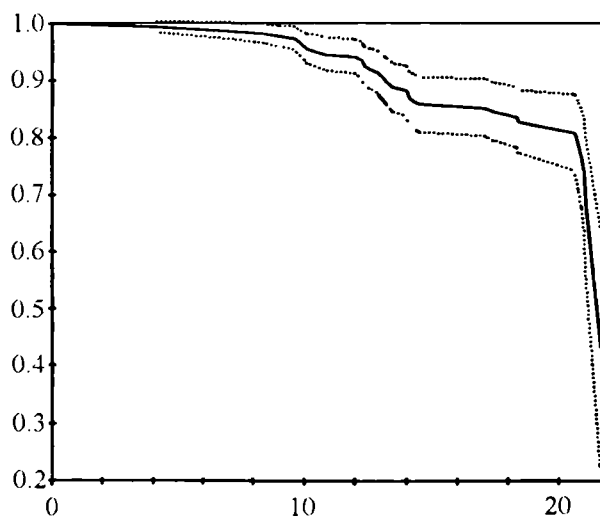
Grade	Number of Sockets	% of Total (115)
I	47	41
II	39	34
III	16	14
IV	13	11

Despite the variable radiographic appearances all these 115 patients had excellent clinical function. More worrying was that demarcation accelerated with time and that those sockets with poor radiographic appearance were probably potential failures. Severe demarcation and eventually migration represents loss of bone stock, which makes revision surgery more difficult, so a conflict arises as to whether a "pre-emptive" revision operation should be performed on the basis of the radiological evidence even though the patient may still have clinically good function.

Schulte *et al.* (1993) presented results of cemented Charnley hip arthroplasties after a minimum follow up period of twenty years (Figure 2-18).



(a)



(b)

Figure 2-18: The survivorship of hip replacement components.

(Shulte *et al.*, 1993)

The curves show the probability of retention of the original prosthesis on the y axis against time in years on the x axis. Radiographic evidence of definite or probable loosening of the femoral component or aseptic loosening confirmed at revision (a) and radiographic evidence of definite or probable loosening of the acetabular component or aseptic loosening confirmed at revision (b) were the endpoints. The dotted lines represent 95% confidence levels.

Their results demonstrate the rate of acetabular loosening, whether judged by radiographic evidence, or confirmed at revision, was 2 to 3 times that of the femoral component. Wroblewski (1986) reported that in three major series, the incidence of acetabular loosening as determined radiographically was 22-25% after 10 years. Significantly, it can also be seen that very long periods of follow up are needed to

demonstrate any notable effects of improvements in technique with follow-up studies using either clinical, or conventional radiographic assessment.

However, recent studies have used a special radiographic technique, Röntgen stereophotogrammetric analysis (RSA) to enable accurate measurements in three dimensions of the position of implants within the body. The positional accuracy of this technique is claimed to be 10-250 μm . RSA is thus sensitive enough to be suitable for the analysis of implant stability under load and with respect to time (migration), non-invasively *in vivo* (Selvik, 1989). Significantly, there is evidence that the early migration of implants in bone is correlated with and therefore may predict clinical survivorship. This has been shown with relatively long periods of follow-up (10 years) by Grewal *et al.* (1992) for knee prosthesis and in the shorter term (3 to 24 months post-operatively) by Önsten *et al.* (1993) for acetabular cup migration. Snorrason *et al.* (1993) have used RSA to evaluate several factors affecting the success of hip replacements with cemented acetabular components. They considered that detection of early migration indicated an inferior bone cement interface and that the poor primary fixation that this implied indicated that the fate of a cemented prosthesis might be revealed in the first post-operative months. In support of this evidence are the studies of Carlsson and Gentz (1984) and Hodgkinson *et al.* (1988) who found that even minor radiological defects in the cement bone interface appearing in the first post-operative year lead to 35-40% radiological loosening after ten years. Although the relationship between acetabular component migration in the early post-operative years and later clinical loosening requiring revision is not quite clear, the RSA technique shows great promise as a method of evaluation of implants and implantation techniques in one or two years instead of the ten or fifteen of a clinical trial and with smaller patient groups. With careful analysis and/or the assistance of computerised image analysis, it even appears that some of these benefits can be realised with conventional monoplane radiography (Stocks *et al.*, 1995), which has the additional benefit of being applicable retrospectively.

Improvements in cementing technique have led to a valuable increase in the survivorship of cemented hip replacements (Malchau and Herberts, 1996). Hodgkinson *et al.* (1993) reported an improvement in post-operative radiological appearance of the cement-bone interface with flanged compared to unflanged cups

which was reflected in the radiological appearance at 10 years where 43% of flanged sockets showed no evidence of radiolucency as against 30% of the unflanged group. It is clear then that aseptic loosening, in particular of the acetabular component, makes the most significant single contribution to the overall long term failure rate of cemented total hip replacement.

2.4.1 Causes of Aseptic Loosening

It is likely that the process of aseptic loosening is the result of a combination of factors, the importance of each depending on the particular prosthesis design and technique of insertion. Huiskes (1993) has recently defined a series of "failure scenarios", which are helpful in attempting to classify the potential failure processes of total hip replacement. Classification of the scenarios that are probably most relevant to the cemented total hip replacement, particularly the acetabular cup, are:

- (i) The "accumulated damage scenario", where the cement-bone interface eventually fails as a result of the mechanical stresses placed upon it.
- (ii) The "implant-reaction scenario". In this case wear particles from various sources stimulate the resorption of bone at the cement-bone interface.
- (iii) The "bone adaptation scenario". The bone response to the changed stress patterns causes bone hypertrophy in highly stressed areas and resorption in areas of low stress.
- (iv) The "destructive wear scenario". This is the "simple" case of mechanical wear of and eventually loss of continuity of the bearing surfaces. This is an important materials problem, since it represents the limiting lifetime of all types of prosthesis, but will not be considered further here.

There is some debate as to whether the "accumulated damage scenario" or the "implant reaction scenario" relates most strongly to the acetabulum in cemented joint replacement. Schmalzried *et al.* (1992) emphasise the cellular response to UHMWPE wear particles in the acetabulum and mechanical failure of the cement and cement-prosthesis interface in the femur. However, the recent RSA studies have correlated early migration rate and long term stability in both knee prosthesis (Grewal *et al.*, 1992) and in the shorter term (3 to 24 months) in acetabular cups (Önsten *et al.*, 1993)

Snorrason *et al.* (1993) considered that detection of early migration indicated an inferior cement-bone interface and that the poor initial fixation this implied indicated that the long term prognosis of a cemented prosthesis might be revealed in the first post-operative months.

2.4.1.1 Accumulated Damage

In the accumulated damage scenario two factors are important - the stresses at the interface and the strength of the interface. High stresses and low strength (under static or cyclic loading) contribute to more rapid failure of the interface. Stresses are to some degree controllable by the surgeon, by the adjustments to hip biomechanics possible during joint replacement, but mainly depend on the implant design and the materials from which it is made (section 2.3) and patient related factors such as activity and body weight. Interface strength, especially with cemented implants, depends to a great extent on the skill of the surgeon and the surgical technique (Lee and Ling, 1984). In the case of cemented joint replacements, two major factors are thought to contribute to production of an interface with insufficient strength - surgical trauma and insufficient contact/interlock between cement and intact bone (section 2.5).

The process of inserting an implant causes acute bone necrosis, due to damage to the blood supply and the thermal and chemical effects of the bone cement. In post-mortem studies of total hip replacement, Willert and Puls (1972), quoted in Feith (1975), found a zone of necrotic bone and marrow up to 3mm thick around a cemented prosthesis a few weeks after implantation. The mechanical processes of preparing the bone surfaces for an implant can damage vascularisation which will lead to bone (cell) death. As with any wound, there is an acute immune response during which macrophages and foreign body giant cells proliferate. It has been shown that large numbers of active macrophages are implicated in aseptic loosening and bone resorption.

Bone cement may cause tissue necrosis in two ways; by chemical toxicity or by heat damage. Linder (1977) and Feith (1975) showed that, in rabbits, any necrotic effects due to chemical trauma from the monomer were overwhelmed by the mechanical damage due to the surgical procedure and thermal damage generated by the polymerisation. It is well established that excessive heat can cause tissue injury. The

temperature that the bone reaches during cement insertion depends principally on the (time dependent) rate of heat generation in the cement and on the rate that heat is transferred from source (the cement) to sink (effectively the bone and prosthesis), mainly by conduction.

In the rabbit, Eriksson and Albrechtsson (1983) showed that the threshold temperature for impaired bone regeneration was 44-47°C for 1 minute exposure. At higher temperatures the threshold time decreases.

Temperatures at the "interface" between cement and bone have been measured *in vivo*, by Meyer *et al.* (1973), with maximum temperatures of 70°C in the region of the lesser trochanter, and *in vitro* by DiPisa *et al.* (1976) who recorded a very similar temperature at the base of the "acetabulum" on insertion of a polyethylene acetabular component into a temperature controlled glass model. Experiments of this type are rather difficult to perform, since the cement bone interface is a poorly defined region in which steep temperature gradients exist, making positioning of any temperature probe crucial.

Huiskes (1980) tried to quantify thermal necrosis using a finite element model to predict necrotic zones in the acetabulum. Time-temperature damage threshold curves derived for epithelial cells by Moritz and Henriques (1947) were used in combination with the results of an axisymmetric finite element model, to generate a "necrosis map" (Figure 2-19). Lundskog (1972) showed that the response of epithelial cells to thermal insult was substantially the same as bone cells (osteocytes).

Using a parametric finite element analysis of a cemented femoral prosthesis, Huiskes (1980) predicted a significant increase in the maximal bone temperature with increasing cement thickness. Revie *et al.* (1994) similarly demonstrated in an experimental study using polypropylene model acetabula that increasing the cement mantle thickness leads to a higher "necrosis index", a damage criterion they defined using similar time-temperature damage threshold curves to Huiskes. They also demonstrated that cementation pressures (44 kPa) increased curing temperatures by an insignificant amount, with a slight reduction in curing time. Suggested methods of reducing the extent of thermal necrosis include varying the properties of the cement such as the mixing ratio and constituents to modify the heat generating reaction

(Meyer *et al.*, 1973; Feith, 1975; Huiskes, 1980), pre-cooling the cement and implants to improve their efficiency as heat sinks (DiPisa *et al.*, 1976; Huiskes, 1980), pre-cooling the bone (Huiskes, 1980) and reducing the quantity of cement used (Huiskes, 1980).

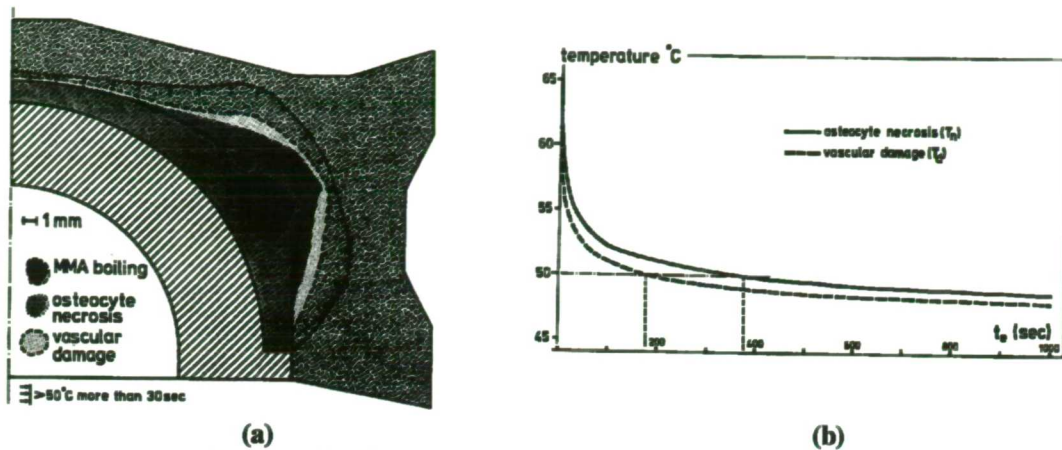


Figure 2-19: Thermal necrosis due to acrylic bone cement.
(a) necrotic zones after cup cementation, as predicted by finite element analysis, and (b) necrosis thresholds as defined by Moritz and Henriques (Huiskes, 1980)

Immediately after prosthesis insertion, the tissues in contact with the implant consist of necrotic and shattered trabeculae, structurally intact bone, tissue debris and blood (Lee and Ling, 1984). Evidence suggests that, although intimate bone-cement contact is possible, some fibrous interposition may be present from the start. The fibrous tissue layer may be stable for a long period of time, but in some cases may grow progressively and become extensive. It is probably also possible for the fibrous layer to be partially eliminated by processes of metaplasia (Charnley, 1979), given suitable mechanical conditions. Repair of the peri-prosthetic tissue occurs in the light of the new mechanical environment. Living bone will continue with the normal processes of remodelling and under appropriate mechanical conditions, dead bone can be substituted by living bone (Ling, 1986). However, mechanical failure of the necrotic bone may occur before this process is complete if static or cyclic stress levels exceed the static or fatigue strength of the bone. Necrotic bone is less strong and stiff than living bone and has lower fatigue strength (Carter *et al.*, 1981). Should the necrotic bone layer fail before it can be substituted by living bone or a layer of blood clot is interposed between the implant and the bone, relative motion at the implant-bone interface can occur. These movements, termed micromotion, can occur if an implant is not rigidly mechanically coupled to the surrounding bone. Brunski *et al.* (1979) have shown that a fibrous tissue layer forms around endosseous implants loaded after

implantation, whereas direct or nearly direct bone contact can be achieved around non-functional ones. It was proposed that the small amplitude relative motions (micromotion) between implant and bone were the cause of fibrous tissue encapsulation. Swanson (1977) suggested that low amplitude micro-movements are acceptable provided that they do not steadily increase in amplitude with successive load applications and do not lead to damage accumulation in the bone. Pilliar *et al.* (1986) have shown that micromotion greater than 150 μm is sufficient to prevent bone ingrowth into porous coated implants in dogs. Securely fixed implants with bone ingrowth showed micromotions less than 30 μm when mechanically tested after sacrifice.

2.4.1.2 Implant Reaction and Wear

The dynamic coefficient of friction of a healthy animal joint is ≈ 0.002 . For a typical artificial joint combination of stainless steel on UHMWPE, the value of the dynamic coefficient is 20 to 25 times higher (Black, 1988). In current artificial joints lubrication mechanisms similar to the natural joint do not occur and friction and wear rates are higher. Wroblewski (1985) measured the wear of high density polyethylene acetabular cups retrieved at revision. For cups retrieved when revision was due to a fractured femoral component, the mean linear rate of wear was 0.12 mm year^{-1} (range 0.02 to 0.28 mm year^{-1}). For other cases, including loosening of either component, the mean wear rates were higher (mean 0.30 mm year^{-1} , range 0.07 to 0.52 mm year^{-1}). The direction of socket wear was quite variable in both the medial-lateral and anterior-posterior planes. Pederson *et al.* (1995) recently performed a retrospective radiographic study of wear. Linear wear rates for both 22 and 28mm diameter heads were similar to Wroblewski's study, but it was noted that volumetric wear rate for the 28 mm head was almost double that of the 22 mm head.

Wear of the acetabular cup results in the femoral head "boring" into the cup, progressively restricting the range of movement of the joint and increasing the likelihood of impingement of the femoral component and consequent shock loading of the cup. However, the most serious consequence of wear seems to be the generation of particulate debris. This debris can stimulate cells to resorb bone and form a thick fibrous layer at the bone cement interface. In a cemented hip joint prosthesis there are

several possible sources of wear debris: the articulating surface itself, the implant cement interface, the bone cement interface and, increasingly with more modular designs of prosthesis, the implant-implant interfaces. It has recently also been found that metallic implants are covered in milligrams to tens of milligrams of particulate debris from the manufacturing process "off the shelf", each milligram representing more than one million particles (Merchant *et al.*, 1995).

The presence of cells thought to be active in bone resorption such as macrophages, multinuclear giant cells and osteoclasts, together with particles of implant material has been reported by many studies of fibrous membranes obtained at revision operations (Schmalzried *et al.*, 1992; Revell *et al.*, 1997). In the laboratory it has been shown that particles of many materials, including PMMA, polyethylene and titanium, can trigger processes which culminate in bone resorption, but the mechanisms by which the particles provide the stimulation and the predominant paths to bone resorption around an implant are still debated. Yao *et al.* (1995) have shown by challenging osteoblast-like cells in culture with a variety of materials (commercially pure titanium, silver, polystyrene) and particle sizes, that particle size, at least for this type of cell, is more significant than composition. Small particles (1 μm) suppressed collagen expression by their cells, whereas larger particles (20 μm) had no effect, compared to controls. This effect was independent of material. They suggested that since osteoblast collagen synthesis is vital in bone formation and remodelling, it is possible that wear debris is detrimental to the bone repair process and that suppression of this function by wear debris might be an important contributor to loosening. Similarly, for human macrophages challenged with PMMA particles, González *et al.* (1995) showed that no proliferative cell response occurred, but the size and the dose of particles were important in determining macrophage release of cytokines and lysosomal enzymes. Non-phagocytosable particles (200 μm) had little effect on release of these factors.

2.4.1.3 Bone Adaptation

The shape and mechanical properties of a mature bone are governed by a combination of genetic and developmental factors and the loading history of the bone. Under normal conditions, the rate of bone deposition and repair matches the rate of bone resorption and fatigue damage accumulation and no net change in bone morphology is observed, although continual bone turnover occurs. Should the mechanical demands

made on a bone alter, as for example when a prosthesis is implanted, the bone has the capacity to adapt its structure in response. According to the theory of adaptive bone remodelling ("Wolff's Law") bone responds to its mechanical environment by depositing material in areas that are highly stressed and resorbing material in areas that are less stressed. This may be manifested as external modelling, characterised by new bone formation at the cortical surface, or internal remodelling, involving a change in density of the cortical or trabecular bone and possibly rearrangement and change in the orientation of trabeculae. Stress shielding, or stress protection, occurs where areas of bone experience much lower stresses when an implant is introduced than in the normal case. According to Frost (1992), the biological response of bone can be divided into at least four "fuzzy" windows, depending on the level of mechanical usage. These are classified as the "disuse" window, the "adapted" window, the "mild overload" window and the "pathologic overload" window, depending on the relationship between the actual bone strain and the bone failure strain (Figure 2-20). Normally bone is in the "adapted" window, but the introduction of a prosthesis changes the mechanics of the bone and will most likely shift the response. In the pelvis the articular cartilage and at least some of the subchondral bone layer of the acetabulum are replaced by a relatively thick polyethylene cup and bone cement layer. The subchondral and trabecular bone then experiences an altered mechanical environment (Dalstra, 1993). The effects of adaptive bone remodelling are probably less significant in the acetabulum than in the femur, where much stiffer and bulkier implants are used and the insertion of an intramedullary device represents a greater departure from the normal situation. In any case clinical evidence for implant failure directly attributable to adaptive bone remodelling is lacking, although change in stress patterns in bone after implantation is certain.

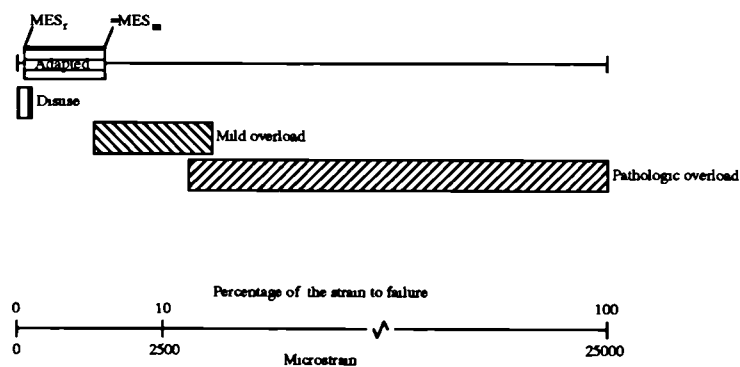


Figure 2-20: The "windows" of bone response to mechanical stimulus. (Frost, 1992)

2.5 Aspects of Fixation with Acrylic Bone Cement

In view of the late complications of cemented acetabular cups and the suspected role of quality of initial fixation in long term success, recently supported by RSA studies, there is surprisingly little work on the strength and stability of entire acetabular reconstructions, as compared to that on the strength of the bone cement interface, and how it is best achieved. Much of the recent work concentrates on cementless fixation methods. In one of the earliest studies Andersson *et al.* (1972) examined the strength of the bone-prosthesis bond in the acetabulum with reference to the technique of surgical preparation. Compressive loads up to 3920 N were maintained perpendicular to the acetabular mouth while a torsional moment (torque) was applied to the cup and the torque at failure recorded. Overall, providing cartilage was removed, but the subchondral plate preserved and the acetabular fossa thoroughly cleaned, failure torque was considerably greater than 100 Nm. The eventual failure was always between cement and bone, and fragments of bone often remained attached to the cement. If the compressive load was increased, the failure torque was similar, but if greatly reduced or removed the failure torque was reduced by about 50 %. Anchoring holes appeared to have only a small effect when a compressive normal load was present, although the results of Chen *et al.* (1974) showed somewhat higher torsional strengths than Andersson *et al.* despite using a purely torsional test. Oh (1983) has shown in a model, again with purely a torsional load, that in the absence of other fixation, distributed small anchoring holes provided a torsional strength of up to 157 Nm. Many small holes were more effective than fewer, larger ones as more cracks would need to be nucleated and propagated before failure. Volz and Wilson (1977) also performed a torsional test that did not include a compressive load. Acetabula prepared by reaming with preservation of subchondral bone showed failure at an average torque of 33 Nm, rising to 43 Nm if the cup was fully seated with the cup rim flush with the mouth of the acetabulum. In the latter case the failure torque was calculated to correspond to shear stresses at the bone cement interface of 0.8 MPa. Failure torques were lower than the comparable results of Andersson *et al.*, but discontinuities in the load time curve were used to identify failure rather than the sudden increase in rotation of Andersson *et al.* Removal of the subchondral plate and

the use of anchoring holes was associated with an increase in the failure torque to 70 Nm if the cup was fully seated and 50 Nm if not. For the former the corresponding shear stress was 1.3 MPa. This probably reflects the higher shear strength of an interface between cement and cancellous bone as compared to an interface with cortical or sclerotic subchondral bone, but the absence of compressive perpendicular load resulted in the role of the subchondral plate in resisting compression being ignored. Ohlin and Balkfors (1992) studied the failure torque of cemented cups retrieved at autopsy after 3-14 years of implantation and compared these with freshly cemented sockets in cadaver bones. Failure moment in the two groups was 80 and 86 Nm respectively, a similarity that surprised the authors. In contrast to Andersson *et al.*, failure was not restricted to the cement bone interface - failure between socket and cement and cracks within the cement were universally observed.

Considering the micromotion between implant and bone, Perona *et al.* (1992) have measured that between cup and peri-acetabular bone for various uncemented and cemented implants. They applied loads stepwise between 0 and 2354 N in an anatomical direction to cups fixed in cadaveric acetabula, measuring the resulting micromotion at the ilium, ischium and pubis. Cemented cups showed by far the least micromotion, the direction of which was inconsistent - the cups sometimes displacing supero-laterally and sometimes supero-medially. Micromotion was mainly evident at the ilium (range of -31 to 131 μm at maximum load) and pubis (-6 to 67 μm) and much reduced at the ischium (-23 to 11 μm). This data matches reasonably well the stress distributions in the analysis of Dalstra (1993).

2.5.1 The Strength of the Bone-Cement Interface

In vivo the cement bone interface at the acetabulum is predominantly subjected to mixed mode compression and shear loading. In most situations compression testing of interfaces is not particularly useful since even a completely unbonded interface will support compressive loads up to the compressive failure strength of the weakest material. Hence tensile and shear tests are usually employed. Tensile tests are sensitive to interface conditions and, unlike some shear tests, the interface is not isolated so the whole cement-bone region is therefore tested. The results of interface shear strength testing of implants tend to divide the bone-implant combinations into

three groups; those surrounded by fibrous encapsulation with shear strength of less than 1 MPa, those tolerated by the host bone with shear strengths of 3-10 MPa and those that produce a vital bond with bone with shear strengths up to 60 MPa (Tanner, 1994).

The goal of modern cementing techniques is to enhance the fixation of implants by improving the strength of the cement and the bone-cement interface. Elevated pressure during curing may help to reduce porosity of cement (Bayne *et al.*, 1975), which improves its mechanical properties (Davies *et al.*, 1989). Intrusion of cement into cancellous bone by cement pressurisation has been shown *in vitro* to give the bone cement interface higher tensile (Krause *et al.*, 1982a; Eftekhari and Nercessian, 1988; Kuivila *et al.*, 1989; Mann *et al.* 1997) and shear strength (Krause *et al.*, 1982a; Lavernia *et al.*, 1988; Ober *et al.*, 1989). For a cancellous bone-cement interface loaded in tension, penetration of the bone cement to less than a certain depth (related to the mean cancellous cell size) will result in failure by pull out of the cement "fingers" from the bone (Askew *et al.*, 1984, Krause *et al.*, 1982a). Penetration deeper than this threshold level results in interdigitation of the cement into the bone which leads to failure of the bone itself. For an interface between bone cement and low to medium density, reasonably homogeneous cancellous bone, there will thus be an optimum penetration depth for achieving maximal interface strength. Askew *et al.* (1984) suggested that the optimal depth is ≈ 4 mm. In trabecular bone of high density failure in the bone cement can occur; it should be noted that pelvic trabecular bone is fairly low density (Dalstra *et al.*, 1993).

While pressurisation of cement into cancellous bone has been shown to increase the strength of the bone cement interface, usually (depending on surgical technique) only part of the reamed acetabular surface is cancellous, although fixation holes may be drilled through the subchondral plate near the rim to expose cancellous bone. Data concerning the strength of interfaces between non-cancellous surfaces and acrylic cement is scant. Balu *et al.* (1994) measured the shear strength of the bone-cement interface formed within sections of femoral diaphyses. The interfacial shear strength for un-reamed femoral sections was of the order of 3 MPa. Intramedullary reaming with conical reamers was found to significantly reduce the interfacial shear strength by

reducing the roughness of the endosteal surface, emphasising the role of mechanical interlock.

2.5.1.1 Variables Controlling Cement Penetration into Cancellous Bone

A freshly cut surface of viable cancellous bone consists of a mixture of exposed trabeculae, bone marrow, bone debris from the surgical preparation and blood. For bone cement to intrude into the cancellous spaces, the pressure applied must be sufficient to overcome the viscous resistance of the cement to flow into the cancellous spaces, to displace any marrow, blood and debris and to overcome the bleeding pressure of the bone. Provided cement can be made to penetrate the cancellous bone, the cement and bone are joined by a composite layer composed of a continuous cement phase reinforced with bone trabeculae.

Noble and Swarts (1983) studied the penetration of acrylic bone cements into cancellous bone plugs completely cleaned of fat, debris and soft tissue, in order to evaluate the relationship between osseous structure and cement penetration. Here resistance to flow arises purely from the viscous interaction of the fluid bone cement and the cancellous bone. The bone samples were then orientated in a mould so that bone cement was introduced with trabecular orientation parallel to the applied pressure gradient. The relationships between depth of penetration and cement formulation and bone structure were independently evaluated for a constant applied pressure of 35 kPa. A fairly strong linear relationship (correlation coefficient 0.83-0.94) was observed for the increase in depth of penetration with increase in cancellous cell volume. Penetration depth was not found to be strongly related to porosity. This suggests that, at least for significantly anisotropic specimens and within a narrow range of porosity, the geometry and orientation of the cancellous cells relative to the applied pressure gradient is more important than their absolute volume.

The relationship between penetration depth and porosity for cancellous bone of human and bovine origin over a wide range of porosity has been studied by Rey *et al.* (1987). The specimens were also dried and defatted, but were not deliberately orientated in any particular material direction. Their data did show a strong relationship between porosity and cement penetration depth.

Recently Beaudoin *et al.* (1991) developed a micromechanically based model of polymethylmethacrylate flow in cancellous bone, defining a trabecular bone "unit cell" which was then used to generate a finite element model. The geometry of the model could be manipulated to simulate the various morphological parameters such as porosity, trabecular spacing and surface to volume ratio, enabling parametric studies. Increasing depth of penetration was strongly related to reducing surface to volume ratio. This was broadly consistent with the relationship between cancellous cell volume and penetration observed by Noble and Swarts. The model was also able to predict the relationship between porosity and penetration depth observed by Rey *et al.* The results of these three studies are summarised in Figure 2-21.

Several authors have studied the relationship between cement properties and cement penetration. The significant property of cement in this respect is its viscosity, which in turn is related to formulation, mixing and handling techniques. The viscosity of several acrylic bone cements has been studied by Krause *et al.* (1982b). They found that the rheological behaviour of bone cements in the implantation "time window" was that of a non-Newtonian pseudoplastic fluid and that the dependence of the viscosity function on strain rate and time could be described by a time dependent power law type expression. Highly significant differences were found between different cement formulations.

Noble and Swarts, in their study of cement penetration in dried bone, found that penetration decreased linearly with increase in the cement viscosity as measured at 50% of final penetration depth.

Where marrow and fat are present, they must be displaced by the bone cement, preferably without entrainment, such that penetration can be achieved. Efforts are usually made to remove fat and marrow from the prepared cancellous bed during surgery by brushing and/or pulsatile lavage. This bone preparation has a highly significant effect on cement penetration (Askew *et al.*, 1984) and hence interface strength (Halawa *et al.*, 1978; Krause *et al.*, 1982a).

Bone, like any other vascularised tissue, bleeds when damaged. Shelley and Wroblewski (1988) simulated the effects of a blood pressure of 25 mmHg (3.3 kPa) on cement penetration in a model acetabulum and found that, on release of pressurisation, this was sufficient to displace cement even 5 minutes after insertion.

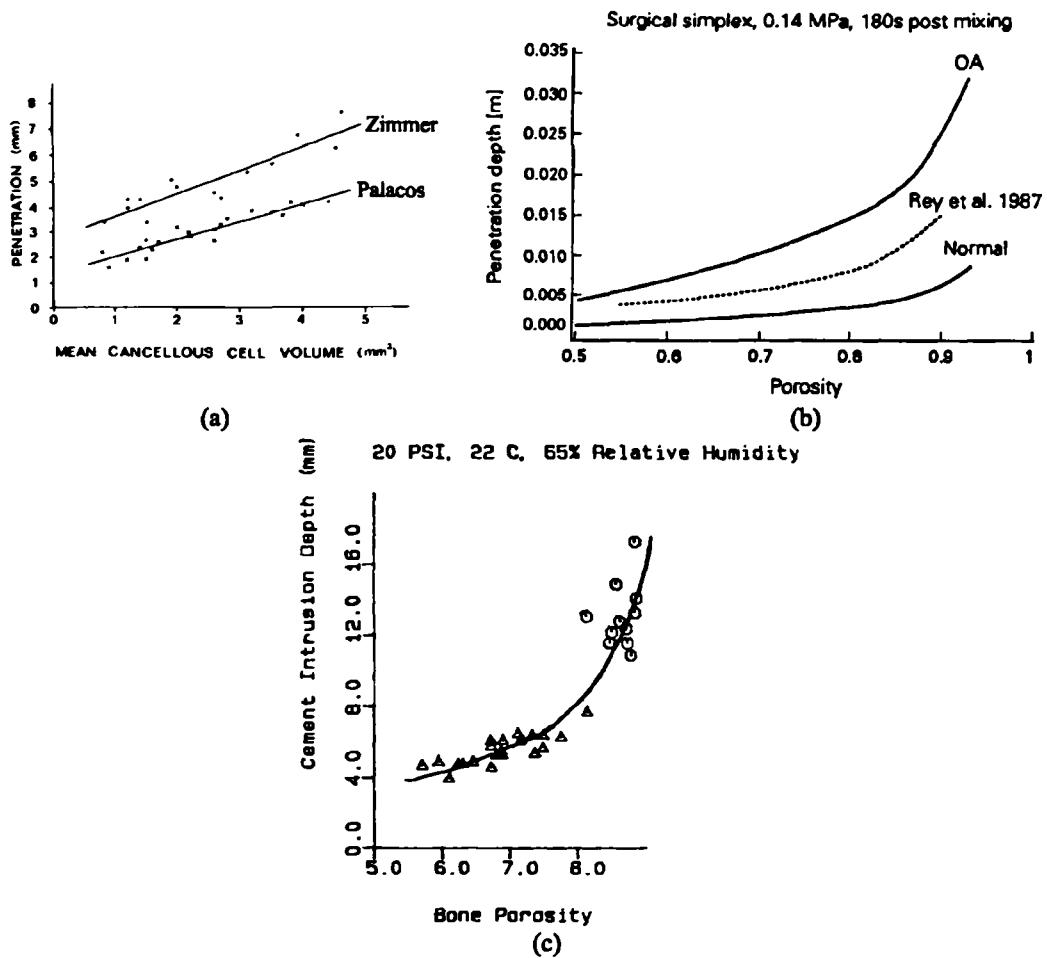


Figure 2-21: Cement penetration into cancellous bone.

(a) Cement penetration as a function of cancellous cell volume for two types of bone cement (Noble and Swarts, 1983); (b) Cement penetration as a function of porosity as predicted by F.E.A. (Beaudoin *et al.*, 1991); (c) Cement penetration as a function of porosity (Rey *et al.*, 1987).

2.5.1.2 Pressures Required to Achieve Penetration

The level of pressurisation needed in practice to achieve the "required penetration" has recently been studied *in vitro* by Juliusson *et al.* (1994). Femoral heads obtained at arthroplasty were drilled to simulate the anchoring holes commonly made intra-operatively in the subchondral plate of the acetabulum, thoroughly cleaned by pulsatile lavage and cement introduced via a cement gun with a special silicone elastomer nozzle to avoid cement leakage at the periphery. The duration of pressurisation was between 20 and 60 seconds. In this study the effects of blood pressure were not modelled, although a later study from the same group did include this (Juliusson *et al.*, 1995). In this case it was found that cement pressures

approaching 0.3 MPa were needed to achieve penetration of 4 mm. No correlation was found between penetration and duration of pressurisation.

2.5.2 Intra Operative Pressurisation of Bone Cement

Two separate modes of cement pressurisation can be envisaged (Spierings, 1993); a closed system in which a hydrostatic pressure is developed by use of a suitable device (Figure 2-22(a)) and an open system as achieved for example on cup insertion (Figure 2-22(b)). The closed system has the obvious difficulty of achieving an efficient seal between the pressurising device and the rim of the acetabulum, especially in view of the highly irregular geometry of this region. In the open system pressure gradients are produced in the cement by the resistance to flow of the cement itself.

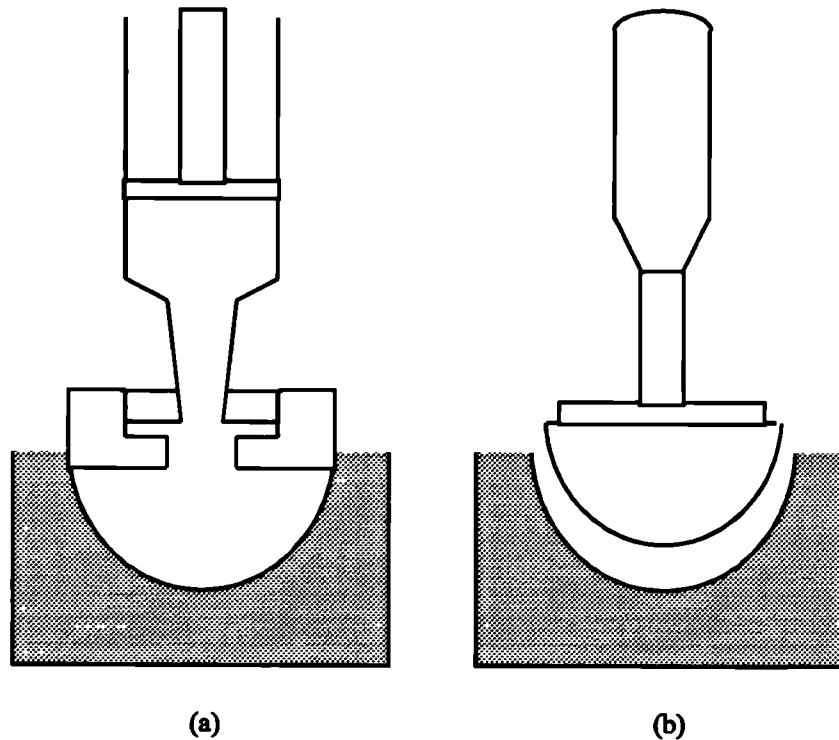


Figure 2-22: Approaches to cement pressurisation.
(a) Pressurisation of a closed system and (b) pressurisation in an open system.
(Spierings, 1993)

In the routine method of cup fixation, insertion of the cup into the prepared acetabulum causes cement to pour out around the periphery of the cup. Flow of cement is indicative of failure to achieve hydrostatic pressurisation.

The pressure developed on insertion of acetabular cups of varying design has been studied by Oh *et al.* (1985), Shelley and Wroblewski (1988) and Beverland *et al.*

(1993). Oh *et al.* compared the effect of four types of cup with differing flange designs on pressures measured in the lower portion of a model acetabulum. The results showed a trend for higher pressure under cups with more complete flanges which reflects the increased resistance to escape of the liquid cement at the periphery provided by the flange. However the cups were inserted by a materials testing machine operating in stroke control and unrealistically high insertion forces were produced on inserting, in particular the continuous flanged cups (forces approached 2500 N). Shelley and Wroblewski compared the peak pressure generated at the pole of a model acetabulum for the Charnley "ogee" cup and a scalloped cup when inserted under a constant load of ≈ 78 N. The unflanged socket produced a peak pressure of ≈ 5.9 kPa, the ogee socket ≈ 23.7 kPa. Beverland *et al.* (Figure 2-23) found that insertion of an unflanged cup produced a higher pressure (measured at a similar location to Shelley and Wroblewski) than the flanged cup (insertion force 98 N). This was attributed to the trimmed flange making sufficient contact with the acetabular wall to oppose the insertion force. Under a custom designed acetabular cup the cement pressure was still higher. The pressures measured in all cases were notably higher than those reported by Shelley and Wroblewski.

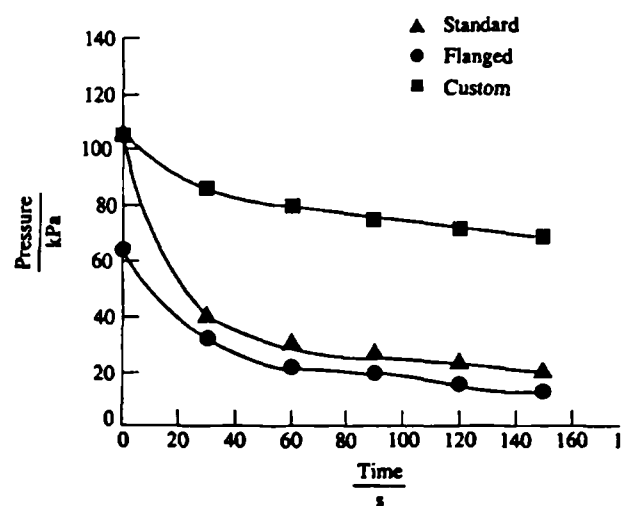


Figure 2-23: Cement pressure-time curves during acetabular cup insertion. (Beverland *et al.*, 1993)

Several devices are on the market that aim to improve pressurisation in the acetabulum. All rely on the use of a compliant material/structure to attempt to seal the irregular edge of the acetabulum while allowing sufficient displacement to pressurise the bone cement. The Exeter pressuriser is basically a silicone elastomer balloon attached to a handle that enables saline solution to be driven into the balloon to

expand it against the rim of the acetabulum and hopefully occlude irregularities. Subsequently, owing to the deformability of the balloon, load applied to the handle results in pressurisation of the cement. Lee and Ling (1974) evaluated the pressuriser by measuring the pressure produced in bone cement in real acetabula at a point between the centre of the cross sections of the ilium and ischium. Typical results showed a peak pressure of the order of 100 kPa and maintenance of the pressure above 35 kPa was achieved for a significant time (1½ to 2 minutes). When bone was dissolved away from cement, the acetabula in which the pressuriser had been used showed superior interdigitation of the cement.

The Oh-Harris pressuriser uses a silastic seal, shaped so its surface approximates to the rim of the acetabulum, attached to a gun with an advanceable plunger to apply pressure to the contained cement once the seal has been established. In tests using PMMA cement 3½ minutes from mixing (Oh *et al.*, 1983), pressures of 113, 120 and 149 kPa were measured at pressure transducers located in the ilium, ischium and base of acetabulum respectively. This was compared to finger packing where pressures were 53, 8 and 23 kPa for the same locations. Interdigitation of cement was noted similar to that seen by Lee and Ling (1974).

2.5.2.1 Side Effects of Cement Pressurisation

Some side effects have been reported with cement pressurisation additional to those attributable to the PMMA bone cement itself. These are mainly cardiovascular problems due to reaction of the circulatory system to emboli produced by air, fat and marrow squeezed into the blood stream by the bone cement (Wenda *et al.*, 1988).

2.5.2.2 Alternative Techniques to Produce Cement Penetration

Somville *et al.* (1987) described *in vitro* evaluation of a technique in which cement was injected behind a flanged acetabular cup temporarily held in position by screws. Pressure measured during injection showed peaks up to 140 kPa.

Draenert (1989) has demonstrated a vacuum technique designed to improve cement penetration and reduce the risk of complications associated with cement pressurisation. The technique involves sealing the iliac segment of the acetabulum by the application of a silicone elastomer capped cement delivery tube and applying a

vacuum via a hole drilled above the supero-lateral edge of the acetabulum. The vacuum helps to remove blood and marrow from the iliac region of the acetabulum and to draw cement into the cancellous spaces. No figures were given to demonstrate improved cement intrusion.

3. Acetabular Cement Pressurisation During Total Hip Replacement

3.1 Rationale

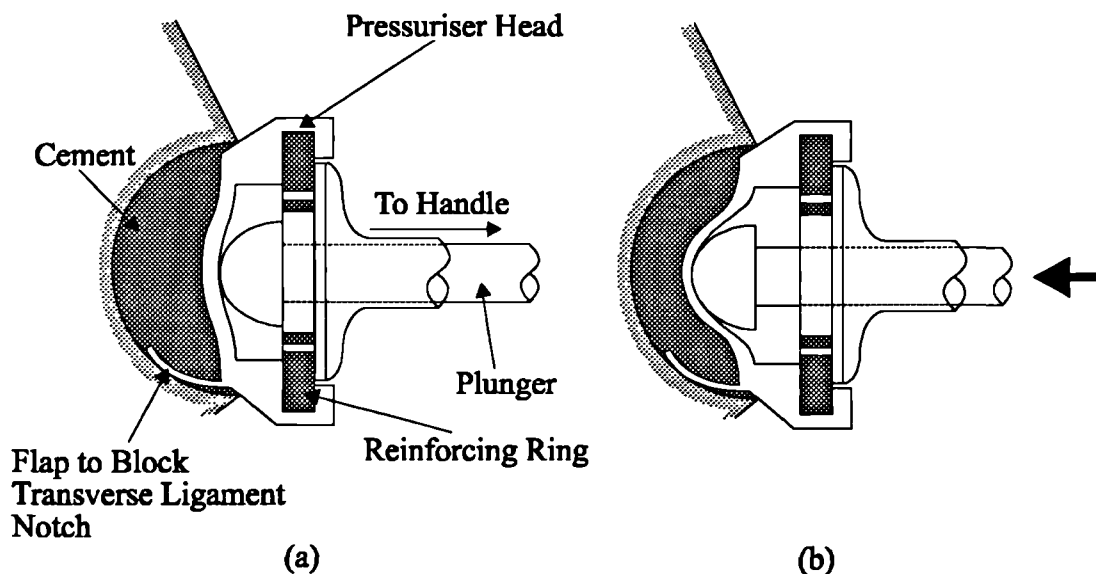
Although *in vitro* studies have demonstrated the efficacy of some pressurisation devices (Lee and Ling, 1974; Oh *et al.*, 1983), per-operative control of cement pressurisation in the acetabulum remains difficult due to the acetabular anatomy, in particular the discontinuity of the acetabular wall under the transverse ligament, the cotyloid notch. Two series of laboratory investigations have been conducted into the efficacy of cement pressurisation techniques in the acetabulum. Initially (“Machine Control”), a universal testing machine was used to compare cement pressurisation by the insertion of an acetabular cup of typical design and a novel design of cement pressuriser. However, it became apparent that although these controlled tests were useful, because they eliminated the influence of the surgeon and the particular surgical technique employed, they created a somewhat unrealistic situation. It has been shown that the expertise of the surgeon who performs the operation is one of the most important determinants of the success of an arthroplasty procedure with a given implant. Thus, in subsequent comparative studies of cementing techniques, reported as “Manual Control”, an experienced orthopaedic surgeon was employed to perform simulated operations in the laboratory. Two digital cement packing techniques - “finger packing” and “hand packing”, cup insertion, the pressuriser described in “Machine Control” and two further novel pressuriser designs were compared, together with an existing commercial device, the “Exeter” pressuriser (Howmedica, Park Royal, London, U.K.). Finally, per-operative measurement of cement pressure is described, obtained using an instrumented version of one of the devices described in section 3.2. In addition to providing validation of the laboratory methods, these measurements provide useful feedback to the surgeon and demonstrate the efficacy of the particular design of cement pressuriser *in vivo*. An additional goal in the long term is to elucidate the role of cement pressure on acetabular fixation.

3.2 Laboratory Studies

3.2.1 Introduction

3.2.1.1 Machine Control

The pressuriser used in this series is a new device, designed by Dr F.P. Bernoski of Weisteinde Zieckenhuis, Den Hague, The Netherlands (Figure 3-1). It consists of a moulded silicone elastomer head shaped to occlude the mouth of the acetabulum, with a flap to cover the cotyloid notch. The pressuriser head contains a peripheral reinforcing ring which is attached to a handle to position the device in the acetabulum and apply a sealing force (Figure 3-1a). The handle incorporates a central plunger, which is designed to be advanced once a seal has been achieved to displace the central diaphragm of the head and hence generate pressure in the cement (Figure 3-1b).



**Figure 3-1: Schematic of the Bernoski cement pressuriser.
Shown (a) prior to and (b) after the application of the pressurisation force.**

The machine control tests had two aims:

1. To compare the duration, distribution and magnitude of the pressure generated by insertion of an acetabular cup and the new cement pressuriser.
2. To determine the effect of cement leakage through the transverse ligament notch on the pressure attained and the efficacy of the flap in preventing this leakage.

3.2.1.2 Manual Control

The purpose of the second series of tests was to evaluate acetabular cement pressurisation *in vitro* under conditions similar to those in a real operation. Clinically a variety of finger packing techniques, insertion of an acetabular cup with a cement restricting flange and/or various pressurisation tools may be used. Two prototype designs of pressuriser developed at the Unit for Joint Reconstruction in conjunction with DePuy CMW (CMW Laboratories, Blackpool, U.K.) were compared with an established device, the Exeter pressuriser, and the new ("Bernoski") pressuriser tested with machine control. Further comparisons were made with two manual techniques, the first in which the adducted fingers of one hand are pressed against cement and acetabular rim with the other and the second in which the cement is simply finger packed, and with insertion of a flanged acetabular cup (DePuy International, Leeds, U.K.). The first of the new devices (UJR 1) aims to create a closed, cement filled space within the acetabulum by means of a compliant elastomer seal, similar in principle to the Exeter and Bernoski devices although using different design features to achieve the seal (Figure 3-2).

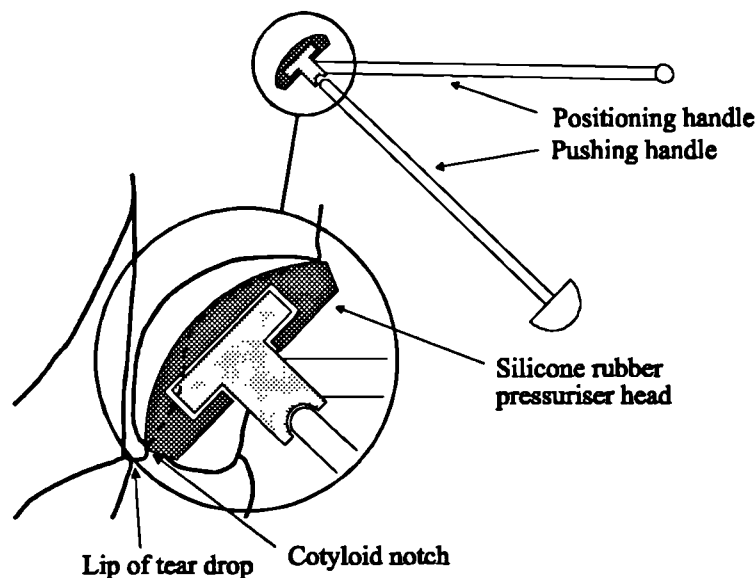


Figure 3-2: Schematic of UJR 1.

The second device (UJR 2) attaches to a standard cement gun to allow cement to be pressure-injected into the acetabulum. It incorporates a trimming aid from an "Ogee" flanged acetabular cup (DePuy International, Leeds, U.K.), which may be trimmed to fit the particular acetabulum into which the cement is introduced (Figure 3-3).

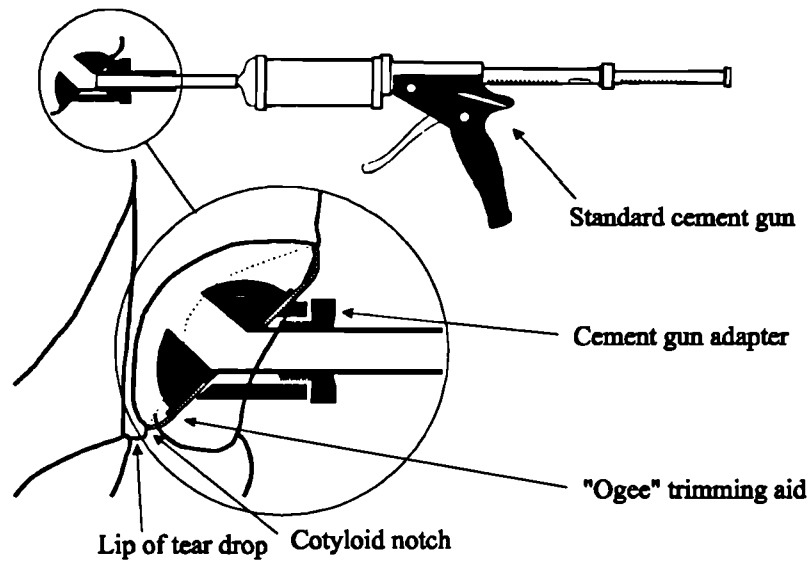


Figure 3-3: Schematic of UJR 2.

3.2.2 Methods

3.2.2.1 Machine Control

The acetabulum of a "Sawbones" hemi-pelvis (Sawbones Europe AB, Malmö, Sweden) was reamed to a hemispherical shape 54 mm in diameter. Two pressure transducers were mounted, one (model 4045A, Kistler Instruments Ltd, Hartley Wintney, U.K.) at the pole of the acetabulum and the second (EPX series, Entran Ltd, Watford, U.K.) in the ilium approximately 10 mm from the acetabular rim. Temperature coefficients of sensitivity and zero drift were less than 2% per 55°C and less than 2% of full scale per 55°C respectively for the Entran transducer and less than 1% and 0.5% of full scale for the Kistler transducer. Given the small temperature changes in the cement during the pressurisation period as compared to the peak temperatures during cure and the temperature compensation of the transducers, the error due to thermal effects during pressurisation was assumed to be negligible. The sensing membrane of the Kistler transducer was larger (10.5 mm diameter) than the Entran transducer (3.5 mm diameter) and it was for this reason that the Kistler transducer was placed at the pole of the acetabulum where the pressure is more uniform over a wider area. A photograph of the instrumented model with the Bernoski pressuriser approaching the acetabular mouth is shown in Figure 3-4.

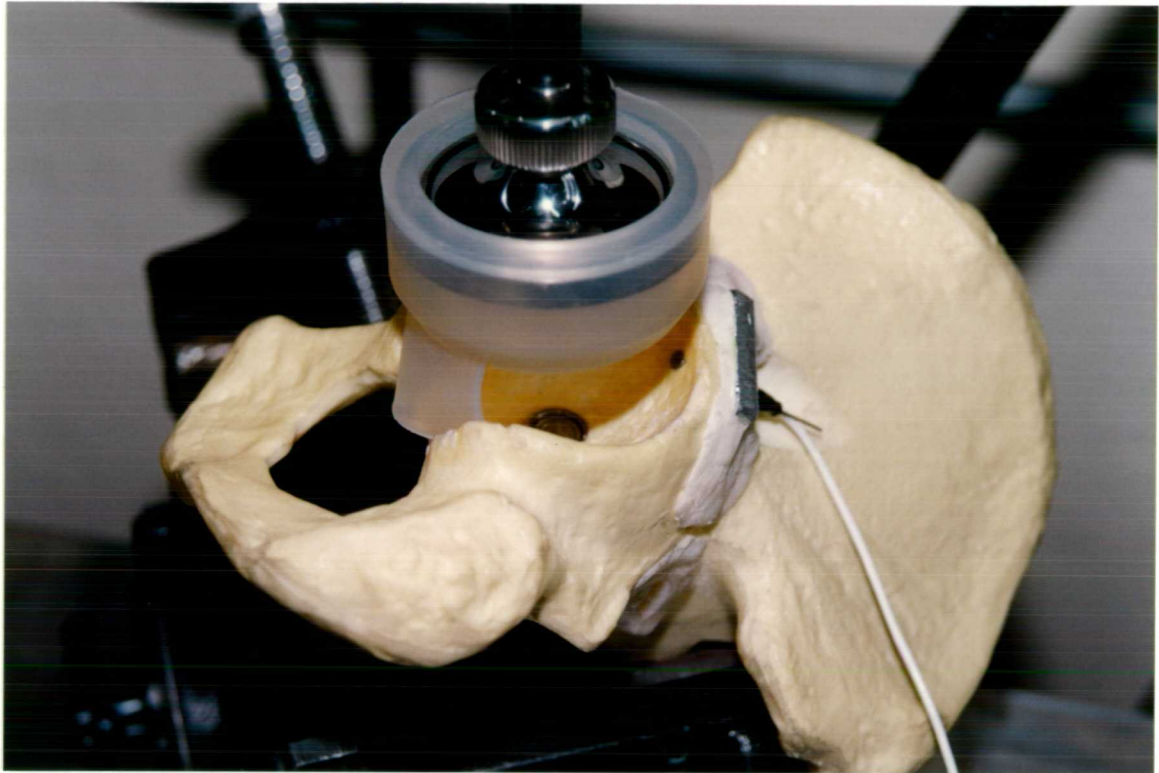


Figure 3-4: The instrumented model acetabulum with the Bernoski device.

The hemi-pelvis was mounted in a vice fixed to the lower table of a servo-hydraulic materials testing machine (ESH Testing Ltd, Brierley Hill, U.K.) with the mouth of the acetabulum horizontal. The pressure transducers and the outputs of the materials testing machine were connected to an IBM compatible PC (PC2286/40, Amstrad PLC, Brentwood, U.K. with Microsoft DOS 5.0 operating system) running specially written software via an analogue-to-digital converter card (AD1200, Brainboxes, Liverpool, U.K.), sampling at 20 Hz for each input, to allow near-continuous recording of pressure, force and actuator displacement. Boneloc bone cement (Polymers Reconstructive A/S, Farum, Denmark) was mixed in the Boneloc "Vacuum Pac" mixing system and delivered to the acetabulum with the dedicated applicator gun, according to the manufacturer's instructions. Although Boneloc cement has been withdrawn from the commercial market because of problems with subsidence of femoral stems, attributed to creep of the cement (Thanner *et al.*, 1995), its handling characteristics in the post mixing phase are similar, at least qualitatively, to conventional PMMA cements, particularly the lower viscosity cements such as CMW 3. Four minutes after mixing the cup was inserted or the pressurisation started. All tests were carried out at a laboratory temperature of $21\pm 1^\circ\text{C}$ and humidity of $40\pm 15\%$, both measured within 0.5 m of the apparatus. Three groups each of three tests were

performed, using the following to pressurise the cement:

1. An acetabular cup (Ultima UHMWPE Cup; Johnson & Johnson Orthopaedics, New Milton, U.K.) size 54 mm. This has a 50 mm diameter body, to allow a 2 mm cement mantle, a 53 mm diameter flange, to allow a 0.5 mm peripheral gap for cement extrusion, and PMMA spacers to prevent bottoming out.
2. The pressuriser without flap closing the acetabular mouth.
3. The pressuriser with flap closing the acetabular mouth and covering the acetabular notch.

In each case the cup or the central plunger of the pressuriser, as applicable, was pressed into the acetabulum by the testing machine, operating in load control mode with a constant force of 210 N applied, thus providing a controlled simulation of the action of a surgeon during an operation. The orientation of the apparatus was such that the cup was inserted with the flat face parallel to the mouth of the acetabulum. In the case of the pressuriser tests, the reinforced upper rim of the pressuriser was clamped to the acetabulum with a force of 100 N. This simulated the force applied by the surgeon via the metal reinforcing ring by the cup pressuriser handle when used clinically. These forces were considered to be representative of the maximum forces applied per-operatively after experiment with a pusher and weighing scales.

3.2.2.2 Manual Control

A "Sawbones" hemi-pelvis was again used, but this time the reaming was carried out to achieve a more realistic shape representative of a surgically prepared arthritic acetabulum, with less deepening of the acetabulum and hence a larger radius of curvature than the model described above. The acetabulum was fitted with the pressure transducers described above, in similar positions to the machine control series, and connected to the same monitoring and recording equipment. An improved computer program was written to allow real time display as well as recording of the cement pressure. The hemi-pelvis was mounted securely in a vice fixed to a workbench, simulating the orientation of the acetabulum in a lateral surgical approach with the patient supine. CMW 1 or CMW 3 bone cement was mixed and loaded into the dedicated applicator gun according to the manufacturer's instructions. For UJR 2,

cement was retained in the barrel until pressurisation started. For the remaining techniques, the cement was simply delivered to the acetabulum with the gun. At 2 minutes after mixing for CMW 1 cement and 4 minutes for CMW 3 cement, use of the pressurisation device, finger packing or cup insertion commenced and the pressures achieved recorded. All tests were carried out at a laboratory temperature of $20\pm 2^{\circ}\text{C}$ and humidity of $30\pm 10\%$, both measured within 0.5 m of the apparatus.

3.2.3 Results

3.2.3.1 Machine Control

Representative plots of pressure measured at the pole and rim of the acetabulum are shown in Figure 3-5 and Figure 3-6 respectively. On each curve, zero time refers to the time of application of the force to the cup or pressuriser, 4 minutes from the start of mixing. Cement pressurisation was continued only until 7 to 8 minutes from mixing so the cement mass could still be removed easily from the model acetabulum. Solidification time of the cement is difficult to define precisely, but was qualitatively complete at 10 minutes from mixing. The peak and mean pressures recorded are shown in Figure 3-7 and Figure 3-8 respectively, averaged for the three tests with each device. Mean pressures were calculated by integrating the pressure time curve numerically using the trapezium rule and dividing the area under the curve obtained by the time for which pressurisation was maintained.

Introduction of the cup alone lead to a rapid, but transient, pressure rise at the pole of the acetabulum and a smaller rise at the rim. For both locations the pressure then dropped approximately exponentially, falling to the baseline value after approximately 20 seconds. Peak pressures measured were 120 kPa at the pole and 55 kPa at the rim. In each test cement extruded from between the cup flange and the rim of the acetabulum and through the transverse ligament notch. This cement outflow was itself indicative of pressure gradients in the acetabulum. The peak pressure value at both locations was coincident with the "bottoming out" of the cup as indicated by cessation of displacement of the testing machine actuator at constant force.

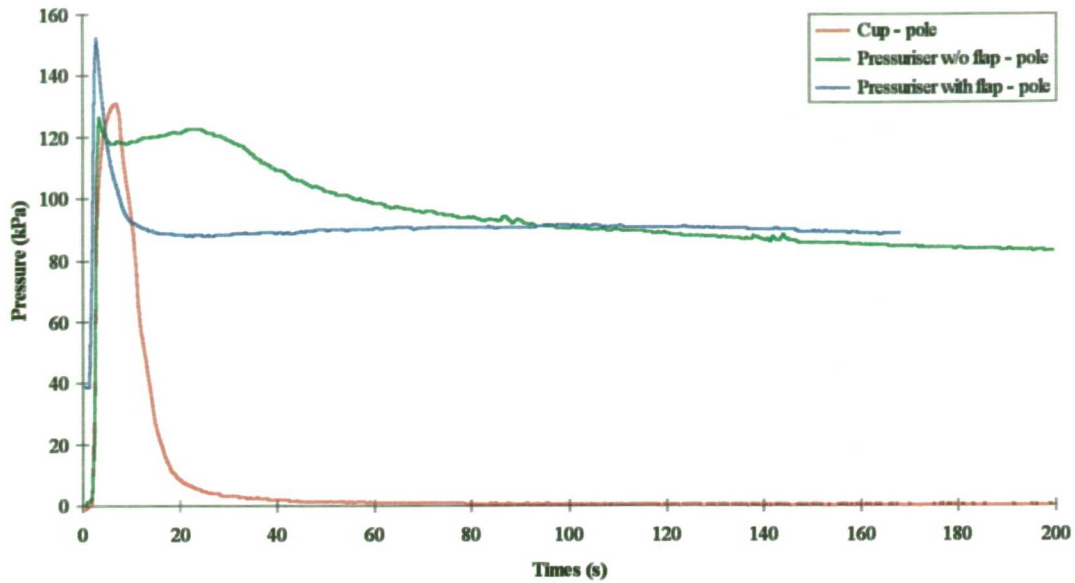


Figure 3-5: Pressure measured at the pole of the acetabulum.

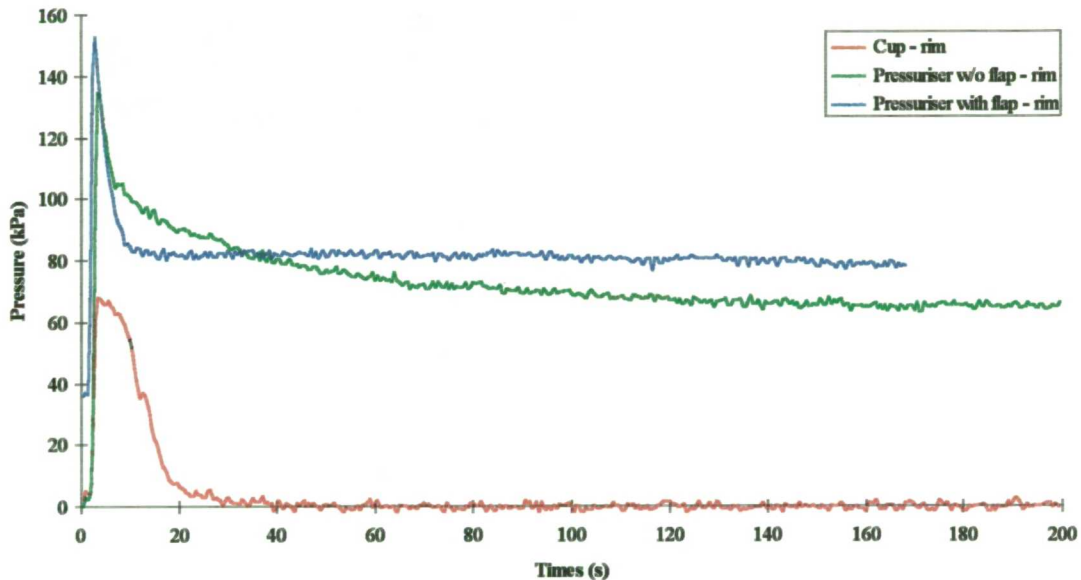


Figure 3-6: Pressure measured at the rim of the acetabulum.

With the pressuriser with no flap, the pressure measured at the pole was similar to that generated by cup insertion. The pressure at the rim was, however, much higher than that produced by cup insertion and comparable to the pressure at the pole. As with cup insertion, the peak pressure was reached almost immediately. A relatively rapid fall off to a plateau then occurred as the bevelled leading edge of the pressuriser head wedged into the rim of the acetabulum. During this time there was some leakage of cement from the rim and the transverse ligament notch. The pressure then dropped very gradually for the remainder of the test. Some leakage, from the transverse ligament notch only, continued for most of the test.

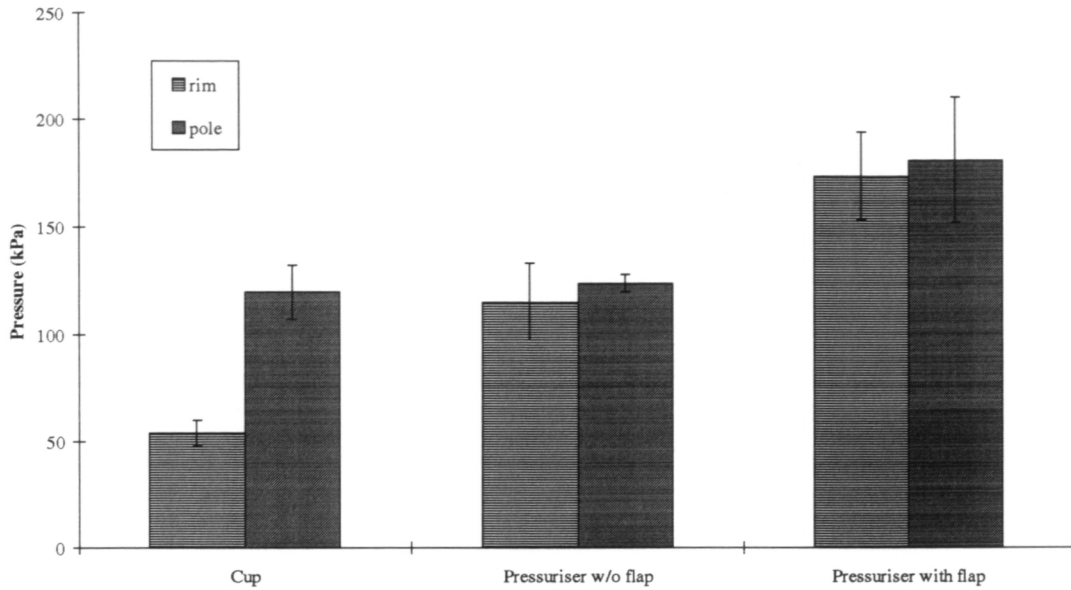


Figure 3-7: Peak pressures recorded. (Error bars represent 1 standard deviation).

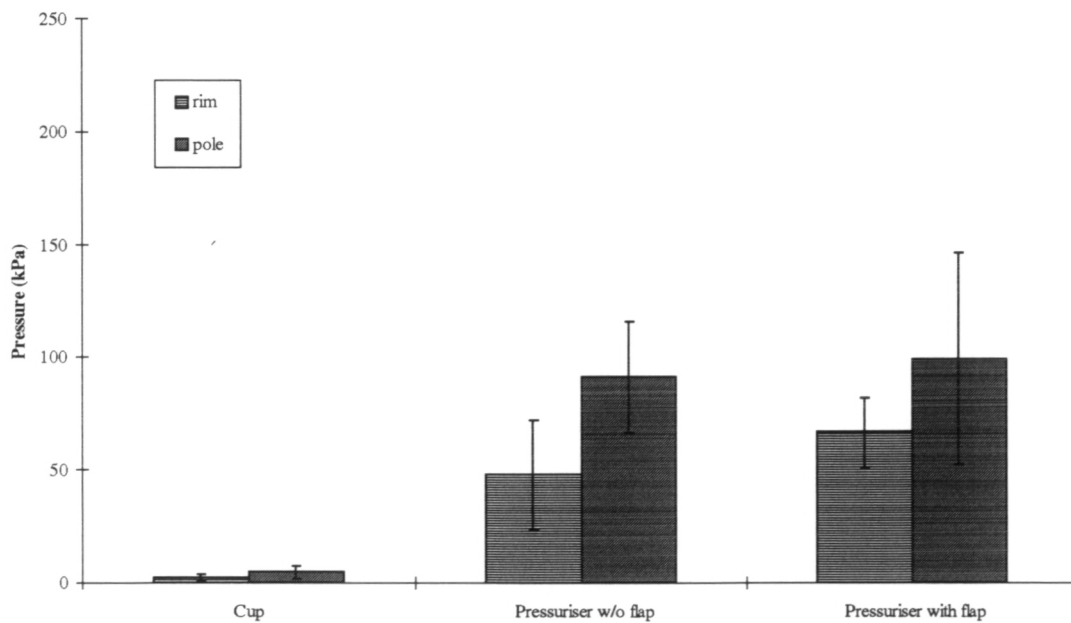


Figure 3-8: Mean pressures recorded. (Error bars represent 1 standard deviation).

The addition of the flap to prevent cement leakage through the transverse ligament notch further increased both the peak pressure and the plateau pressure. The flap reduced the initial leakage and visual observation showed the flap was indeed effective in preventing cement flow through the transverse ligament notch. Significantly, the rim pressure and pole pressure were similar when either pressuriser variant was used. The pressuriser with flap showed the highest peak pressure, of the

order of 180 kPa, at both the pole and the rim. The highest sustained pressure (80-90 kPa) was also produced with this device.

Statistical analysis of the peak pressure data at the pole and rim was performed using Student's *t*-test. At the pole, there was no significant difference between the cup and the pressuriser without flap ($p = 0.6$), but the pressuriser with flap produced significantly higher pressure than both the cup alone ($p = 0.035$) and the pressuriser without flap ($p = 0.036$). At the rim, the pressuriser with flap produced greater pressures than the pressuriser without a flap ($p = 0.021$) which in turn was greater than the pressure with the cup alone ($p < 0.005$).

Similar analyses for the mean pressures showed that at the pole mean pressures for both the pressuriser without flap ($p < 0.005$) and with flap ($p = 0.025$) were significantly higher than those for the cup. There was no statistical difference between the two designs of pressuriser. At the rim the pressuriser without flap ($p < 0.032$) and with flap ($p < 0.005$) were significantly higher than those for the cup. Again the difference between the two pressuriser designs was not statistically significant.

3.2.3.2 Manual Control

Figure 3-9-Figure 3-15 show plots of pressure vs. time from mixing for use of the UJR1, UJR2, Exeter and the Bernoski pressurisers, insertion of the "Ogee" flanged cup and the finger packing and hand pressurisation techniques respectively, as measured at the pole and the rim of the model acetabulum whilst using CMW 1 cement. The curves had substantially the same shape with CMW 3 cement. Mean pressures and peak pressures averaged for the three tests with each technique/cement combination are shown in Figure 3-16 to Figure 3-19. The mean pressure was obtained by numerically integrating the positive portions of the pressure time curve using the trapezium rule and dividing by the corresponding pressurisation time.

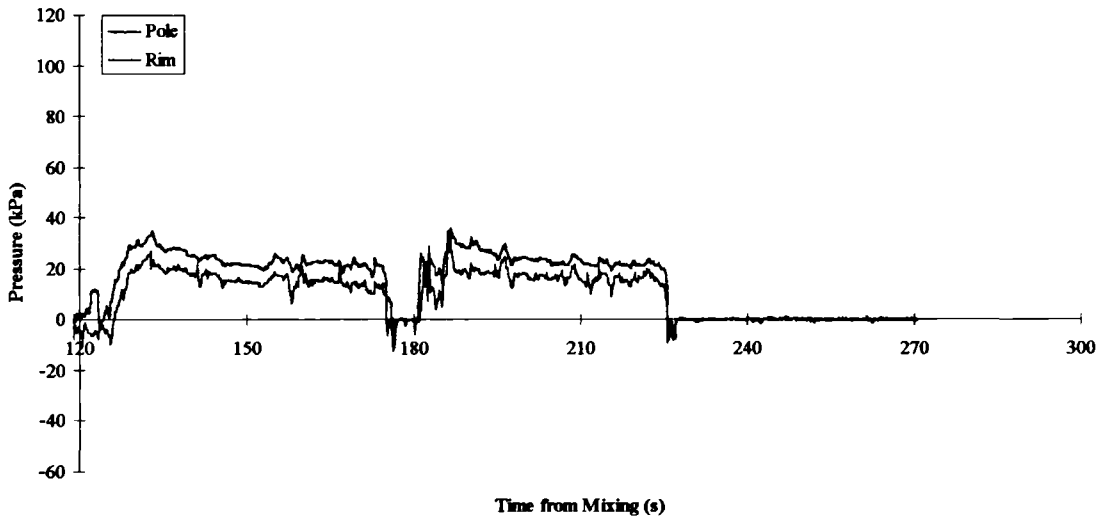


Figure 3-9: Pressure recording, UJR 1 pressuriser.

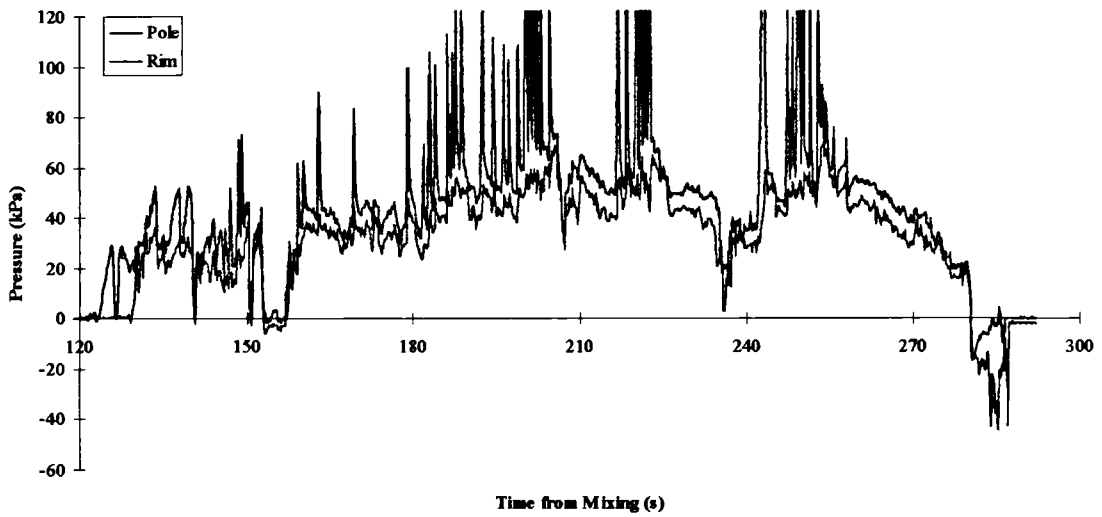


Figure 3-10: Pressure recording, UJR 2 pressuriser.

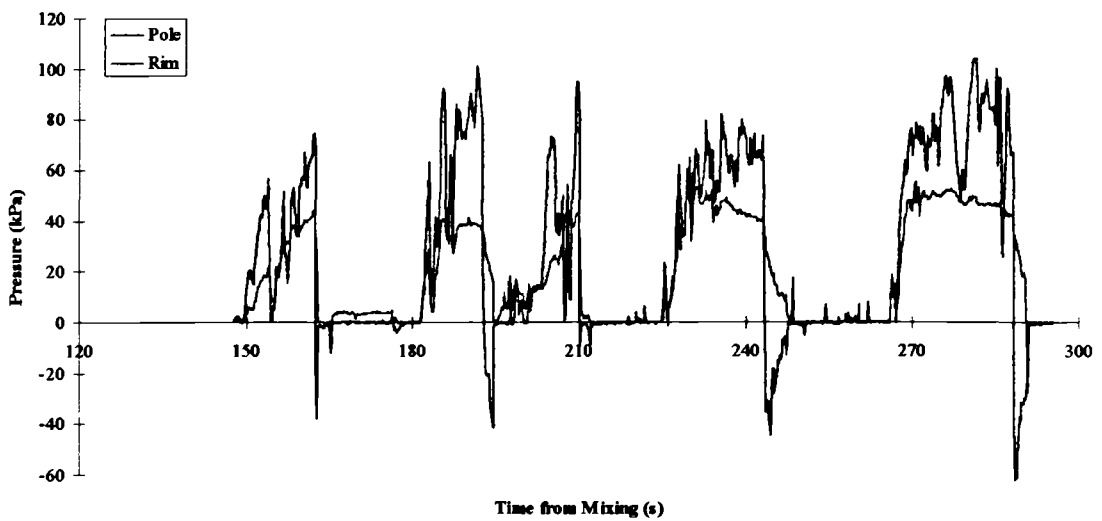


Figure 3-11: Pressure recording, Exeter pressuriser.

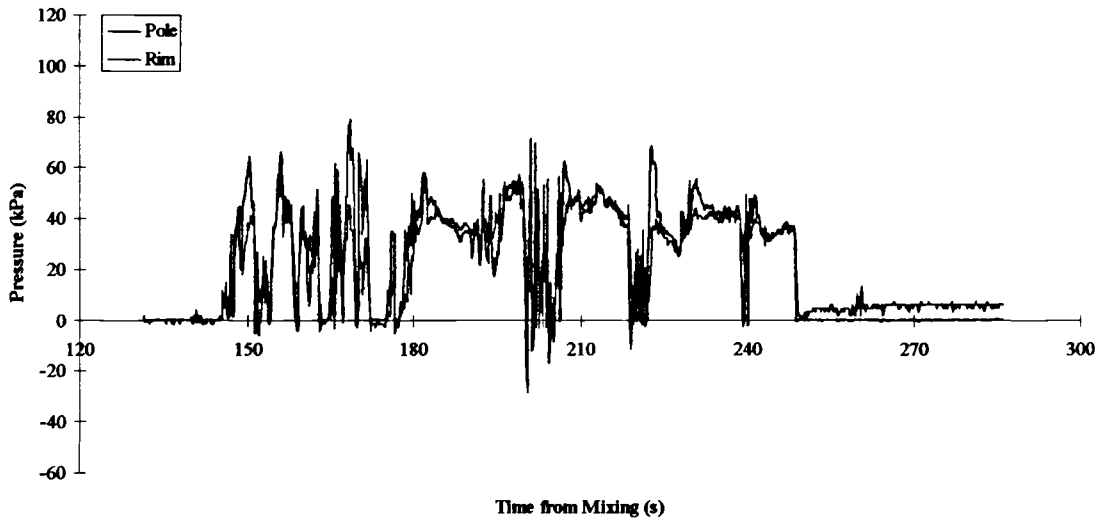


Figure 3-12: Pressure recording, Bernoski pressuriser.

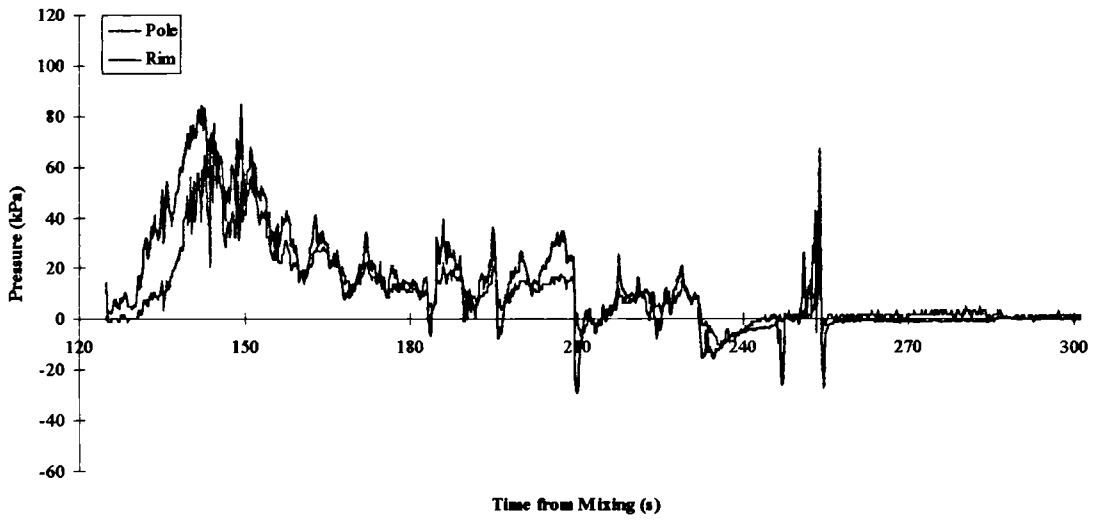


Figure 3-13: Pressure recording, "Ogee" flanged cup.

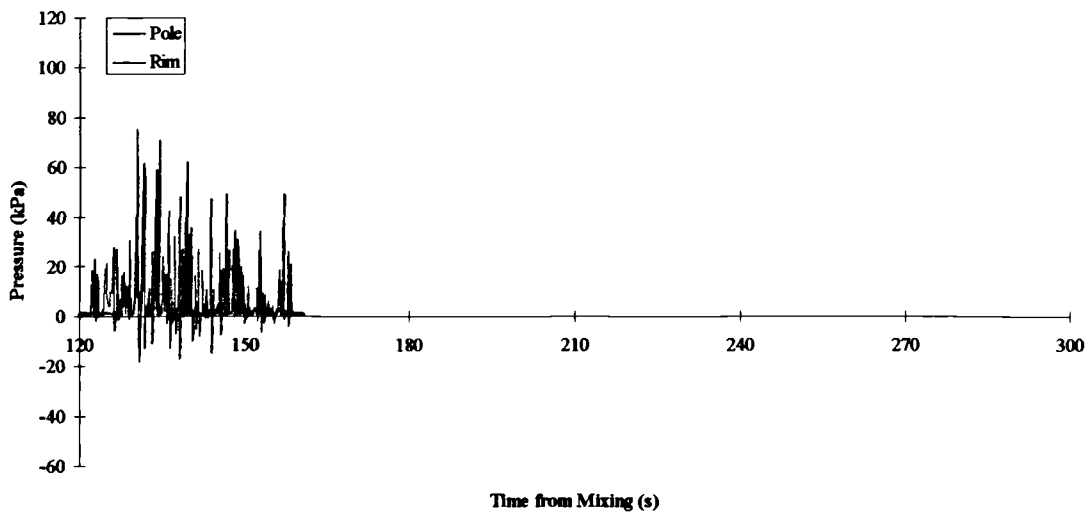


Figure 3-14: Pressure recording, finger packing.

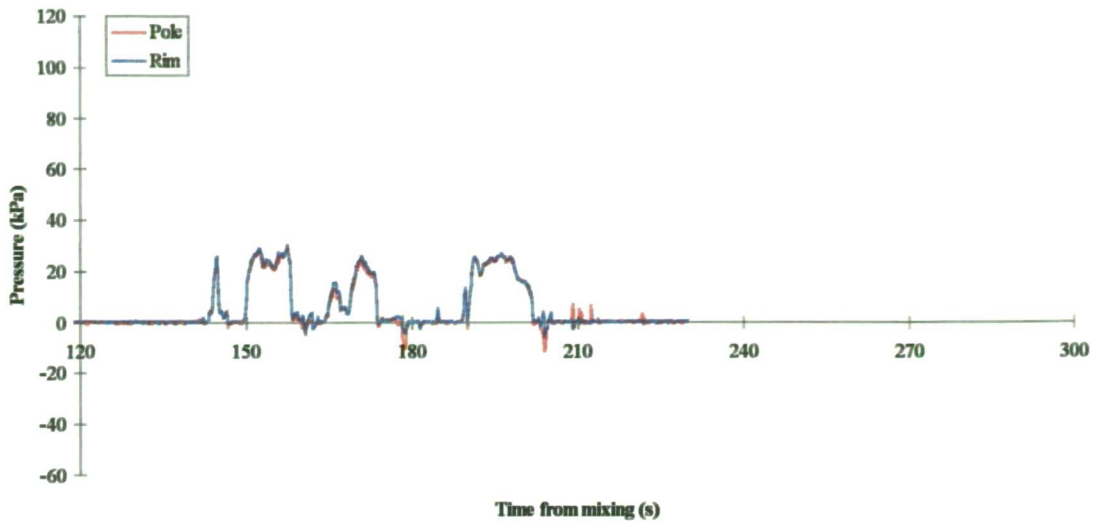


Figure 3-15: Pressure recording, hand pressurisation technique.

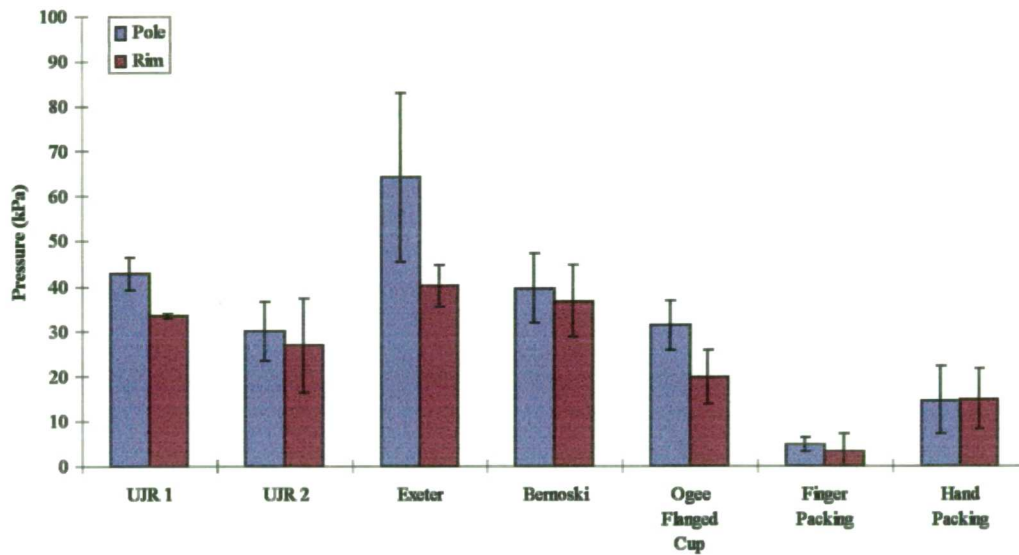


Figure 3-16: Mean pressure for various cementation techniques - CMW 1 cement. (Error bars represent 1 standard deviation).

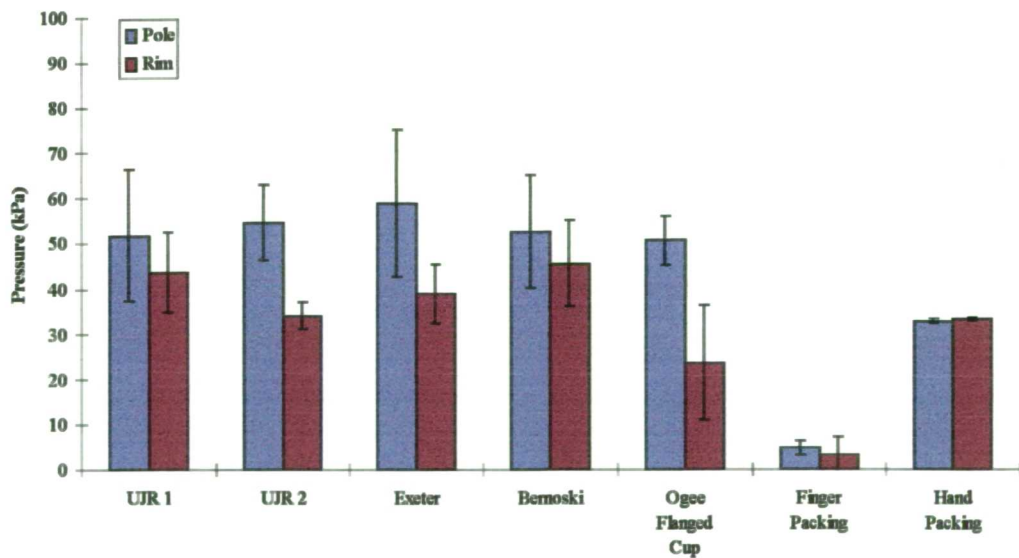


Figure 3-17: Mean pressure for various cementation techniques - CMW 3 cement. (Error bars represent 1 standard deviation).

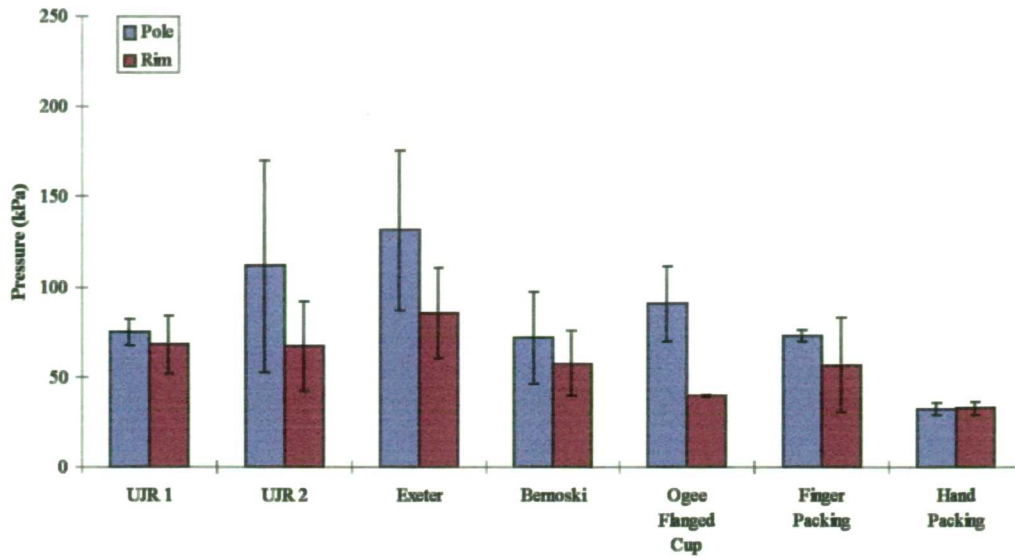


Figure 3-18: Peak pressure for various cementation techniques - CMW 1 cement. (Error bars represent 1 standard deviation).

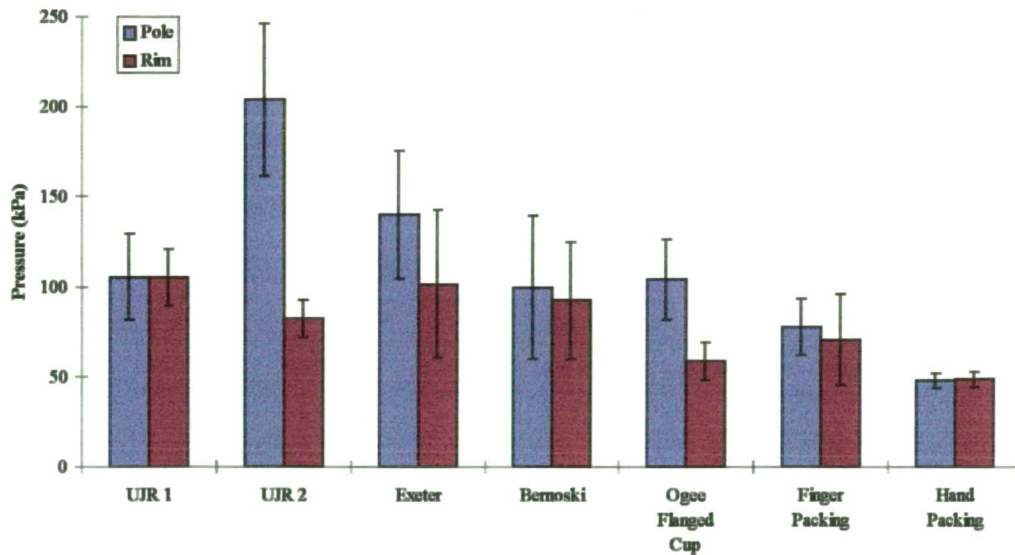


Figure 3-19: Peak pressure for various cementation techniques - CMW 3 cement. (Error bars represent 1 standard deviation).

Statistical analysis of the mean and peak pressures at the rim and pole for the two cements was performed using Student's *t*-tests, although due to scatter and the small number of observations in each group the validity of the analysis is in question. Those comparisons which showed statistically significant differences at the $p = 0.05$ level are shown in Table 3-1.

**Table 0-1: Comparisons showing statistically significant differences at the $p = 0.05$ level.
Numbers are p values for the comparisons.**

	Mean Pressure, Pole						Peak Pressure, Pole			
	CMW1			CMW3			CMW1	CMW3		
	Finger Packing	Hand Packing	Finger Packing	Finger Packing	Hand Packing	Hand Packing	Hand Packing	UJR 2	Finger Packing	Hand Packing
UJR 1	0.000	0.012	0.010				0.008	0.046		
UJR 2	0.016		0.001						0.016	0.028
Exeter	0.011		0.009							
Bernoski	0.002	0.038	0.003							
Flanged Cup	0.003		0.001	0.043						
Finger Packing				0.000			0.001			

	Mean Pressure, Rim						Peak Pressure, Rim		
	CMW1			CMW3			CMW3		
	Flanged Cup	Finger Packing	Hand Packing	Finger Packing	Hand Packing	Hand Packing	Hand Packing	Hand Packing	Hand Packing
UJR 1	0.000	0.000	0.018	0.004				0.029	
UJR 2				0.001				0.041	
Exeter	0.010	0.001	0.022	0.002					
Bernoski	0.039	0.003		0.002					
Flanged Cup		0.026							
Finger Packing					0.002				

There were no statistically significant differences in mean pressure between any of the pressurisers and only between UJR1 and UJR2 with CMW3 cement was there a statistically significant difference in peak pressure. With the exception of the flanged cup at the rim with CMW3 and hand packing at both locations with CMW1, mean pressures were higher for all the alternative techniques than for finger packing.

All four pressurisation tools were able to produce sustained cement pressurisation at both the pole and the rim of the acetabulum. The mean pressures were comparable for all except UJR 2 with CMW1 cement (discussed in detail in the final paragraph of this section). The consistently lower pressures recorded at the rim reflect slight leakage of the cement and loss of hydrostatic pressure with all the devices. The mean pressures were similar to those achieved with machine control.

High pressure spikes were seen on all the traces but in particular with UJR 2 with CMW3 cement where transient pressures at the pole reached 200 kPa. In general the spikes were higher at the pole than the rim. In the case of UJR 2, these spikes were coincident with pulls on the trigger of the cement gun, which would be expected to produce high transient pressures in the region of the cement exit hole of the pressuriser, located directly above the pole transducer. A comparable effect was seen with the Exeter pressuriser. In some cases, a combination of cement leakage and the flexibility of the balloon seal allowed this device to behave like a piston in a cylinder bore and hence generate high, but transient pressures. Occasionally this pistoning effect led to “bottoming out” of the Exeter pressuriser, which made re-packing of the cement necessary.

Peak pressures with finger packing and hand packing were low, but in the same range as the other techniques. Mean pressures for finger packing were very low, however, due to the transient nature of the technique (Figure 3-14).

All methods showed higher pressures at the pole than at the rim, indicating pressure gradients in the cement. During cup insertion, the difference between pole and rim pressures was usually the greatest.

The repeatability of pressurisation showed considerable variation between the devices. Strict control of the experiments was deliberately avoided to replicate the variability inherent in the use of such devices during an operation. The experiments using

machine control showed better repeatability (Bernoski *et al.*, accepted). With this in mind, the Exeter pressuriser with both cements and UJR 2 with CMW1 cement showed the greatest range of trace to trace variation in peak pressure. This was approximately reflected in the mean pressure. These observations may reflect the difficulty in fully visualising the acetabulum, in particular the regions of cement leakage, with the Exeter device. Overall, UJR 1 with CMW1 cement and UJR 2 with CMW3 cement showed the least variation.

Negative pressure spikes were seen on removal of all the devices from the cement. The effect was much more pronounced if the device was removed at an early stage as, for example, when re-packing the cement was required with the Exeter device. This problem was worst with UJR 2, which as a prototype was made from materials with higher adherence to the partly cured cement than the elastomers used for the other devices. With the devices manufactured from elastomeric materials, the general appearance of the cement mass in the acetabulum suggested clean separation of the pressuriser head from the cement.

CMW3 cement seems to offer a slight advantage in both peak and mean pressure when used in the manner described. As used here, with a cement gun, CMW3 cement was much easier to handle because of the extended time at relatively low viscosity. It was difficult to fill the acetabulum by extrusion of CMW1 from the cement gun at only two minutes from mixing in comparison with CMW3 at four minutes. Subsequent pressurisation of CMW1 using UJR 2 was also impaired. Both of these problems, however, are simply consequences of the difficulty of extruding cement through the relatively long, small bore delivery nozzle used in this prototype design.

3.2.4 Discussion

The increasing rate of late acetabular component failure is causing clinical problems (section 2.4). Since the early 1970's pressurisation has been known to improve "interlock" by causing penetration of cement into cancellous bone and thus increasing the strength of the bone-cement interface (Krause *et al.*, 1982a; Askew *et al.*, 1984; Mann *et al.*, 1997). Cement penetration of 3-5 mm is believed to be the optimum (Huiskes and Sloof, 1981; Krause *et al.*, 1982a; Askew *et al.* 1984; Walker *et al.*, 1984). Clinical evidence seems to support these laboratory studies in that cement

pressurisation is effective in improving the long term success of the acetabular cup (Malchau and Herberts, 1996). Surgical skill and experience also seem to contribute significantly and the “average” orthopaedic surgeon can expect worse results than those in specialised centres (Malchau *et al.*, 1993). Simplification of the technique of cement pressurisation may increase the reproducibility of the procedure: rather than concentrating on improving the best results, it may be more important to improve the worst.

The optimum technique for achieving the required cement penetration is unknown. Pressurisation of cement is easier in the femur than in the acetabulum. In the femur simply inserting the prosthesis into the cement filled intramedullary canal generates peak pressures of 220 kPa (Davies and Harris, 1993). Achieving such pressures in the acetabulum is rather more difficult, owing to its geometry. Cement penetration depends on factors that are (partially) under the surgeon’s control, such as cement viscosity, preparation of the bone bed and insertion force if using a flanged cup as a pressurisation device (Chapter 4), and those which are not, such as bone porosity and bleeding pressure. From the studies of Askew *et al.* (1984) and Juliusson *et al.* (1994) it appears that relatively short pulses (5-10 seconds) of elevated pressure are as effective as sustained pressure in realising cement penetration. The literature suggests that short duration peak pressures of 75-100 kPa are sufficient to achieve the required cement penetration into a clean cancellous surface. The results of Noble and Swarts (1983) indicate pressures of 35-50 kPa sustained for 30-60 seconds produce near optimal cement penetration into thoroughly cleaned low density cancellous bone. Short high pressure pulses need to be superimposed on a sustained background pressure to avoid displacement of cement by blood pressure or possibly elastic recovery of the cement. Pressure above 5 kPa (37.5 mmHg) would seem to be sufficient to resist these effects (Shelley and Wroblewski, 1988). Juliusson *et al.* (1995) found that the presence of blood in the cancellous spaces before pressurisation began reduced penetration by 50% and explained this strong influence of circulation by the incompressibility of the trapped fluid. This is likely to be the reason why thorough cleaning of the bone bed produces dramatic effects on cement penetration.

In these experiments, machine controlled insertion of an acetabular cup produced peak pressures of 120 kPa at the pole and 55 kPa at the rim. This compares with the 106

kPa peak pressure measured by Beverland *et al.* (1993) at the pole of a simulated (non-hemispherical) "revision" acetabulum using an unflanged cup and an insertion force of approximately 100 N and a peak pressure of 6 kPa reported by Shelley and Wroblewski (1988) for an unflanged cup with an insertion force of approximately 80 N. Of the two variations of the Bernoski pressuriser tested using machine control, that incorporating a flap to seal the cotyloid notch was the most effective in increasing the magnitude of both the peak pressure (180 kPa) and the sustained pressure (80-90 kPa). The rim pressure and pole pressure were nearly equal when either of the two variations were used. The absence of the flap would be expected to allow cement to pour through the cotyloid notch and indeed some leakage was observed. If the rim transducer had been closer to the acetabular notch, it is expected that the measured pressure would have been lower, since the flow from the acetabular notch indicates a local cement pressure gradient in this region. However, the cotyloid notch of the model acetabulum was wide and shallow and could be partially sealed even by a pressuriser without flap. If an acetabulum with a deep notch had been used, as can occur in some patients, the effect of the flap might have been even more pronounced.

Manual cup insertion generated transient pressurisation that, while of longer duration than with machine control, showed similar characteristics with a relatively rapid rise to a peak pressure followed by more gradual decay. Under manual control the profile could be modified by the surgeon by increasing force on the cup inserter in the latter stages, but this technique could also result in cup mal-position and in the worst case direct contact between cup and bone. With this method, there may be a conflict between effective cement pressurisation and control of position of the cup.

Technique was important for all the devices in determining the pressures measured. The various large spikes visible on many of the traces occurred when a conscious effort was made to push harder, with a "pistoning" motion, on the pressurising device. In separate tests where the surgeon viewed the pressure display on the computer screen, greater control over the pressure was possible.

A common clinical technique relies on finger packing of the cement into the bone followed by impaction of the acetabular cup. Although finger packing has previously been shown to generate reasonable pressures, especially in fixation holes drilled through the subchondral plate, laminations may be introduced into the cement and

pressurisation is likely to be patchy (Oh *et al.*, 1983). The present results showed finger packing to be ineffective in maintaining mean pressure in comparison to all the other methods.

The design of a device to achieve a closed cavity is complicated by the irregular acetabular rim and particularly the presence of the cotyloid notch. With the exception of UJR 2, which is a cement injection device based on a cement gun, all the pressurisers had a compliant head designed to deform under load and seal the acetabulum, thus confining the cement. Thus it is not surprising that no clear-cut advantage was demonstrated for any particular device. All the pressurisation tools demonstrated sustained cement pressurisation at both the pole and the rim of the model acetabulum. The highest peak pressure was obtained with UJR 2 and CMW3 cement, the highest mean pressure with the Exeter pressuriser and CMW1 cement. Overall, UJR 1 with CMW1 cement and UJR 2 with CMW3 cement showed the least variation of the tested combinations. UJR 1 is one of the simplest designs imaginable, which makes it “user friendly”. The Exeter pressuriser, for example, is a rather complex device with which practical difficulties, mainly fluid leakage from the balloon seal, are often experienced. Its use typically results in somewhat uneven pressurisation of cement due to the pistoning effect mentioned above.

The significance of fixation at the rim of the acetabulum has not been addressed in the literature. While pressurisation of cement into cancellous bone has been shown to increase the strength of the bone cement interface (Krause *et al.*, 1982a; Eftekhar and Nercessian, 1988; Lavernia *et al.*, 1988; Kuivila *et al.*, 1989; Ober *et al.*, 1989), it is usual, depending on surgical technique, for only part of the reamed acetabular surface to be cancellous. The peripheral non-cancellous areas do not readily accept cement, although fixation holes may be drilled through the subchondral plate near the rim to expose cancellous bone. In these areas cement pressurisation may serve to drive out trapped blood, marrow and air and hence ensure intimate contact of cement and bone. It seems that secure fixation is necessary in the periphery of the acetabulum, in particular in the region of the ilium (Charnley zone 1) where radiolucencies are most commonly observed on anterior-posterior X-rays and where stresses at the interface with an implanted acetabulum are highest (Dalstra and Huiskes, 1995; section 5). Improved rim fixation may also help prevent the ingress of wear debris to the back of

the acetabulum which is considered by some to be the major factor in acetabular loosening (Schmalzried *et al.*, 1992).

3.3 Per-operative Cement Pressurisation Measurements

An instrumented pressuriser has been designed to allow the per-operative measurement of acetabular cement pressurisation. Measurements made at sixteen primary hip replacement operations are described and compared to the *in vitro* work described above.

3.3.1 Design and Testing of the Instrumented Pressuriser

The instrumented pressuriser is a modification of UJR 1 described above (Figure 3-2). The principal modification is the inclusion of a pressure transducer mounted in the adapted pressuriser backing plate and protruding through a central hole in the elastomer pressuriser head (Figure 3-20). Cooling the elastomer head in liquid nitrogen facilitated the machining of the transducer hole and the counter-bore to accommodate the boss on the backing plate. The sensing diaphragm of the transducer is positioned slightly interior to the surface of the pressuriser head to provide it with some mechanical protection. The mounting configuration ensures that spurious strains are not produced in the sensing diaphragm by contact with rigid materials.

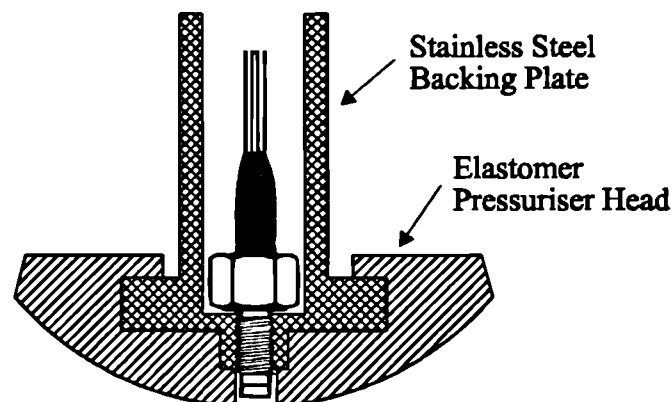


Figure 3-20: Detail of pressure transducer mounting in the instrumented pressuriser.

3.3.1.1 Pressure Transducer and Data Acquisition System

A flow diagram of the data acquisition system is shown in Figure 3-21.

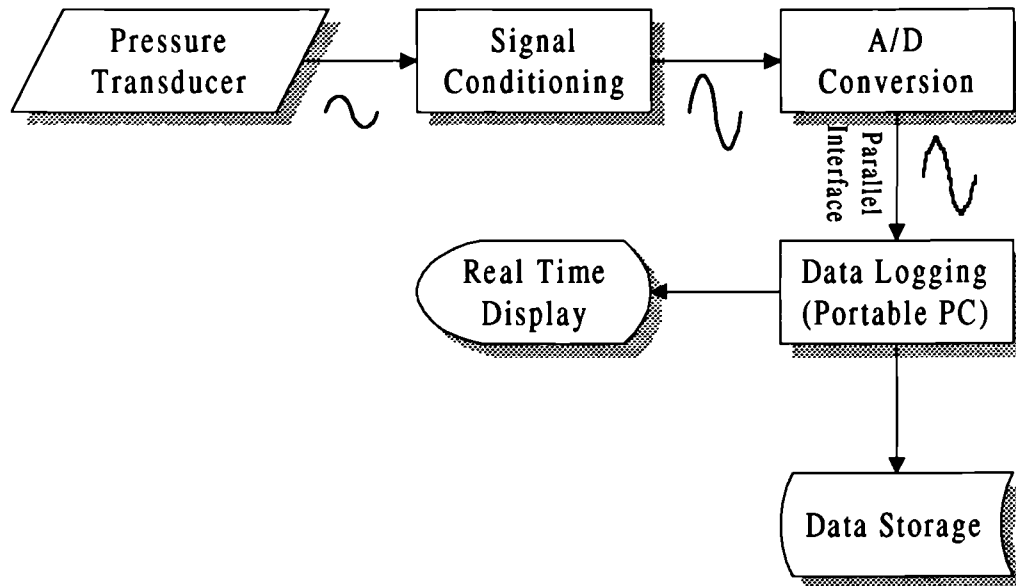
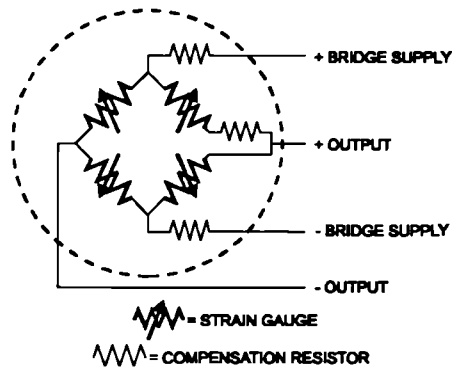
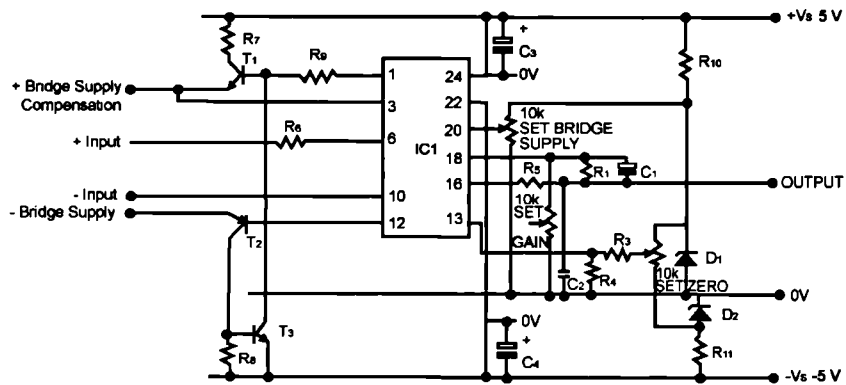


Figure 3-21: Flow diagram of data acquisition and storage scheme.

The pressure transducer (EPX series, Entran Ltd, Watford, U.K.) is a strain gauged diaphragm type, the strain gauges being connected in a full Wheatstone bridge configuration (Figure 3-22 (a)). To permit sterilisation, the transducer was factory sealed at one atmosphere pressure, the leads given a waterproofing treatment and extended to 2 metres in length. The transducer is temperature compensated in the range 20°C to 80°C and performs to the same specifications described in section 3.2.2.1. Signal conditioning was by a standard strain gauge amplifier (RS Components, Corby, U.K.) (Figure 3-22 (b)), for which a regulated power supply was provided by a custom circuit operated by two 9 volt PP3 batteries (Figure 3-22 (c)). The output of the strain gauge amplifier was connected to a 10 bit analogue-to-digital converter (PICO ADC-11, Pico Technology, Cambridge, U.K.) interfaced to a portable computer (386SX-20, Sanyo Ltd, Watford, U.K., running Microsoft DOS 5.0) via the parallel port. Custom written software was used to log the data and display it in real time. All the electrical components of the system were powered by batteries to minimise the electric shock risk to the patient. Battery operation provides a floating power supply (no ground connection) and hence ground leakage currents, as described in British Standard 5724 Section 1.1 Part 1 (1992), cannot flow. Indeed any current flow through the patients tissues requires at least a dual fault condition with both transducer bridge supply wires broken.

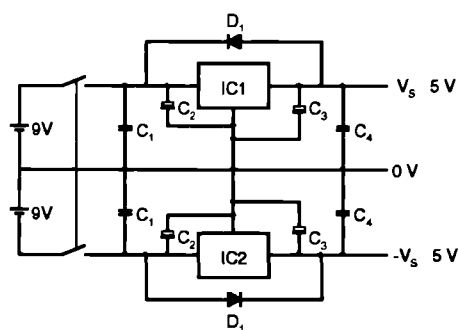


(a)



- | | | |
|---------------------------------|------------|-------------|
| C1 = 100nF | R4 = 2.2kΩ | R10 = 680Ω |
| C2 = 10nF | R5 = 10Ω | R11 = 680Ω |
| C3 = 10μF | R6 = 100Ω | T1 = BD 135 |
| C4 = 10μF | R7 = 47Ω | T2 = BD 136 |
| R1 = 100kΩ | R8 = 10Ω | T3 = BC 108 |
| R3 = 100Ω | R9 = 1kΩ | D1 = 1N827 |
| D2 = 1N827 | | |
| IC1 = RS Strain Gauge Amplifier | | |

(b)



- | | |
|-------------|-------------|
| C1 = 100nF | C3 = 10μF |
| C2 = 10μF | C4 = 100nF |
| D1 = 1N4001 | IC1 = 78L05 |
| IC2 = 79L05 | |

(c)

Figure 3-22: Components of the instrumentation.
 (a) strain-gauged-diaphragm pressure transducer, (b) strain gauge amplifier. (c) power supply.

The assembled apparatus is shown in Figure 3-23.



Figure 3-23: The instrumented acetabular cement pressuriser and recording apparatus.

3.3.1.2 Calibration and Testing

To test the system, acetabular cementing was simulated using the instrumented acetabulum described in section 3.2.2.2. Simultaneous computer recordings were made to compare the outputs of the pressure transducer in the pressuriser and those in the acetabulum. Three runs were made using CMW 3 cement mixed according to the manufacturers instructions and delivered to the acetabulum at 4 minutes from mixing, whereupon pressurisation was commenced. The data from a typical run are shown in Figure 3-24. It can be seen from these plots that the pole pressure is most comparable to the pressuriser pressure. This was expected since in use the pole of the device was in the pole of the acetabulum. The device is thus likely to give a reliable measure of pole pressure in the acetabulum per-operatively. Section 3.2.3.2 showed that the pole pressure is a reasonable measure of the overall pressurisation of cement, particularly for the device (UJR1) on which the instrumented pressuriser is based.

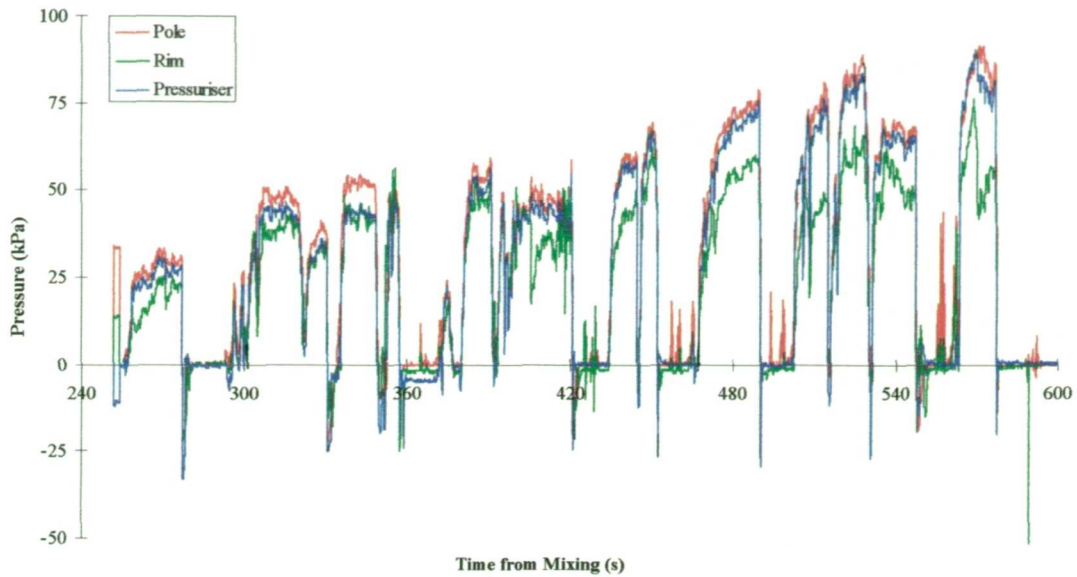


Figure 3-24: The instrumented pressuriser tested in the instrumented acetabulum.

3.3.2 Methods

The components of the pressuriser handle, the pressuriser head and the transducer were double packed and autoclave sterilised on a low temperature (120°C) programme to comply with the maximum temperature allowed for the pressure transducer. During the operation, the components were unpacked aseptically and assembled by a scrubbed assistant. When required the assembly was handed to the surgeon for trial positioning (Figure 3-25). Once the trial was complete and the surgeon was satisfied with the size of pressuriser head, the electrical connection for the pressure transducer was handed to an assistant outside the sterile field and plugged into the amplifier and computer ready for data collection. The electronics were switched on at least five minutes before use to ensure thermal equilibrium had been reached and there would be no amplifier drift during measurement. Palacos R bone cement was mixed using the CEMVAC vacuum mixing apparatus and syringed into the surgeon's hand at 1 to 2 minutes from mixing according to preference. The operating theatre was at a constant temperature of 21°C. During the mixing time the pressure reading from the transducer was adjusted to zero under software control. The surgeon then introduced the cement to the acetabulum and commenced use of the device (Figure 3-26). Pressurisation was typically continued for 1 minute before the pressuriser was removed and a Charnley flanged acetabular prosthesis inserted. Load was maintained on the prosthesis until the cement was judged to have set, approximately ten minutes

from mixing. Two senior surgeons, one of whom also performed the *in vitro* tests described earlier, performed all the operations. Details of the patient group, who all received Charnley total hip replacements for osteoarthritis, are shown in Table 3-2. The average age at operation was 63 years and there were 10 men and 6 women.

Table 3-2: Details of patients for the per operative cement pressure measurements. The “head” column gives the diameter of the elastomer pressuriser head used in mm.

Patient	Age	Sex	Surgeon	Hip	Head	Comments
MK	51	M	2	Ⓛ	63	
EJ	75	M	2	Ⓡ	63	
EH	66	F	2	Ⓛ	63	
BG	75	F	2	Ⓛ	50	Protrusion acetabulum, bone graft used
JR	74	F	2	Ⓡ	50	
BH	77	F	2	Ⓛ	63	
RT	62	M	2	Ⓛ	50	
PH	64	F	2	Ⓡ	50	
EW	54	F	2	Ⓛ	50	Surgeon unhappy with choice of head size
NJ	72	F	2	Ⓡ	50	
RH	69	F	1	Ⓡ	50	
GR	69	F	1	Ⓛ	50	
ED	81	F	1	Ⓛ	50	
DB	73	M	1	Ⓛ	50	Right (contralateral) hip arthodesis
RM	37	M	1	Ⓛ	50	Right (contralateral) hip osteotomy
CJ	62	M	1	Ⓛ	50	

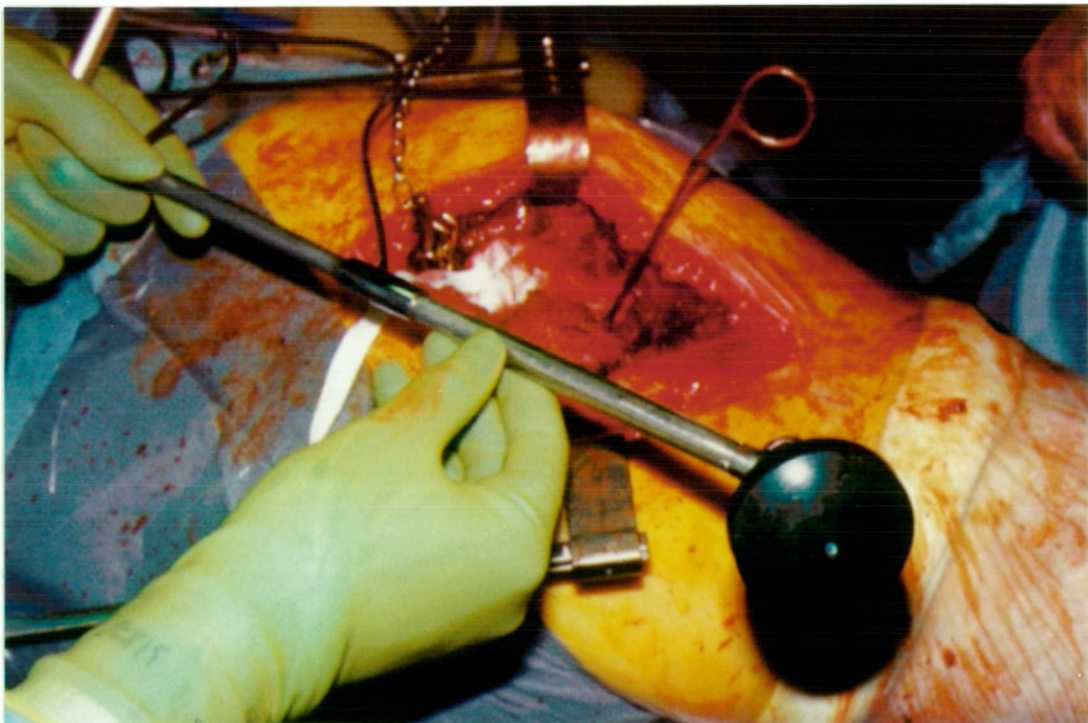


Figure 3-25: The instrumented pressuriser.

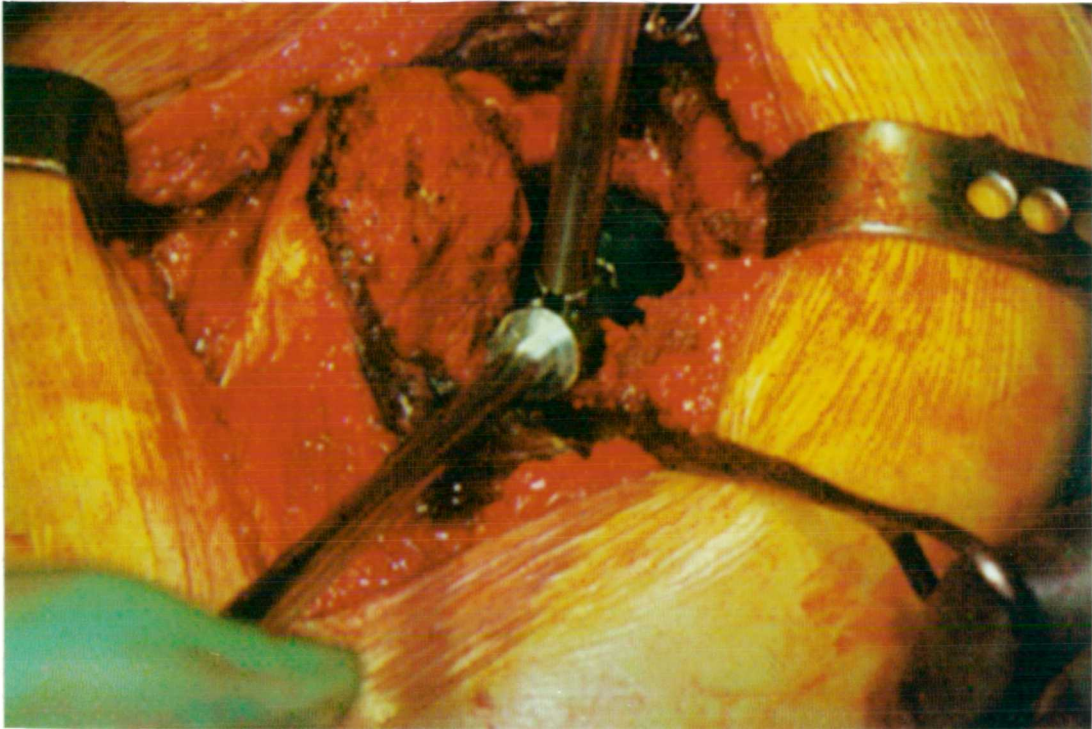


Figure 3-26: The instrumented cement pressuriser in use.

3.3.3 Results

Figure 3-27 is an example of the pressure traces obtained per-operatively. The initial flat portion of the curve between 80 and 90 seconds from mixing represents the pressure signal before software “zeroing” and demonstrates the stability of the transducer output. At the onset of pressurisation, seating of the pressuriser in the acetabulum generated a transient pressure spike, followed by a rapid rise to a high value on commencement of the major pressurisation effort. On removal of the device from the cement, negative pressure spikes were observed, particularly if early re-packing of cement was necessary due to excessive leakage. However the general appearance of the cement mass in the acetabulum suggested clean separation of the pressuriser head from the cement. It appeared that the negative spikes were due to adherence of the cement to the diaphragm of the transducer rather than being an indication of a vacuum effect or adherence of the cement to the pressuriser head itself.

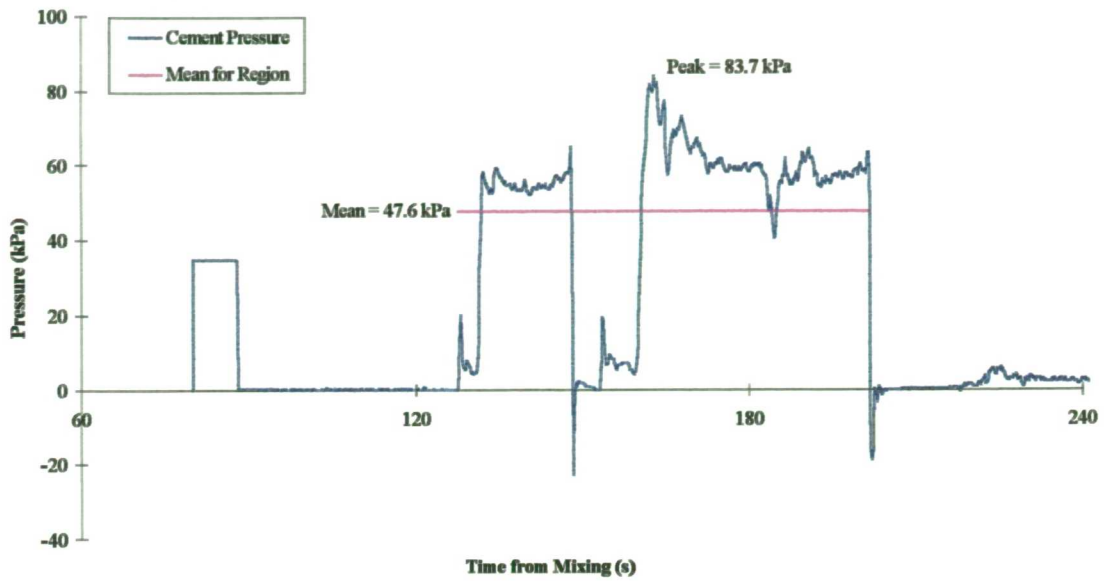


Figure 3-27: Representative per-operative pressure recording.

The mean (calculated as described in section 3.2.3.1) and peak cement pressures for a total of 16 operations performed by the two orthopaedic surgeons are shown in Figure 3-28. There was no significant difference between either the peak or mean pressures for the two surgeons at the 5% level (two tailed t-test assuming unequal variances).

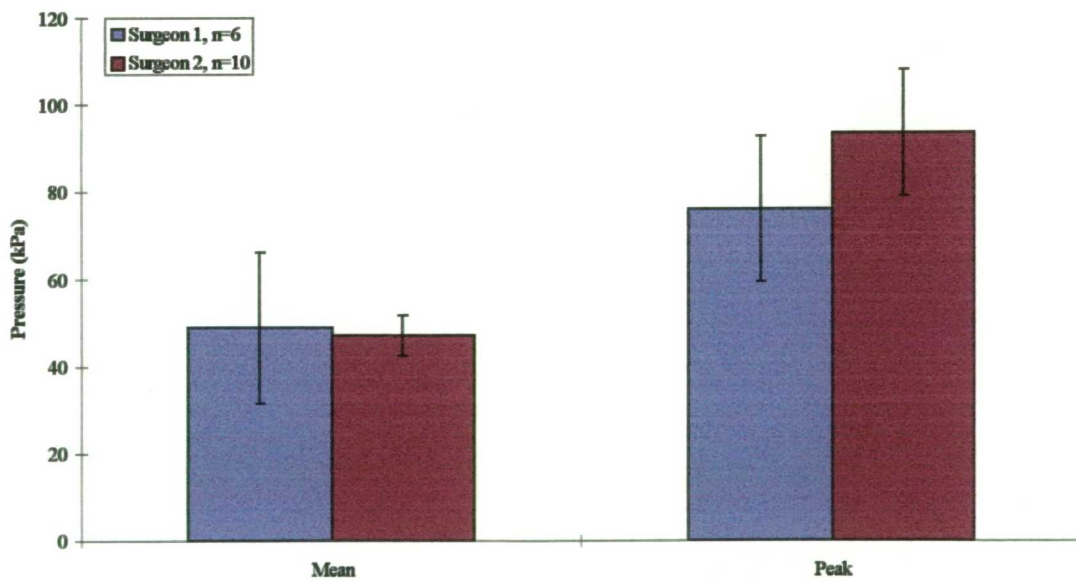


Figure 3-28: Mean and peak per operative cement pressures.

A typical post operative X-ray appearance is shown in Figure 3-29. No obvious radiolucencies are visible on this radiograph.



Figure 3-29: Post operative radiograph after use of the instrumented pressuriser.

3.3.4 Discussion

The per-operative measurements are useful for several reasons. Since the pressurisation required for optimal cement penetration into thoroughly cleaned low density cancellous bone is reported to be of the order of 35-50 kPa for 30-60 seconds (Noble and Swarts, 1983), the present data show that this can be attained *in vivo* using a simple and inexpensive device. Although the surgeon did not observe the measured cement pressure per-operatively, the feedback provided to the surgeon by reviewing the pressure measurements post-operatively with regard to his own cementing technique was felt to be useful. The per-operative pressure measurements also showed satisfying agreement with the laboratory studies, validating their use for the comparison of cementing techniques. A future goal may be to perform cement pressure measurements as a fairly routine part of hip replacement operations, which would provide objective measurement of cementing quality and contribute to establishing clinically the relationships between cement pressure, radiographic appearance and the development of aseptic loosening.

3.4 Summary and Conclusions

Two series of laboratory investigations have been conducted into the efficacy of cement pressurisation techniques in the acetabulum. Initially a universal testing machine was used to control cement pressurisation by the insertion of an acetabular cup of typical design and a novel design of cement pressuriser (the “Bernoski” pressuriser) into an instrumented model acetabulum. In subsequent comparative studies of cementing techniques an experienced orthopaedic surgeon was employed to perform simulated operations in the laboratory with a similar instrumented model. Two digital cement packing techniques, cup insertion, the pressuriser used under testing machine control and two further novel pressuriser designs were compared, together with an existing “benchmark” commercial device. Finally, per-operative measurements of cement pressure were described, obtained using an instrumented pressuriser.

Under machine control, cup insertion produced transient cement pressurisation, with peak pressures of 120 kPa at the pole and 55 kPa at the rim. Of the two variations of the “Bernoski” pressuriser tested in this way, that incorporating a flap to seal the cotyloid notch was the most effective in increasing the magnitude of both the peak pressure (180 kPa) and the sustained pressure (80-90 kPa). The rim pressure and pole pressure were similar when either of the two variants were used.

Manual cup insertion generated transient pressurisation that, while of longer duration than with machine control, showed similar characteristics with a relatively rapid rise to a peak pressure followed by more gradual decay. Relying on the cup alone to pressurise cement may generate a conflict between effective cement pressurisation and control of position of the cup. Finger packing was ineffective in maintaining mean pressure in comparison to all the other methods.

The similar design, with the exception of the cement injection device UJR 2, of all the pressurisers meant no clear-cut advantage was demonstrated for any particular device, all demonstrating sustained cement pressurisation at both the pole and the rim of the model acetabulum. The highest peak pressure was obtained with UJR 2 and CMW3 cement, the highest mean pressure with the Exeter pressuriser and CMW1 cement. Per-operative pressure measurements showed satisfying agreement with the laboratory studies, validating their use for the comparison of cementing techniques.

Technique was important for all the devices in determining the pressures attained. The various large spikes visible on many of the traces occurred when a conscious effort was made to push harder, with a “pistoning” motion, on the pressurising device. In separate tests where the surgeon viewed the pressure display on the computer screen, greater control over the pressure was possible. Although the surgeon did not observe the measured cement pressure per-operatively, the feedback provided to the surgeon by reviewing the pressure measurements post operatively with regard to his own cementing technique was felt to be useful.

4. Modelling of Cement Flow During Acetabular Cup Insertion

Joint prostheses intended for use with cement can be considered as cement pressurisation devices. Since cement pressurisation with the prosthesis relies on the displacement (flow) of the fluid cement and the viscous resistance of the cement to this displacement, it is particularly suited to mathematical modelling. This chapter describes the characterisation of a representative viscosity for various commercially available bone cements and the permeability of cancellous bone, parameters which required definition for the subsequent development of a suitable modelling technique based on the finite element method. The results of benchmark finite element models and laboratory experiments have been compared to validate the modelling technique, which was then used to predict the pressurisation and consequent penetration of bone cement into cancellous bone during insertion of two representative designs of acetabular prosthesis.

4.1 Parameter Definition

4.1.1 The Rheological Behaviour of Acrylic Bone Cements by Oscillating Plate-on-Plate Rheometry

4.1.1.1 Theory

An elastic material subject to a shear strain will instantaneously develop a shear stress proportional to the shear strain, the constant of proportionality being the shear modulus. If the shear strain is made to vary in time (e.g. sinusoidally), the shear stress will vary exactly in-phase with the shear strain. For a purely viscous material subjected to the same sinusoidally varying shear strain, the shear stress varies exactly $\frac{\pi}{2}$ radians out-of-phase with the shear strain, or alternatively the shear stress is exactly in-phase with the shear strain rate. There is then a linear relationship between shear stress and shear strain rate, the constant of proportionality being the Newtonian viscosity. For a viscoelastic material, the shear stress is out-of-phase with the shear

strain by the loss angle δ ($0 < \delta < \frac{\pi}{2}$), or alternatively is displaced from the shear strain rate by the angle $\frac{\pi}{2} - \delta$. In such a material viscous flow and elastic deformation occur simultaneously. The material response of such a material can be represented by a complex number, the complex viscosity η^* where:-

$$\eta^* = \eta' - i\eta'' = \frac{\tau(t)}{\dot{\gamma}(t)} \quad \text{Equation 4-1}$$

where η' and η'' are the real and imaginary parts of the complex viscosity respectively, $\tau(t)$ is the shear stress, $\dot{\gamma}(t)$ is the shear strain rate and t is time.

The real part of the complex viscosity, η' , is a measure of the viscous contribution to the overall material behaviour, while the imaginary part, η'' , measures the elastic contribution. The ratio of the real and the imaginary parts is equal to the tangent of the phase angle between shear strain and shear stress and is used as a measure of the viscous or elastic nature of the material.

4.1.1.2 Method

The rheological behaviour of five conventional polymethylmethacrylate (PMMA) acrylic bone cements, CMW 1 and CMW 3 (DePuy CMW, Blackpool, U.K.), Palacos LV30, Palacos LV40 and Palacos R (Schering Plough, Welwyn Garden City, U.K.) and one modern copolymer formulation, Boneloc (Polymers Reconstructive A/S, Farum, Denmark), were measured using an oscillating plate-on-plate rheometer (RHEOLAB MC100 with US 200 software, Physica Meßtechnik GmbH, Germany; measurements performed by Dr Sanjukta Deb at the IRC in Biomedical Materials, QMW, London). Although Palacos LV30 and Palacos LV40 have nominally the same composition, differing in the final volume of the mix, they were treated as different cements in this study. These cements represent a broad spectrum of those in current surgical use from subjectively the lowest (Palacos LV) to highest (CMW1) viscosity. All the powder and all the liquid supplied in the manufacturer's pack were mixed in a glass beaker for 30 seconds at room temperature and a small sample (approximately 5 cm³) immediately transferred to the base plate of the rheometer. The rheometer head was lowered to give a plate to plate spacing of 1 mm and the test commenced. The temperature of the bone cement was maintained at 21.9 °C by the thermostatically controlled lower plate of the rheometer. The oscillating frequency was 1Hz with an

oscillation amplitude of 0.5% of one revolution ($\frac{\tau}{100}$). The geometry of the testing domain produced shear strain rates in the cement varying from 0 to 0.5 sec^{-1} (Appendix A).

4.1.1.3 Results

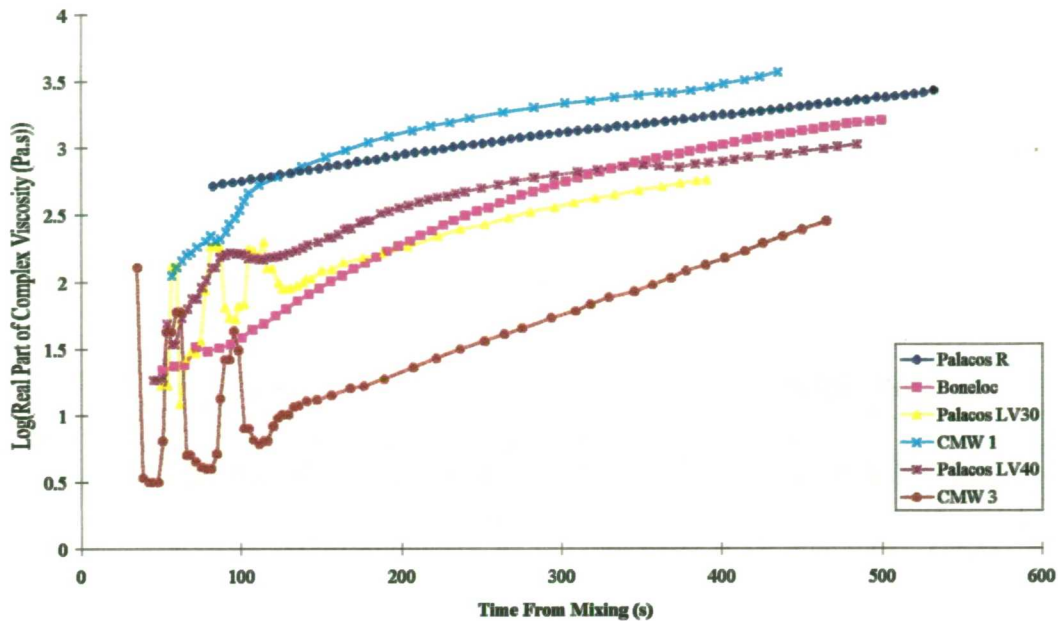


Figure 4-1: Real part of complex viscosity, η' , for commercial acrylic bone cements.

Figure 4-1 shows the real part of the complex viscosity for the six bone cements vs. time from mixing. Some cements showed an initial settling period, during which rapid changes to η' apparently occurred, but thereafter all the cements behaved similarly, with $\log(\eta')$ increasing approximately linearly with time. The conventional PMMA cements were ranked throughout the curing period, after 120 seconds, in order of increasing viscosity, CMW3, Palacos LV30, Palacos LV40, Palacos R, CMW1. Taking the rate of change of viscosity with time as a measure of the rate of cure, it can be seen that all the conventional cements have similar curing kinetics. The sixth cement, Boneloc, incorporates higher methacrylates and showed a more rapid rate of change of viscosity/rate of cure, consistent with its different chemical formulation. Linear approximations to the curves of $\log(\text{real part of complex viscosity})$ vs. time from mixing in the window from 120 to 480 seconds from mixing were made using the method of least squares. These relationships (Table 4-1) were then assumed to describe a linear (Newtonian) viscosity, η (Pa s), for the bone cement at time t (s). The

table shows slope and intercept (m and c) for the regression equation (Equation 4-2) describing the relationship between viscosity and time:-

$$\log \eta = mt + c \quad \text{Equation 4-2}$$

Viscosity can thus be recovered from these relationships by:-

$$\eta = 10^{(mt+c)} \quad \text{Equation 4-3}$$

Table 4-1: Linear relationships for log (real part of complex viscosity) vs. time.

Cement Type	Relationship			Validity
	Slope	Intercept	R ²	
Palacos R	1.53x10 ⁻³	2.63	0.993	100<t<500
Boneloc	3.44x10 ⁻³	1.62	0.957	150<t<500
Palacos LV30	2.90x10 ⁻³	1.69	0.998	150<t<350
CMW 1	1.99x10 ⁻³	2.70	0.975	150<t<400
Palacos LV40	2.04x10 ⁻³	2.12	0.917	150<t<450
CMW 3	4.20x10 ⁻³	0.49	1.000	150<t<450

Figure 4-2 shows the loss angle tan delta vs. time from mixing which gives a measure of the relative contributions of the viscous and elastic components of the material behaviour.

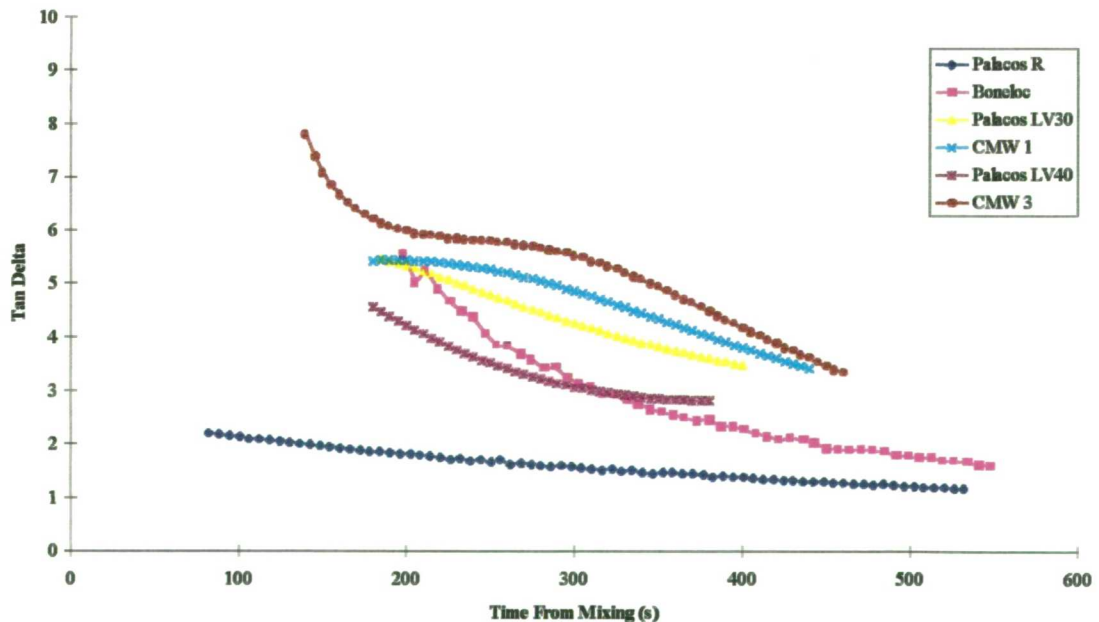


Figure 4-2: Tan delta for commercial acrylic bone cements.

The higher tan delta, the more “liquid” is the character of the material. In general there was a relatively high early rate of decrease of tan delta. For Palacos R, Boneloc and

Palacos LV40, the rate of change of tan delta decreased smoothly and towards the end of the measurement time it appeared that tan delta was approaching a constant value, in accordance with the continuing viscoelastic behaviour of the fully cured cement. The remaining cements, Palacos LV30, CMW1 and CMW3, showed similar behaviour after an intermediate period when the rate of change of tan delta was low (the slight plateaux on the curves). The ranking of the cements according to tan delta is somewhat different to the ranking according to viscosity; in descending order of tan delta, CMW 3, CMW 1, Palacos LV30, Palacos LV40, Palacos R. CMW 1 cement despite being “high viscosity”, showed anomalously low elasticity. Again the copolymer Boneloc cement behaves differently, showing a more rapid rate of change of tan delta in the central portion of the graph.

4.1.2 The Permeability of Cancellous Bone

The simplest treatment of flow through a porous medium is Darcy’s law which states that the average velocity perpendicular to a section through a block of porous material is proportional to the pressure gradient perpendicular to the section with a constant of proportionality k , called the permeability, viz:-

$$v_x = \frac{Q}{A} = \frac{-k}{\eta} \frac{dP}{dx} \quad \text{Equation 4-4}$$

where v_x is the velocity perpendicular to the section, Q is the volumetric flow rate, A is the area of the section, η is the fluid viscosity, P is pressure and x is the spatial co-ordinate perpendicular to the section.

Numerous relationships exist to describe the permeability in terms of the geometry of the pore spaces. The most commonly used is the Carmen-Kozeny equation (Kay and Nedderman, 1985) which models the porous material as a bundle of narrow tubes and expresses the pressure gradient $\frac{dP}{dl}$ across a bed of porous material of length l in the flow direction as:-

$$v_m = - \left(k_0 \frac{S^2}{\varepsilon^3} \left(\frac{l_e}{l} \right)^2 \right)^{-1} \frac{dP}{dl} \frac{1}{\eta} \quad \text{Equation 4-5}$$

where v_m is the superficial flow velocity through the bed, l_e is the effective length of the flow channels, S is the total wetted surface per unit volume, ε is the porosity and k_0 is a constant.

Thus by comparison with Darcy's law the permeability can be expressed as:-

$$k = \left(k_0 \frac{S^2}{\epsilon^3} \left(\frac{l_e}{l} \right)^2 \right)^{-1} \quad \text{Equation 4-6}$$

The value of the constant k_0 for flow channels of circular cross section is 2 and, for an isotropic network of flow channels, where the average angle of passage of cement through the channels is 45° , l_e/l becomes equal to $\sqrt{2}$. Then Equation 4-6 simplifies to:-

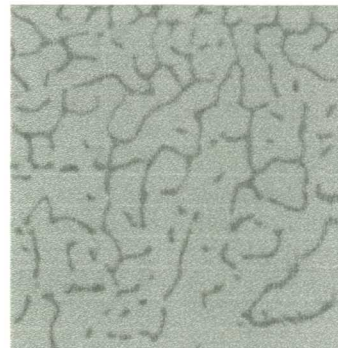
$$k = \left(\frac{4S^2}{\epsilon^3} \right)^{-1} \quad \text{Equation 4-7}$$

and the two parameters required for the specification of permeability are the wetted surface area per unit total volume, S , and the porosity, ϵ .

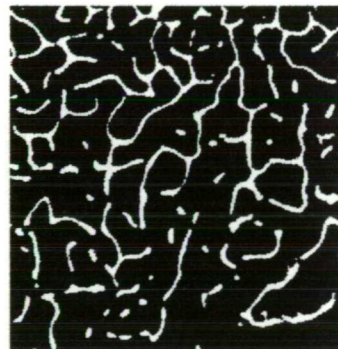
4.1.2.1 Method

Eleven specimens of cancellous bone from various sources (bovine proximal tibia - 8 specimens, bovine calf acetabulum - 2 specimens, human vertebra - 2 specimens, human proximal tibia - 4 specimens) were defatted by water jet and cleaned of residual fat and marrow by soaking overnight in 1,1,1 trichloroethane. The apparent dry density of the specimens was established by weighing the specimens on an analytical balance and measuring the specimen dimensions with Vernier callipers. The specimens were then prepared histologically by dehydration in graded aqueous alcohol solutions, decalcification in EDTA, embedding in paraffin wax, sectioning by microtome (slice thickness $3.5 \mu\text{m}$) and staining with haematoxylin and eosin. Digital images of the sections were then produced by photographing the sections on a light table using a Kodak DCS420 24 bit digital camera fitted with a Nikon macro lens. The images were transferred from the camera, converted to grey scale and stored on computer disk for processing using the image analysis program UTHSCSA ImageTool (developed at the University of Texas Health Science Center at San Antonio, Texas and available from the Internet by anonymous FTP from <ftp://maxrad6.uthscsa.edu>). An IBM compatible PC running Microsoft Windows 95 was used for all the digital image processing. The images were reduced interactively to binary images by grey level thresholding using the original image as a reference and then the automatic object detection algorithm invoked. The detected objects were then

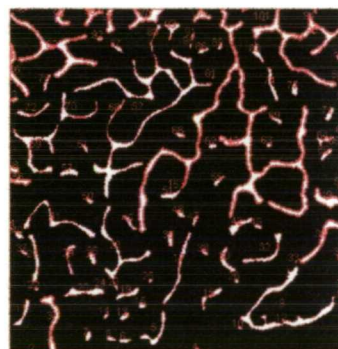
processed to give object perimeters and areas. An assessment of the errors involved in this process is given in Appendix B. The steps in the extraction of required parameters are illustrated in Figure 4-3.



(a)



(b)



(c)

Figure 4-3: Steps in extracting morphological parameters using ImageTool.
(a) raw image after conversion from 24 bit colour to grey-scale, (b) binary image after grey level thresholding and (c) extraction of objects in the image with the object detection algorithm

By the principle of Delesse (Delesse, 1847, cited in Whitehouse, 1974), the area fraction of porosity in the section is numerically equal to the volume fraction of porosity in the sample. Since bone area was derived by the image analysis, porosity is equal to $(1 - \text{area fraction of bone})$.

The wetted surface area to total volume ratio is related to the total boundary length per unit area of test specimen, B_A , by the relationship (Whitehouse, 1974):-

$$S = \frac{4B_A}{\pi} \quad \text{Equation 4-8}$$

Permeability was then calculated using Equation 4-7.

4.1.2.2 Results

Figure 4-4 shows a plot of permeability vs. apparent dry density. Fitting a straight line through the data using the method of least squares gives the regression equation:-

$$k = -2.76 \times 10^{-11} \rho_{ad} + 1.69 \times 10^{-8} \quad (R^2 = 0.63) \quad \text{Equation 4-9}$$

where ρ_{ad} is the apparent dry density.

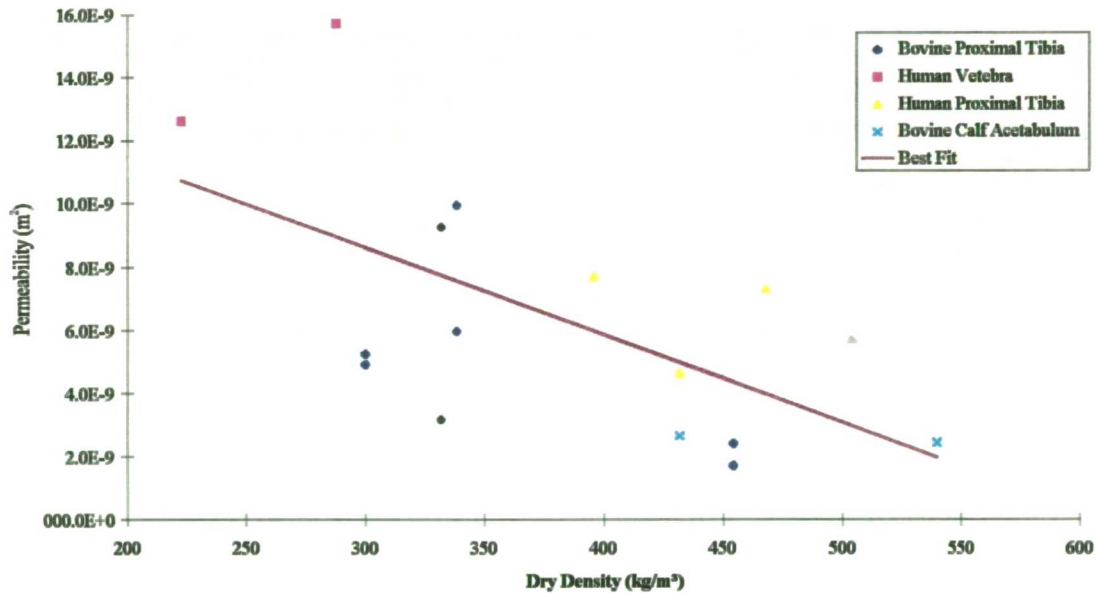


Figure 4-4: Permeability of cancellous bone vs. apparent dry density.

4.2 Development of Modelling Technique

4.2.1 Theory

The incompressible isothermal flow of a Newtonian (linear) fluid can be completely described by the continuity (conservation of mass) equation and the Navier-Stokes (momentum) equation, given by Equation 4-10 and Equation 4-11 respectively.

$$\frac{\partial \rho}{\partial t} + (\nabla \cdot \rho \bar{v}) = 0 \quad \text{Equation 4-10}$$

$$\rho \frac{D\bar{v}}{Dt} = -\nabla P + \eta \nabla^2 \bar{v} \quad \text{Equation 4-11}$$

where ρ is the fluid density, t is time, \bar{v} is the fluid velocity, P is pressure and η the fluid viscosity.

The resistance to fluid flow produced by the porous cancellous bone was modelled by Darcy's law (Equation 4-4), expressed in co-ordinate free vector notation as:-

$$\bar{v} = -\frac{k}{\eta} \nabla P \quad \text{Equation 4-12}$$

the constant of proportionality being k , the permeability of the solid medium.

4.2.2 Method

The modelling of cement flow during insertion of a prosthesis into a bone bed is complicated by the changing shape of the fluid domain. To overcome this problem the method summarised in the flow chart (Figure 4-5) was adopted, with the finite element method used to discretise the fluid domain and solve the fluid flow equations. In the finite element formulation the resistance to flow presented by the cancellous bone was implemented by incorporating extra resistance terms into the momentum equations in the elements representing cancellous bone, this formulation being equivalent to Darcy's law. Prosthesis insertion was simulated by applying a constant velocity at all the boundary nodes associated with the exterior surface of the prosthesis. By calculating the steady state velocity and pressure solution to the Navier-Stokes and continuity equations and integrating the pressure over the same set of nodes, a linear relationship was established for insertion force vs. insertion velocity to allow the development of cement penetration based on a constant applied force, a more realistic simulation of the action of a surgeon during an operation. A new solution was then calculated based on the cup insertion velocity extrapolated to the required insertion force and the bone cement domain modified based on the velocity of the prosthesis and the exit velocity of the bone cement through the porous cancellous bone. Using this method, it was possible to simulate prosthesis insertion under constant applied force or constant insertion velocity. Bone cement was in all

cases assumed to behave as a linear viscous (Newtonian) liquid. Since the prosthesis reaches its final position in the bone bed and total cement penetration typically occurs within a few seconds of the application of pressurisation force (Walker *et al.*, 1984), no attempt was made to model the increase in viscosity with time for the curing cement. Cancellous bone was modelled as an isotropic porous material. It was further assumed that the flow was incompressible and isothermal, that gravitational forces could be neglected and that quasi steady state conditions were maintained (Tadmor and Gogos, 1979). Laminar flow was a natural consequence of the fluid properties, fluid domain shape and insertion velocities/forces considered. The analyses was carried out using the ANSYS/FLOTRAN commercial finite element package (release 5.3) running under Microsoft Windows 95 on an IBM compatible PC.

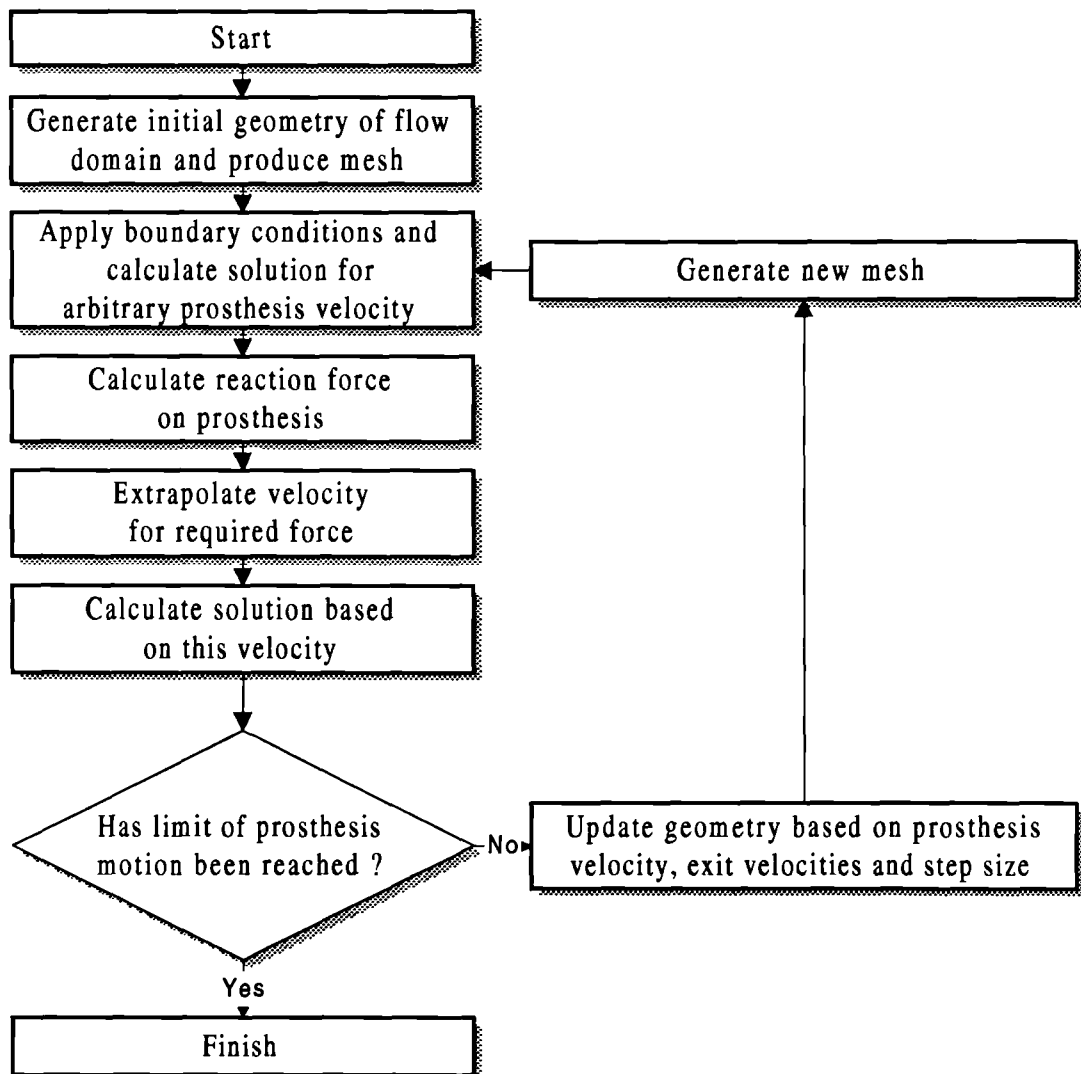


Figure 4-5: Flow chart showing cement flow modelling technique.

4.3 Experimental Validation of Modelling Technique

The finite element modelling technique was tested against two experimental protocols. The first (Acetabular Model) involved simulation of the insertion of two designs of acetabular cups into a model acetabulum. This was to validate the assumption of linear viscosity and the quasi steady state assumption made in the modelling formulation. The second protocol (Porous Material Model) was intended to evaluate the predictions of flow into cancellous bone by placing a cylindrical porous ceramic disk, designed to have similar morphology to cancellous bone, under the actuator of the testing machine and squeezing bone cement into it with a descending impermeable disk.

4.3.1 Acetabular Model

4.3.1.1 Experimental Methods

The instrumented model acetabulum described in section 3.2.2.1 was held in a vice under the actuator of a servo-hydraulic materials testing machine (ESH Testing, Brierly Hill, U.K.). An attachment to the actuator of the testing machine permitted the insertion of (a) a scalloped rim Charnley acetabular cup, outside diameter 43 mm, and (b) a flanged Charnley acetabular cup, outside diameter 40 mm, with the flange trimmed to fit snugly at the rim of the acetabular cavity (Figure 4-6).

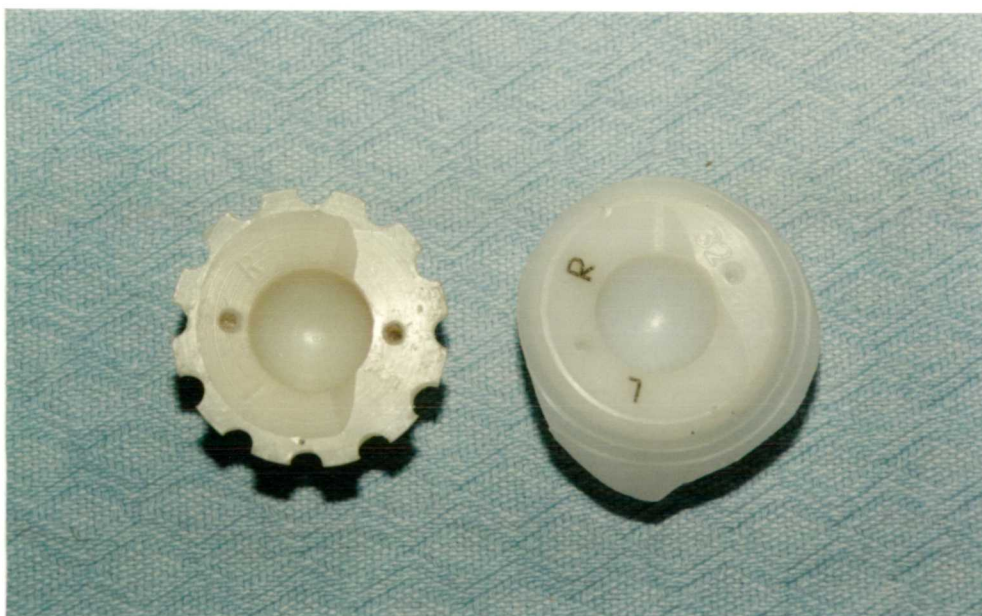


Figure 4-6: A scalloped (left) and a trimmed flanged (right) acetabular cup.

CMW 1 or CMW 3 cement was mixed in a bowl. At three minutes from mixing the cement was placed in the acetabulum and the cup inserted under displacement control at velocities of 1.28, 2.56 or 5.13 mm s⁻¹. Repeated withdrawals and insertions of the cup were made until the cement set. Pressures at the rim and the pole of the acetabulum were measured and recorded according to the method described in section 3.2.2.1.

Displacement control was chosen for two reasons. Firstly, in displacement control the control loop of the testing machine is closed whether a specimen is present or not. With a labile material such as bone cement, true load control presents difficulties and introduces some uncertainties. Secondly, under displacement control high shear strain rates are generated in the cement as the gap between cup and acetabulum narrows. This represents a stern test of the linear constitutive law chosen to model the cement and one in which deviations from linearity, such as shear rate dependent viscosity and/or elastic effects, would be expected to manifest themselves.

4.3.1.2 Finite Element Models

Initial finite element models of the bone cement domains were generated to represent the geometry of the model acetabulum and the two acetabular cups. Three dimensional and axisymmetric finite element meshes were compared to evaluate the effects of the irregular acetabular rim on cement pressure. In the both the three dimensional and the axisymmetric models the rim of the scalloped cup and the flange of the flanged cup were represented by areas concentric with the cup body and with total area equal to the total area of the rim minus the scallops or the trimmed flange respectively. The three dimensional and axisymmetric finite element meshes of the bone cement domain with the cup in the initial position are shown in Figure 4-7.

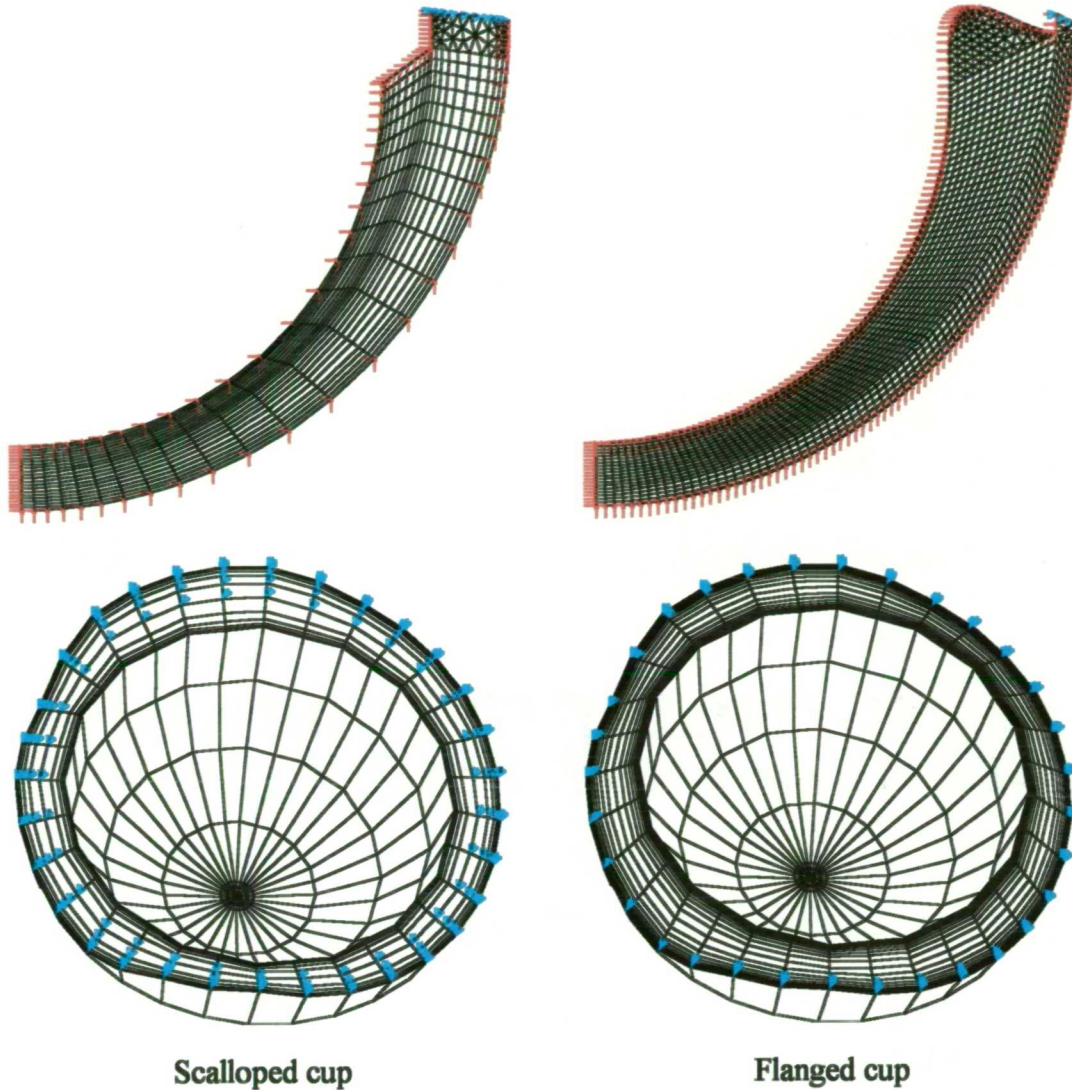


Figure 4-7: Initial axisymmetric and 3D meshes of bone cement flow domains.

▶ indicate boundaries on which velocity was specified, **▶** where pressure was specified. Velocity specifications are not shown on the three dimensional models for clarity.

To simulate cup insertion, velocity of the cup surface (including rim/flange) was specified as 1.28, 2.56 or 5.13 mm s⁻¹ as in the experiments. In the axisymmetric models the velocity component across the axis was set to zero. In the exit areas between rim and acetabulum (scalloped cup) and flange and acetabulum (flanged cup), pressure was specified as zero. Wall boundary conditions (all velocity components zero) were assumed elsewhere. Viscosity was specified for each model according to the insertion time in the relevant experiment and the viscosity time relationships reported in Table 4-1. The density of liquid bone cement is not commonly reported in the literature. Haas *et al.* (1975) report the density of cured bone cement to be approximately 1.2 × 10³ kg m⁻³ and the shrinkage on cure to be approximately 8%. Therefore assuming constant mass, $\rho_l \approx 0.92\rho_s = 1.1 \times 10^3 \text{ kg m}^{-3}$,

where ρ_l and ρ_s are the density of the liquid and solid respectively. In the three dimensional models strain rates were calculated, using the macro described in Appendix C to extract the components of the strain rate tensor. An effective strain rate was then calculated from the second invariant of the strain rate tensor, J_2 , given by:-

$$J_2 = \frac{1}{6} \left[(\dot{\epsilon}_{11} - \dot{\epsilon}_{22})^2 + (\dot{\epsilon}_{22} - \dot{\epsilon}_{33})^2 + (\dot{\epsilon}_{33} - \dot{\epsilon}_{11})^2 + 6(\dot{\epsilon}_{12}^2 + \dot{\epsilon}_{23}^2 + \dot{\epsilon}_{31}^2) \right] \quad \text{Equation 4-13}$$

where $\dot{\epsilon}_{ij}$ are components of the strain rate tensor. This is analogous to the von Mises stress in solid mechanics, which is the second invariant of the deviatoric stress tensor (Dieter, 1988).

4.3.1.3 Results

Figure 4-8 shows finite element model predictions of the pressure distributions for scalloped and flanged acetabular cups inserted under displacement control at a velocity of 2.56 mm s^{-1} . Viscosity was 895 Pa s . Pressures are shown normalised to the maximum pressure, which is noted at the bottom-right of each plot. Discrepancies of 10%-20% can be seen between the peak pressures predicted by the axisymmetric and three dimensional models, although pressure distributions are similar. There are some differences at the margins of the models, which can be explained by small differences in the geometric representation of the cups in these regions.

Figure 4-9 shows typical experimental pressure time curves for the scalloped and flanged cups. The peak rim pressure was approximately 50% of the peak pole pressure for the scalloped rim cup and approached 100% of the peak pole pressure for the flanged cup.

A comparison of some representative experimental curves and the corresponding finite element predictions are shown in Figure 4-10.

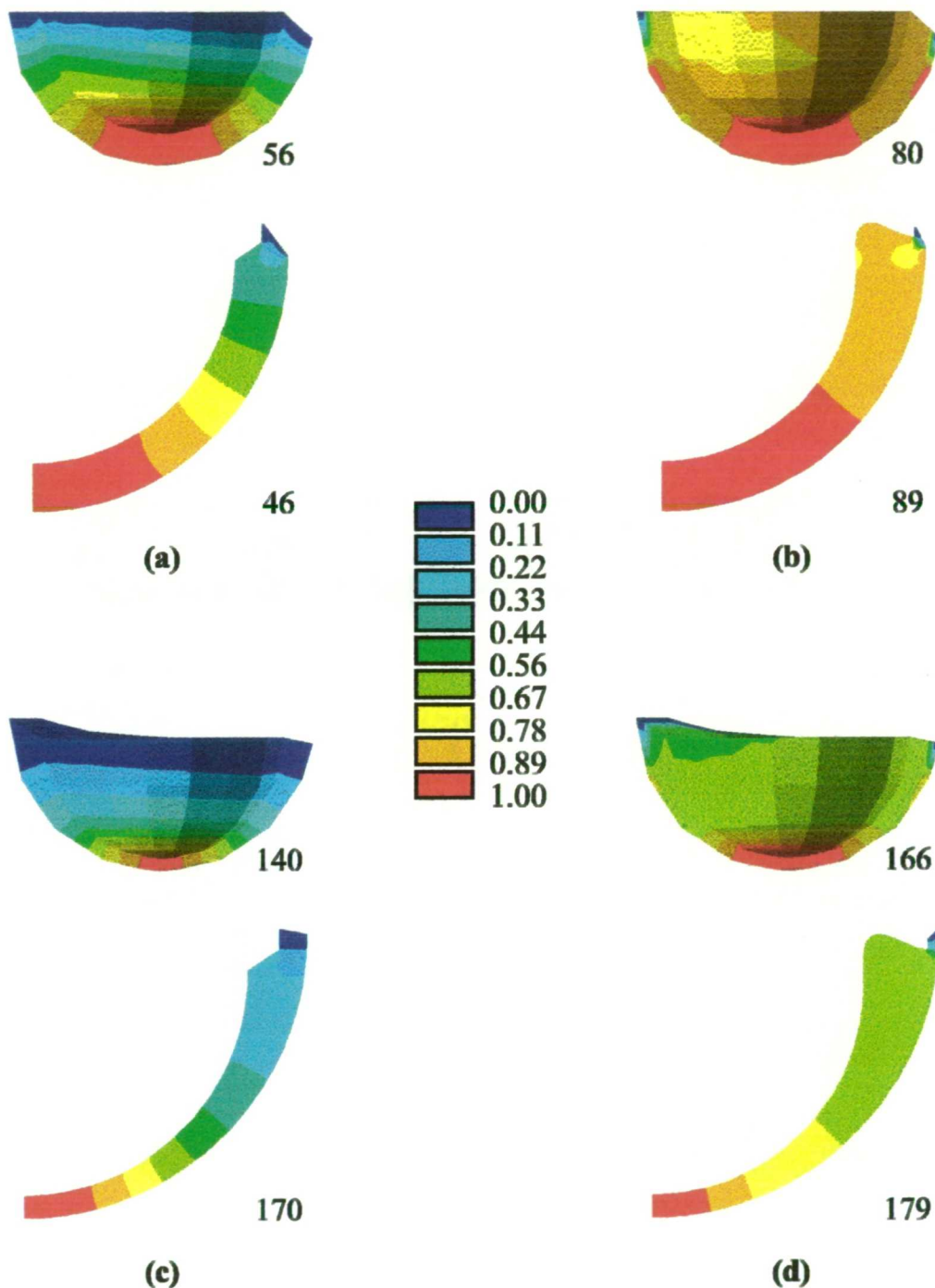
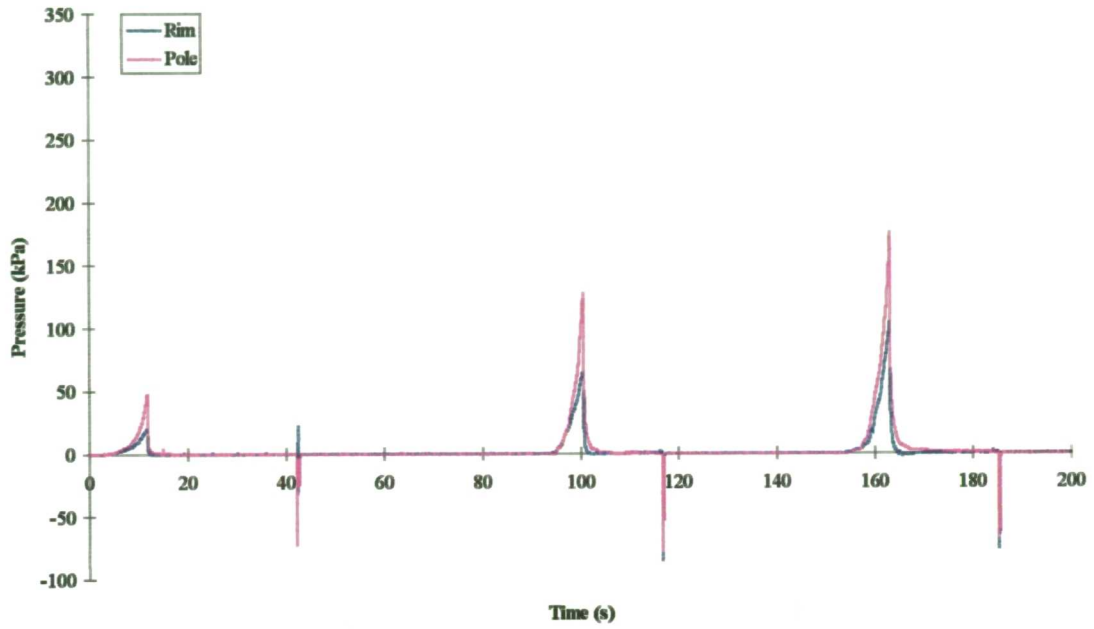
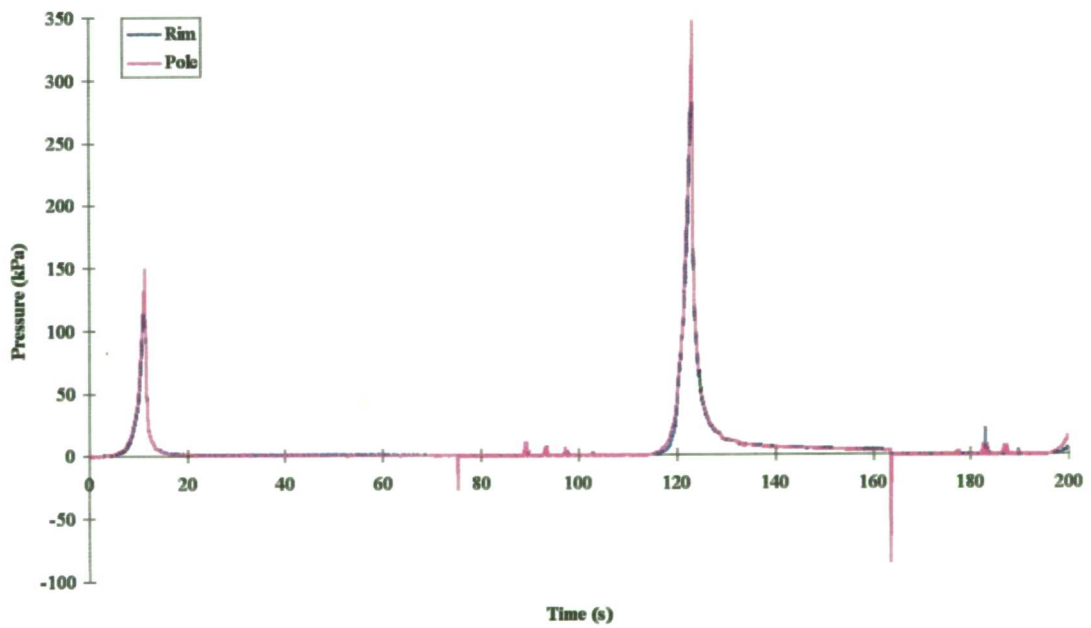


Figure 4-8: Cement pressure distributions during acetabular cup insertion.
(a) Unflanged cup with cup apex to acetabular apex separation of 5.5 mm
(b) flanged cup, separation 5.5 mm (c) unflanged cup, separation 2 mm
(d) flanged cup, separation 2 mm.
Figures at the bottom-right of each plot are maximum pressure in kPa.

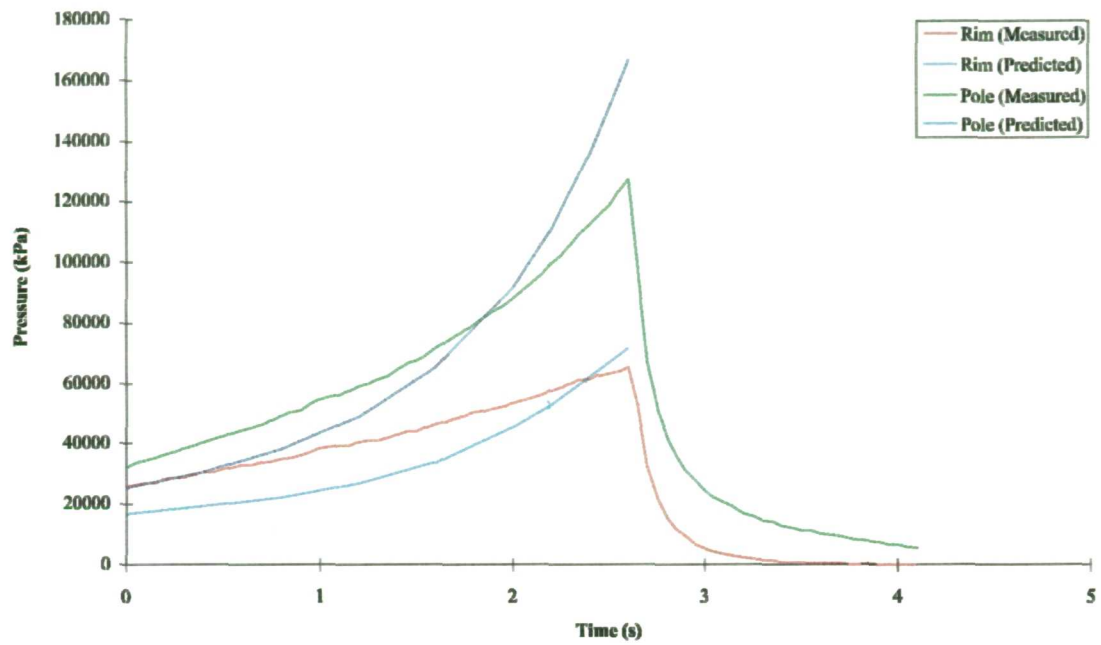


(a)

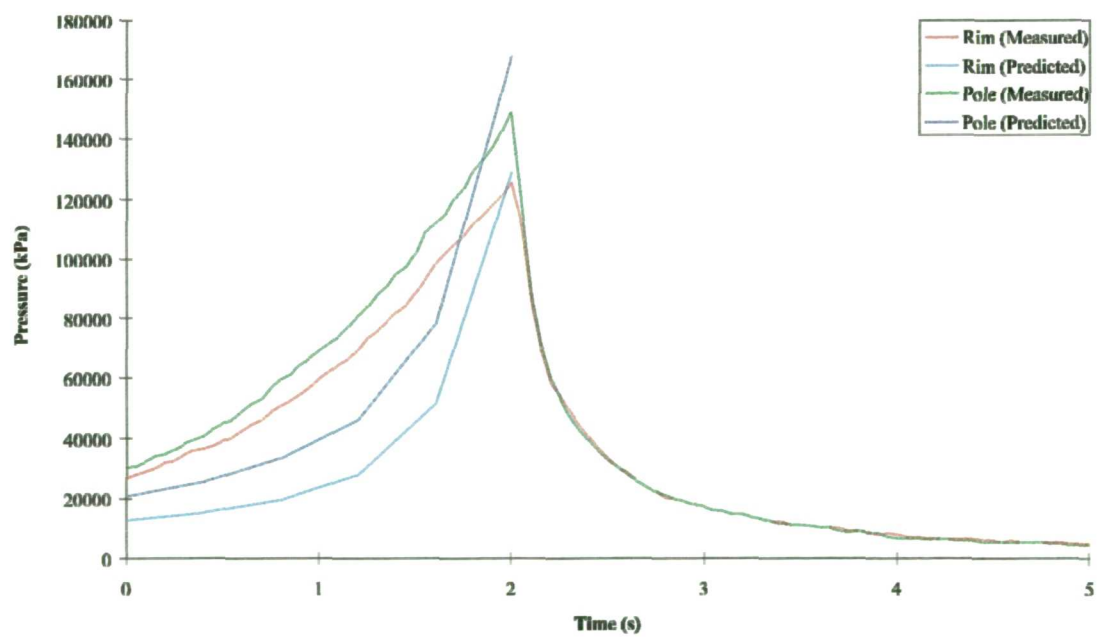


(b)

Figure 4-9: Experimentally determined pressure vs. time curves, repeated cup insertion.
(a) Scalloped rim cup, CMW1, time zero = 3 min. from mixing, stroke rate 2.56 mm s^{-1} .
(b) Flanged cup, CMW1, time zero = 3 min. from mixing, stroke rate 2.56 mm s^{-1} .



(a)

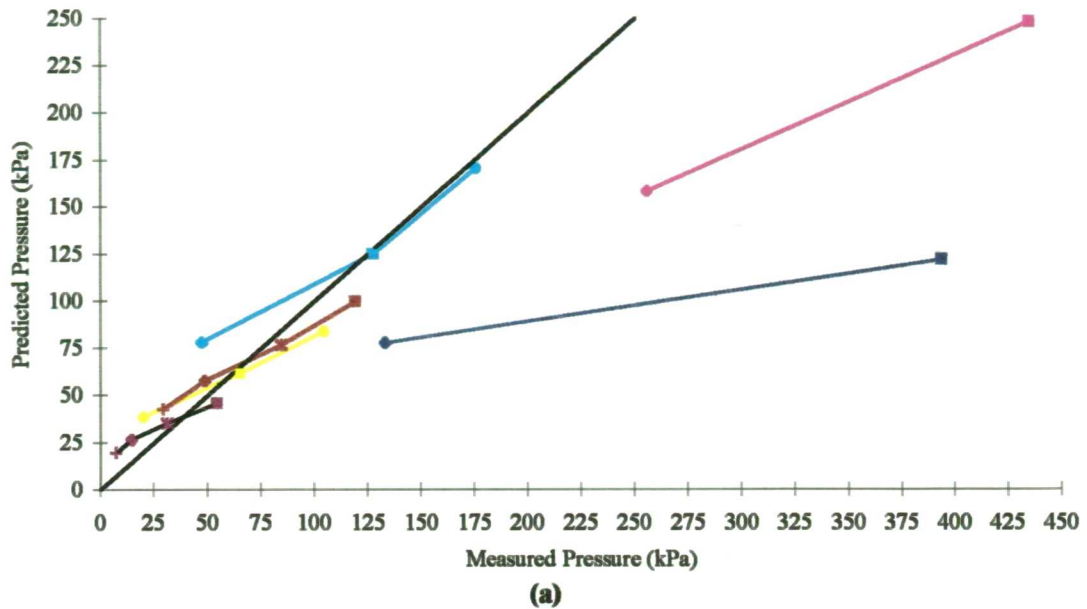


(b)

Figure 4-10: Comparison of measured and predicted pressure vs. time curves.
(a) Scalloped cup, CMW1 cement, time zero = 4½ minutes from mixing, stroke rate=2.56 mm s⁻¹.
(b) Flanged cup, CMW1 cement, time zero = 3 minutes from mixing, stroke rate=2.56 mm s⁻¹.

The model was generally less successful in predicting the experimental results for CMW1 cement than for CMW3. In the early stages of cup insertion, where the gap between cup and acetabulum was relatively large, the finite element models usually underestimated the cement pressure by between 10 and 20 %. In the latter stages the agreement was better. The errors were found to depend on the type of cement, the cup insertion velocity and the time from mixing. The errors may occur for a number of reasons in addition to those associated with the simple treatment of the constitutive behaviour of the cement; in the early stages of the experiment the finite element models do not represent the experimental geometry well, since the cement tends to pool in the apex of the acetabulum. Comparison of the peak pressures generated at the rim and pole transducers and the corresponding finite element predictions are shown in Figure 4-11 and Figure 4-12. In these figures, the shape of the data point marker indicates the insertion time (from mixing of the bone cement) and hence the cement viscosity. The colour of the data point marker indicates the insertion velocity and the location in the acetabulum at which pressure was sampled. The lines join data points obtained at a given location with the same cup insertion velocity.

The measured and predicted peak pressures are generally in good agreement. This is particularly true for CMW3 cement and for the measurements soon after cement mixing. The results for CMW1 cement are poorer, which indicates that the major source of error, at least for the peak pressure predictions, is the assumption of Newtonian behaviour for the liquid bone cement, rather than inadequate representation of the geometry of the flow domain.



+ $t = 124, \eta = 657$ $\diamond t = 184, \eta = 895$ $\times t = 238, \eta = 1183$ $\square t = 280, \eta = 1470$ $\circ t = 334, \eta = 1942$

■ Rim, $v = 5.13$ mm/s	■ Rim, $v = 2.56$ mm/s	■ Rim, $v = 1.28$ mm/s
■ Pole, $v = 5.13$ mm/s	■ Pole, $v = 2.56$ mm/s	■ Pole, $v = 1.28$ mm/s

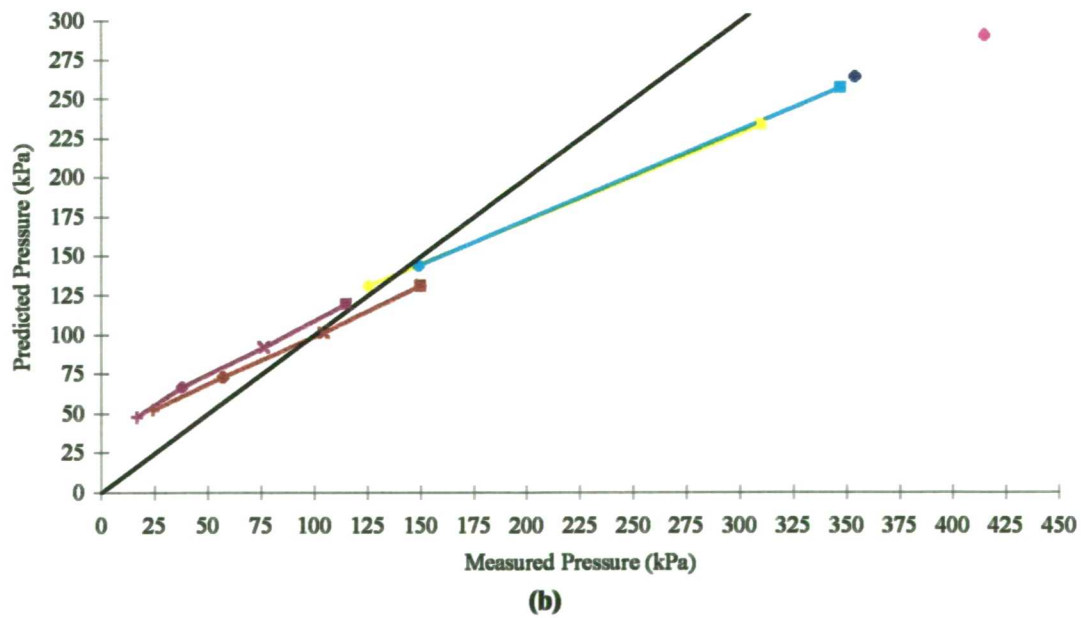
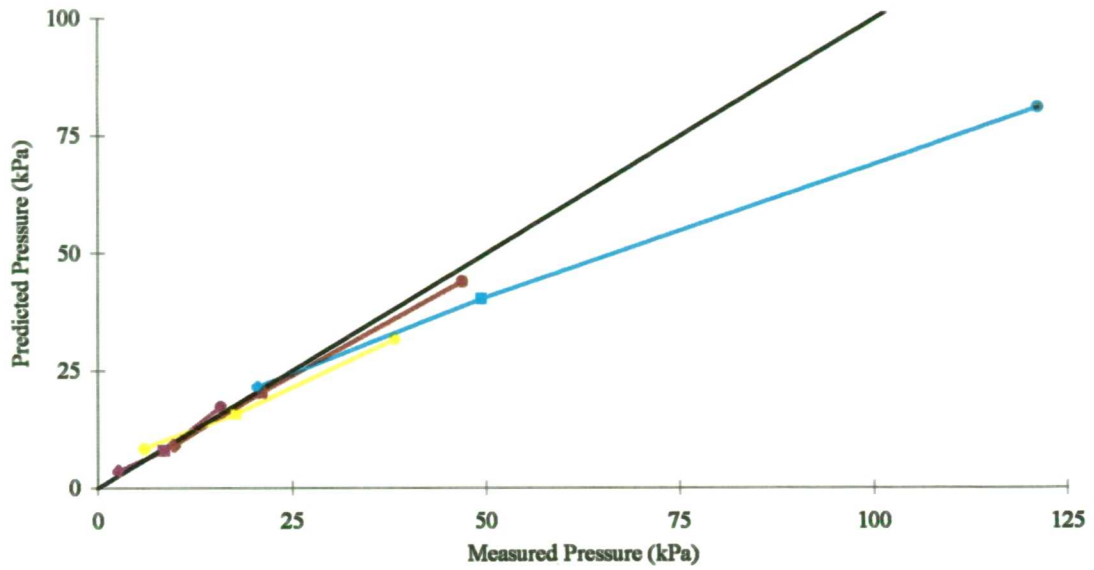
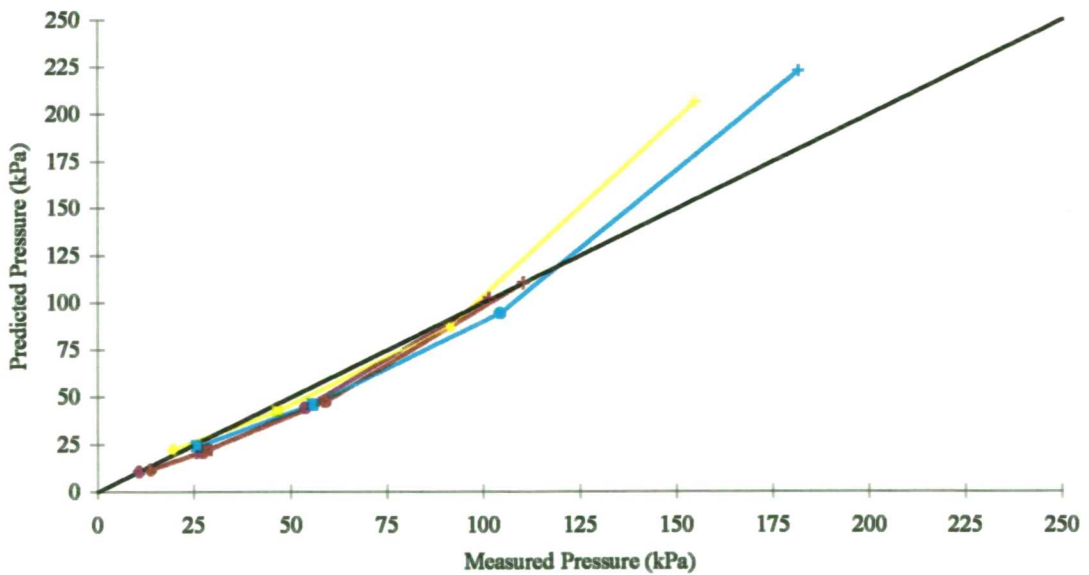
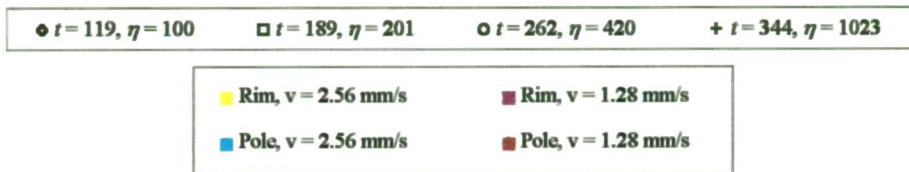


Figure 4-11: Comparison of predicted and measured pressures for CMW 1 cement. (a) Scalloped cup and (b) flanged cup. The heavy black line represents a 1:1 relationship.



(a)



(b)

Figure 4-12: Comparison of predicted and measured pressures for CMW 3 cement. (a) scalloped cup and (b) flanged cup. The heavy black line represents a 1:1 relationship.

Strain rates are shown in Figure 4-13 for the flanged and unflanged cups as the cup approaches the acetabulum. Results for cup-acetabulum separations at the pole of 5.5 and 2 mm are shown. A comparison is made between the strain rates generated by velocity (2.56 mm s^{-1}) and force (100 N) controlled cup insertion.

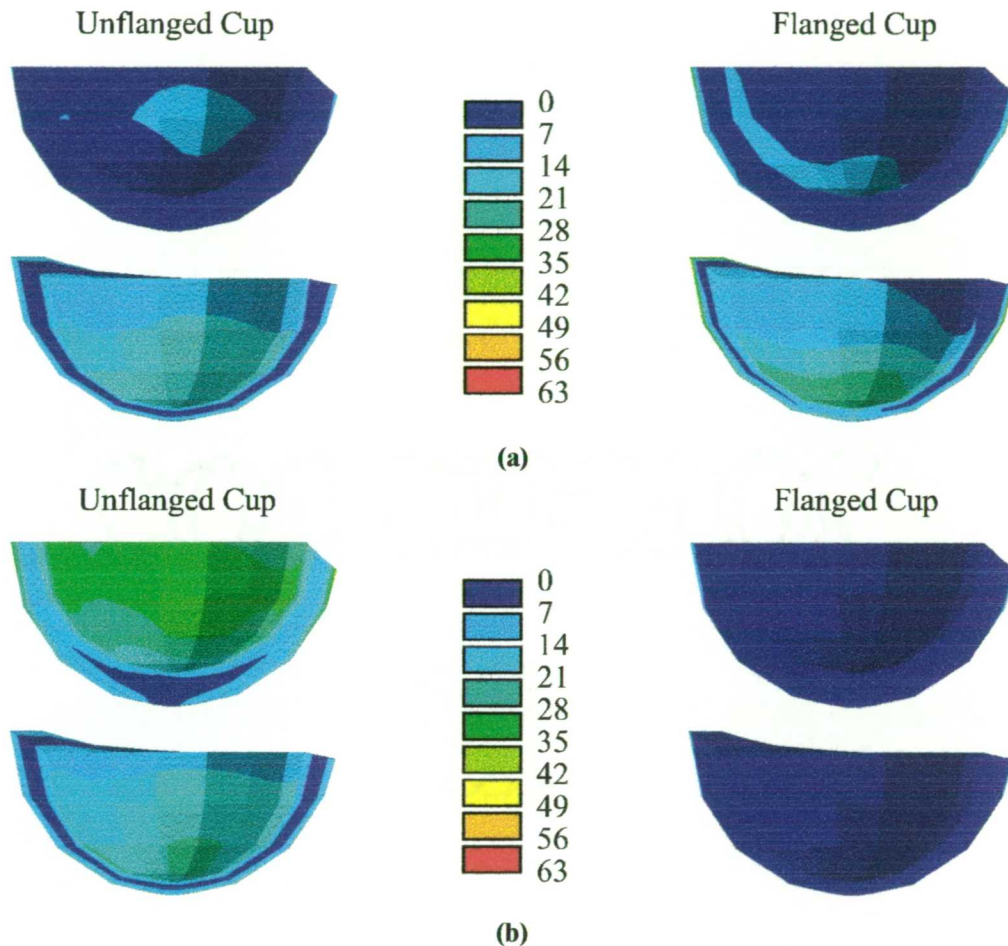


Figure 4-13: Strain rates during cup insertion (s^{-1}). Results for (a) velocity (2.56 mm s^{-1}) and (b) force (100 N) control.

Since strain rates are controlled by the velocity of cup insertion, the velocity controlled results are independent of cement viscosity. However, in the force controlled case the instantaneous cup velocity depends on the cement pressure which in turn depends on the cement viscosity. Thus under force control strain rate becomes a function of viscosity. Results in Figure 4-13 (b) are presented for a cement viscosity of 500 Pa s . Strain rates varied from 0 to 63 s^{-1} . However, regions of high shear rate were localised to geometric restrictions in the flow domain, such as close to the flange of the flanged cup throughout the insertion process and near the apex of the acetabulum for both cup designs as the gap between cup and acetabulum closed. In the velocity controlled case, strain rates were highest for the flanged cup, being dominated

by the narrow gap between flange and acetabulum. In the force controlled case, strain rates were highest for the unflanged cup because its velocity of approach was higher.

4.3.2 Porous Material Model

4.3.2.1 Experimental Methods

In this experiment an open pore hydroxyapatite ceramic foam with an apparent density of 400 kg m^{-3} and a permeability of $2.5 \times 10^{-7} \text{ m}^2$ (North Wales and Oswestry Tissue Bank, Wrexham, U.K.) was used to simulate cancellous bone. A disk of the porous ceramic material was placed on the base-plate of an ESH materials testing machine (Figure 4-14). CMW1 cement was mixed as described above and at three minutes from mixing placed on the top surface of the porous disk. The impermeable plate mounted on the actuator of the testing machine was lowered from an initial separation of 11.5 mm to a final separation of 2.5 mm at a constant velocity of 1.28 mm s^{-1} , resulting in cement penetrating the porous surface and exuding from the gap between plate and disk at the circumference. After the cement had cured, the cement penetration was measured (with correction for magnification) from a plane X-ray taken perpendicular to the axis of rotational symmetry of the disk.

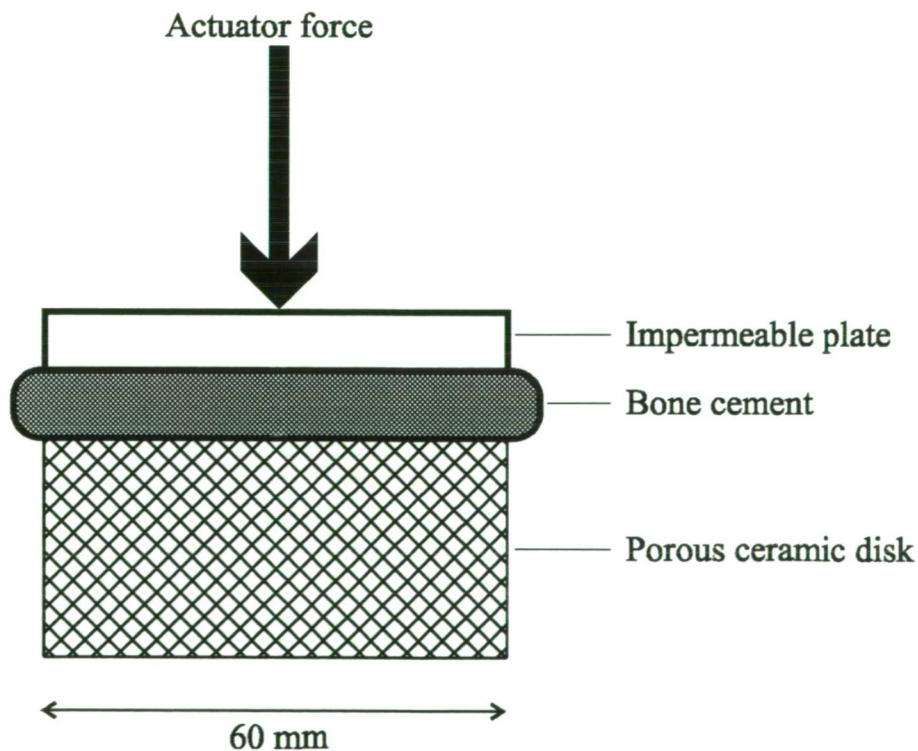


Figure 4-14: Schematic of the porous disk experiment.

4.3.2.2 Finite Element Model

The methodology used was similar to that described in section 4.3.1.2. Axisymmetric finite element models were used; the initial finite element mesh is shown in Figure 4-15. As boundary conditions, the component of velocity across the axis was set to zero and pressure was specified as zero at the cement exit regions between the bottom of the impermeable top plate and the top of the porous disk and at the penetrating front of bone cement. Cement viscosity and density were specified as described in section 4.3.1.2.

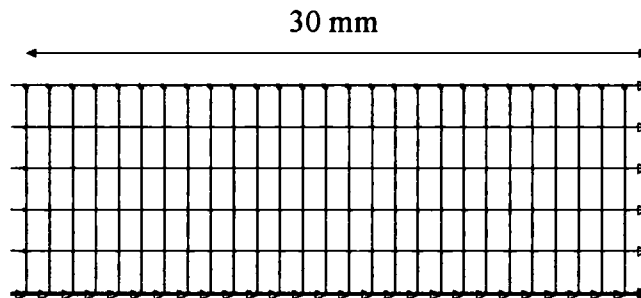


Figure 4-15: Initial finite element mesh for the porous disk simulation.
□ indicate boundaries on which velocity was specified, ▷ where pressure was specified.

4.3.2.3 Results

The development of cement penetration was followed in the finite element model by tracking the locations of nodes on the exterior edge of the mesh representing the cement front. The mesh at three stages in the development of the cement penetration is shown in Figure 4-16.

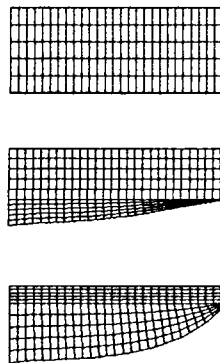


Figure 4-16: Development of the mesh showing three stages of cement penetration.

Figure 4-17 shows the final finite element mesh overlaid on an X-ray of the corresponding experiment. The good agreement between the predicted penetration over the whole of the specimen is evident.

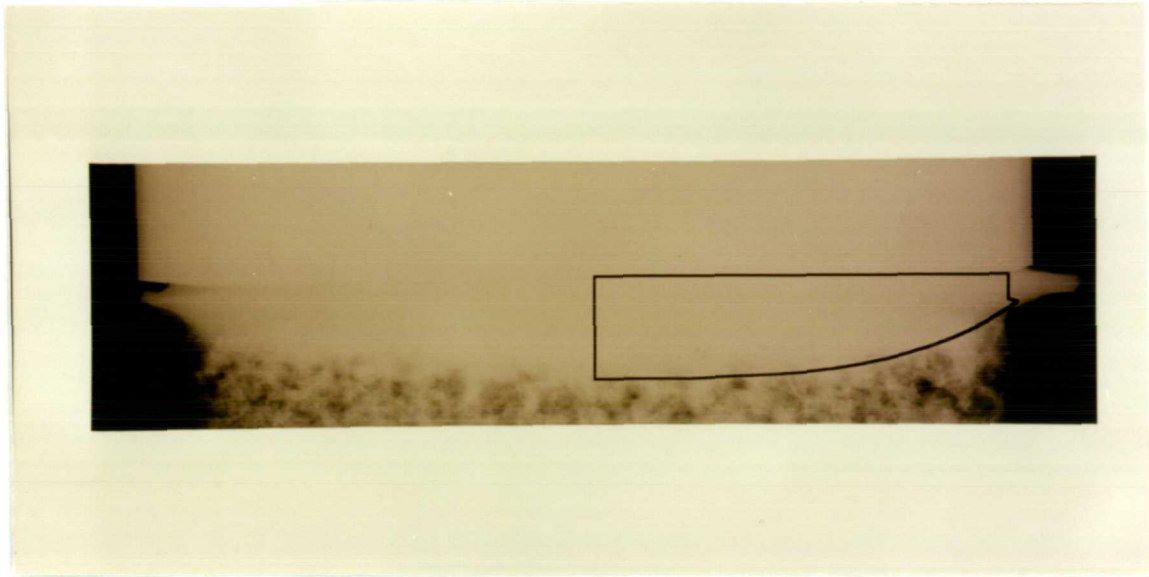


Figure 4-17: Predicted penetration profile superimposed on an X-ray of the porous disk.

4.4 Parametric Analysis of Cement Penetration During Acetabular Cup Insertion

The enhanced initial fixation brought about by careful preparation of the bone bed and cement pressurisation are considered to be responsible for the reduction in the rate of aseptic loosening with modern surgical techniques (Malchau and Herberts, 1996). Various studies suggest that cement pressurisation and subsequent penetration of cement into cancellous bone produces a stronger interface (Krause *et al.*, 1982a; Askew *et al.*, 1984). Prosthesis design is important for cement pressurisation (Shelley and Wroblewski, 1988; Beverland *et al.* 1993) and appears to be clinically significant since improvements in the radiographic appearance of the cement bone interface for flanged cups are observed in the long term (Hodgkinson *et al.*, 1993). To analyse the effect of varying parameters such as the design of the prosthetic cup, the viscosity of the bone cement and the permeability of the cancellous bone, the modelling technique developed above was used.

4.4.1 Method

Axisymmetric finite element meshes of the acetabulum with an unflanged and flanged cup are shown in Figure 4-18. The deep region of the acetabulum was assumed to be covered by solid subchondral bone plate while the peripheral region was cancellous

bone. Cup insertion under force control was simulated, using a force of either 100 N or 200 N, as described in section 4.2.2. At the axis of symmetry the velocity component across the axis was set to zero. On the exit boundaries, at the outer edge of the cancellous bone and between cup body and acetabulum (unflanged cup) and flange and acetabulum (flanged cup), pressure was specified as zero. Wall boundary conditions (all velocity components zero) were assumed elsewhere.

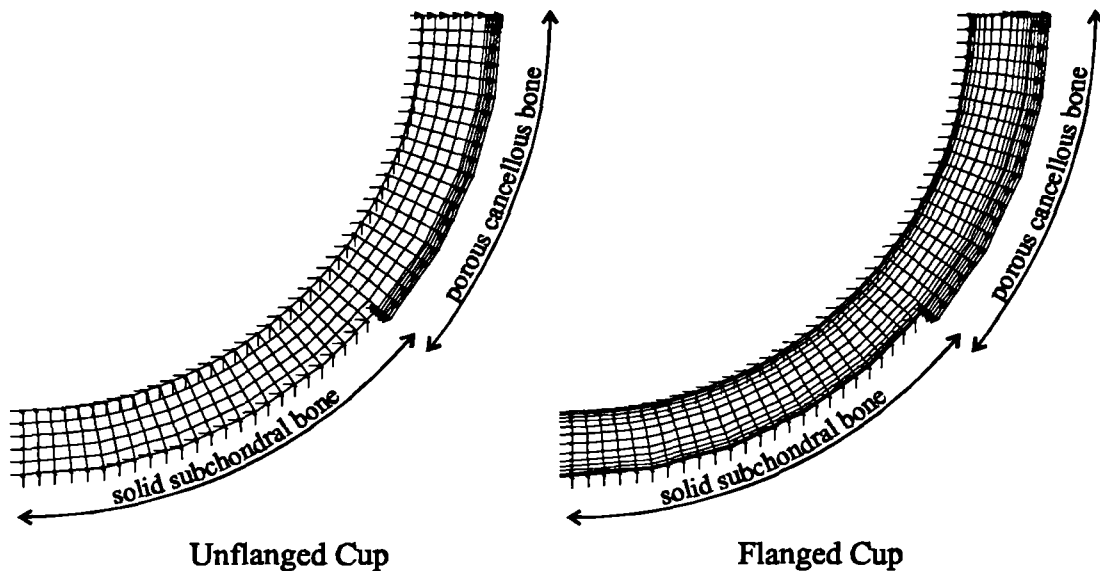


Figure 4-18: Finite element meshes of acetabula with unflanged and flanged cups.

Parametric analyses were carried out, varying cup insertion force as described above and assuming cement viscosity of either 500 or 1000 Pa s. These values were intended to be representative of those encountered in clinical use of the cement and are in accordance with those measured in section 4.1.1. In addition the permeability of the cancellous bone was varied from 10^{-9} to 10^{-7} m^2 . The permeability of normal cancellous bone ranges from 2×10^{-9} to 10^{-8} m^2 , corresponding approximately to apparent wet densities of 1100 to 800 kg m^{-3} respectively. However pathological changes to cancellous bone as a result of arthritic conditions range from extensive cyst formation to appreciable densification (Grennan, 1984). Due to the uncertainty of these changes a larger range of permeability was adopted.

4.4.2 Results

Figure 4-19 shows cement pressure distributions for two prosthesis positions and two prosthesis designs. The pressure was always highest at the pole of the acetabulum. Gap closure between prosthesis and bone bed produced steeper pressure gradients.

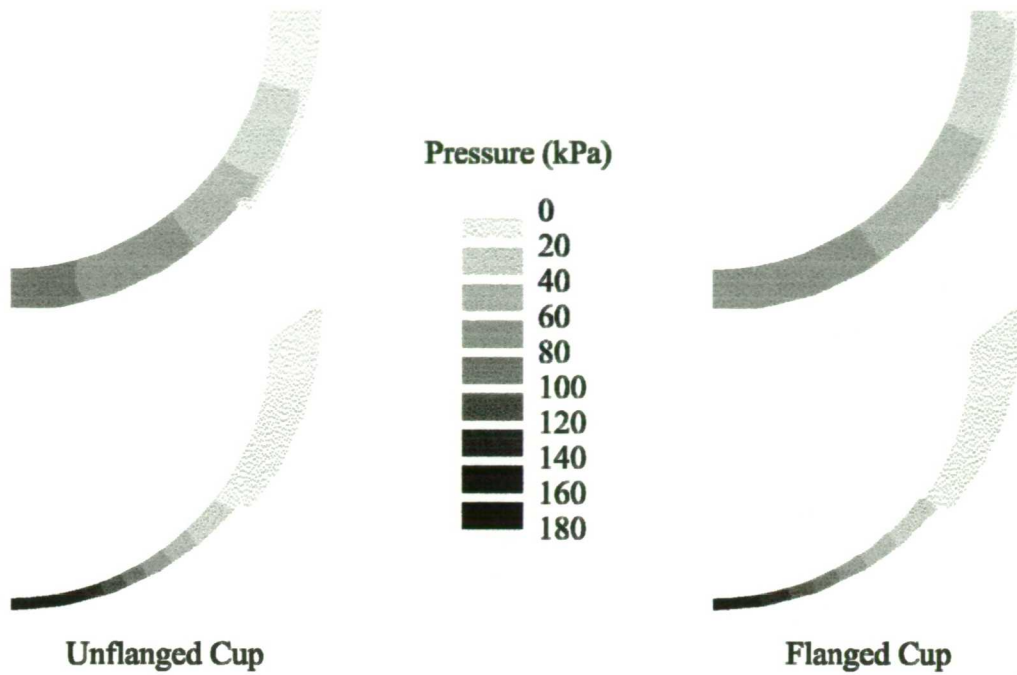


Figure 4-19: Cement pressure distributions at two cup positions for 100 N insertion force.

Further results are presented as cement penetration in the radial direction for the cancellous bone region. Figure 4-20 to Figure 4-22 show the results of the parametric analyses for the two prosthesis design variations. The development of cement penetration is shown as the gap between prosthesis and bone narrows from 8 to 1 mm. Cement penetration varied from negligible (Figure 4-22) to more than 5 mm (Figure 4-21).

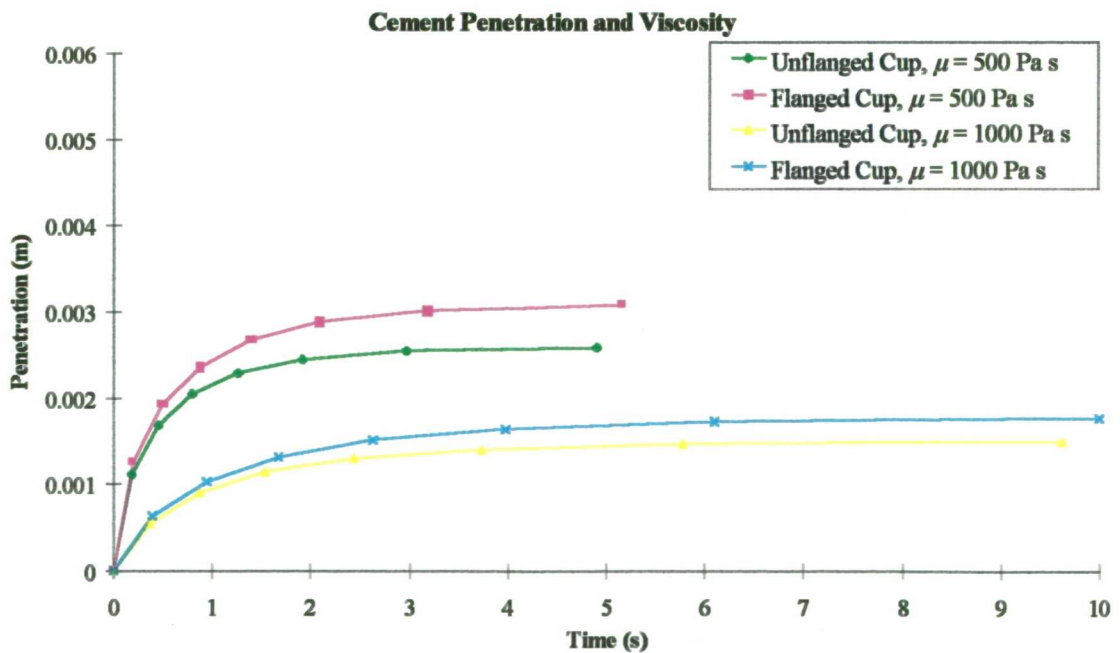


Figure 4-20: Predicted relationship between cement penetration and cement viscosity.
 ($k = 10^{-7} \text{ m}^2, F = 100 \text{ N}$)

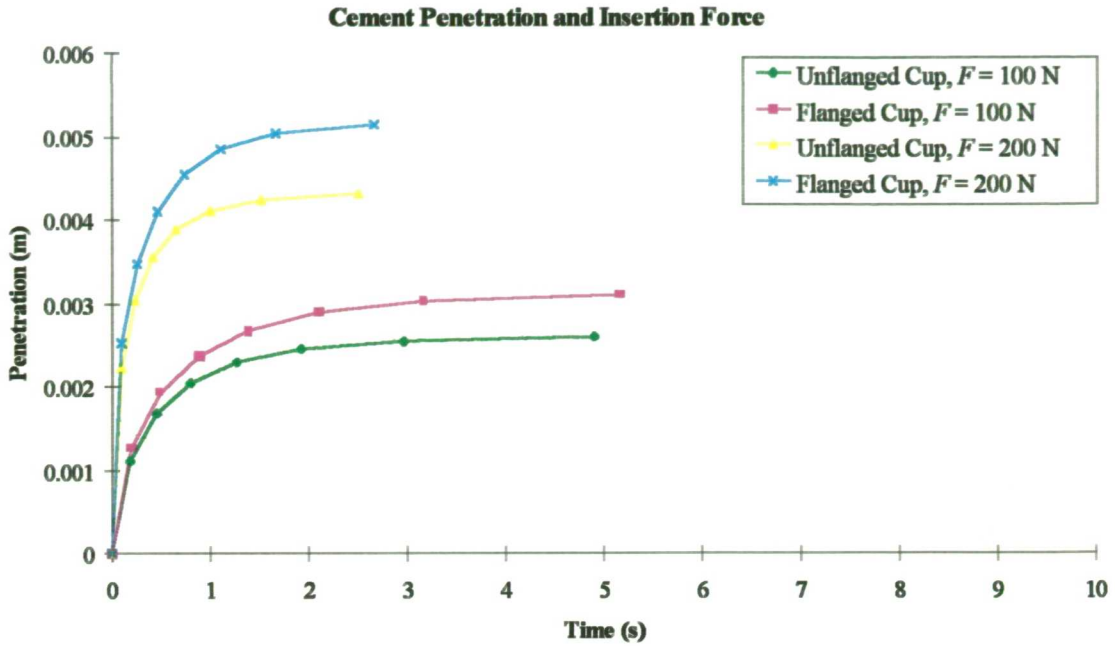


Figure 4-21: Predicted relationship between cement penetration and insertion force.
 $(k = 10^{-7} \text{ m}^2, \eta = 500 \text{ Pa s})$

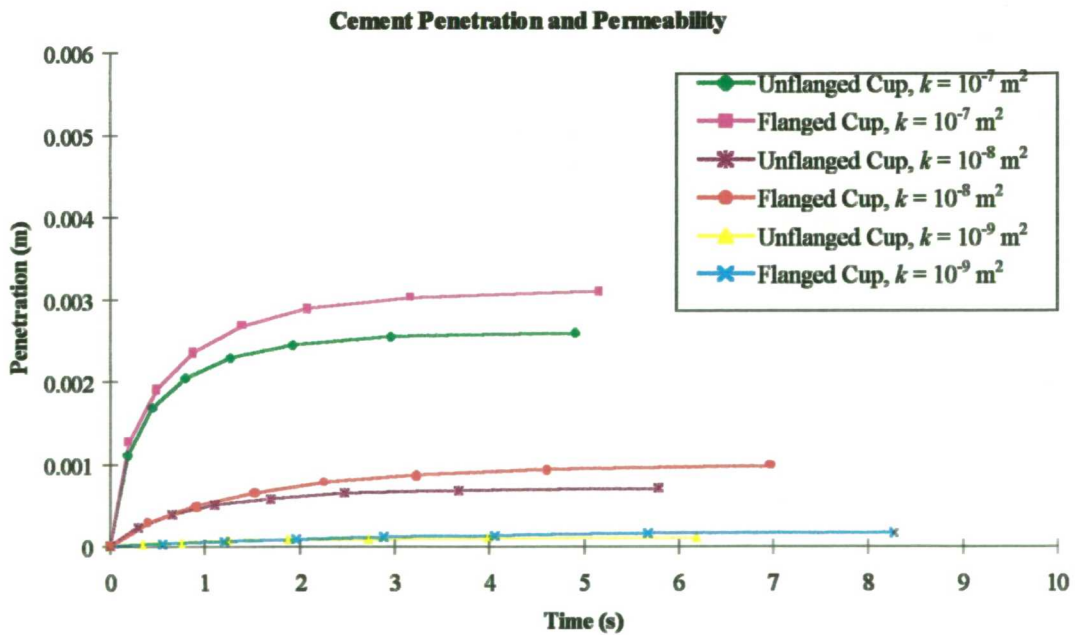


Figure 4-22: Predicted relationship between cement penetration and bone permeability.
 $(F = 100 \text{ N}, \eta = 500 \text{ Pa s})$

4.5 Discussion

Bone cement is rheologically an extremely complex material. After mixing its behaviour changes from that of a labile liquid to a rigid solid in approximately 6 to 10 minutes. During this time the material's response to an applied load changes from

depending principally on the rate of loading to depending principally on the amount of loading. Acrylic bone cements are known to exhibit viscosity that decreases with shear rate, described as pseudoplastic behaviour. A power law model was used by Krause *et al.* (1982b) to describe the behaviour of Zimmer LVC, Zimmer MMH65 and Surgical Simplex. Such materials cannot in general be fully described by the Newtonian viscosity. However, a sensible choice of constitutive equation (material model) for a given flow situation depends on the magnitude of the various effects and the accuracy of the required predictions. Indeed the dominant non-linear effect appeared to be increasing elasticity as the cement cured (Figure 4-11 and Figure 4-12). Inclusion of the shear rate dependent viscosity, noted by other authors (Krause *et al.*, 1982b; Beaudoin *et al.*, 1991), in the model was not found to be necessary to predict successfully experimentally determined cement pressures without penetration of cancellous bone. In this study, a simple measure of the cement viscosity was made at a single average shear rate (Appendix A), which proved to be significantly lower than the peak strain rates encountered during the cup insertion process. However, consideration of the strain rate distribution during cup insertion indicates that the average shear rate used in the rheometric testing was not hugely different from the average shear rate experienced by the cement during cup insertion. This may explain why such a simple constitutive law gave reasonable results in the latter experimental and finite element modelling. It is worth noting that similar analyses for femoral component insertion indicate that shear rates are much lower than in the acetabulum, since for the same insertion force, the prosthesis insertion velocities are much lower (New, unpublished data).

Although the conventional cements are all nominally polymethylmethacrylate formulations, large differences in viscosity were found. These differences may be explained by differences in powder particle size and molecular weight distribution, different accelerator composition and the effects of various copolymer species such as styrene (Lautenschlager *et al.*, 1987). The chemical make up of Boneloc differs considerably from the conventional cements, the pre-mixed cement having a powder component composed of poly(butylmethacrylate-methylmethacrylate) copolymer and a monomer component composed of a mixture of methylmethacrylate, *n*-decyl methacrylate and isobornyl methacrylate. There are also modifications to the

accelerator system and thus the different curing kinetics of this cement are easily explained.

The permeability measurement technique developed here to obtain permeability from theoretical relationships between morphology, measured by computerised image analysis, and resistance to flow. The results show reasonable agreement with those of Beaudoin *et al.* (1991), who obtained permeability directly from measurements of pressure drop across human proximal tibial cancellous bone specimens through which a Newtonian fluid was flowing. Beaudoin *et al.* (1991) give the relationship for permeability against apparent wet density, ρ_{aw} , as:-

$$k = -1.85 \times 10^{-11} \rho_{aw} + 2.69 \times 10^{-8} \quad \text{Equation 4-14}$$

When the present results are recast in terms of apparent wet density (using the measured porosity and assuming a marrow density of 800 kg m^{-3}), the regression equation is:-

$$k = -3.63 \times 10^{-11} \rho_{aw} + 4.29 \times 10^{-8} \quad (R^2 = 0.52) \quad \text{Equation 4-15}$$

These adjusted results are compared with those of Beaudoin *et al.* in Figure 4-23.

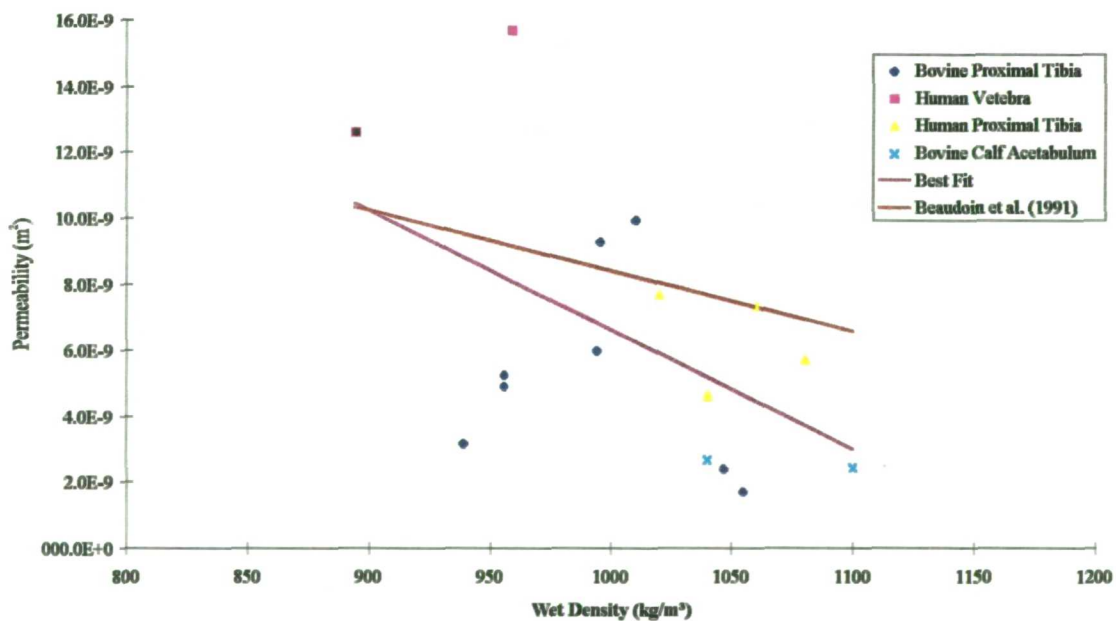


Figure 4-23: Permeability of cancellous bone vs. apparent wet density.

Durst *et al.* (1987) described the underestimation of the experimentally determined pressure drop by theoretical relationships based on the bundle of smooth channels approximation, such as Equation 4-7, by factors of 2 to 3. However these errors are typical of porous materials, such as gravel beds, in which the cross section of the flow

channels changes rapidly along the flow path and hence where the fluid is subject to large elongation and contraction as it passes along the flow path. Elongation and contraction dissipates additional energy and adds to the viscous pressure drop in the channels, assumed smooth. In cancellous bone the cross section for flow is relatively large and does not change nearly as rapidly along the flow path. This may explain why large discrepancies are not apparent between the present results and the results of Beaudoin *et al.* (1991). Thus the technique provides a relatively straightforward method of determining cancellous bone permeability, which can be derived after, for example, the infiltration of the bone specimen with bone cement, provided there is sufficient contrast between bone and cement that they can be adequately distinguished.

Many studies have attempted to define the amount of cement penetration required to produce a mechanically optimal cement-bone interface. Generally mechanical properties improve as penetration increases until a plateau is reached, after which no further improvements can be achieved. Further penetration may lead to increased physiologically undesirable effects such as thermal bone necrosis and excessive viable bone becoming engulfed in bone cement. As a result, most authors agree that 2 to 5 mm of cement penetration is optimal (Huiskes and Sloof, 1981; Krause *et al.*, 1982a; Dorr *et al.*, 1984; Walker *et al.*, 1984), which equates to 1-2 pore diameters in cancellous bone. It has been postulated that the final strength of the cement bone interface is principally determined by the strength of the cancellous bone (Majkowski *et al.*, 1994), which is in turn related to the density (Carter and Hayes, 1977b) and hence permeability (Beaudoin *et al.*, 1991). It is not clear, therefore, how bone permeability would affect the interface strength, since less penetration into denser bone may produce a stronger interface. Many authors have tried to address the question of the pressures required to achieve the desired cement penetration in the acetabulum. One study highlighted the need to continue cement pressurisation to prevent displacement of cement by bleeding of the bone (Benjamin *et al.*, 1987). Juliusson *et al.* (1995) found that the presence of blood in the cancellous spaces before pressurisation began reduced penetration by 50% and explained this strong influence of circulation by the incompressibility of the trapped fluid. This is likely be the reason why thorough cleaning of the bone bed produces quite dramatic effects on overall cement penetration. Previous

attempts to use the finite element method (Beaudoin *et al.*, 1991) have sought to model simple laboratory studies, limited to situations where controlled uniform pressure is employed. The uniform pressurisation assumed in these models is often the very thing that is difficult to achieve in practice. In many cases the prosthesis itself is relied on to generate cement pressure and this was the situation modelled in this study.

The modelling technique appears to perform reasonably well, particularly in the prediction of peak pressures and the penetration of cement into cancellous bone. The accuracy of the predictions does, however, appear to be dependent on the cement type, suggesting that the major source of error is the treatment of bone cement as a Newtonian fluid. As mentioned above, the dominant non-linear effect appeared to be increasing elasticity as the cement cured. Overall, these results suggested that the modelling technique was applicable to the parametric analyses that followed.

The analyses of section 4.4 found that 90% of the ultimate cement penetration was achieved within 2-3 seconds of commencing the pressurisation effort. Neglecting the increase in viscosity as the cement polymerises was thus justified. In the model formulation, as soon as the prosthesis stops moving, cement pressure drops instantaneously to zero. This is a consequence of the Newtonian fluid model assumed. The cause of the cessation of cup motion is impingement of some part of it on the acetabulum; with the unflanged cup the apex of the cup meets the depth of the acetabulum. Alternatively, the flange of the flanged cup may meet the side of the acetabulum, depending on flange size. Although experimentally high pressures continue to be measured after this situation has occurred, particularly with the flanged cup, cement penetration is then essentially complete. The continued application of pressure is valuable clinically to prevent the effects of bleeding mentioned above, but does very little to increase penetration of cement, the effect considered here.

The distribution of cancellous bone assumed in the model representing the acetabulum was a considerable simplification of the real thing. Cancellous bone extended from the edge of the acetabulum to the depth, whereas in the great majority of clinical cases a lip of dense bone of variable width will extend from the rim, representing the edge of the pelvic cortex and the remains of the subchondral plate, which may have become thickened and eburnated by the osteoarthritic disease processes. However, the results presented here sampled the cement penetration approximately 10 mm below the rim,

where cancellous bone is quite likely to be exposed during acetabular pressurisation. For this reason the results are presumed to be representative of cement penetration in this area. A further possible criticism of the finite element modelling technique, also applicable to previous laboratory studies, is that a surgeon applies neither a constant force nor constant velocity when inserting a prosthesis. In reality the direction and the magnitude of the push are likely to change, usually in a deliberate attempt to control the extrusion of the bone cement in some way. In principle arbitrary velocity-time or force-time profiles could be applied to the prosthesis to examine these effects, but to compare prosthesis designs the present technique is ideal, since the numerical results are absolutely repeatable and reproducible. From previous literature, constant force experiments seem to be preferable to constant velocity, although a surgeon is neither a constant force or constant velocity device. Also, by incorporating a very powerful method of solving fluid flow equations for arbitrary fluid domains, namely the finite element method, the technique developed here can easily be generalised to any prosthesis-bone cavity geometry. The values for insertion force, cement viscosity and cancellous bone permeability were chosen to be at the extremes of the ranges encountered clinically. Parametric variation showed cement penetration to be greater with flanged cups, reduced viscosity cement, higher insertion force and more permeable bone. Permeability appears to have a very strong effect simply because it was varied by a factor of 100 compared to factors of 2 for the insertion force and cement viscosity. Several studies have attempted to quantify the cement penetration into cancellous bone in the acetabulum using various methods of cement pressurisation. Typically a few small diameter tubes are placed at strategic locations in the acetabulum. While useful for comparative tests, the somewhat arbitrary diameters chosen by various authors make for difficult comparisons with the present study, where an attempt was made to accurately account for the permeability of the cancellous bone. In general, however, the same trends emerge as reported here. As expected, the flanged cup was always at an advantage compared to the unflanged cup, resulting in approximately 20% increase in overall cement penetration in all cases. Halving the cement viscosity or doubling the insertion force both resulted in 40% increase in ultimate cement penetration. These comparisons, together with qualitative comparisons with post-operative X-rays, suggests that the finite element modelling

technique presented is suitable for describing the effects of prosthesis design on cement penetration and for evaluation of design improvements.

With regard to cementing technique, the results suggest that the prosthesis should be inserted with as much force as possible to produce maximum cement penetration. Although the use of reduced viscosity cement would also seem to be advisable, clinical experience shows the “low viscosity” cements to be difficult to handle under surgical conditions. Practical advice would be to insert the cement and then the prosthesis as soon as the cement is judged to be able to reasonably support its own shape. Since body forces (gravity) on the bone cement were not considered, this particular effect cannot be assessed from the current models. If these effects were to be considered, a more sophisticated treatment of cement viscosity with time would be required.

4.6 Summary

Aseptic loosening is the most common cause of late failure of total hip replacement. Analysis of the Swedish Arthroplasty Register has demonstrated that modern surgical techniques have led to a reduction in the rate of aseptic loosening (Malchau and Herberts, 1996). The enhanced initial fixation brought about by careful preparation of the bone bed and cement pressurisation are considered to be responsible for the improvement. Various studies suggest that cement pressurisation and subsequent penetration of cement into cancellous bone produces a stronger interface (Krause *et al.*, 1982a; Askew *et al.*, 1984). Prosthesis design is important for cement pressurisation (Beverland *et al.*, 1993; Shelley and Wroblewski, 1988) and appears to be clinically significant since improvements in the radiographic appearance of the cement bone interface for flanged cups are observed in the long term (Hodgkinson *et al.*, 1993). A model of cement flow during component insertion in joint replacement, based on the finite element method and using simple treatments of cement viscosity and cancellous bone permeability, has been developed and then applied to quantify the effects of prosthesis design on cement penetration into cancellous bone in the acetabulum. Parametric analyses showed cement penetration to be greater with flanged cups, reduced viscosity cement, higher insertion force and more permeable cancellous bone. Cement penetration varied from negligible (less than 0.5 mm) to

more than 5 mm. The trends were in agreement with those reported in the literature and appeared reasonable in comparison to typical post-operative radiographic appearances.

5. Mechanical Aspects of Acetabular Cup Fixation

5.1 Introduction

The mechanism of failure of cemented acetabular cups is still debated (section 2.4). Recent studies have emphasised the role of cellular reactions to particulate debris arising from wear of the cup articulating surface, but there is considerable evidence that the initial quality of fixation is an important determinant of long term success. Understanding of the mechanics of the pelvis and of acetabular reconstruction remains incomplete, especially with regard to sub-optimal component fixation (partial debonding at the cement-bone interface). Thus structural finite element analyses of the innominate bone in various configurations have been performed. Using these models, modifications to acetabular mechanics induced by the implantation of acetabular prostheses have been investigated. Additionally, the effects of sub-optimal fixation have been studied.

5.2 Methods

All the structural finite element models used are derived from the nodal, connectivity and material properties definitions of Dalstra (1993). The full details of the development of this model, which includes validation with a strain gauge study, are given in Dalstra *et al.* (1995), but a brief summary and a description of some necessary modifications is given below. All structural analyses were performed with the ANSYS general purpose finite element package (releases 5.0a and 5.3) and its integrated pre- and post-processing modules (ANSYS Inc, Houston, Pennsylvania, USA), running on various IBM PC compatible computers with Microsoft Windows 95 and MS-DOS 6.0 operating systems.

5.2.1 The Basic Finite Element Mesh

The basic mesh consists of elements that describe the cortical shell and the cancellous bone of the bulk of the pelvis. The geometry of the model was defined by manually sectioning and digitising slices from the pelvis of an 87 year old male. The digitised sections were then divided into 4 node quadrilaterals which, when the sections were

stacked, were connected to form 8 node brick elements representing the cancellous bone. The faces of the brick elements on the surface of the model were then overlaid with 4 node membrane elements to represent the cortical shell. Young's moduli were assigned to the brick elements by superimposing the mesh on a dual energy quantitative CT scan, from which the Young's modulus of the cancellous bone was derived with the empirical relationship:-

$$E = 2017.3 \left(\frac{\rho_{Ca-eq}}{0.626} \right)^{2.46} \quad \text{Equation 5-1}$$

where E is Young's modulus and ρ_{Ca-eq} is the calcium equivalent density, a calibrated quantity derived from X-ray absorption values. Poisson's ratio for these elements was assumed to be 0.2. The thickness of the cortical shell was also measured from the CT scan slices and assigned to the nodes of the relevant membrane elements. Young's modulus and Poisson's ratio for the cortical shell were assumed to be 17 GPa and 0.3 respectively. All materials were assumed homogeneous, isotropic and linear elastic.

5.2.2 Modifications

Due to differences between the MARC finite element program (MARC Analysis Corporation, Palo Alto, USA) used by Dalstra and ANSYS, certain changes had to be made to the basic model. A computer program was written to modify elements too distorted to be acceptable to ANSYS. Some 15% of the original 8 node brick elements were transformed into 6 node prisms and 4 node tetrahedra. Fortunately, since such mixed meshes can perform poorly, only 15 tetrahedral elements were required. Similarly, 55% of the original 4 node membrane elements were transformed to 3 node triangles because of excessive deviation from planarity ("warping"). These adjustments were made by modifying the element connectivity and did not affect the positions of nodes and hence the geometry of the model. Care was taken to ensure that the correct distribution of material properties and membrane thickness was preserved. The modified finite element mesh, the distribution of Young's modulus in the cancellous bone and the distribution of cortical thickness are shown in Figure 5-1. In total the model comprises approximately 700 nodes and 1300 brick and membrane elements. Comparative tests with the results of Dalstra (1993) showed negligible differences in the results due to the mesh modifications and the different FE codes.

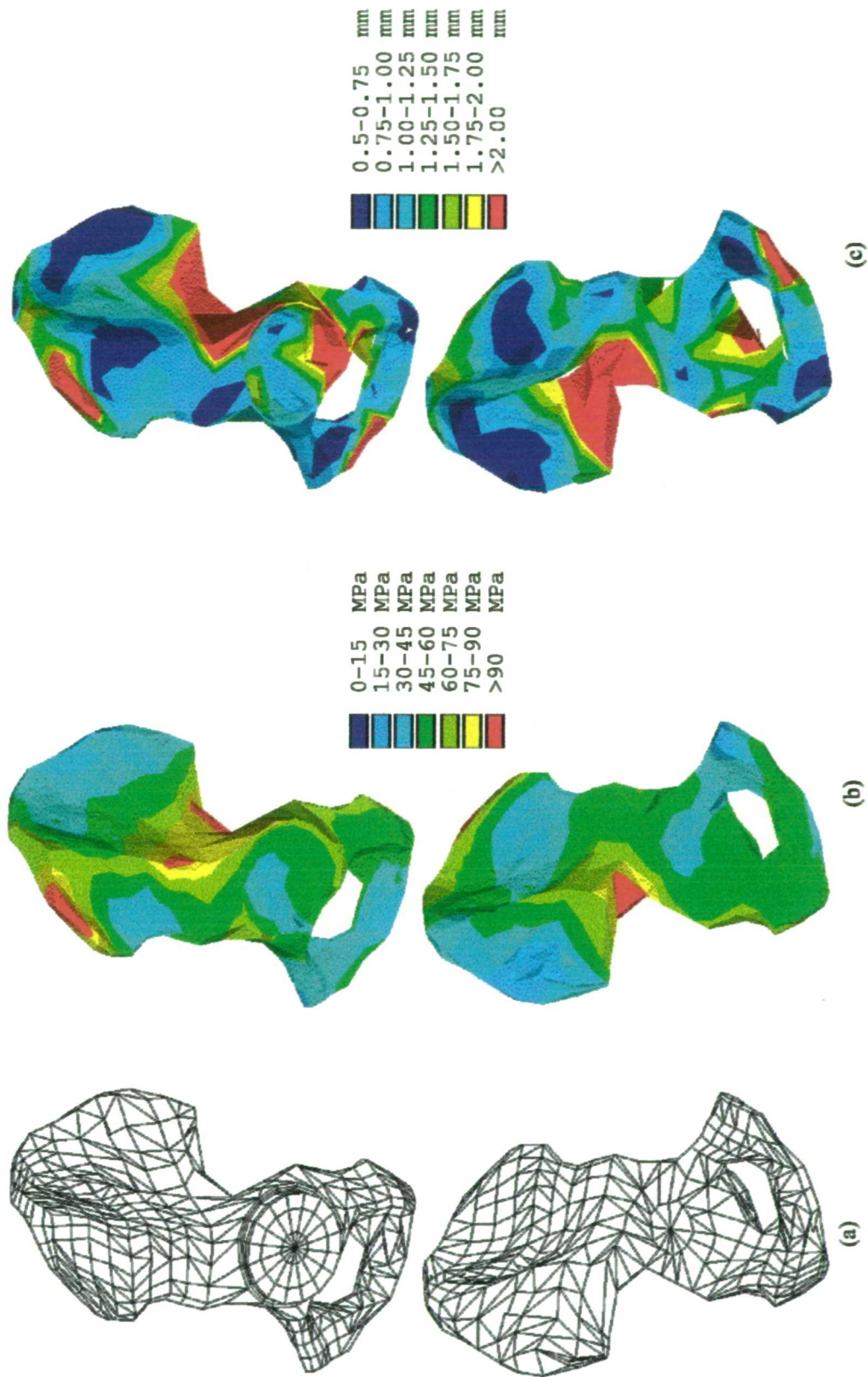



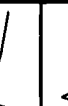






Figure 5-1: Lateral (top) and medial (bottom) views of the finite element model. (a) Modified finite element mesh, (b) Young's modulus distribution in the cancellous core, (c) Thickness distribution in the cortical shell.

5.2.3 Applied Loads

Force vectors representing 22 muscles acting across the hip joint and the hip joint reaction force during 8 "snapshots" of the gait cycle were available for application to the model (Table 5-1). The magnitudes and directions of the muscle forces were derived by Dalstra from the studies of Crowninshield and Brand (1981) and Dostal and Andrews (1981) respectively and the hip joint reaction force from Bergmann *et al.* (1993). Muscle insertions are shown in Figure 2-3.

Table 5-1: Hip joint force and muscle forces for eight load cases during gait. (N)

	1	2	3	4	5	6	7	8
								
Hip joint reaction force	426	2160	1876	1651	1180	187	87	379
Gluteus minimus	228	140	263	228	175	123	114	219
Gluteus medius	1018	1053	1474	1509	1412	982	105	421
Gluteus maximus	842	930	167	377	456	491	114	482
Tensor fasciae latae	0	132	88	158	149	88	70	96
Adductor brevis	0	114	0	0	0	202	0	114
Adductor longus	0	88	0	0	88	158	70	140
Adductor magnus	0	0	0	0	132	263	0	0
Semimembranosus	579	368	333	368	421	298	61	421
Semitendinosus	0	140	105	246	316	368	105	0
Biceps femoris (long head)	298	202	88	70	123	114	79	377
Gracilis	0	0	0	0	88	158	70	140
Sartorius	0	88	0	0	35	158	88	88
Iliacus	0	0	0	228	307	272	0	0
Psoas	149	0	316	175	88	175	105	140
Gemellus inferior	0	0	0	0	0	140	79	149
Obturator externus	0	0	0	0	123	167	135	123
Obturator internus	167	123	0	61	61	149	123	0
Pectineus	0	0	175	96	0	149	0	0
Piriformis	202	175	0	0	0	0	123	228
Quadratus femoris	61	96	0	0	88	184	0	0
Gemellus superior	140	88	123	79	0	0	158	202
Rectus femoris	0	123	0	0	0	175	105	96

The most important muscles not included in this model are the erector spinae, the internal and external obliques and quadratus lumborum. These muscles do not cross the hip joint and are principally active on the contralateral side during the stance phase of gait, since they function to stabilise the upper body with respect to the pelvis (Cunningham's Textbook of Anatomy, 1972).

To describe correctly the transfer of load between the femoral head (femoral prosthesis) and the acetabulum (acetabular cup), a portion of the femoral head (femoral prosthesis) was included in all models. The femoral section was coupled to the acetabulum by contact elements supporting only compressive load transfer at the interface, since the contact between head and cup was in all cases assumed to be frictionless.

5.2.4 Solution

Since the models include non-linear contact elements, initial solution of the finite element displacement equations required iterative techniques. Once contact was established, however, the solution proceeded as for a linear problem unless the contact status of a contact element changed. Other non-linearities such as large deflections and stress stiffening may occur in the pelvis under physiological loading, but were considered to be of secondary importance and were omitted. Under these conditions, typical total solution time was 2 hours using a Pentium 120 PC with 32MB of RAM.

5.2.5 Hoffman Failure Criterion for Cancellous Bone

Failure criteria provide methods for comparing the actual state of stress in a material to some allowable state of stress and hence determine whether failure is likely to occur. The von Mises criterion, developed to predict yielding in ductile metals, assumes failure (yielding) will not occur providing the von Mises equivalent stress remains below the uniaxial yield stress of the material. Applying the simple von Mises yield criterion to cancellous bone is difficult since failure under pure hydrostatic stress is excluded, clearly a problem for a porous material, and no allowance is possible for differences in tensile, compressive and shear strength. The Hoffman failure criterion (Hoffman, 1967) has been used previously to describe the failure of cancellous bone (Stone *et al.*, 1983) and bone implant interfaces (Weinans *et al.*, 1993). The Hoffman

criterion has been modified to allow its use in problems involving multiaxial stresses in cancellous bone (Equation 5-2). Failure is said to have occurred when the left hand side of this equation, the Hoffman failure index, exceeds the critical value 1. Although this criterion may not predict failure under hydrostatic stress, it does allow for different tensile, compressive and shear strengths.

$$\frac{1}{2F_t F_c} \left[(\sigma_y - \sigma_z)^2 + (\sigma_z - \sigma_x)^2 + (\sigma_x - \sigma_y)^2 \right] + \left(\frac{1}{F_t} - \frac{1}{F_c} \right) (\sigma_x + \sigma_y + \sigma_z) + \frac{1}{F_s^2} (\tau_{yz}^2 + \tau_{zx}^2 + \tau_{xy}^2) > 1$$

Equation 5-2

where σ_x , σ_y and σ_z are the component normal stresses, τ_{xy} , τ_{yz} and τ_{zx} are the component shear stresses and F_t , F_c and F_s are the tensile compressive and shear strengths respectively. The relationships of Kaplan *et al.* (1985) and Stone *et al.* (1983) (Equation 5-3 to Equation 5-5) were used to calculate the tensile, compressive and shear strength for each cancellous bone element based on its apparent density (calculated from the CT density of Dalstra (1993)).

$$F_c = 3 \cdot 24 \cdot 10^7 \rho^{1.85}$$

Equation 5-3

$$F_t = 1 \cdot 45 \cdot 10^7 \rho^{1.71}$$

Equation 5-4

$$F_s = 2 \cdot 16 \cdot 10^7 \rho^{1.65}$$

Equation 5-5

5.3 Analyses

To investigate the effects of assumptions regarding the loading of the pelvis and the kinematic boundary conditions applied, three finite element models representing the normal pelvis were used. The first modelled the full pelvis by reflecting the hemi-pelvis mesh in the plane of the pubic symphysis and connecting the two halves by solid elements (Young's modulus of 11.5 MPa, Poisson's ratio 0.45), assumed to be representative of symphyseal fibrocartilage. Both sacroiliac joints were assumed to be "built-in", i.e. all degrees of freedom at the nodes attached to the element faces representing the joint surfaces were specified as zero. The second modelled the hemi-pelvis with both the sacroiliac joint and the pubic symphysis "built-in" and the third the hemi-pelvis with just the sacroiliac joint "built-in".

The subchondral bone layer of the lunate surfaces was modelled with membrane elements, 2 mm thick, with a Young's modulus of 2 GPa and a Poisson's ratio of 0.3,

and the cancellous bone underlying the lunate surface modelled with solid elements as previously described for the basic mesh (sections 5.2.1-5.2.2). The distribution of Young's modulus in the underlying cancellous bone is shown in Figure 5-2. Articular cartilage (Young's modulus 11.5 MPa and Poisson's ratio 0.45) with a thickness of 2 mm was assumed to cover the lunate surfaces and the femoral head. To avoid confusion, henceforth "subchondral bone" will refer to the cortical layer modelled with membrane elements and "sub-lunate cancellous bone" to the layer of cancellous bone immediately below it. There is no sharp anatomical distinction between the cancellous bone of this region and that in the bulk of the pelvis. In all cases the loaded (left) side of the pelvis had the muscle forces and hip joint reaction force corresponding to the early single leg stance phase of gait applied (load case 2, Table 5-1).

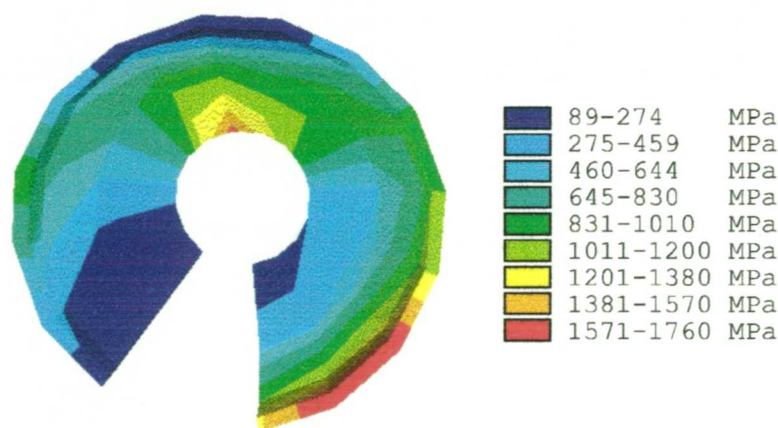


Figure 5-2: Young's modulus distribution in the sub-lunate cancellous bone.

The effects of the replacement of the normal acetabular joint surface with a cemented polyethylene cup were examined. Recent studies of reconstructed femora in various configurations have indicated that, after prosthesis implantation, peak cancellous bone stresses can be an appreciable fraction of, and may even exceed the strength of, the bone and also that these stresses correlate with early migration (Taylor *et al.*, 1995). Based on these observations it has been suggested that migration is caused by the collapse and subsequent remodelling of cancellous bone (Taylor and Tanner, 1997). In view of this hypothesis, the cancellous bone stresses in the normal and in the reconstructed acetabulum have been compared to the bone strength using the Hoffman failure criterion. Since stresses at the bone-cement interface are also highly significant, these were also considered. The nodal force method described by Kuiper (1993),

which divides the nodal forces that act between the elements of the materials adjacent to the interface by the area attributed to the nodal points, was used to calculate interfacial stresses, resolved into tilting and twisting shear stress and normal stress components according to Figure 5-3.

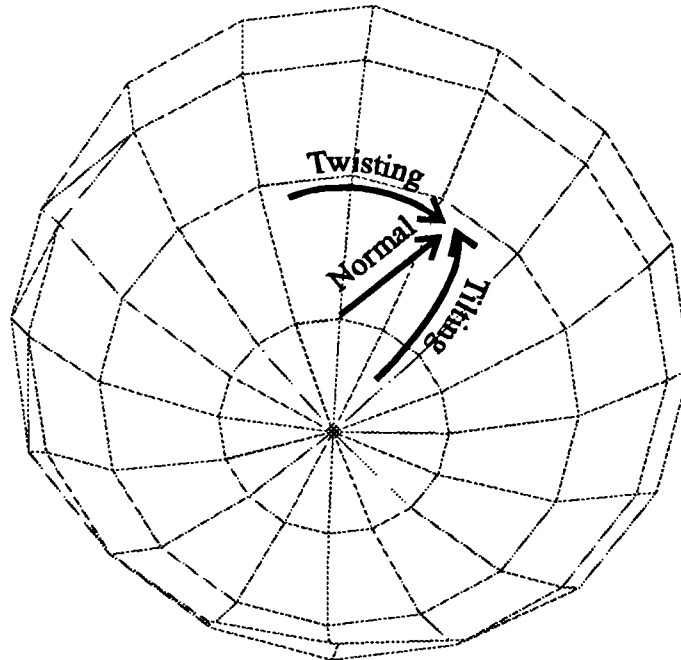
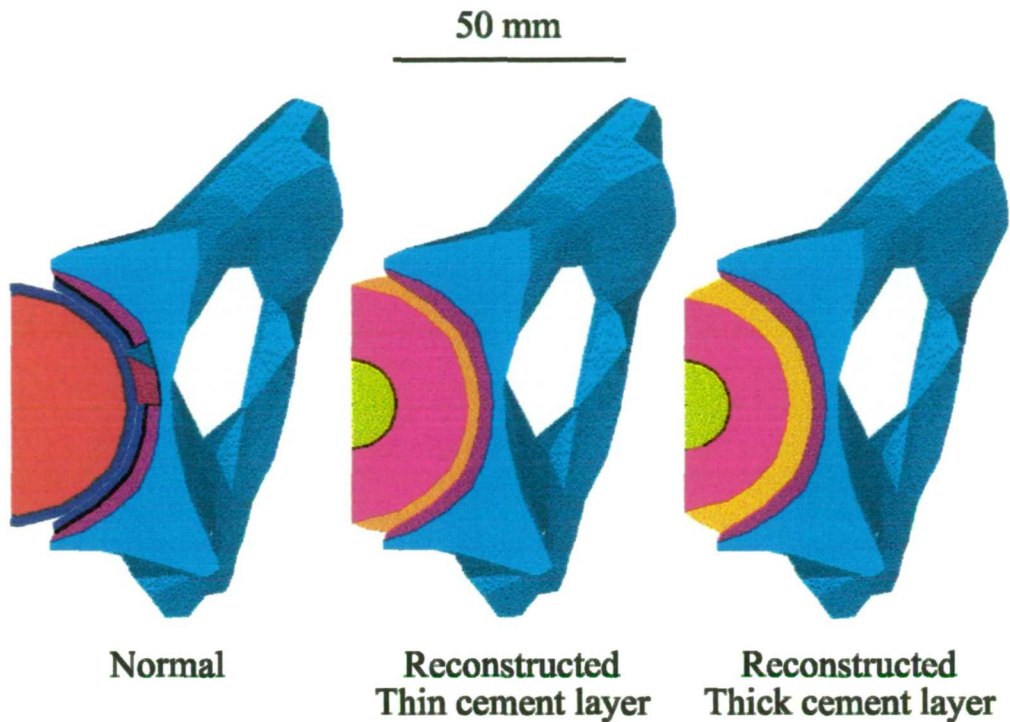


Figure 5-3: Positive direction of normal, twisting and tilting shear stress.

The hemi-pelvis model with built-in pubic symphysis and loaded with load case 2 (Table 5-1) was used to analyse the stresses in the normal pelvis and two variations of a pelvis implanted with a cemented all-polyethylene prosthesis. Two cement mantle thicknesses were studied (3 mm and 6 mm, with 18 mm and 15 mm cup thicknesses to keep the total cement plus cup thickness constant) (Figure 5-4). In the implanted models, the acetabular floor region between the lunate surfaces was filled with 8 node brick elements (Young's modulus 622 MPa and Poisson's ratio 0.2), approximating the shape of a typical pre-implantation acetabulum. Two separate cases were considered for each implanted model in which the subchondral bone plate was assumed to have been removed by reaming, or retained. The results of the finite element analyses were then used to define a Hoffman failure index for each cancellous bone element based on the equations presented in section 5.2.5.












Key	Material	Young's Modulus	Poisson's Ratio
	Pelvic cancellous bone	Variable (see text)	0.2
	Subchondral bone	2×10^9	0.3
	Sub-lunate cancellous bone	Variable (see text)	0.2
	Articular cartilage	11.5×10^6	0.45
	Bone cement	2.5×10^9	0.3
	Acetabular cup	1×10^9	0.4
	Femoral cancellous bone	800×10^6	0.2
	Femoral prosthesis	210×10^9	0.3
	Pelvic cortical bone	17×10^9	0.3

Figure 5-4: Sections through the normal and implanted acetabula.

To simulate debonding of the cement bone interface, the model with the thick cement layer and retention of the subchondral bone had successive layers of nodes associated with element edges at the perimeter of the cement-bone interface separated by inserting gap elements which only allowed transmission of compressive and (in the case of a non-zero coefficient of friction) shear forces across the interface. The model was analysed in four configurations, the first assuming a fully bonded cement bone interface and the second, third and fourth assuming one, two and three circumferential

layers of nodes were released at this interface respectively. The release of one, two and three layers corresponded to debonded layers 10, 23 and 36 mm deep respectively, extending from the acetabular rim towards the pole (Figure 5-5). These models will henceforth be referred to as the “one layer”, “two layer” and “three layer” debonded models.

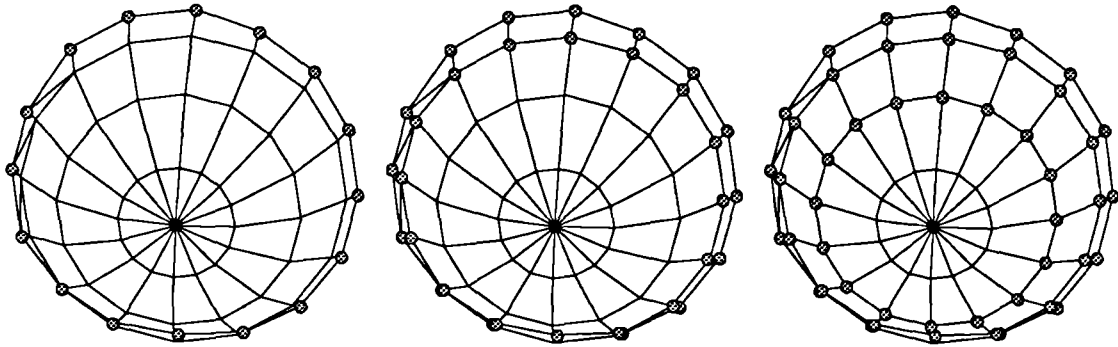


Figure 5-5: Locations of debonding for the one-, two- and three layer debonded models.

Since the gap size was chosen arbitrarily, the effect of the initial gap size was investigated by comparing 0.1 mm and 0.5 mm gaps. To investigate the effects of friction on the interface, a Coulomb friction model with a friction coefficient (μ) of 0.25 was assumed. This value lies between those for surfaces with a fairly effective lubricant and ones with no lubricant (O'Connor, 1968). The load transfer behaviour of the gap elements is illustrated in Figure 5-6, where F_N is the force normal to the interface, F_T is the force tangential to the interface (friction model only), $((u_N)_i - (u_N)_j)$ and $((u_T)_i - (u_T)_j)$ are the relative displacements of the gap element nodes in the normal and tangential directions respectively and K_N and K_T are the normal and tangential contact stiffnesses. If the gap element closes when loads are applied to the structure, equal and opposite normal contact forces are applied to the nodes of the gap element which are shared by solid elements on either side of the interface, according to the relationships of Figure 5-6. The normal contact stiffness constant K_N was in all cases assumed to be equal to the average stiffness of the cancellous bone elements attached to the contact element node. K_T was assumed to be equal to K_N . The two effects of interest in this case were the alterations to the stresses in the acetabulum and the micromotion between cement and bone brought about by the debonding. In this thesis the term “micromotion” is used exclusively to describe small sliding displacements between two materials at a non-bonded interface. An alternative definition of

micromotion is the elastic and plastic deformation of the materials at the interface (Taylor and Tanner, 1997).

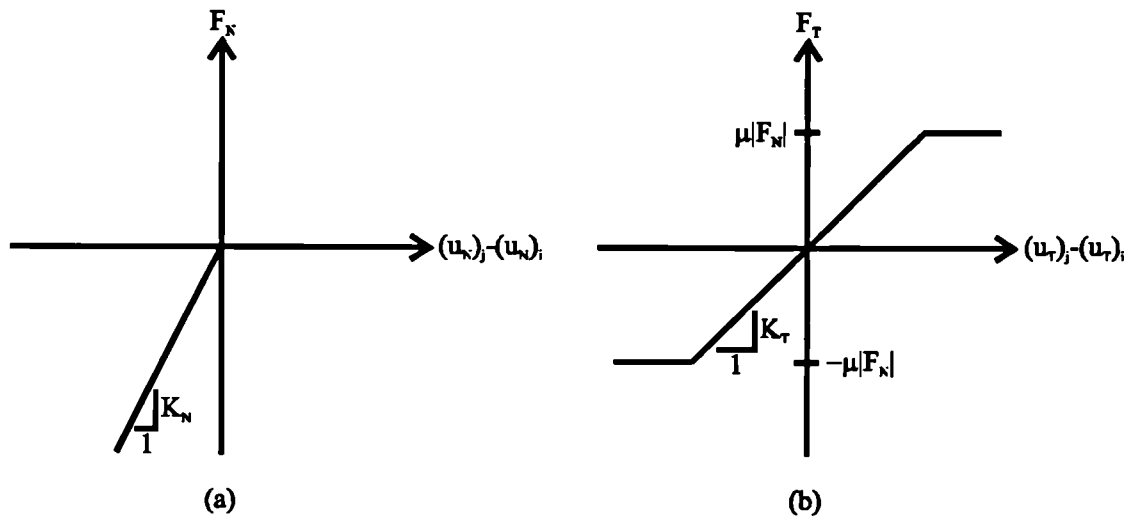


Figure 5-6: Force deflection relationships for contact (gap) elements.
 (a) normal and (a) perpendicular to the interface.

5.4 Results

5.4.1 The Effect of Boundary Conditions on Pelvic Mechanics

The effect of changes in the kinematic boundary conditions on nodal displacements are shown in Figure 5-7. Peak displacements in the iliac wing were virtually unchanged by the choice of boundary conditions, in all cases being in the region of 6 mm under the action of the hip abductor muscles. Near the pubic symphysis, displacements were, predictably, highest when the symphysis was unrestrained, with up to 6 mm of posterior-medial displacement. The presence of a contralateral hemi-pelvis reduced displacement at the pubis to about half that seen for the unrestrained symphysis. Generally the displacements in the hemi-pelvis were least with the built-in pubic symphysis, intermediate with the full pelvis and most with the free pubic symphysis.

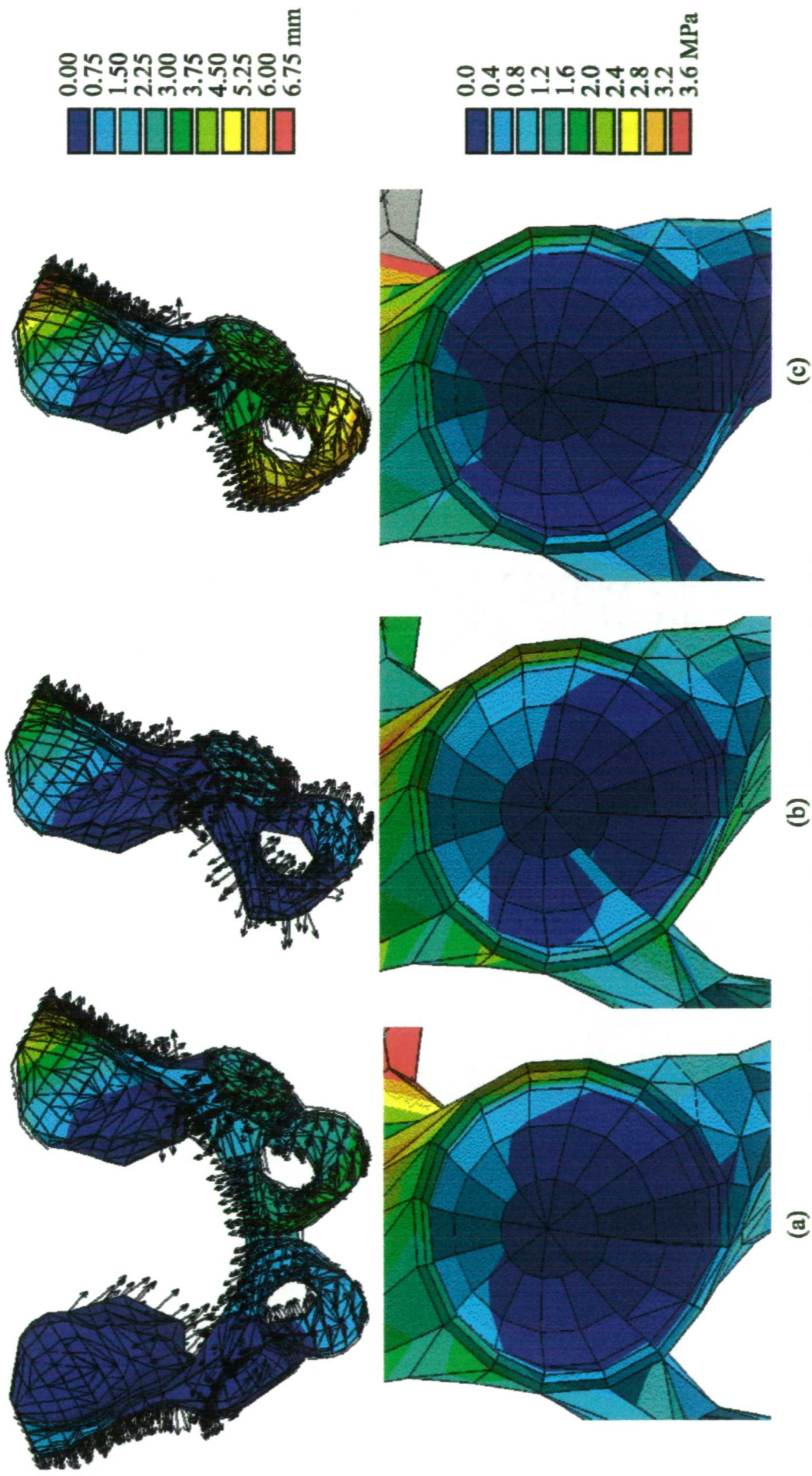


Figure 5-7: Pelvic deformation and von Mises stress in the sub-lunate cancellous bone. (a) a full pelvis with both sacroiliac joints built-in, (b) a hemi-pelvis with built-in pubic symphysis and built-in sacroiliac joint and (c) a hemi-pelvis with free pubic symphysis and built-in sacroiliac joint. For displacements (top), contours represent the magnitude and the arrows represent the direction of the displacement vector.

The overall pattern of the von Mises stresses in the cancellous bone underlying the subchondral bone plate were similar for the built-in pubic symphysis model and the full pelvis model. Stresses were marginally higher for the built-in pubic symphysis model, particularly in the region of the pubic bone. Allowing the pubic symphysis to move freely reduced stresses in the depth of the acetabulum and produced high stress in the region of the greater sciatic notch. There was a general trend to increase the area under higher stresses as the pubic symphysis became progressively more constrained.

5.4.2 Load Transfer in Normal and Reconstructed Acetabula

Figure 5-8 compares the peri-acetabular displacement fields for the normal and reconstructed acetabula for load case 2 (Table 5-1). In the reconstructed case the overall displacements are smaller, particularly in the superior quadrant, suggestive of significant stiffening of the acetabulum by the implant.

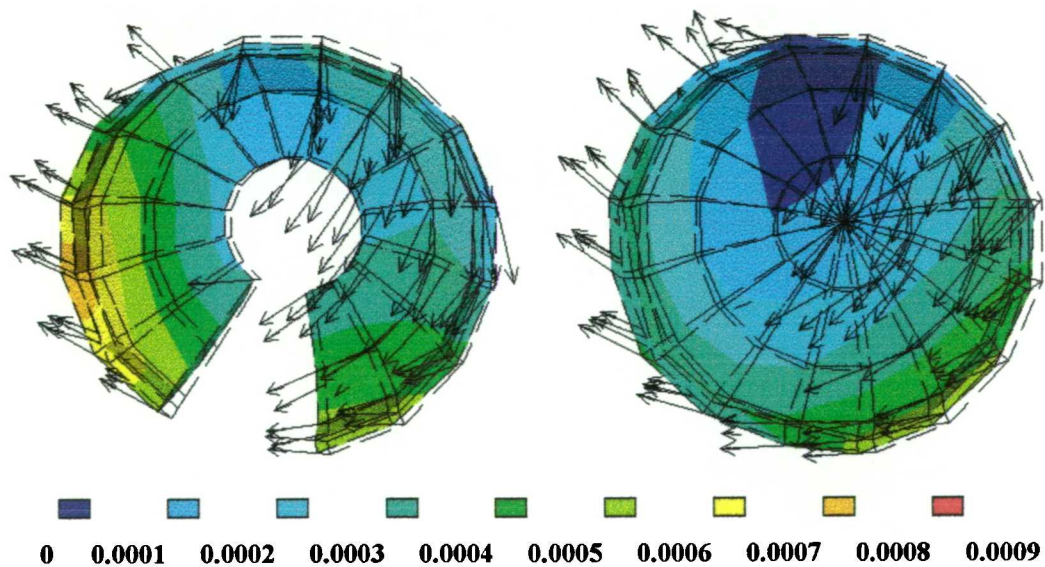


Figure 5-8: Peri-acetabular displacements in normal and reconstructed acetabula. Contours represent magnitude (mm) and arrows direction of the displacement vector.

Von Mises stresses in the cancellous bone and the distribution of the Hoffman failure criterion for the normal and both reconstructed models without the subchondral plate are shown in Figure 5-9. Peak stresses in the sub-lunate cancellous bone in both reconstructed acetabula were lower than in the normal acetabulum and stresses were distributed over a wider area. In the reconstructed cases significantly more stress was transferred through the rim of the acetabulum. Changing cement thickness produced minimal changes in both the displacement and stress fields.

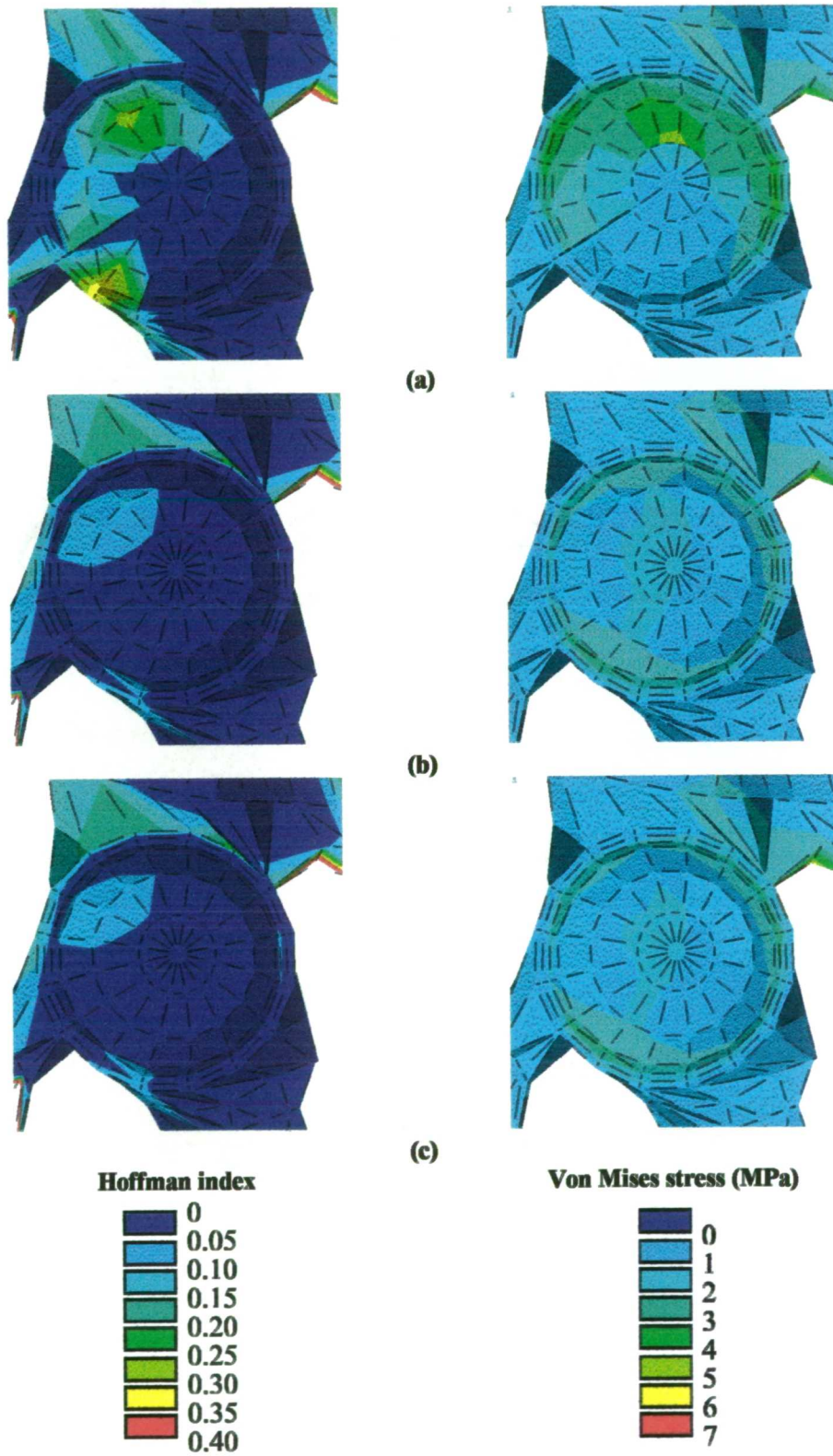


Figure 5-9: Distribution of the Hoffman criterion and von Mises stress. (a) Normal, (b) thin cement layer and (c) thick cement layer.

In the normal acetabulum the maximum value of the Hoffman index in the region of the acetabulum was less than 0.4 (greater than 1 represents failure). In both reconstructed acetabula the maximum value was reduced to below 0.15, again there was virtually no difference between the two cement thicknesses.

Comparing the effect of removal or retention of the subchondral plate, small differences were seen in the cancellous bone von Mises stresses and the Hoffman index. The differences were most clearly manifested in the interface stress components as shown in Figure 5-10 and Figure 5-11. Where the subchondral plate was sacrificed, peak stresses at the interface were slightly raised, but overall the differences were negligible. Compared to the bulky acetabular cup and bone cement, the stiffness of the subchondral plate is small, so it contributes relatively little to the stiffness of the acetabulum.

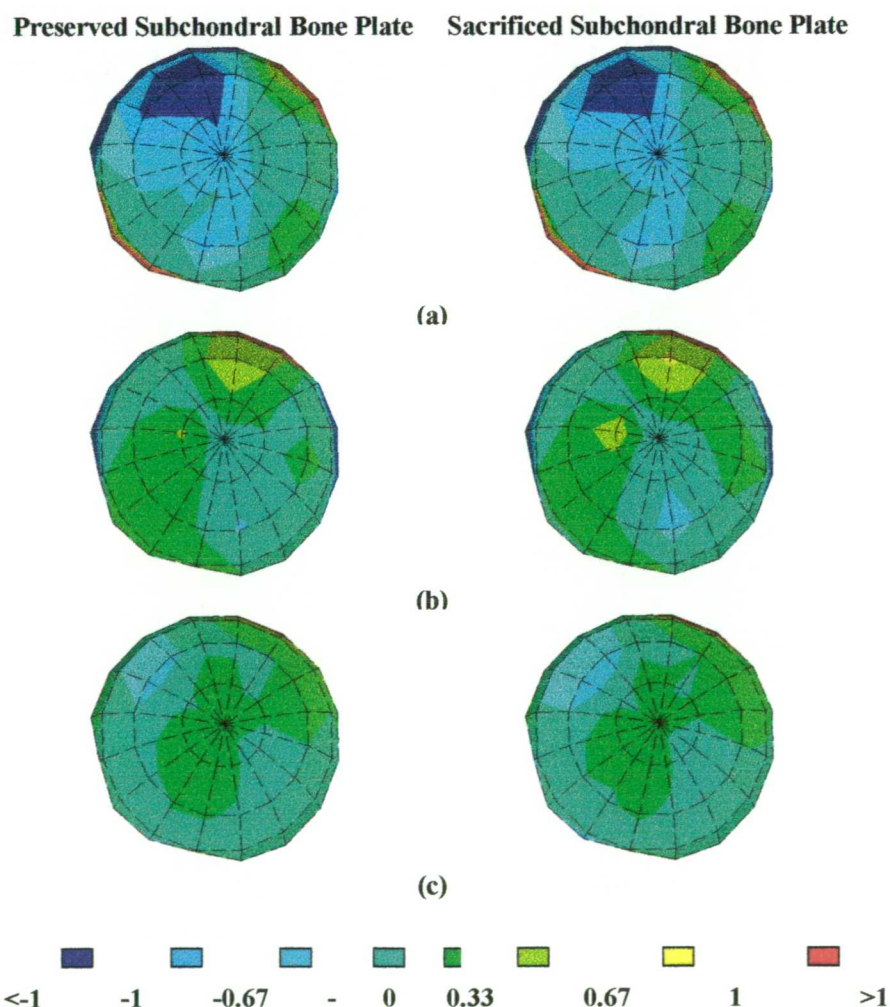


Figure 5-10: Effect of sacrifice of the subchondral plate on interface stress. Results for thick cement model (a) normal, (b) twisting and (c) tilting stresses (MPa)

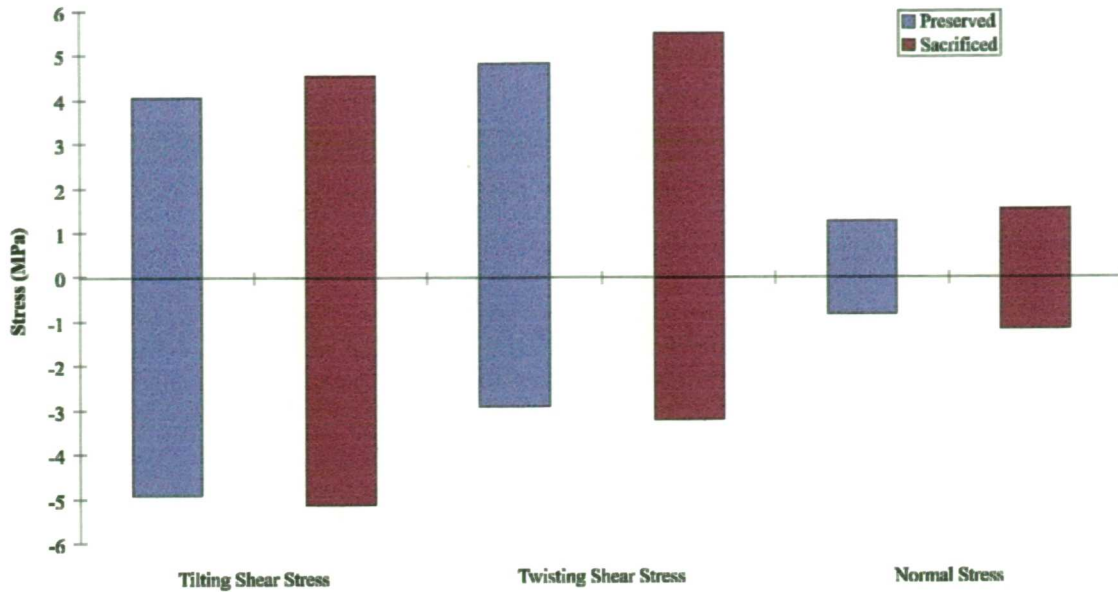


Figure 5-11: Maximum and minimum values of the interface stress components. Results for thick cement model with preserved and sacrificed subchondral bone plate.

5.4.3 The Effect of Prosthesis Debonding on Acetabular Mechanics

Figure 5-11 shows the micromotion at the bone cement interface for three locations around the acetabular rim of the frictionless, 0.1 mm gap (“baseline”) model for the two layer debonded case.

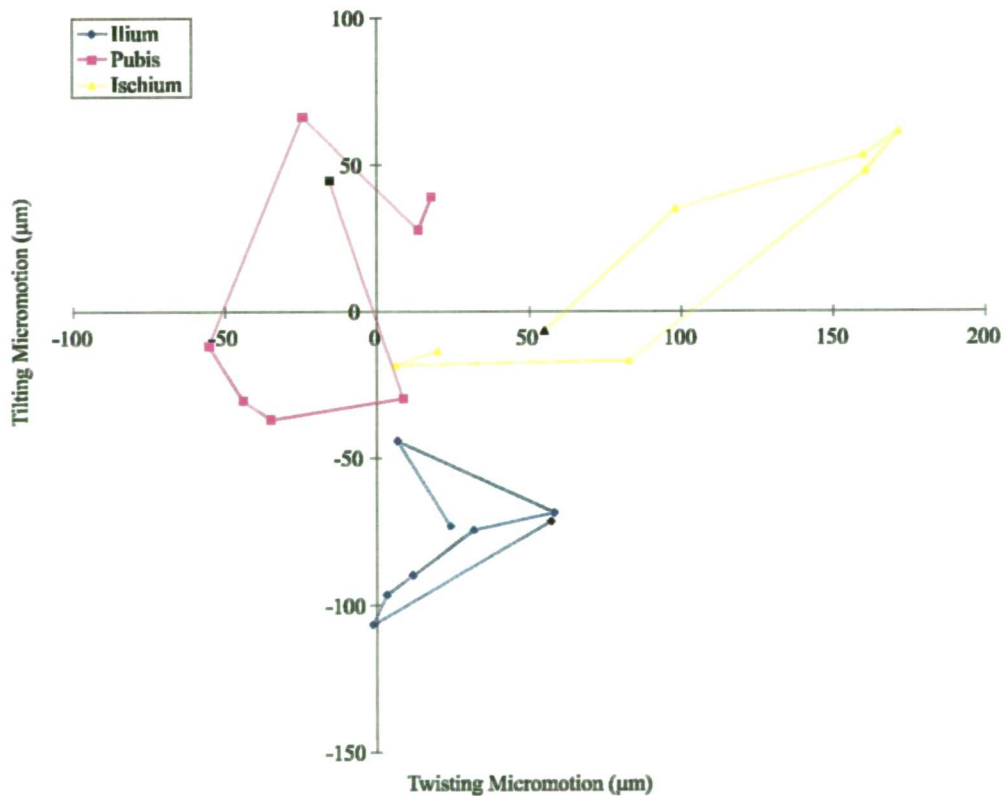


Figure 5-12: Tilting and twisting micromotion at the ilium, ischium and pubis. Results for the two layers debonded baseline model. Black markers represent load case 1, the line joins the points that represent the further load cases in the order they appear in Table 5-1.

The position of each point represents the relative displacement parallel to the interface of the two nodes of selected gap elements at the ilium, ischium and pubis for the eight load cases representing the complete gait cycle defined in Table 5-1. In the unloaded model, the relative displacement in both directions is zero. Tilting and twisting micromotions as defined in Figure 5-3 are shown on the y and x axes respectively.

Figure 5-13 shows the amplitude of the micromotion over the gait cycle for the one, two and three layers debonded baseline model. At all locations, except the ilium in the twisting direction, the range of micromotion increases almost linearly with the amount of debonding. With a single debonded layer, representing a debonded width of 7-12 mm depending on position, micromotion parallel to the interface in both directions was greater at the ilium than at the pubis or ischium. Twisting micromotion dominated at the ilium, the total motion over a complete gait cycle being 55 μm in twisting and 30 μm in tilting. This is in accordance with the path the hip joint reaction force vector sweeps in the acetabulum, since the range of the locus of the vector is greater around the symmetry axis of the cup than perpendicular to this axis. A similar effect was observed at the ischium and the pubis, although at the pubis the two sliding components were closer in range. With two layers debonded, this situation was reversed, micromotion at the ilium being least. With three layers debonded, the micromotions at the ilium and pubis were similar and significantly less than that at the ischium. In all cases the relative size of the two components depended on both location and the amount of debonding. At the ischium the tilting component was always less than the twisting. At the pubis, with the exception of the one layer model, the twisting was less than the tilting. At the ilium twisting was greater than tilting in all except the case with two layers debonded.

The effect of friction on the micromotion at the ilium is shown in Figure 5-14. Friction had a small effect, decreasing the amplitude of micromotion. Adding friction to an interface model makes the response of the system dependent on loading history. The application and then removal of load on the system may or may not result in the model returning to its original configuration - it is generally non-conservative. Despite this, in the present model each successive loading cycle generated substantially the same micromotions. This invites the conclusion that in the present model frictional forces were substantially less than elastic restoring forces in the loaded structure.

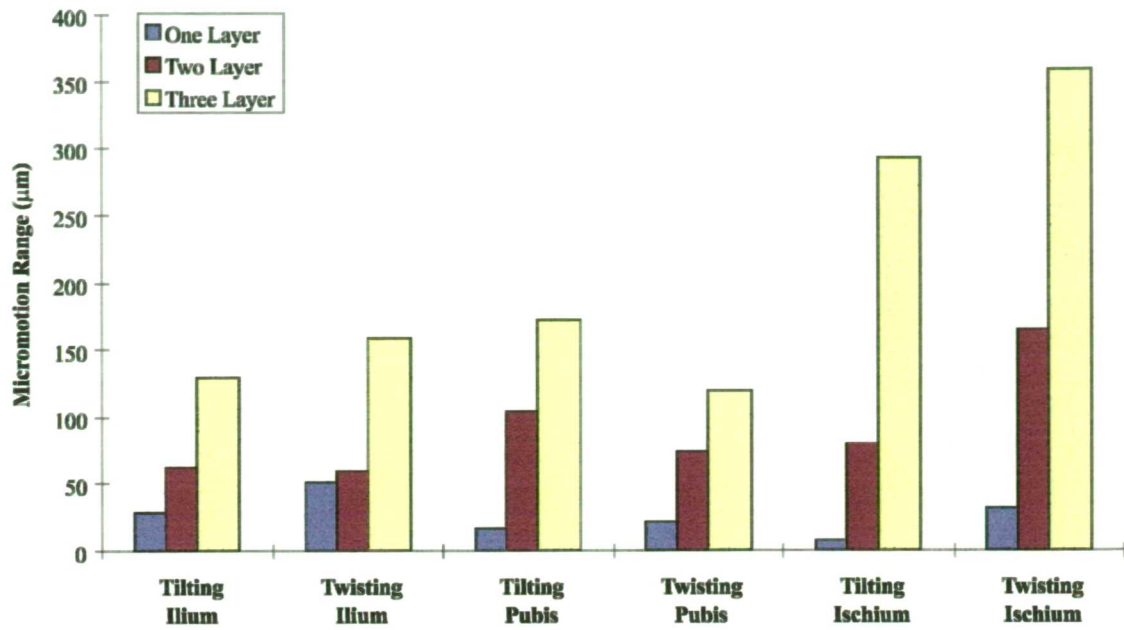


Figure 5-13: Tilting and twisting micromotion at the ilium, pubis and ischium. (baseline model)

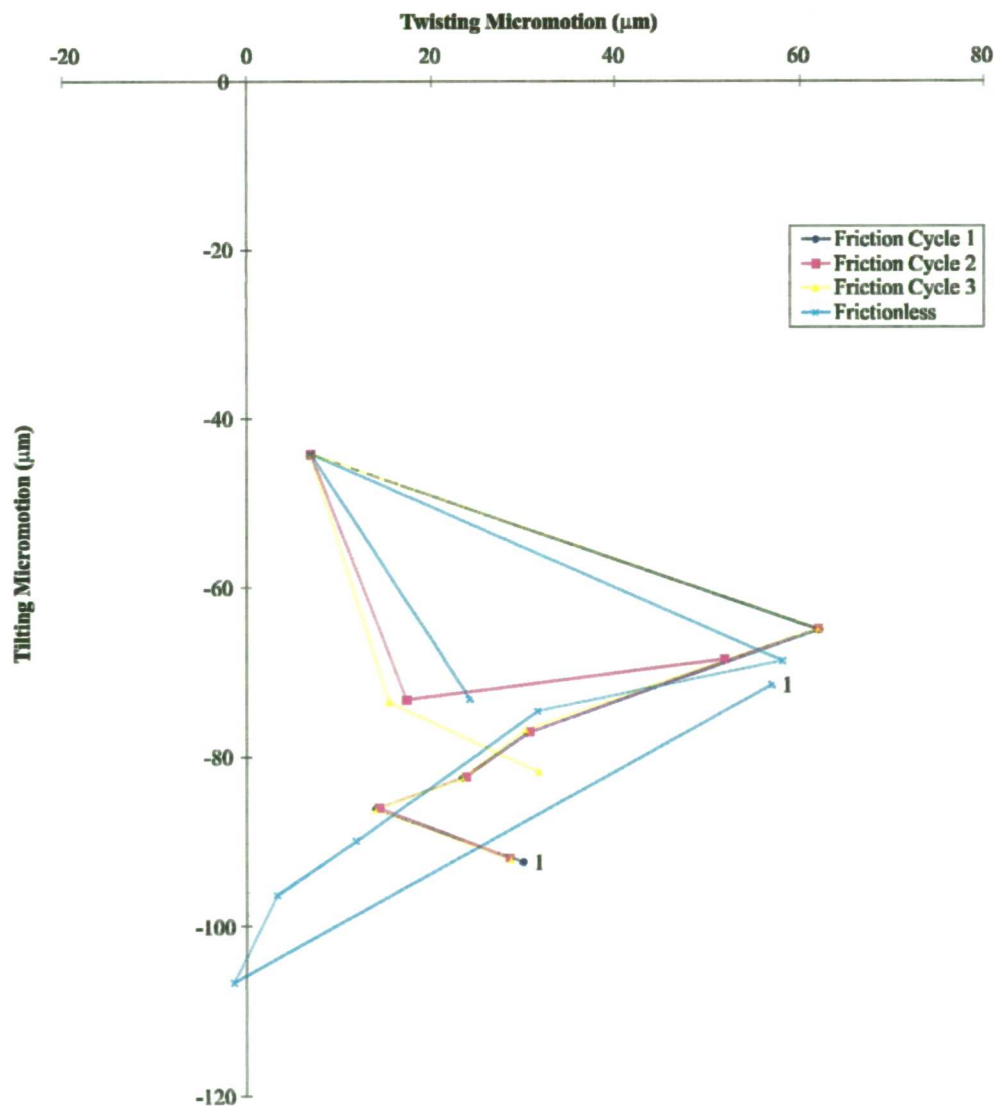


Figure 5-14: The effect of friction on micromotion at the ilium.

Figure 5-15 summarises the range of motion at the three locations as a result of varying the model parameters.

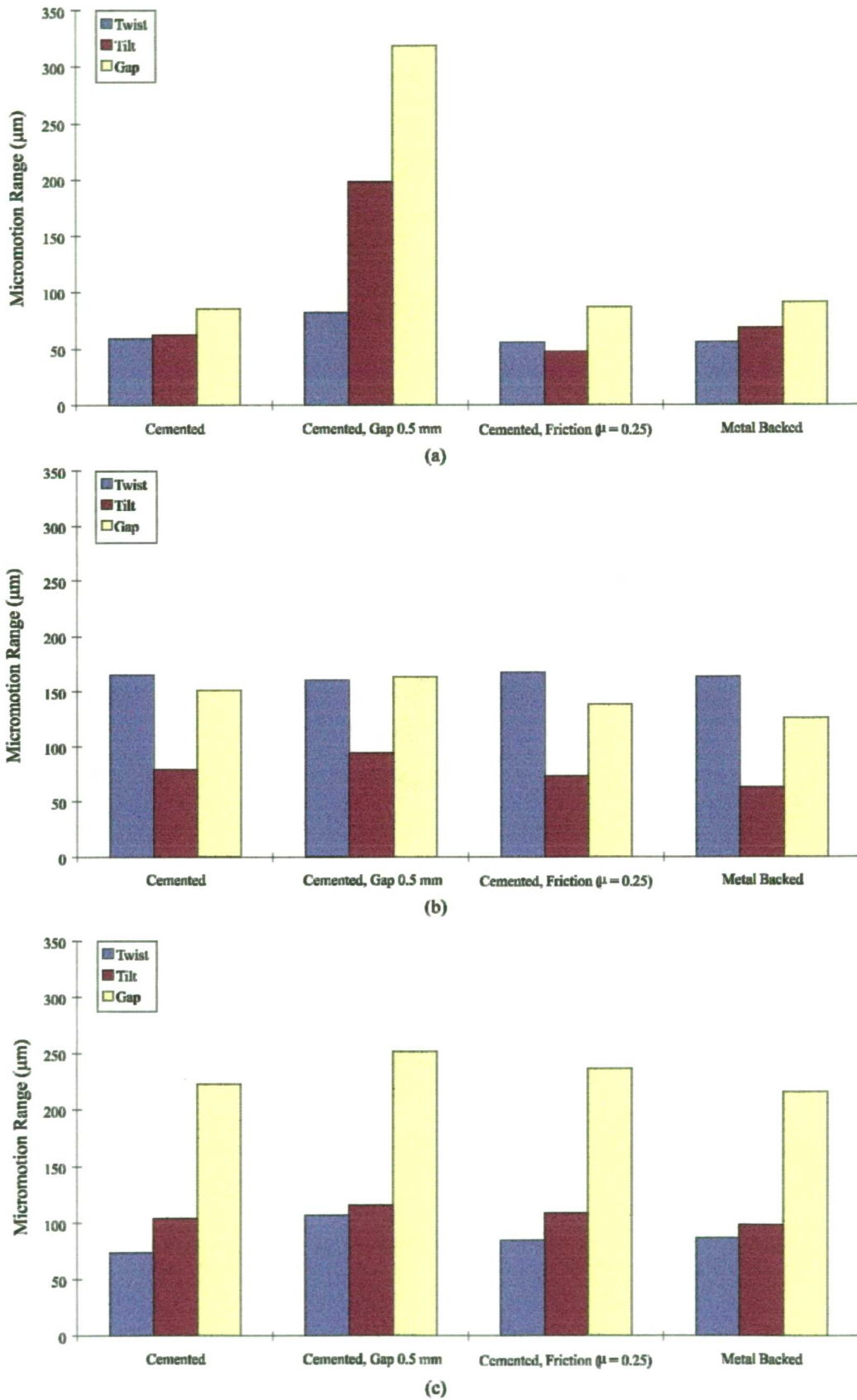


Figure 5-15: Effect of varying model parameters on the range of micromotion. Results at (a) the ilium, (b) the ischium and (c) the pubis.

The assumed size of the gap between cement and bone was by far the most significant parameter. Increasing this gap greatly increased micromotion at the ilium, since most load transfer occurred at this site once debonding was included. Friction had a relatively small influence on the micromotion where little debonding was present, progressively increasing as the amount of debonding increased. A small decrease in micromotion for one layer debonded was noted at the ilium, accompanied by a slight increase at the pubis and almost no change at the ischium. As more debonding was introduced the effect of friction became slightly more noticeable, decreasing micromotion at the ilium and particularly making changes in the distribution of interface stresses. Metal backing made small changes, comparable in magnitude to the effect of friction. Gap size made significant changes to the micromotion at the ilium, but not at the ischium and pubis, again reflecting the direction of the hip joint reaction force. The effect of prosthesis debonding on the interface stresses is shown in Figure 5-16. These results are for a frictionless model with a gap size of 0.1 mm using the second load step in the gait cycle (peak hip joint reaction force).

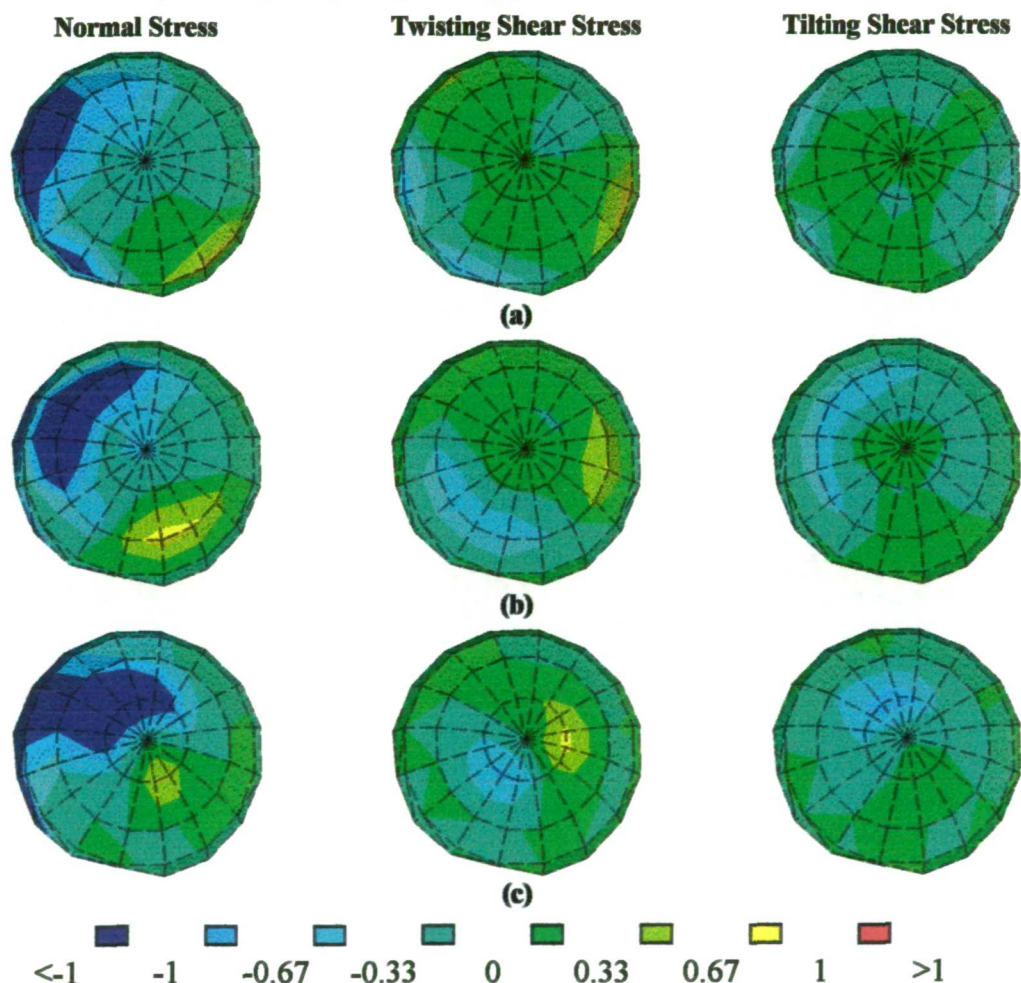


Figure 5-16: The effect of debonding at the cement bone interface on interface stresses. Stress (MPa), frictionless model with (a) one layer, (b) two layers and (c) three layers debonded.

Figure 5-17 shows results for the two layer debonded model when friction and increased gap size were introduced. As with micromotion, friction had a relatively small influence where little debonding was present, progressively becoming more important as the amount of debonding increased. The small decreases in micromotions were accompanied by negligible changes in the peak values of the interface stress components. As more debonding was introduced the effect of friction became more noticeable, decreasing micromotion at the ilium and particularly making changes in the distribution of interface stresses. With a gap size of 0.1 mm the cup tilts towards the anterior superior wall and makes contact by closing the gap, thus transferring load by compressive contact. With a gap size of 0.5 mm, this mechanism was not evident, resulting in increased tensile stresses at the bond line opposite the contact area in the small gap model. Compared to the bonded case, stresses were much lower. In the bonded models the stiffness of the cortical shell causes high stress at the rim.

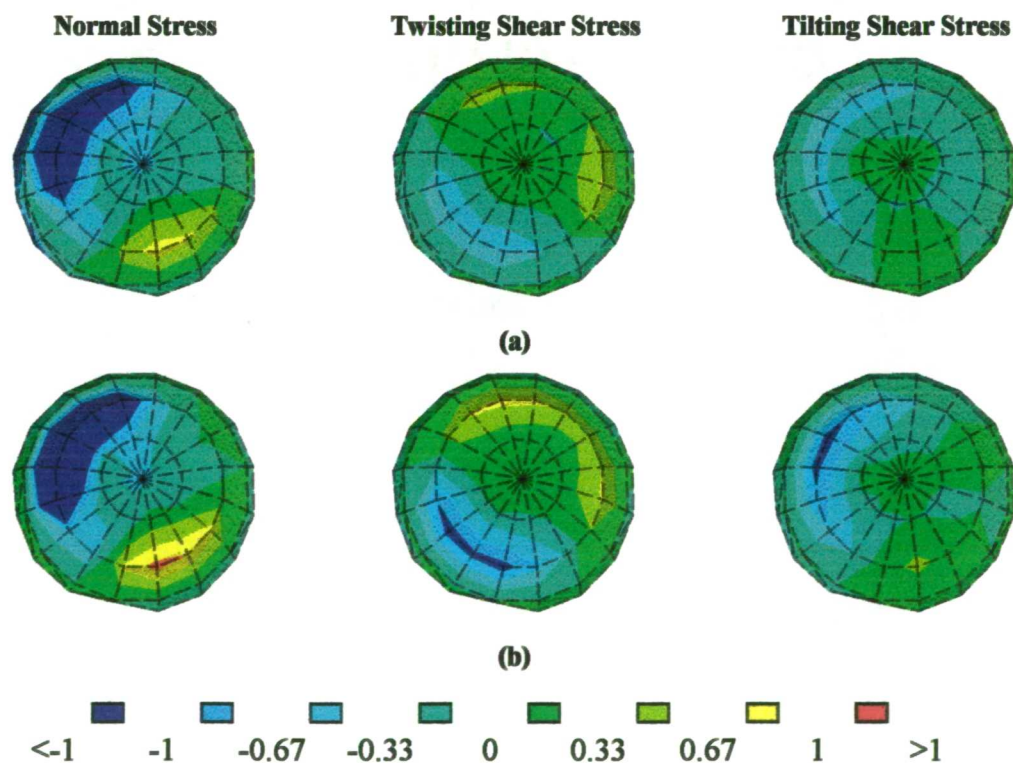
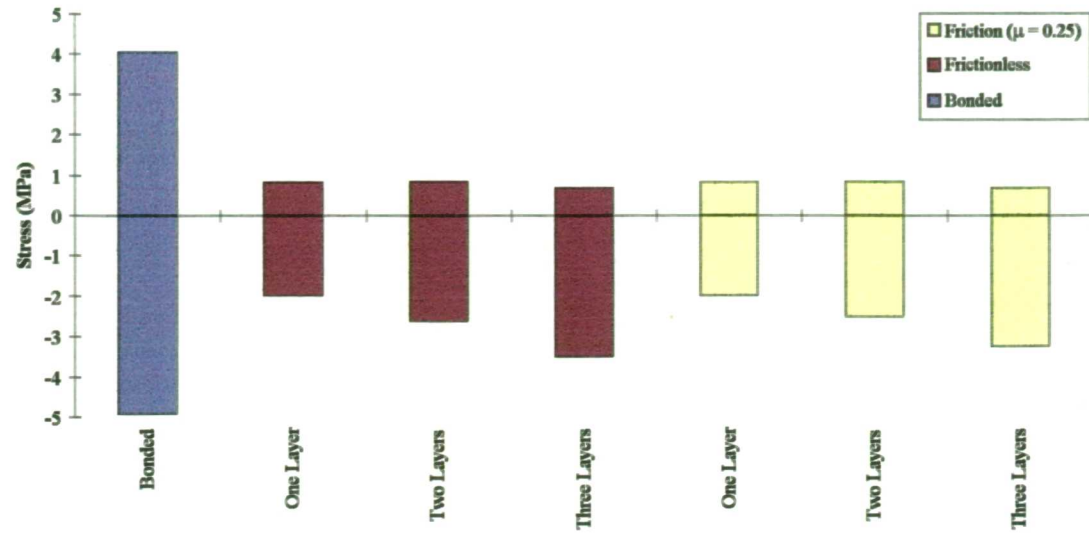
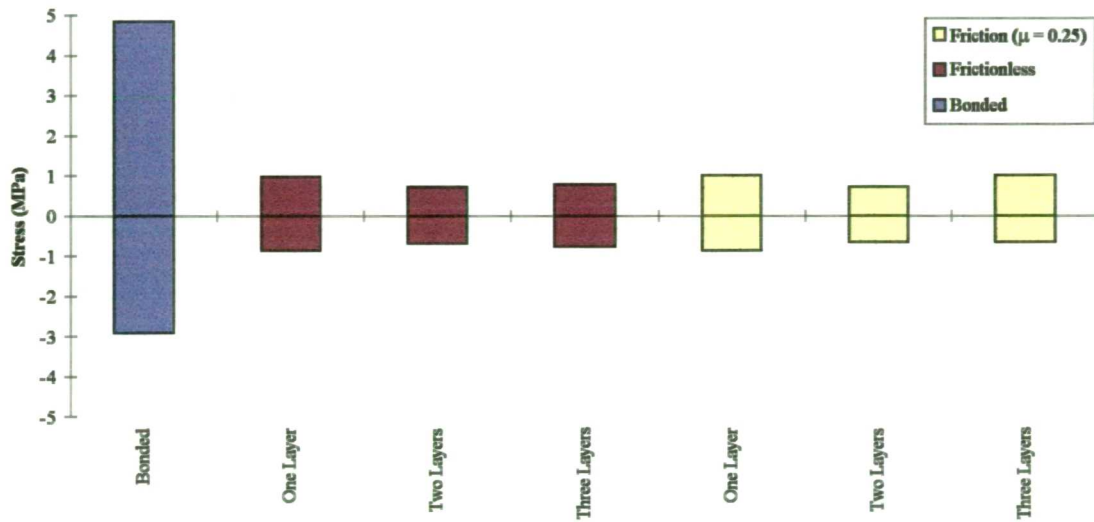


Figure 5-17: The effect of debonding at the cement bone interface on interface stresses. Stress contours (MPa) for two layer debonded model with friction ($\mu = 0.25$) and a gap size of (a) 0.1 mm and (b) 0.5 mm

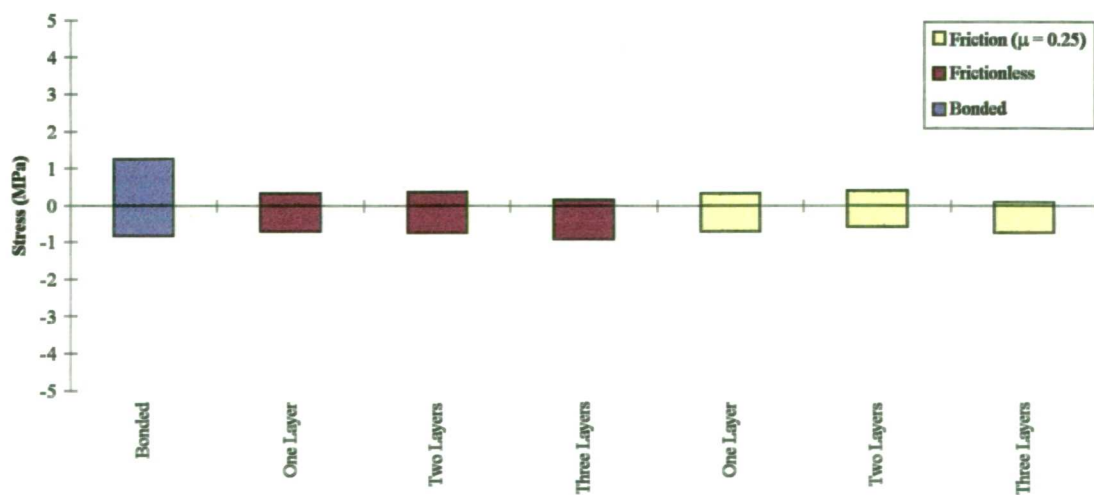
Figure 5-18 summarises the interface stress at the ilium, ischium and pubis for the various models. The maximum and minimum interface stresses are shown and compared to the equivalent fully bonded model.



(a)



(b)



(c)

Figure 5-18: Maximum interface stresses for the bonded and debonded models. (a) normal interface stress, (b) twisting component of the shear stress and (c) tilting component of the shear stress.

In light of these results, it is instructive to review the various models with regard to the gross effects on load transfer in the acetabulum (Figure 5-19). In the normal hip the load appears to be shared between the cancellous bone in the depth, which transfers load into the medial cortex, and the lateral cortex. In the reconstructed hip assuming perfect bonding between bone and cement over the whole surface of the cement mantle, more load is transferred into the lateral cortex and less via the cancellous bone, as indicated by the different stress distributions. As debonding, simulated by releasing element connectivity around the rim of the acetabulum and inserting gap elements, progresses, the subchondral bone layer transmits loads into the lateral cortex and the cancellous bone regains a more significant role in load transmission. Gap size appeared to have a relatively small effect. It is interesting to note that now the removal of the subchondral plate has a more significant effect on the distribution of load between the cortices and the cancellous bone, with larger increases in cancellous bone stresses than demonstrated with the perfectly bonded models described above.

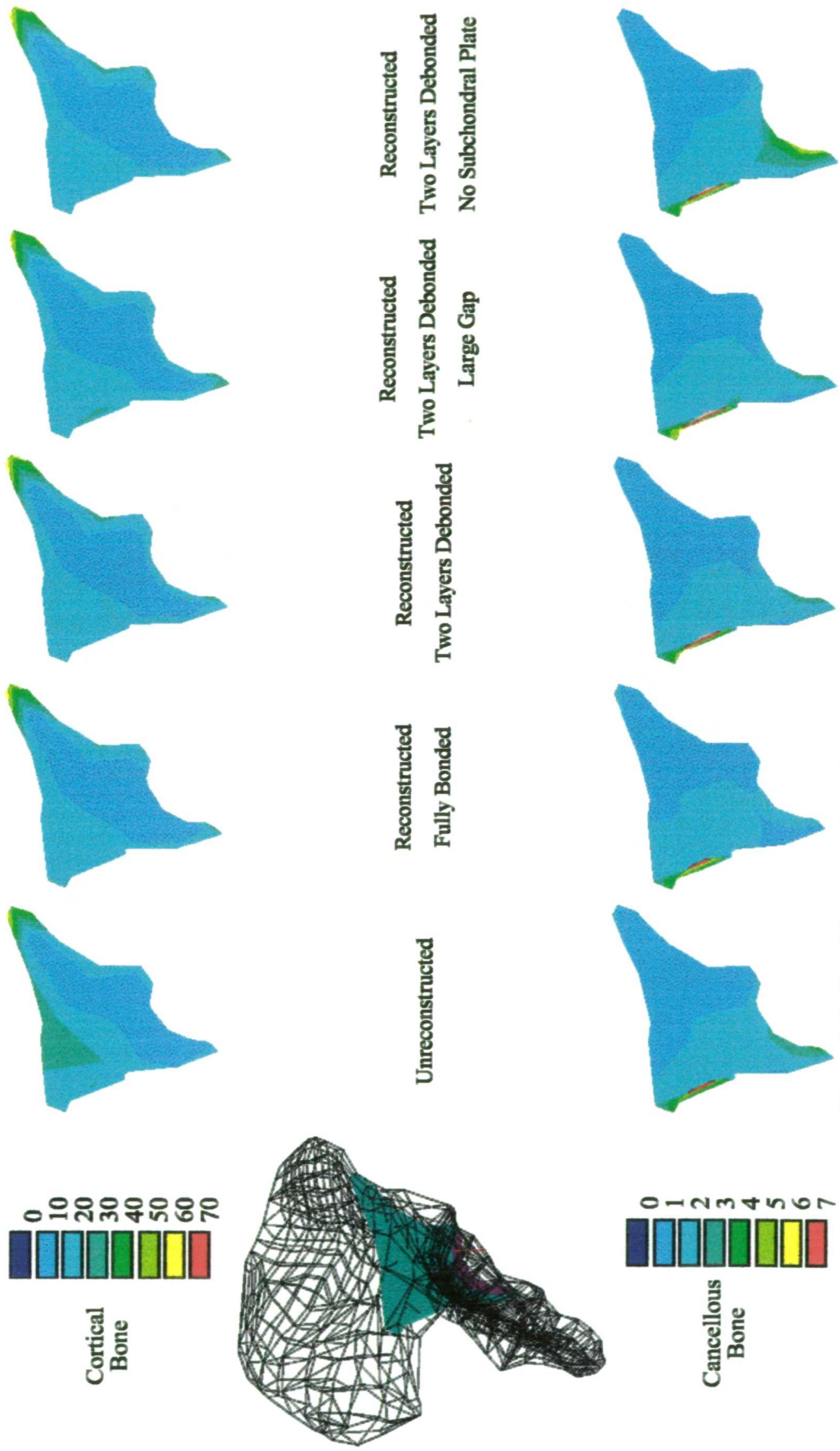


Figure 5-19: Von Mises stress in cortical and cancellous bone for various models. The cutting plane (which contains the hip joint reaction force vector shown as a red arrow) is indicated on the left.

5.5 Discussion

Recent work at the University of Nijmegen has revealed the inadequacy of two dimensional and axisymmetric finite element models in predicting the mechanical behaviour of the acetabulum (Dalstra and Huiskes, 1995). Two dimensional models are inherently too flexible since they cannot account for reinforcement by the anterior and posterior acetabular walls, whereas axisymmetric models are too stiff because the acetabular wall is assumed to be circumferentially continuous with no allowance for the acetabular notch. The effects of these modelling assumptions are highly significant and in the past may have lead to misleading conclusions about the effects of implant design on the mechanics of the acetabulum, e.g. the role of metal backing. Three dimensional models are thus prerequisite for modelling the acetabulum, despite the increased complexity of mesh generation and the computational effort required.

For the purposes of this discussion, the hemi-pelvis is mechanically linked to the rest of the body via muscles and three joints, the hip joint, the sacroiliac joint and the pubic symphysis. During the single leg stance phase of gait the weight of the upper body is transferred into the pelvis principally via the ipsilateral sacroiliac joint and secondarily via the contralateral innominate bone, the pubic symphysis and by direct bearing of the abdominal viscera on the medial surfaces of the iliac wings. The hip joint is stabilised by the muscles that cross the hip - at the hip the ligamentous structures and the joint capsule only operate at the extremes of the range of motion of the joint. The hemi-pelvis is thus essentially a beam, albeit one of intricate geometry and subject to complex loading, supported at the two non articulating joints, the pubic symphysis and the sacroiliac joint. The constraints applied to the finite element models at these joints define their ability to transmit forces and moments. Anatomically the sacroiliac joint is characterised by strong ligamentous support and an interlocking surface which appears to indicate "design" for resistance to bending and shear loading. Building in the sacroiliac joint(s) in the finite element models

allows it to generate forces and moments exactly equal and opposite to the out of balance forces that result from the out of balance applied loads, seemingly in keeping with the physical structure of the joint. The behaviour of the pubic symphysis is more difficult to predict, so the effects of varying the boundary condition at the pubic symphysis have been studied. It was found that while the overall displacement field of the loaded hemi-pelvis was strongly affected by the boundary conditions, the second order quantities strain and stress were much less affected. The patterns of von Mises stresses around the acetabulum were not greatly different for the built-in pubic symphysis model and the full pelvis model. Stresses were marginally higher for the built-in pubic symphysis model, particularly in the region of the pubic bone. Allowing the pubic symphysis to move completely freely reduced stresses in the depth of the acetabulum and produced higher stresses in the region of the greater sciatic notch. The general trend was to increase the area under higher stresses as the pubic symphysis became progressively more constrained. It was thus concluded that some constraint was necessary at the pubic symphysis to represent the stiffness of the contralateral hemi-pelvis and produce realistic load transfer. To provide this constraint a built-in pubic symphysis, in which all degrees of freedom of the nodes at the pubic symphysis were set to zero, was assumed in all latter models. Although this constraint is not completely consistent with the anatomy of the pubic symphysis, the differences in the strain and stress fields between the full pelvic model and the built-in pubic symphysis model were small, and thus the built-in pubic symphysis was applied to all subsequent models. This has the additional benefit of maintaining consistency with previous work (Dalstra, 1993).

Muscle forces have a considerable influence on the displacement, strain and stress fields in the pelvic bone (Dalstra, 1993). When muscle forces are omitted the pelvis becomes loaded in a three point bending mode and maximum stresses occur around the supports of the sacroiliac joint and the pubic symphysis. The peak von Mises stresses at the superior rim of the acetabulum are reduced by 15%. With the exception

of the models considering the micromotion produced by a debonded cement bone interface, where multiple load cases representing the complete gait cycle were used (Table 5-1), the representative load case chosen simulated the beginning of the single support phase of gait with the hip in 18° of flexion. It was at this stage that Dalstra (1993) found the highest peri-acetabular stresses.

In the normal acetabulum there appear to be two mechanisms for the transfer of the hip joint reaction force into the pelvis. The load is shared between the cancellous bone in the depth of the acetabulum and the pelvic cortex at the acetabular rim depending upon the relative stiffness of each. In the unreconstructed case the hip joint reaction force causes the acetabulum to bulge in the superior and posterior directions, becoming more ovoid in shape with the major axis of the ovoid approximately coincident with the line of action of the hip joint reaction force. The principal effect of acetabular reconstruction is to stiffen the acetabulum. The presence of the relatively stiff acetabular cup suppresses the deformation of the acetabulum and causes the acetabulum to behave as a more rigid body and hence to tend to retain its approximately hemispherical shape. In the reconstructed acetabulum loads are not transmitted as efficiently as in the natural situation. If a fully bonded prosthesis is assumed, most of the load is transferred at the rim and the cancellous bone in the depth is stress shielded compared to the normal acetabulum. This is a more extreme version of what happens in the normal joint, where the articular cartilage and subchondral plate combined, which are less stiff than the polyethylene cup and cement combined, transfer load directly into the lateral cortex and to the medial cortex via cancellous bone (Jacob *et al.*, 1976). With a debonded prosthesis, the character of the load sharing changes, less load is transferred at the rim (cortex) depending on gap size and relatively more at the depth by the cancellous bone. Then the pattern of loading changes and the cancellous bone becomes relatively more highly stressed.

The Hoffman index gives a measure of the load carried by a particular region of bone with respect to its total load carrying capacity. In the normal acetabulum "Wolff's

Law" arguments might suggest that the Hoffman failure index should be evenly distributed over the acetabulum. However, in this study the Hoffman index was considered for only one load case (representing single leg stance phase in walking). Other phases of walking and activities such as stair climbing will produce different stress distributions in the acetabulum owing primarily to changes in the direction of the hip joint reaction force. The concentration of high values of the Hoffman index along the line of the hip joint reaction force is noteworthy - this concentration would be expected to follow the hip joint reaction force as it sweeps the acetabulum.

The reduced values of the Hoffman index and the redistribution of stress in both reconstructed acetabula as compared to the normal case lead to the conclusion that, under the static conditions modelled, cancellous bone is within its load bearing capacity. From these results, it seems collapse and remodelling of cancellous bone is less likely to be a significant failure mechanism in the acetabulum than in the femur. Indeed both the redistribution of stresses in the reconstructed case and the reduction in the Hoffman index throughout the acetabulum appears to indicate "stress shielding" as a result of the introduction of the implant, although the significance of this effect with respect to bone remodelling cannot be addressed here.

In considering the surgical options in acetabular reconstruction, the stress magnitude and distribution are negligibly changed by retention or removal of the subchondral bone plate. The introduction of the relatively stiff implant and cement composite means the subchondral plate contributes little to the overall stiffness of the structure. The major effect of the retention of the subchondral plate can be expected to be deleterious. The hard dense surface it presents, especially in the osteoarthritic case, prevents interlock occurring between cement and bone and hence reduces the strength of the cement bone interface. For the interface stresses the same pattern was observed whether the subchondral plate was removed or preserved. Studies have shown the negligible strength of the interface between bone cement and cortical bone (te Nuyt and Vosseveld, 1996).

In the debonded models it was assumed that some degree of debonding will be present, if not immediately post operatively then shortly after rehabilitation starts. The simplest possible model for describing the mechanics of a debonded interface was adopted, that of frictionless contact. A number of uncertainties were present when assuming this model. The effect of the assumed size of the gap, whether friction was important and the effects of the stiffness of the prosthesis were assessed by varying these parameters. Friction was found to hardly influence the micromotion or the interface stresses. Weinans *et al.* (1990) compared a variety of modelling techniques in the femur and found that the gap element approach, as used here, tended to underestimate micromotions by a factor of 3 to 5 compared to more elaborate techniques involving interposition of non-linear interface layers. However, the present models differ in two important ways. Unlike Weinans *et al.*, it was assumed that a significant area of the cement bone interface was still fully bonded and thus considerable remote resistance to micromotion existed. Weinans *et al.* also set out to model the interposition of a relatively thick layer of compliant tissue in an implanted femur. Thus the loading, the shape and the nature of the secondary stability of the construction was very different to the situation here. The aim of the present study was to simulate the immediate post-operative conditions where the thickness of interposed material is small. The stability of the prosthesis is mainly due to the regions where perfect bonding still remains, i.e. varying amounts of the depth of the acetabulum. The remaining fully bonded interface also provides an explanation for the validity of neglecting friction at the debonded interface since, because of the stored elastic energy in this (deformed) interface, there will always be a significant restoring force to restore the original configuration of the interface when only relatively small loads on the implant are present.

Micromotion at the interface was controlled by the amount of debonding and locally at the ilium by the size of the gap. The magnitude of the micromotion was relatively insensitive to friction and the stiffness of the implant. Debonding allows the cup and

cement to move relative to the bone, but the combination of rigid body motion and deformation makes it somewhat difficult to describe the overall motion of the cup and cement with respect to the bone. However, it appears that there is a combination of twisting about the axis of the cup and tilting about an axis passing slightly deep to the centre of rotation of the cup and through the acetabular notch. In the early stages of debonding the motion is greatest at the ilium, being for both twisting and tilting more than double that at the ilium and pubis. With two layers debonded the largest motion transfers to the ischium and the pubis, a trend which continues with three debonded layers. In the fully bonded case the peak interface stress components are higher than in all the debonded cases. This is due to the direct transfer of load from the extreme edges of the cement mantle to the pelvic cortex, which is stiffer than the acetabular cancellous bone. If the layer of nodes at this location is released and a gap interposed, this mechanism of load transfer is much reduced even for a gap size of 0.1 mm. A larger gap (0.5 mm) allows more movement of the cement and cup at the ilium, however in neither case was the deformation enough to allow contact at the ilium in the location for which results are presented, since the motion was smaller than the initial gap size. This suggests that in the small gap case, load transfer still partially occurs at the cortex. The contact regions are reflected in the stress plots (Figure 5-16 and Figure 5-17) where, in the small gap case, considerable loads are still transferred at the superior acetabular rim. The increase in stress as more layers are debonded is explained by the reduction in surface area available for elastic load transfer. It is also of note that, even with large debonded areas, the cancellous bone stresses remain low.

Various clinical follow up studies have shown that all end stage fixation failures (aseptic loosening) are characterised by the formation of a fibrous interfacial layer which allows gross motion of the prosthesis. Several pathways by which this end stage is reached are possible. There is considerable evidence that all prostheses migrate to some degree from the first day post-operatively. It is also reasonably clear that the magnitude of this migration in the first few years post implantation is a strong

indication of the total lifetime of the prosthesis (Stocks *et al.*, 1995). This would appear to support theories that failure to achieve adequate fixation per-operatively is a strong causative factor. Numerous radiological studies of the acetabulum, although considered to be of limited quantitative value (Schmalzried, personal communication) show that radiolucent lines appear first in the regions of the superior rim (Charnley zone I) and the inferior rim (Charnley zone III) and as time passes progress inwards towards the depth (Strömberg *et al.*, 1996). Bos *et al.* (1995) reported the reorganisation of trabeculae into a neo-cortex parallel to the cement mantle and connected to the pelvic cortex. The thickness of the neo-cortex was correlated with the patient's body weight. In 15 of 25 acetabula there was also focal metaplasia to cartilage in direct contact with the cement. In the reconstructed acetabulum the medial wall had thinned to a mean of 5 mm after a mean implantation time of seven years, compared to 12 mm in non-implanted controls. Schmalzried *et al.* (1992) found intimate bone contact over extensive areas in the depth of the acetabulum. The present results suggest that the assumption of a fully bonded interface removes the driving force for the neo-cortex formation reported by Bos *et al.* and the thickening of the bone abutting the cement reported by Schmalzried *et al.* However, these clinical observations may represent the consequences of a sequence of events initiated by rim debonding.

5.6 Critique

As always, the results of the present analyses need to be interpreted within the limits of the assumptions that are made in their formulation. The most ill defined feature is the anatomy of the acetabulum, as presented to a surgeon during a hip replacement procedure. In a normal acetabulum a thin layer of subchondral cortical bone underlies the articular cartilage and overlies a trabecular network of supporting cancellous bone. In severe cases of osteoarthritis the cartilage will have worn through and there will usually be a substantial thickening and eburnation (polishing) of the

subchondral bone plate. In this situation the supporting cancellous bone often contains fluid filled cysts and has little residual load bearing capacity, also the lunate surface of the acetabulum may have disappeared leaving an almost hemispherical dome. The eburnated bone has very little prospect for achieving an interlock fixation with acrylic cement, so holes are drilled in it. The arthritic acetabulum therefore presents a spectrum of pathological changes in the supporting bony structures, from the nearly normal to those cases with a thick eburnated subchondral surface and rarefied supporting cancellous bone, which present different problems in achieving fixation. None of these factors are examined in the present study and their effects on the mechanics of the pelvis are largely unknown, but clinically they influence the potential success of the operation. In the femur, where the region affected by arthritic changes is usually completely removed, these problems do not arise.

Much of work assumed a fully bonded interface. Whether this hypothetical situation can be achieved in practice is dubious, particularly when cement is in contact with a relatively smooth subchondral bone plate. The description of the interface is complex and necessarily must be simplified, both geometrically and with regard to its load transfer behaviour. An attempt was made to address the problem of sub optimal cement bone bonding by frank debonding of the cement bone interface around the acetabular rim. Debonding at the acetabular rim may arise in two ways. It might occur rapidly post operatively due to a failure of cementation technique, or it may occur late in the lifetime of a prosthesis. Although these results provide an indication of the effects of prosthesis debonding in the immediate post-operative period and how these effects depend on the amount of debonding, they should be interpreted with care when trying to extrapolate to late stage debonding associated with aseptic loosening, paying due attention to the fact that bone is a dynamically adaptable material that constantly changes its properties in response to the loads applied to it in accordance with "Wolff's Law". The assumptions made in these models about the structure and properties of the bone that surrounds the acetabulum (that they remain unchanged

throughout) can only be expected to be sensible for debonding occurring at an early stage, before significant adaptive changes have taken place. The essentially non-linear processes of debonding and adaptive bone remodelling have been linearised in this case, completely ignoring the effects of bone adaptation. To truly model the progression of debonding a full non-linear simulation of the remodelling process may be required. Having said this it is also difficult to identify the starting point for the prosthesis debonding and the two layer and even three layer debonded models may well be realistic starting points given the presence in some cases of quite extensive radiolucent lines on post-operative X-rays.

5.7 Summary and Conclusions

1. The choice of kinematic boundary conditions has a profound influence on the displacements of the pelvis, but the second order quantities strain and hence stress are much less affected.
2. Muscle forces also have a strong effect on the displacements of the pelvis. However in the region of the acetabulum, the distribution of strain and stress is dominated by the hip joint reaction force.
3. The bonding assumed at the interface between cement and bone has a significant effect on the distribution of load throughout the acetabulum.
4. In the perfectly bonded case, the retention or sacrifice of the subchondral plate has only a small effect on the load transfer in the acetabulum. In the normal hip the subchondral plate transfers the joint contact forces into both the underlying cancellous bone and the cortical shell, but the replacement of the compliant cartilage layers and the femoral head by a much stiffer construction negates this role. Compared to the stiffness of the prosthetic components, the contribution of the subchondral plate is negligible. However, when debonding is assumed at the cement bone interface, the subchondral plate appears to play a more important role, but since the interface strength between cement and the subchondral bone plate is

much less than that between cement and good quality cancellous bone, debonding is less likely to occur in the first place in the latter case.

5. Peak interface stresses were much higher in the fully bonded acetabulum owing to load transfer at the rim into the stiff cortical bone of the pelvis.
6. Micromotion in the debonded case was controlled by the amount of debonding and locally at the ilium by the size of the gap. The magnitude of the micromotion was relatively insensitive to friction and the stiffness of the implant.

6. Stability of Cemented Acetabular Cups Under Dynamic Loading

Kloss (1996) designed a new joint simulator which has now been validated. This device has been used to investigate the relationship between cement pressurisation, especially pressure distribution, and acetabular component fixation. The mechanical stability of acetabular cups implanted with the conventional technique and using a cement pressurisation tool were compared directly. Finite element modelling and mechanical testing of the proposed loss of fixation at the rim of the acetabulum for conventional cementing techniques has been performed.

6.1 Design and Validation of a New Joint Simulator

6.1.1 Description

The Unit for Joint Reconstruction (UJR) Joint Simulator has been designed to provide a laboratory simulation of the motion and loading in a normal human hip when used in conjunction with a servo-hydraulic universal testing machine. The principal feature of the machine is a large space for specimen mounting, in contrast to most other joint simulator designs that are intended for wear studies and hence have restricted specimen space. The flexibility of the design also means it can easily be adapted for the testing of other multiple degree-of-freedom joints. Two views of the UJR Joint Simulator, mounted in an ESH servo-hydraulic testing machine, are shown in Figure 6-1. The major components are (A) the simulator mechanism, (B) the simulator control unit, (C) the universal testing machine control unit, (D) the load frame and (E) the data logging computer (Amstrad 20286, Amstrad, U.K.)

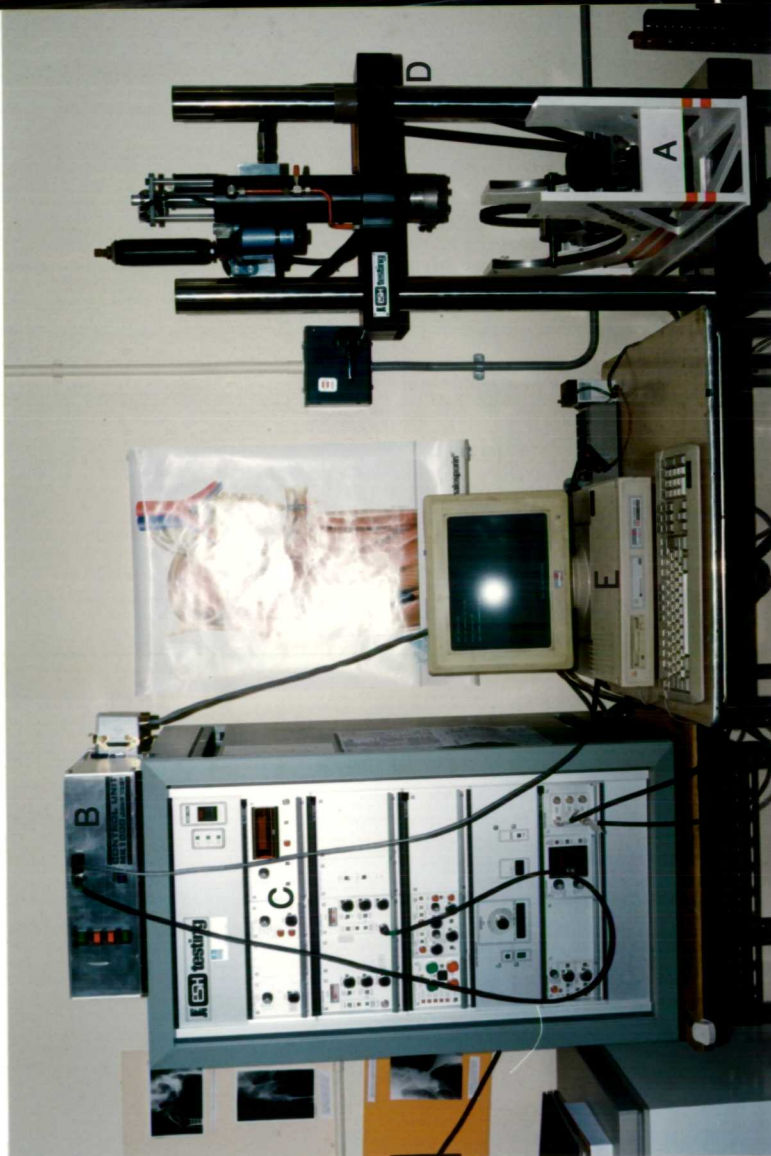
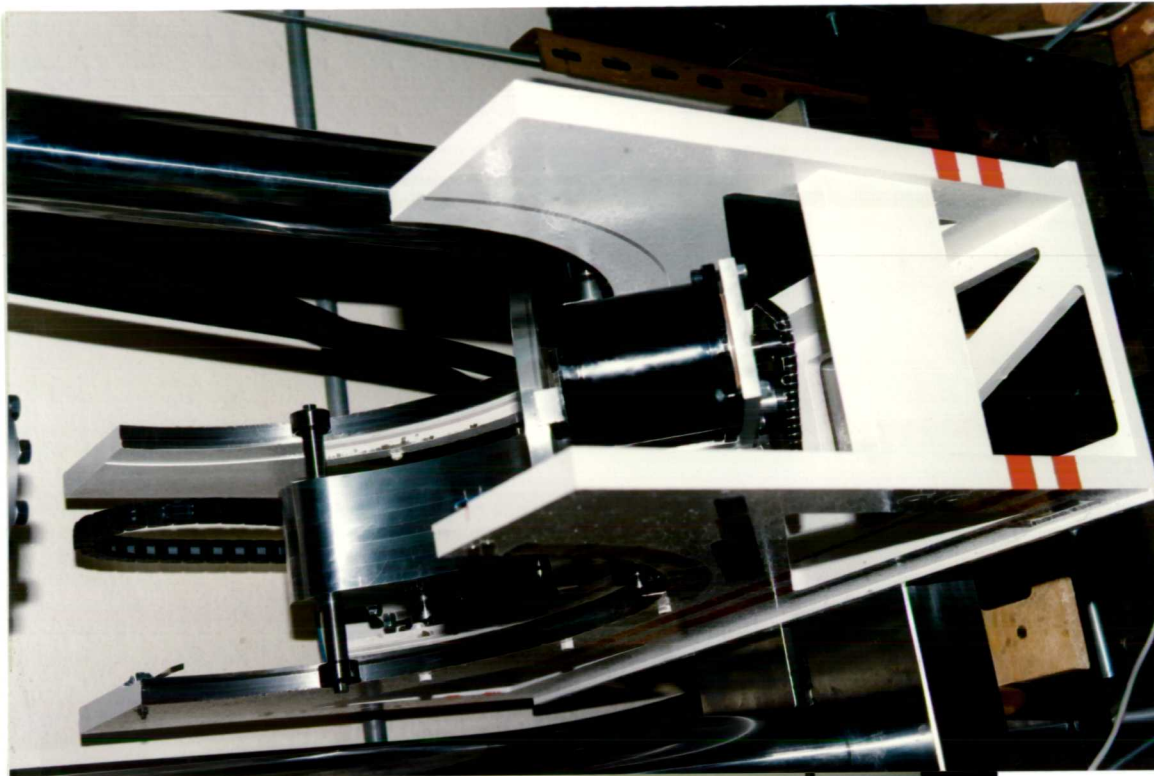


Figure 6-1: Two views of the Unit for Joint Reconstruction Joint Simulator

6.1.2 Mechanical Design

The apparatus (Figure 6-2) consists of a rigid steel frame (components A) that is bolted to the base plate of the servo-hydraulic universal testing machine. An aluminium slide block (B) is supported on two shafts (C) with end bearings that run on semi circular rails (D) incorporated in the frame. A stepper motor (E) mounted on the slide block drives two shaft mounted pinion gears (F) that engage with semi-circular racks (G) mounted below the rails. Torque is transmitted from motor to shaft by sprockets and chain (H). A second stepper motor (I) drives a rotating table (J), also via sprockets and chain (K) about an axis perpendicular to the axis of rotation of the slide block. The driven axes allow positioning of the acetabular cup^a any specified orientation relative to the actuator of the materials testing machine.

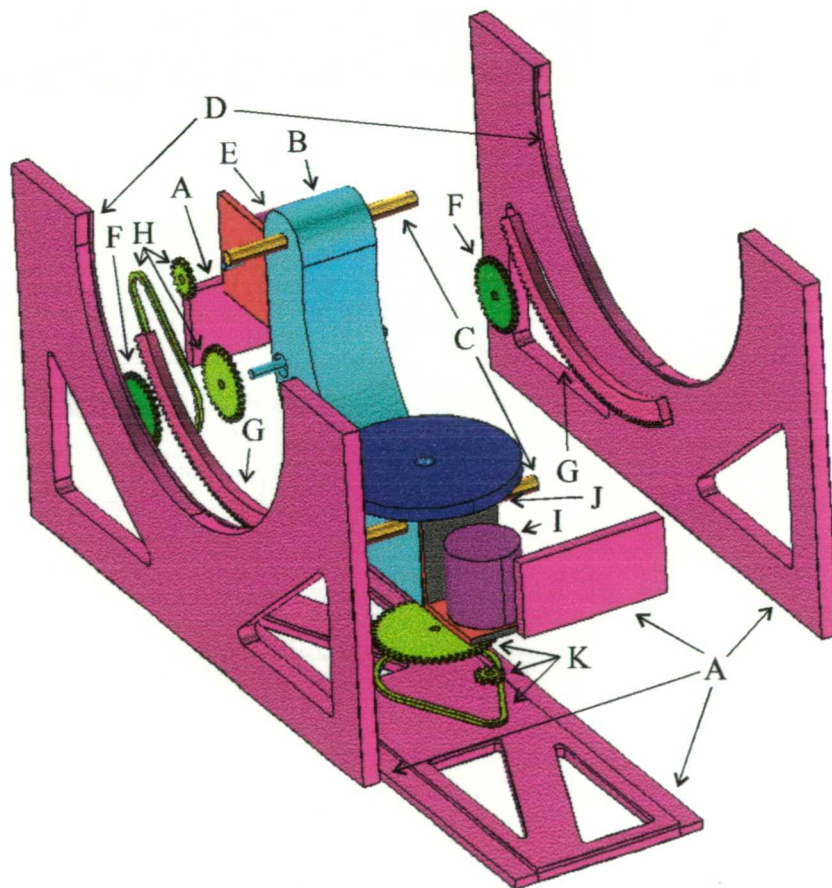


Figure 6-2: The principal mechanical components of the UJR Joint Simulator.

Fixed to the actuator of the testing machine is a loading stem that accepts a modular prosthetic femoral head with a standard taper ($5^{\circ}40'$). Incorporated into the fixture is a biaxial linear slide that transmits only axial forces perpendicular to the sliding surface.

This biaxial slide allows for the inevitable misalignments in the load train introduced when potting the specimens and by specimen deformation under load and prevents the introduction of side loads into the specimen and the testing machine actuator.

6.1.3 Operation and Validation

The operation of the machine and the procedures for its validation are discussed here with respect to the acetabular specimens described latter in this chapter, however the fundamental principles are widely applicable. The acetabular specimen under test is mounted such that the centre of rotation of the acetabulum (the geometric centre of the cup bearing surface) is coincident with the intersection of the axes of rotation of the two driven axes of the Joint Simulator. This intersection is arranged to lie along the line of action of the testing machine actuator and hence force can be applied along any line passing through the intersection of the two axes and any point on the surface of a partial spheroid acetabular cup.

The functional relationships between the components of the simulator are shown in Figure 6-3. Overall control of the system is provided by the simulator control unit. This unit provides power and command signals to the motors from a programmable control board, which also generates an 8 bit digital output that, after suitable digital-to-analogue conversion and filtering, is used as a command signal for the load servo controller of the universal testing machine. The control board is programmed using a proprietary "C" type control language from a remote computer via an RS-232 (serial) data link. Thus control programs can be written and downloaded to the control board such that the motions of the two driven axes and the load applied by the materials testing machine are correctly synchronised. Arbitrary load and motion profiles may be programmed. The outputs of the testing machine control system (load and stroke) together with additional signals from specimen mounted transducers are logged by the data logging computer fitted with an analogue-to-digital converter card (AD1200, Brainboxes, Liverpool, U.K.) and running suitable custom written software.

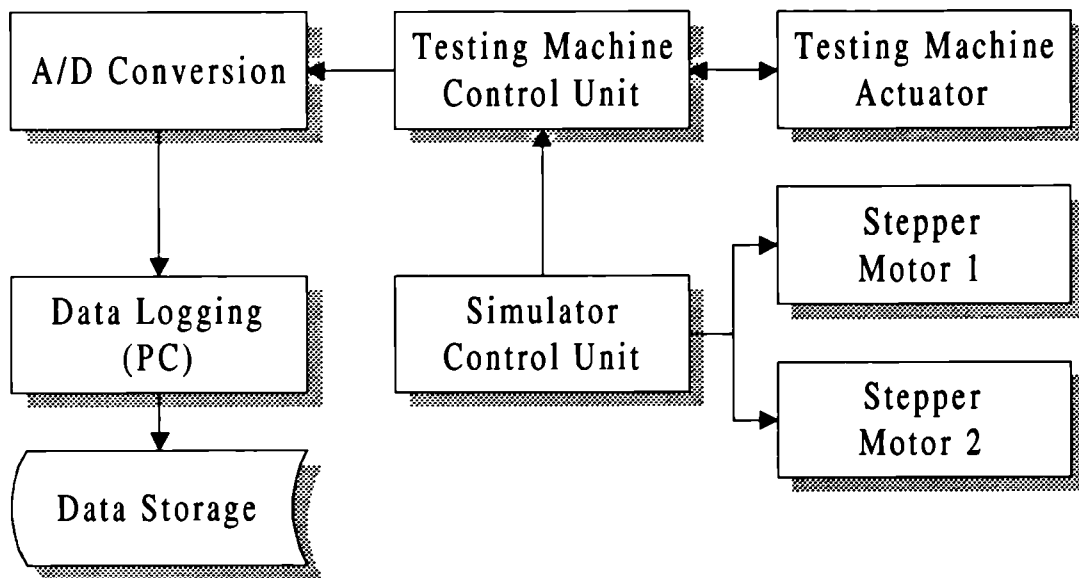


Figure 6-3: Functional diagram of the UJR Joint Simulator.

Double headed arrows indicate bi-directional processes, e.g. closed loop (servo) control.

6.1.3.1 Verification of Load Cycle

Tests to prove the adequacy of positional and load control were required since the control system for the motors is of an open loop design, there being no feedback signal to the simulator control unit from the stepper motors driving the rotation axes or the actuator of the servo-hydraulic testing machine. A specimen was mounted in the simulator as described in section 6.2.1.1. A simplified gait cycle was used which encompasses the important features of normal gait. The face of the acetabular cup was initially positioned at an angle of 38° to the vertical plane and rotated about the axis of the rotating table (Figure 6-2, J) so that the bisector of the angle between the pubic bone and the ischium was aligned with the long axis of the joint simulator. This position thus represents the 0° location. Sinusoidal load and angle functions were generated and used to program the stepper motor control board such that the required load and motion cycles were properly synchronised (Figure 6-4). The locus of the hip joint reaction force vector on the acetabular cup is shown in Figure 6-5.

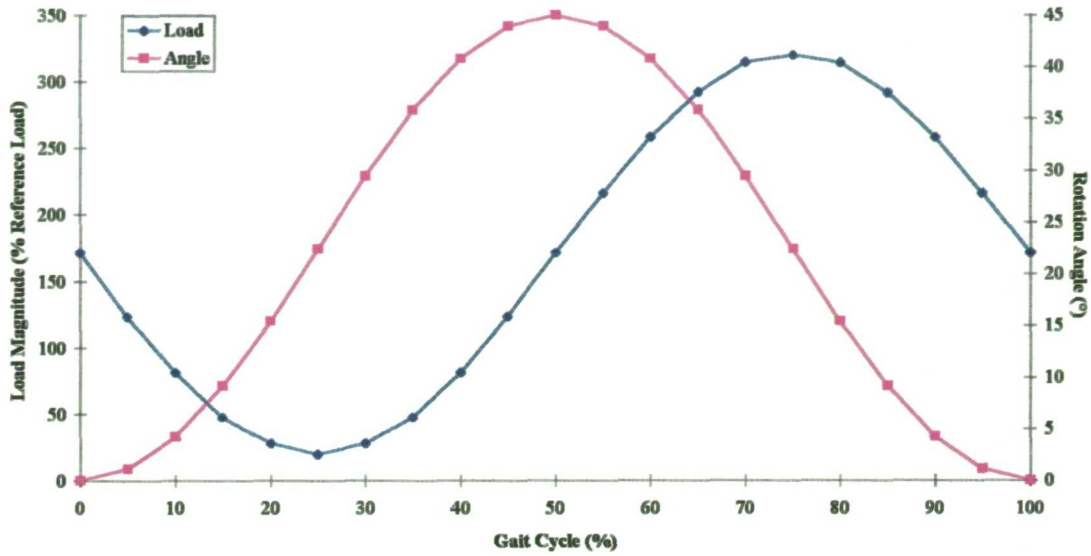


Figure 6-4: Simulated gait cycle: magnitude and orientation of the hip load.

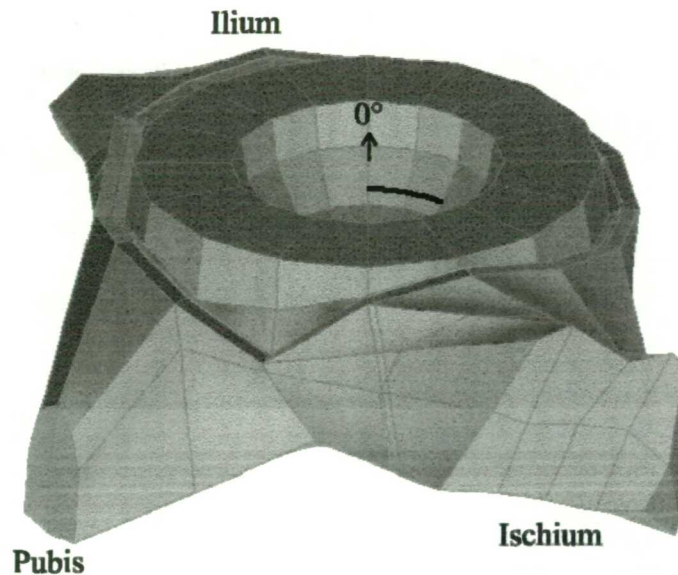


Figure 6-5: View of a mounted specimen along the axis of the testing machine actuator. Shows the locus of the hip joint reaction force vector (thick line on inner surface of cup).

Figure 6-6 shows the result of the load test. It can be seen that there is relatively small error (root mean square error of 3.9 %) between the command signal and the load measured on the ram of the testing machine. A large proportion of this error is due to a slight phase lag of the true (measured) load with respect to the command signal, this is particularly evident where there is a combination of high load and high loading rate as can be seen in Figure 6-6.

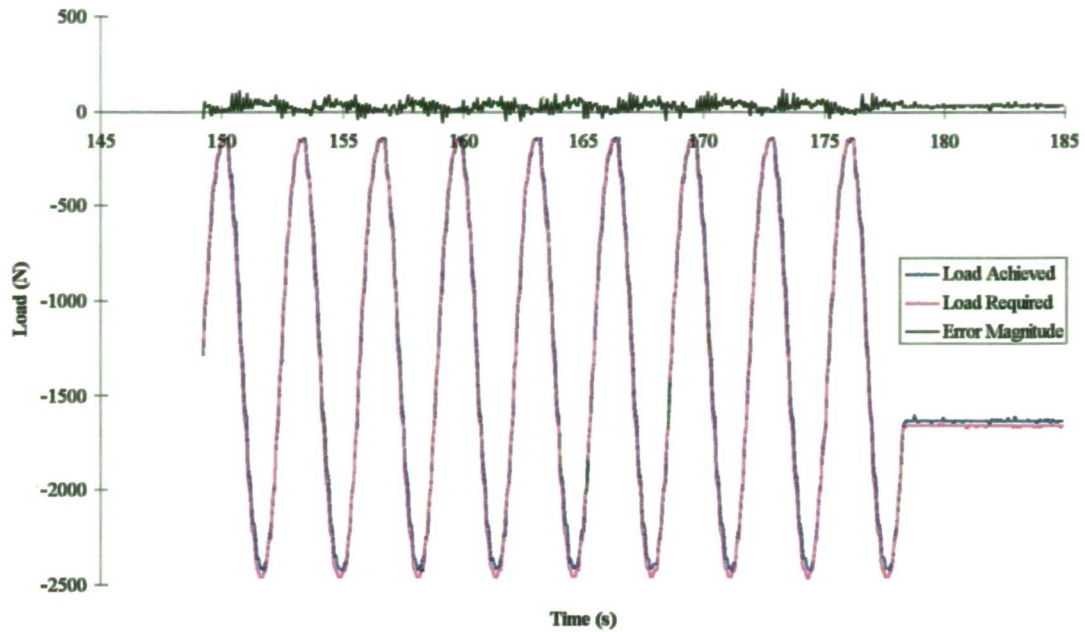


Figure 6-6: Comparison of command and output signals of the UJR Joint Simulator.

The positional control of the table and slide was verified by making a pencil mark at the extreme range of each motion. After 70 cycles, the total positional error was less than 2 degrees, less than 0.03° per cycle. If long term tests were required the cumulative effect of such an error might become significant. However it would be easy to add a limit switch to provide a datum position which could be re-acquired as necessary to prevent the accumulation of such errors. Provision for such limit detection is made for in the motion control unit. Overall this system performed adequately.

6.2 The Effect of Cementing Technique on Acetabular Component Fixation

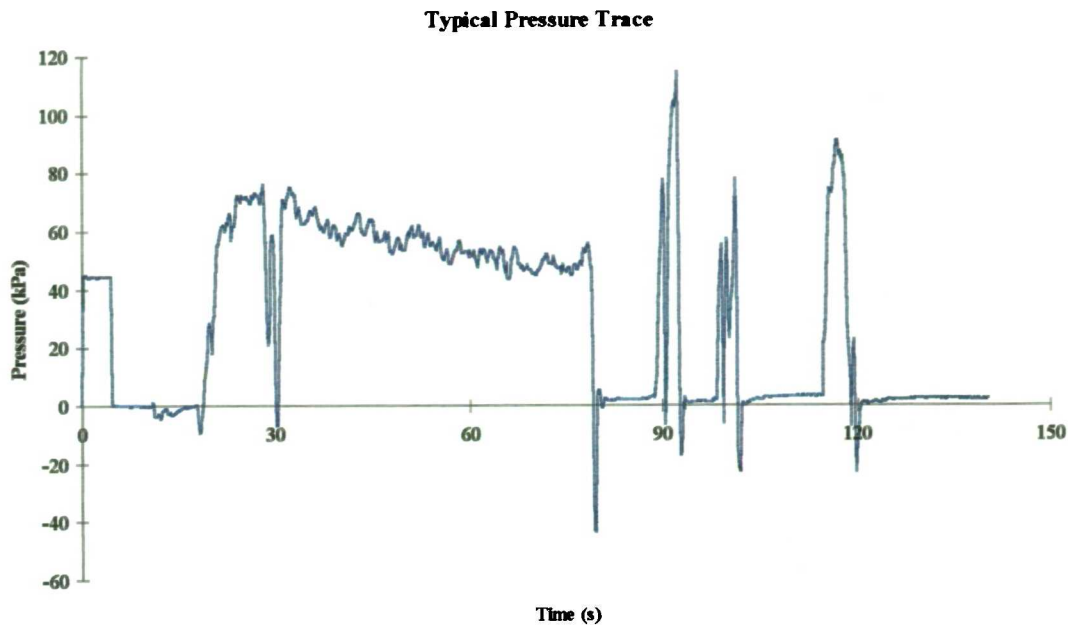
6.2.1 Method

Six segments of frozen bovine calf pelvis were thawed and cleaned of soft tissues and prepared for cup implantation by reaming the acetabula with a 50 mm diameter “cheese grater” type reamer followed by vigorous brushing with a stiff polyethylene fibre brush driven by a power drill (Figure 6-7).



Figure 6-7: The prepared calf acetabulum.

CMW type 1 cement was mixed in a mixing bowl in accordance with the manufacturer's instructions. At three minutes from mixing the cement was delivered to the acetabulum. In group 1 (3 acetabula), a plain UHMWPE cup with 48 mm outside diameter (Ultima, Johnson & Johnson Orthopaedics) and 28 mm bearing surface diameter was immediately inserted and held in place until the cement had cured. In group 2 (3 acetabula), the instrumented acetabular cement pressuriser with a suitable size (63 mm diameter) pressuriser head was used to pressurise the bone cement. Cement pressures were recorded, a typical trace is shown in Figure 6-8. In this trace, the principal pressurisation effort occurs for approximately 1 minute (between $t=20$ and $t=80$ on the trace). The spikes at longer times show when cement was repacked and re-pressurised to ensure sufficient volume of cement in the acetabulum for correct cup seating. Mean and peak pressures for the pressurised group (as described in section 3.3.3) were 41.5 kPa (standard deviation ± 18.8 kPa) and 64.7 kPa (18.8 kPa) respectively, which are comparable to per-operative measurements (section 3.3). After cement pressurisation was complete an identical cup was inserted as in group 1. Prior to mechanical testing a radiograph was taken.



**Figure 6-8: Typical pressure time trace for cement pressurisation in group 2.
Time zero = 3 min. from mixing.**

6.2.1.1 Specimen Mounting

For mechanical testing the prepared acetabula were then potted in Wood's metal (mpt. $\sim 60^{\circ}\text{C}$) in a fixture attached to the Unit for Joint Reconstruction Joint Simulator. To ensure that the centre of rotation of the acetabular cup corresponded to the centre of rotation of the joint simulator (as described in section 6.1.3) the centre of the acetabular cup was mounted precisely on the axis of rotation of the specimen mounting table at a height of 152 mm above the table using a specially designed cup inserter. The slide was moved to the extreme position with the table horizontal. The position of the testing machine actuator was then fixed by placing a gauge block of known length between the actuator and table. Knowing the length of the cup inserter, the displacement transducer of the testing machine was used to accurately position the whole acetabulum at the correct height. The cup inserter then held the prepared acetabula in the required position while the Wood's metal was poured and allowed to solidify.

To measure motion of the implanted cup relative to the acetabular rim a DC energised linear variable differential transformer (LVDT, Schlumberger Dfg5, RS Components, U.K.) was mounted on the superior rim of the acetabulum using a Steinmann pin and jubilee clip. The sensing armature of the LVDT was attached via a small aluminium

bracket to the acetabular cup (Figure 6-9). Power to the LVDT was provided by a combined power supply/amplifier unit (Entran PS30A). This unit also served to amplify the output from the LVDT to increase sensitivity. The output was then connected to the input of the PC's analogue-to-digital converter card via a passive low pass filter. Between test runs the acetabula were kept under wet paper towels to ensure desiccation did not occur. The laboratory temperature was $19\pm 3^{\circ}\text{C}$ at $51\pm 20\%$ relative humidity.



Figure 6-9: Potted acetabulum ready for testing.

The biaxial slide (A) and the position of the LVDT (B) can be seen.

Cyclic loads were applied in groups of ten load cycles, steadily increasing the load amplitude in six successive groups until the maximum load amplitude of 2.4 kN was reached. For each specimen five experimental runs were carried out to assess the

repeatability of the tests and to accommodate any time dependent conditioning effects. A second radiograph of each acetabulum was taken after testing.

6.2.1.2 Transducer Calibration

Since the LVDT was being used at the limit of its specified performance, it was calibrated after every test using a digital Vernier calliper (Mitutoyo) which in turn was verified against a workshop standard gauge block. A typical calibration curve is shown in Figure 6-10 and remarkably little variation was observed from run to run.

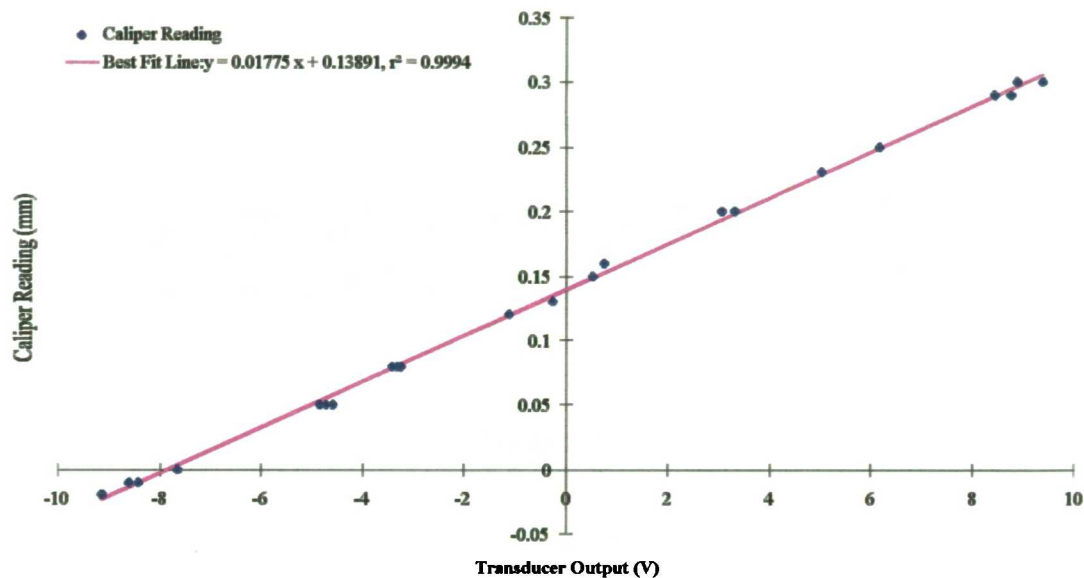


Figure 6-10: A calibration curve for the LVDT.

6.3 Micromotion in the Cemented Acetabular Reconstruction

The results of section 6.2 together with the finite element studies reported in section 5.4.3 prompted a further finite element and experimental study of the debonding mechanisms that might be responsible for the micromotion observed.

6.3.1 Finite Element Models

To investigate further the mechanisms responsible for the micromotion detected in the laboratory study described above and to permit comparison with the results reported in section 5.4.3, finite element models were generated to represent the potted acetabular

segment. Of particular concern are the influence of the different boundary conditions imposed by potting in a rigid material and the influence of the cartilaginous growth plates that are present in the juvenile bovine acetabulum. To simplify the model a uniform material property distribution was assumed for the pelvic cancellous bone and a uniform thickness of 2 mm for the cortical shell. Since the apparent dry density of the bovine acetabular cancellous bone was $\approx 0.48 \text{ kgm}^{-3}$ (section 4.1.2), Young's modulus was set to 0.5 GPa based on the data of Hodgkinson and Currey (1990). Limited data are available for the mechanical properties of growth plates, Alberts *et al.* (1993) used Young's moduli of 6, 20 and 50 MPa for the growth plates of the canine distal femur, which reflects the large range of values reported for the "real time modulus" of articular cartilage. In view of this uncertainty and since the mechanical properties of the growth plate are likely to change as an animal matures (the age of the animals at slaughter was unknown), the median value of 20 MPa was chosen, with Poisson's ratio of 0.4. All materials were assumed to behave as linear elastic continua.

To simulate debonding between cement and bone at the acetabular rim, contact elements were inserted between the nodes of adjacent elements at the interface between cement and bone (detailed in section 5.4.3). The model was analysed in four configurations; the first assuming a fully bonded cement bone interface and then releasing one, two and three circumferential layers of nodes at this interface respectively. The one, two and three layers corresponded to debonded layers extending from the acetabular rim towards the pole, 10, 20 and 30 mm width respectively. Because of the complex bone geometry, a hexahedral mesh could not be generated easily, so cancellous bone, bone cement, the acetabular cup and the prosthetic femoral head were modelled using four node tetrahedral elements with additional rotational degrees of freedom at the nodes (ANSYS type SOLID72). This element was chosen in preference to higher order elements since the ANSYS program does not support contact between elements with mid-side nodes. Also, since contact requires an iterative solution, significant savings in solution times were afforded by the reduced wavefront due to the absence of mid-side nodes. The cortical shell was modelled using three node triangular shell elements having degree of freedom compatibility with the solid elements (ANSYS type SHELL63). The lack of mid-side nodes in the finite elements means that the results cannot be expected to be as accurate as a higher

order mesh of similar refinement. However, given that in this case the first order displacement solution is of interest rather than derived second order solution quantities such as strain and stress, the present mesh seems a reasonable compromise between solution time and accuracy of results. Although the models presented in chapter 5 have a lower mesh density than those presented here and use different finite elements, it is not expected that significant differences between the displacement solutions would exist.

The mesh consists of approximately 5200 solid and shell elements and 1100 nodes. The effect of the potting medium was simulated by constraining the rotational and translational degrees of freedom of the external nodes more than 20 mm from the centre of rotation of the cup in the z direction (Figure 6-11(a), lower view). Loads were applied in 30 load steps, with magnitude and direction taken from the discrete points of Figure 6-4. The model thus had approximately 5500 active degrees of freedom.

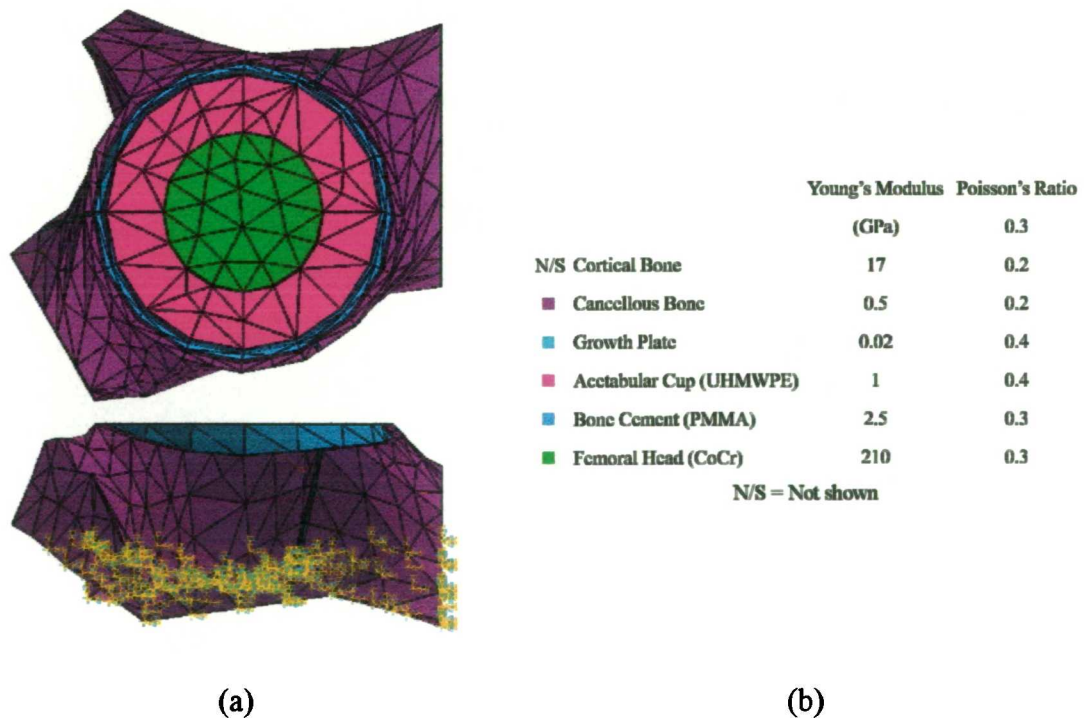


Figure 6-11: Mesh and material property distribution for the finite element models.
(a) Two views of the finite element mesh. Rotation (buff symbols) and translation (cyan symbols) constraints are shown in the lower view. The red arrow represents the applied load for a single load case. (b) Materials properties assigned to the various components.

6.3.2 Laboratory Experiments

To provide some comparative data for the finite element models, two cases were taken from the experiments described in section 6.2. These represented the worst (from the cup insertion group) - case 1 - and the best (from the pressurised group) - case 2 - fixation, as assessed qualitatively from radiographs. In addition a third acetabulum - case 3 - was implanted as described for group 2, but with a layer of PVC electrical insulation tape 25 mm deep placed around the rim of the acetabulum to simulate severe prosthesis debonding in the initial post operative stages.

6.4 Results

Figure 6-12 shows the average micromotion amplitude for the final test run for the two cementation techniques. Given the limited data points and the scatter, there is no statistically significant difference between the two groups ($p = 0.54$, two tailed t-test assuming unequal variance). However the simple observation that the scatter for the cup insertion pressurisation technique is far greater is noteworthy.

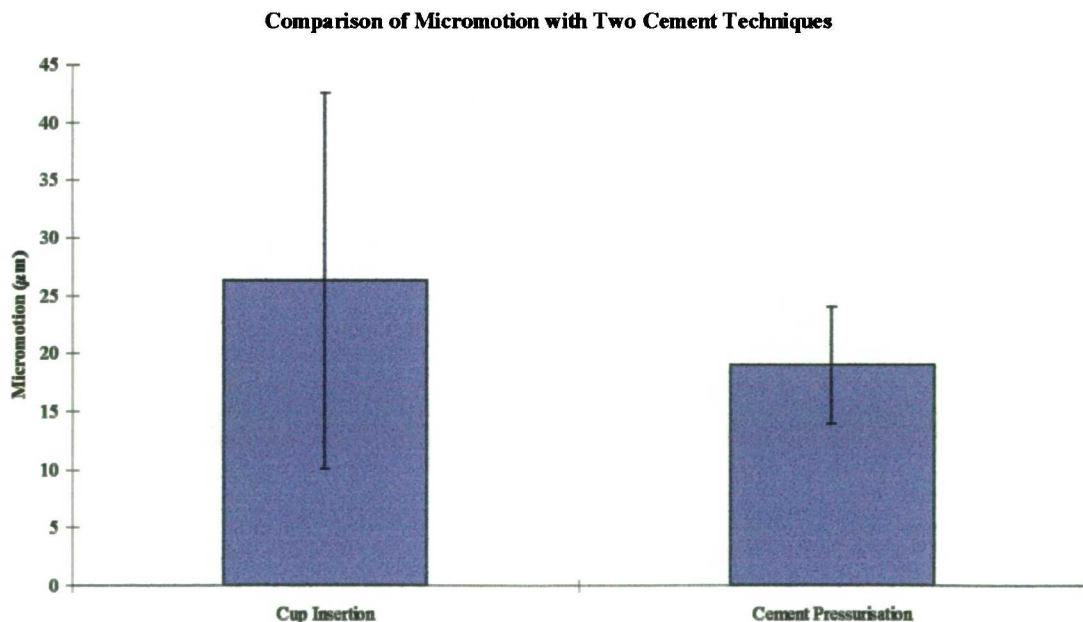


Figure 6-12: Micromotion at the ilium for two cementing techniques. Error bars represent one standard deviation.

The pre-testing radiographs of cases 1 and 2 selected for section 6.3.2 are shown in Figure 6-13.

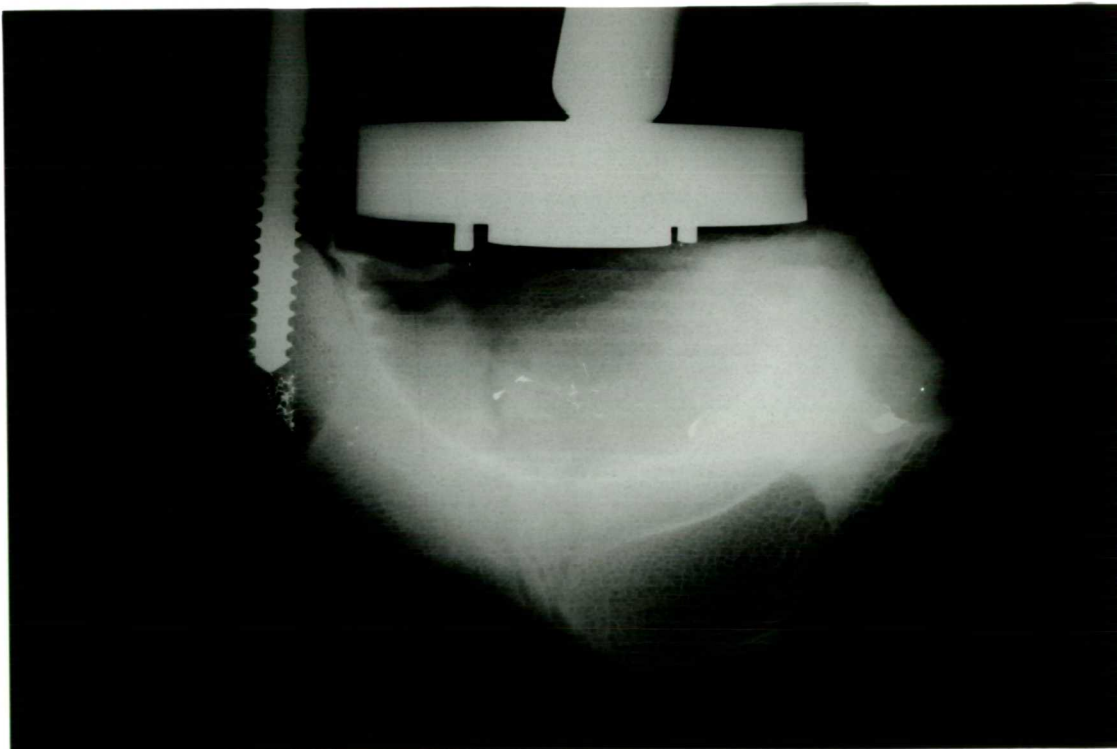
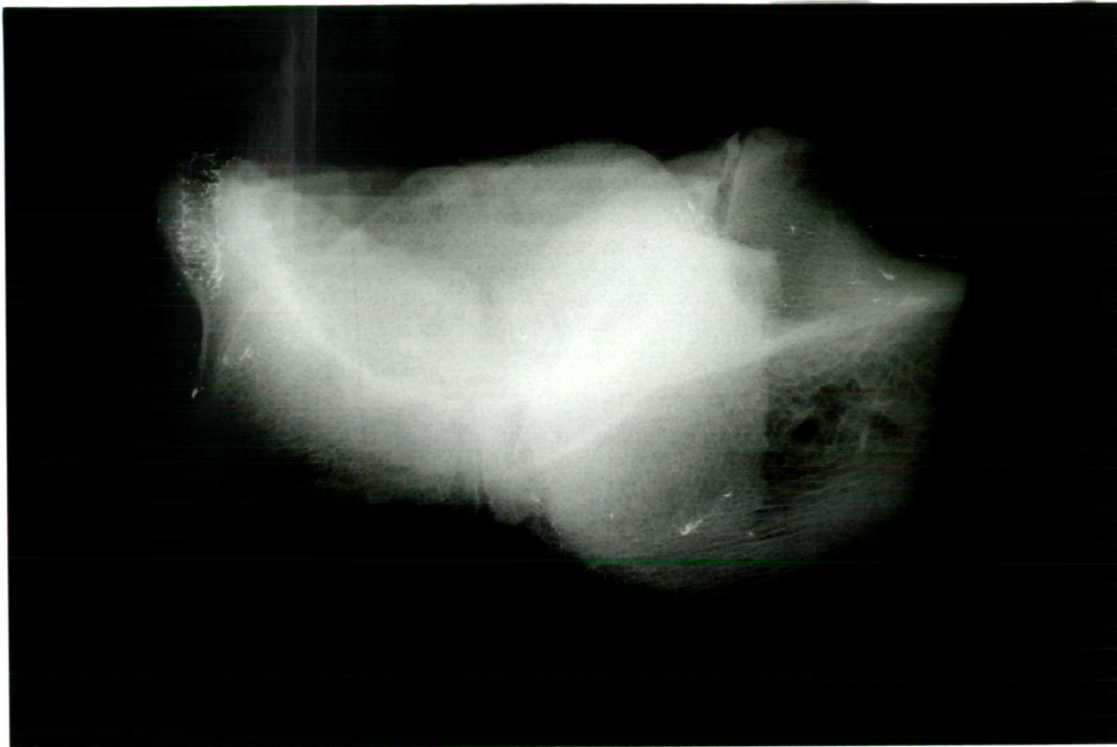


Figure 6-13: Radiographic appearance cement bone interfaces. Qualitatively the worst (case 1, left) and best (case 2, right) are shown.

Some characteristic features emerged in all the laboratory tests. Typically on the first run some settling/conditioning of the specimen was noted. This was observed as a background drift superimposed on the progressive increase in the amplitude of micromotion with the amplitude of the applied load cycles (Figure 6-14). Some small background drift was to be expected, since the minimum load was non-zero and thus scaled with the rest of the load cycle. Of the three specimens compared in the second part of the study, only in case 2 did this settling disappear in the latter tests (Figure 6-15 and Figure 6-16). It is difficult to isolate the origin of this behaviour. The juvenile bovine acetabula contained non-ossified triradial cartilaginous growth plates and the apparent settling behaviour may have been due to consolidation of these relatively compliant layers. It is also possible that the cut trabeculae produced by reaming settled, although the cement would be expected to constrain these trabeculae if sufficiently interdigitated with the bone. In mechanical testing of isolated cancellous bone specimens, the initial “toe” in the stress strain curve is now thought to be an artefact of the cut surface in contact with the loading platens (Keaveny *et al.*, 1994a) which can be eliminated by careful embedding of specimen ends and measurement of strain in a gauge section suitably remote from the region of load application.

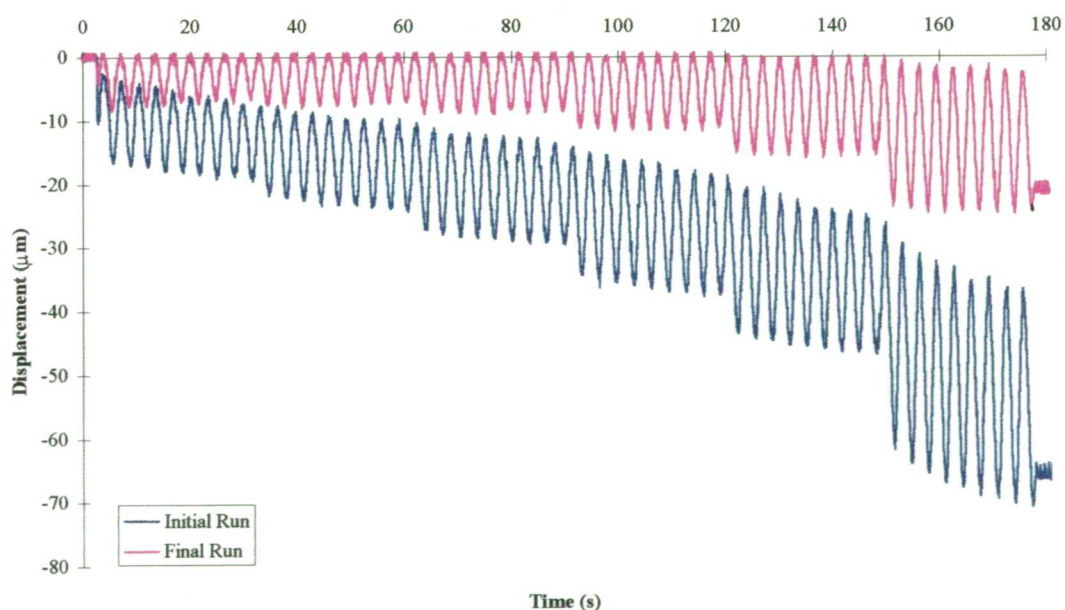


Figure 6-14: Comparison of micromotion variation between 1st and 5th experimental run.

Figure 6-15 shows the micromotion measured on the first of the five runs for each specimen. Figure 6-16 shows the same measurements for the last of the five runs. Case 2, which appeared to be the best fixed of all the specimens tested, showed

different behaviour to the other two. On the initial run, the background drift for this specimen was conspicuously larger than for cases 1 and 3. However, in the final run, this background drift had almost completely disappeared, whereas with cases 1 and 3 it persisted.

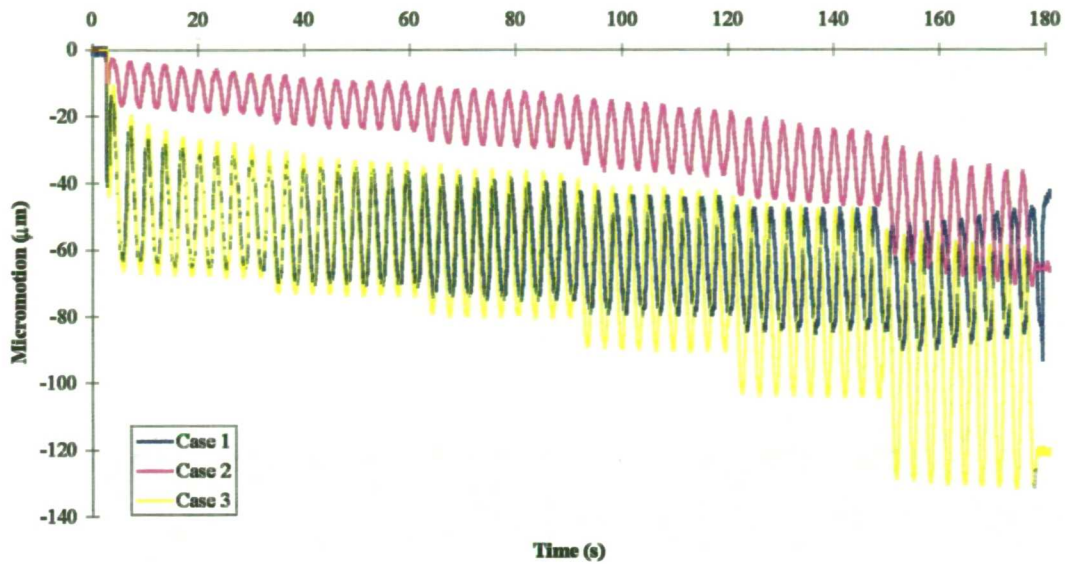


Figure 6-15: Initial run micromotions for the three cases.

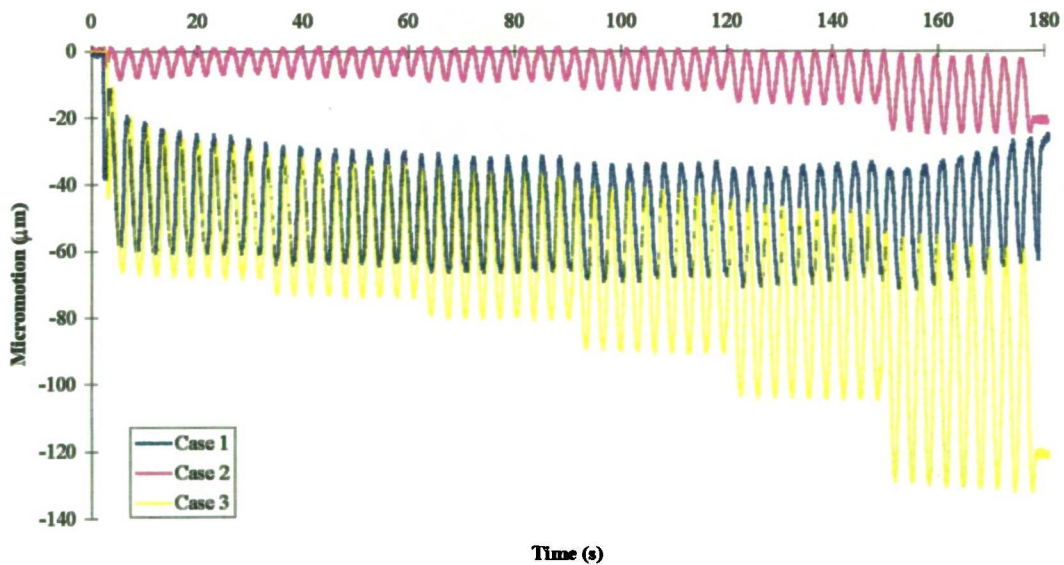


Figure 6-16: Final run micromotions for the three cases.

Figure 6-17 plots the increase in micromotion with load amplitude for the three specimens. It can be seen that the response is almost linear for all cases. However in case 1 the slope of the curve appears to be smaller than would be expected.

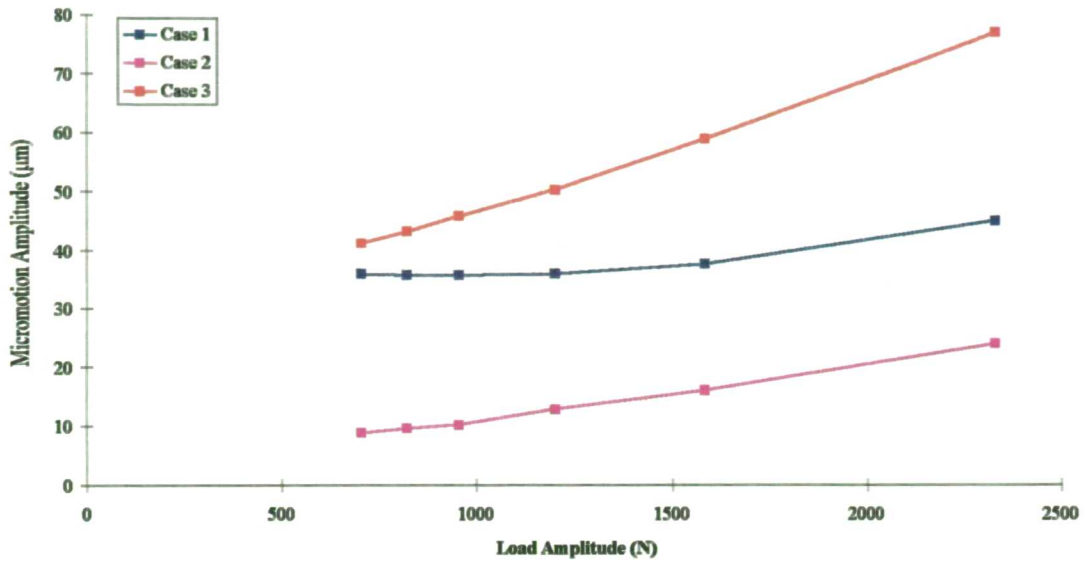


Figure 6-17: Micromotion as a function of load amplitude.

Figure 6-18 compares the results of the finite element models and the experiments for a representative load cycle at maximum load amplitude. In Figure 6-19 the magnitudes of the cyclic micromotions are compared.

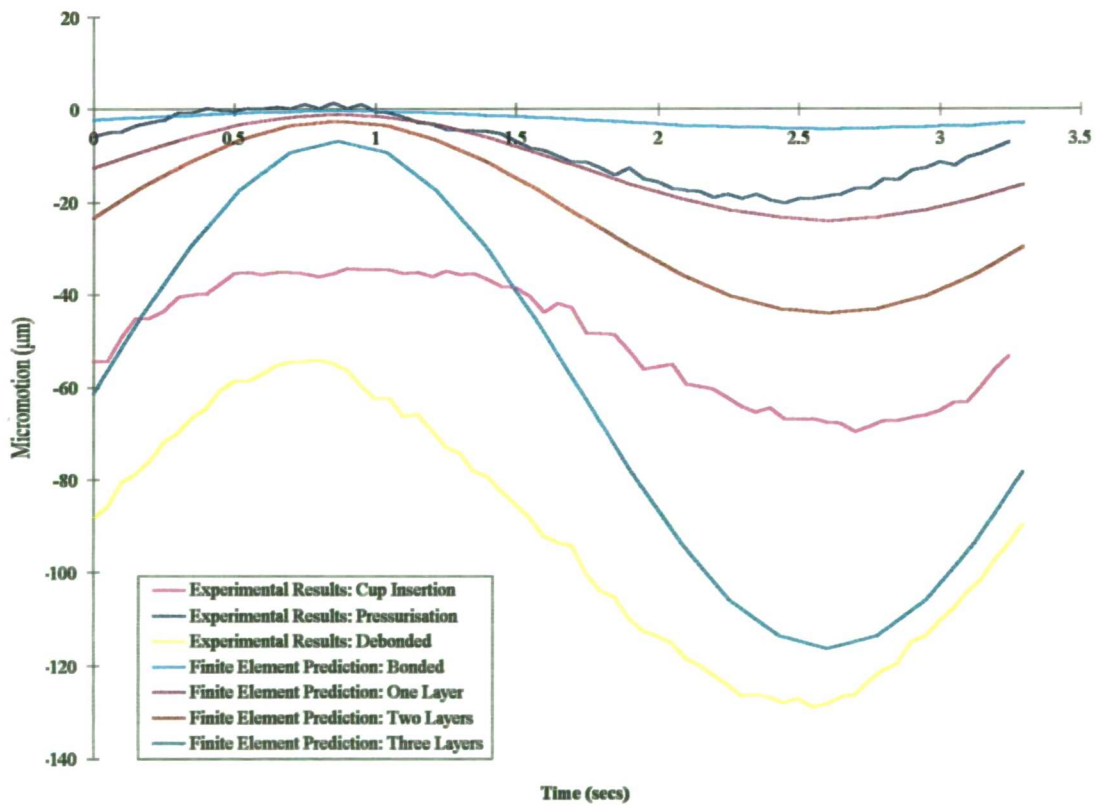


Figure 6-18: Cyclic micromotion: finite element and experimental results.

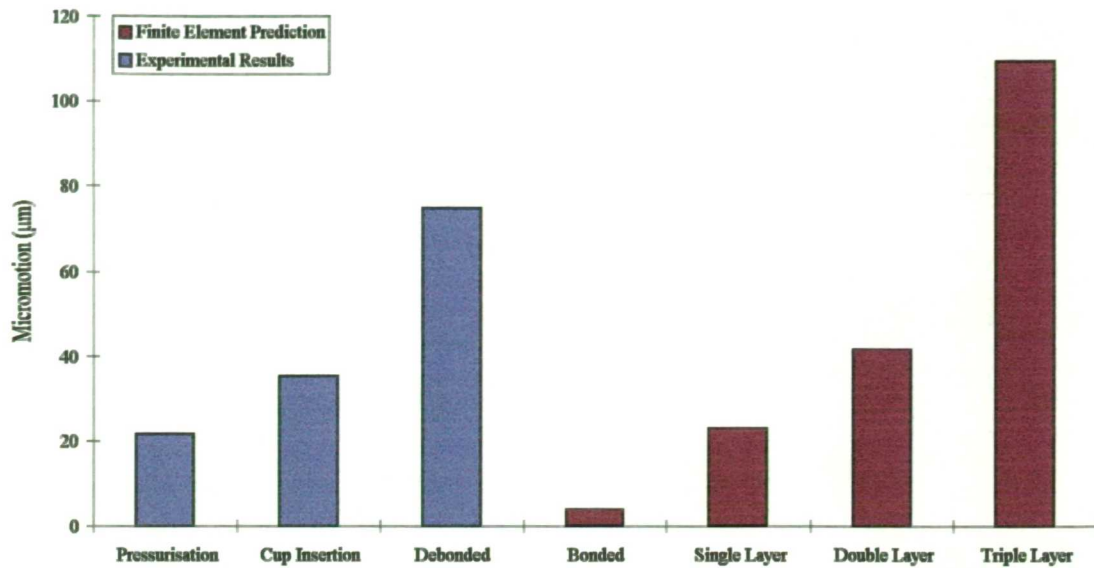


Figure 6-19: Range of micromotion: finite element and experimental results.

There is quite good agreement between the finite element models and the experimental results. Given the only information available about the condition of the interface in the experimental specimens was from plane radiographs, these results must be viewed with some caution. Nevertheless it is tempting to conclude that the finite element models have reasonably captured the behaviour of the partially fixed cup.

To investigate whether the displacements measured by the LVDT could truly be attributed to interface micromotions, the finite element models were re-examined. The absolute interface motions as derived from the relative displacement of the nodes of the relevant interface gap element were compared to the displacement calculated from the relative positions of one node, in the acetabular cup, and a second, in the acetabular rim, corresponding to the locations of the centre of the aluminium bracket and the Steinmann pin mounting the LVDT respectively. The results are presented in Figure 6-20. From these results, it appears that the transducer would overestimate the true interface micromotion, owing to the additional deformation of the intervening material. Although the amount of the overestimation cannot be precisely related to the experimental specimens, it appears that this is a relatively small effect.

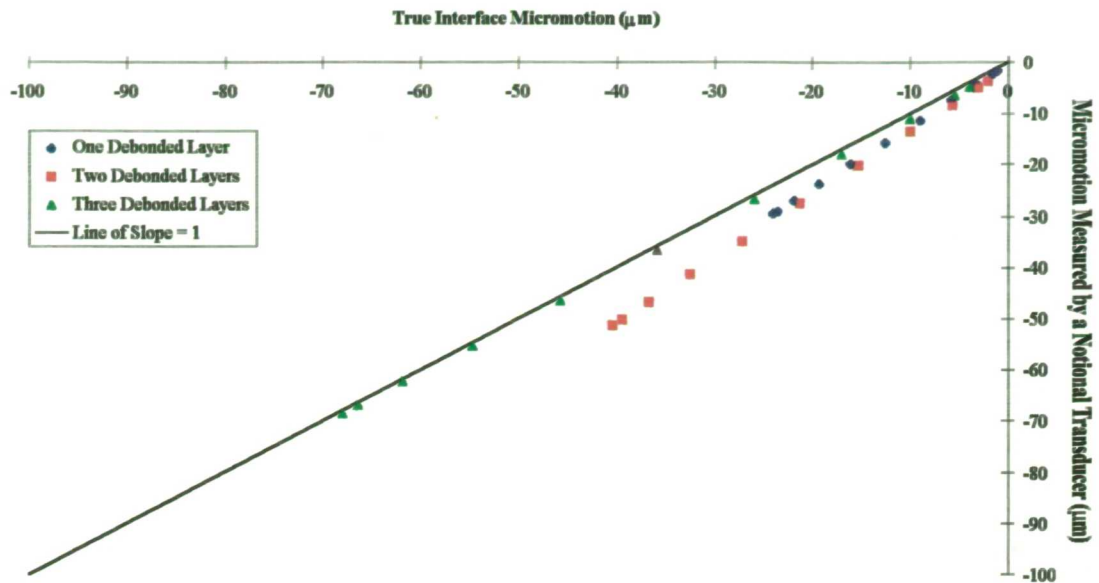


Figure 6-20: Predicted artefact due to remote measurement of interface micromotion.

6.5 Discussion

Comparison of the experimental results with the finite element model provides a useful check of the methodology adopted in Chapter 5 to simulate the effects of prosthesis debonding in a human hemi-pelvis subjected to what was intended to be physiological loading. It also gives an indication how well the laboratory model represents the reconstructed human hip. The finite element predictions compare favourably with the experimental data, which gives some confidence to the micromotion predictions presented in Chapter 5, at least as far as proving the tactic of simply inserting contact elements to represent debonding. The more elaborate treatments of interposed soft tissues as non-linear elastic materials may not be required, at least for comparative studies of methods to augment cemented fixation. Weinans *et al.* (1990) compared a variety of modelling techniques for an uncemented press-fit femoral prosthesis and found that the gap element approach, as used here, tended to underestimate micromotions by a factor of 3 to 5 compared to more elaborate techniques involving interposition of non-linear interface layers. However, the present models differ in two important ways. In the models of Weinans *et al.*, all the resistance to cyclic motion of the prosthesis relative to the bone came from frictional forces or the restoring forces due to deformation of the compliant interposed soft tissue and from macroscopic interference due to the shape of the prosthesis and

the bone bed. The shape of the bone bed was necessarily changed between the “contact” and “compliant layer” treatments and thus changed the properties of the taper coupling between prosthesis and bone. In the present case it was assumed that a significant area of the cement bone interface was still fully bonded and thus considerable remote resistance to micromotion existed, thus the stability of the prosthesis was mainly due to the regions where perfect bonding still remained, i.e. varying amounts of the depth of the acetabulum. Weinans *et al.* also set out to model the interposition of a relatively thick layer of compliant tissue. The aim of the present study was to simulate the immediate post-operative conditions where the thickness of interposed material is small. The support afforded by the remaining fully bonded interface also provides an explanation for the validity of neglecting friction at the debonded interface, since because of the stored elastic energy in this (deformed) interface there will always be a significant restoring force to restore the original configuration of the interface when only relatively small loads on the implant are present. The amount of motion in the finite element models for a given amount of debonding depends most strongly on the material properties assigned to the cancellous bone, since the bony support for the cemented cup arises principally from the cancellous bone, particularly if the prosthesis is debonded at the acetabular rim.

A recent study demonstrated that relatively small changes (compared to the present study) in the boundary conditions of the acetabulum produced significant changes in the contact pressure distribution measured in the normal hip joint (Bay *et al.*, 1997). Stiffening the acetabulum by any means interrupts what appears to be a natural mechanism for increasing the contact area between joint surfaces under load, effectively the flexure of the pubis and ischium about an axis somewhere between the geometric centre of the femoral head and the centre of the acetabular fossa. This effect was also referred to by Massin *et al.* (1993) who described it as “closing the beak” of the acetabulum. The present experiments do not suffer to the extent demonstrated by Bay *et al.*, since the stiffness of the acetabulum has already been considerably increased by the introduction of the prosthesis, which has already gone quite some way to nullify the natural deformation pattern of the acetabulum.

By making comparisons with a finite element model it was possible to separate the true interface micromotion and the measured apparent motion which is a combination

of the true interface micromotion and the deformation of the materials to which the measuring transducer was mounted. It was found in the simulation of the experimental study that tissue deformation could contribute up to 25% of the total measured motions. However, even taking tissue deformation into consideration, the experimentally measured “micromotion” was never as low as predicted by the fully bonded finite element model.

Radiographic studies show that radiolucencies between cement and bone first appear at both the proximal and distal edges of the acetabulum as viewed on an anterior-posterior radiograph and that these radiolucencies progress in time towards the depth of the acetabulum, eventually “cutting out” the cement and cup. The study of autopsy specimens by Schmalzried *et al.* (1992) indicates that these radiolucencies represent a fibrous tissue layer which is circumferential, although this cannot be detected on a conventional anterior-posterior radiograph. Thus the pattern of debonding modelled in this study is probably representative of the true progression of the fibrous interposition. The motions at all three positions was sufficient to jeopardise the possibility of the cement bone interface being reinstated by a healing response. Many studies have looked at the effects of micromotion on potential for ingrowth, usually in connection with uncemented implants, and have shown that gaps *per se* are not particularly harmful, bone being able eventually to bridge gaps up to 2 mm with porous coated (Sandborn *et al.*, 1988) and 0.75 mm with smooth (Thomas *et al.*, 1987) implants. However, if the gap permits micromotion, the amount of micromotion required to prevent gap bridging is very small. If it is assumed that PMMA is essentially bio-inert, it can be assumed that micromotions of more than 150 μm definitely preclude bony apposition, whereas movements of less than 30-40 μm do not prevent apposition (Pilliar *et al.*, 1986; Burke *et al.*, 1991). Since these values are almost universally from animal studies, where healing potential is generally greater than in elderly humans, we may expect that 40 μm is an optimistic estimate of the maximum tolerable micromotion. If this is accepted the micromotions predicted here are worrying, even the smallest amount of micromotion, generated by releasing a single layer of nodes to a depth of 10 mm, is greater than the threshold for apposition. Thus a cemented implant that is even marginally loose at its rim will move more than the tolerable amount and the probability of the interface recovering will thus be small.

7. Conclusions

An extensive body of literature supports, both directly and indirectly, relationships between cup fixation strength, prosthesis survivorship and cementation technique in the acetabulum during total hip replacement. In this thesis some of those factors which may be controlled at the time of operation, or which occur relatively soon post-operatively and are thought to influence the long term success of the acetabular reconstruction, have been investigated.

Various studies have suggested that cement pressurisation and subsequent cement penetration into cancellous bone produces a stronger cement-bone interface (Krause *et al.*, 1982a; Askew *et al.*, 1984; Mann *et al.*, 1997). A range of methods of cement pressurisation were compared using an instrumented model acetabulum. Typically cup insertion lead to a transient pressure rise at the pole of the acetabulum and a smaller rise at the rim, indicating pressure gradients in the cement. Although finger packing generated reasonable peak pressures, pressurisation was patchy and could not be maintained. Two novel cement pressurisers, designed to produce a closed cavity, are described and their use shown to produce effective cement pressurisation in the laboratory. One of these cement pressurisers was then instrumented with a pressure transducer to allow per-operative cement pressure measurements in the acetabulum, the first time such measurements have been described. These measurements showed satisfying agreement with the laboratory studies, helping to validate their use for the comparison of cementing techniques. On average, the mean pressures for two orthopaedic surgeons during 16 total hip replacements were 48.9 kPa (standard deviation 17.4 kPa) and 46.9 kPa (16.7 kPa) and the peak pressures 76.0 kPa (4.7 kPa) and 93.4 kPa (14.5 kPa). No statistically significant difference was found between either the mean or the peak pressures for the two surgeons.

In many operations the acetabular cup itself is used as a pressurisation device, in which case cup design is important for cement pressurisation and penetration of cement into cancellous bone (Beverland *et al.*, 1993, Shelley and Wroblewski, 1988), an effect which appears to be clinically significant since it results in improvements in the radiographic appearance of the cement bone interface in the long term (Hodgkinson *et al.*, 1993). A finite element modelling technique to predict the

pressurisation and penetration of cement into cancellous bone during prosthesis insertion was developed and validated. This model was then used to perform a parametric study of the factors that affect the ultimate cement penetration and consequently the component fixation. These analyses showed cement penetration to be greater with flanged cups, reduced viscosity cement, higher insertion force and more permeable cancellous bone. Cement penetration varied from negligible (less than 0.5 mm) to more than 5 mm. The trends were in agreement with those reported in the literature and appeared reasonable in comparison to typical post-operative radiographic appearances.

Further clinical evidence suggests that dynamic mechanical processes in the short term post operatively determine the lifetime of a prosthesis and consequently that the mechanisms of failure of the cement bone interface that are manifested as prosthesis migration and eventual clinical failure are predominantly mechanical, or at least mechanically triggered (Taylor and Tanner, 1997). The mechanics of cemented acetabular reconstruction remain little studied, particularly with respect to the dynamic aspects of hip joint loading during activity, where both the magnitude and the direction of the hip joint reaction force change significantly with respect to the anatomical axes of the pelvis.

A three dimensional finite element model of the pelvis incorporating a realistic material property distribution and muscle forces (Dalstra, 1993) was used to study the factors that affect the mechanics of the reconstructed acetabulum and an attempt was made to examine the effects of sub-optimal prosthesis fixation (debonding at the acetabular rim). In the normal acetabulum there appear to be two mechanisms for the transfer of the hip joint reaction force into the pelvis. The load is shared between the cancellous bone in the depth of the acetabulum and the pelvic cortex at the acetabular rim according to the stiffness of each. In the reconstructed acetabulum, the presence of the relatively stiff acetabular cup suppresses the deformation of the acetabulum with the result that loads are not transmitted as efficiently as in the natural situation. If a fully bonded prosthesis is assumed, most of the load is transferred at the rim of the acetabulum directly into the cortical shell and the cancellous bone in the depth is stress shielded. With a debonded prosthesis less load is transferred at the rim (cortex) and relatively more in the depth by the cancellous bone, depending weakly on certain

modelling assumptions. In the debonded models, the total range of micromotion between cement and bone over a complete gait cycle was dependent on location in the acetabulum and on the amount of the cement-bone interface assumed to be debonded, but was up to 55 μm for one debonded layer of nodes, representing a debonded width of 7-12 mm. According to published literature and assuming that PMMA is essentially bio-inert, micromotions of more than 150 μm would definitely preclude bony apposition at the cement-bone interface, whereas movements of less than 30-40 μm do not prevent apposition (Pilliar *et al.*, 1986; Burke *et al.*, 1991). Since these values are almost universally from animal studies, where healing potential is generally greater than in elderly patients undergoing hip replacement, it may be that 40 μm is an optimistic estimate of the maximum tolerable micromotion. Even the minimum micromotion was greater than this presumed threshold for apposition. Thus a cemented implant that is even marginally loose at its rim is likely to move locally more than the tolerable amount and therefore the probability of the interface recovering will be small. In addition to these direct mechanical consequences, rim debonding also opens a pathway for wear debris from the articulating surface to reach the depth of the acetabulum and exacerbate loosening by cellular mechanisms leading to bone resorption.

The results of similar finite element models were compared with experimental results from a laboratory model of human acetabular reconstruction, a bovine calf acetabulum, loaded in a newly developed hip joint simulator designed to provide a laboratory simulation of the motion and loading in a normal human hip when used in conjunction with a servo-hydraulic universal testing machine. A simple comparison was made between specimens where a cement pressuriser was either used or not used and in specimens where debonding was deliberately introduced. The results showed that there were measurable differences in the stability of “well fixed” and “poorly fixed” cups and micromotion was found, even in the best fixed case, to be far greater than would be expected from that which could be attributed to elastic deformation of the intervening material. Thus it is reasonable to assume that “perfect” bonding was never achieved in the laboratory and that relatively large micromotion could still occur in specimens that appear radiologically perfectly fixed with no apparent radiolucent lines. These results suggested that rim fixation against the edge of the pelvic cortex may not be achievable

even with the best current cementing technique and thus finite element models which assume complete bonding in this region may be unrealistic.

This experimental study represents a first attempt to relate cement pressurisation and the global fixation status of the acetabular cup. Radiolucencies frequently develop in the short term at the superior acetabular rim. If these radiolucencies are present immediately post operatively the prognosis for the acetabular cup is worse (Strömberg *et al.*, 1996). As well as providing a path for wear debris to reach the cancellous bone supporting the cup in the depth of the acetabulum, the gaps facilitate micromotions that, even if the length of the radiolucent line is as small as 5-10 mm, are already large enough to preclude bone apposition at the cement surface.

8. Future Work

Much of the work described here represents studies which are in many senses preliminary. In particular it remains difficult to answer the surgeon's favourite question - are the results clinically significant?

A particular shortcoming of this project is that no human anatomical specimens have been studied, however, obtaining such specimens is difficult. Computer models need experimental validation, but for practical reasons this can often only be achieved with respect to an experiment that is in itself a model of the real situation, as presented here. The extension of these studies to human specimens is an obvious next step.

The method for simulating bone cement flow during prosthesis insertion is applicable to any cemented prosthesis. It could, for example, be used to predict cement mantle and bone-cement composite thicknesses around femoral components and under tibial trays. The latter is probably the easiest to simulate since the cancellous bone exposed per-operatively has the simplest geometry.

The experimental studies of chapter 6 represent a first attempt at investigating the fixation of acetabular prostheses using an approximation to physiological loading, simulating both the magnitude and direction of the hip joint reaction force during activity. Using bovine acetabula, it was shown that the cementing technique has measurable effects on initial fixation. Much more work is required to establish an optimum cementing technique, but it appears that a pressurisation tool is essential. There is good evidence that mechanical or chemical bonding is required for the long term stability of the interface between implant and bone and that implants that show fibrous tissue between implant and bone (e.g. lucencies on radiographs), while often appearing clinically successful, are meta-stable at best. Present acetabular prostheses appear to fail by the gradual advance of a fibrous tissue layer from the rim to the depth of the acetabulum, radiographic evidence of this mechanism appearing soon after the operation. The present work appears to support the contention that mechanical factors are strongly involved in this mechanism. It is possible that "pre-cracks" present post-operatively or resulting from early localised mechanical failure of the cement-bone interface at the acetabular rim grow principally under the influence of continued

mechanical loading. Despite the complex state of stress at the crack tip, modern techniques that combine fracture mechanics with finite element analysis may be applicable to this situation, particularly in these early stages which appear to be so influential in the outcome of a joint replacement. For laboratory verification of such studies, ideally a non destructive method of measuring the progress of the interface crack would be required. Radiography is generally inadequate for accurately tracking the progress of interfacial cracks, however ultrasonic testing methods are routinely used for assessing the damage levels in composite materials and, despite the complex geometry of the acetabulum, modern digital signal processing techniques may enable information about the interfaces to be extracted.

With the assumption of fully bonded cement bone interfaces, which may not be a good one, stresses predicted by finite element models suggest that, according to “Wolff’s Law” of bone adaptation, the bone should become rarefied in the depth of the acetabulum, whereas autopsy specimens show it to become densified, with the formation of a neo-cortex (Schmalzried *et al.*, 1992; Bos *et al.*, 1995). Debonding of the cement bone interface at the rim of the acetabulum leads to a stress distribution that feasibly might lead to the development of densified bone in the depth of the acetabulum. The application of a bone remodelling algorithm to the acetabulum in both the fully bonded and partially bonded configurations may provide further insight into the mechanism of acetabular loosening.

9. References

- Abendschein W, Hyatt GW.** Ultrasonics and Selected Physical Properties of Bone. *Clinical Orthopaedics and Related Research* 1970; 69: 294-301.
- Ahnfelt L, Herberts P, Malchau H, Andersson GBJ.** Prognosis of Total Hip Replacement, A Swedish Multicenter Study of 4664 Revisions. *Acta Orthopaedica Scandinavica* 1990; 61: Sup. 238.
- Alberts LR, Pao YC, Lippiello L.** A Large Deformation Finite Element Study of Chondrodystasia in the Canine Distal Femoral Epiphyseal Plate. *Journal of Biomechanics* 1993; 26: 1291-1305.
- Andersson GBJ, Freeman MAR, Swanson SAV.** Loosening of the Cemented Acetabular Cup in Total Hip Replacement. *Journal of Bone and Joint Surgery* 1972; 54B; 590-599.
- Askew MJ, Kufel MF, Fleissner Jr PR, Gradisar Jr IA, Salstrom SJ, Tan JS.** Effect of Vacuum Mixing on the Mechanical Properties of Antibiotic-Impregnated Polymethylmethacrylate Bone Cement. *Journal of Biomedical Materials Research* 1990; 24: 573-580.
- Askew MJ, Steege JW, Lewis JL, Ranieri JR, Wixson RL.** Effect of Cement Pressure and Bone Strength on Polymethylmethacrylate Fixation. *Journal of Orthopaedic Research* 1984; 1: 412-420.
- Balu GR, Noble PC, Alexander JW, Vela VL.** The Effect of Intramedullary Reaming on the Strength of the Cement/Bone Interface. Proceedings of 40th Annual Meeting Orthopaedic Research Society 1994: 797
- Bannister GC, Miles AW.** The Influence of Cementing Technique and Blood on the Strength of the Bone Cement Interface. *Proceedings of the Institute of Mechanical Engineers Part H: Engineering in Medicine* 1988; 202: 131-133.
- Bauer TW, Zehr RJ, Ming J, Kambic HE, Bearcroft JA.** Effect of Varying HA and TCP Coating Content on Debris Production and Bone Apposition. Proceedings of 41st Annual Meeting Orthopaedic Research Society 1995: 768
- Bay BK, Hamel AJ, Olson SA, Sharkey NA.** Statically Equivalent Load and Support Conditions Produce Different Hip Joint Contact Pressures and Periacetabular Strains. *Journal of Biomechanics* 1997; 30: 193-196.
- Bayne SC, Lautenschlager EP, Compere CL, Wildes R.** Degree of Polymerisation of Acrylic Bone Cement. *Journal of Biomedical Materials Research* 1975; 9: 27-34.
- Bean DJ, Convery FR, Woo SL-Y, Lieber RL.** Regional Variation in Shear Strength of the Bone-Polymethylmethacrylate Interface. *Journal of Arthroplasty* 1987; 2: 293-298.
- Beaudoin AJ, Mihalko WM, Krause WR.** Finite Element Modelling of Polymethylmethacrylate Flow Through Cancellous Bone. *Journal of Biomechanics* 1991; 24: 127-136.
- Benjamin JB, Gie JE, Lee AJC, Ling RSM, Volz RG.** Cementing Technique and the Effects of Bleeding. *Journal of Bone and Joint Surgery* 1987; 69-B: 620-624.

- Bergmann G, Graichen F, Rohlmann A.** Hip Joint Loading During Walking and Running, Measured in Two Patients. *Journal of Biomechanics* 1993; 26: 969-990.
- Bergmann G, Graichen F, Rohlmann A.** Is Staircase Walking a Risk for the Fixation of Hip Implants ? *Journal of Biomechanics* 1995; 28: 535-554.
- Bernoski FP, New AMR, Scott RA, Northmore-Ball MD.** An *In Vitro* Study of a New Design of Acetabular Cement Pressuriser. *Journal of Arthroplasty* (Accepted).
- Berryman JG.** Measurement of Spatial Correlation Functions Using Image Processing Techniques. *Journal of Applied Physics* 1985; 57: 2374-2384.
- Beverland DE, Kernohan WG, Nixon JR, Orr JF, Watson P.** Pressurisation of Bone Cement Under Standard, Flanged and Custom Acetabular Components for Total Hip Replacement. *Proceedings of the Institute of Mechanical Engineers Part H: Engineering in Medicine* 1993; 207: 19-23.
- Biomaterials and Implants Research Advisory Group.** Report to the United Kingdom Department of Health, 1996, 7.
- Black J.** Orthopaedic Biomaterials in Research and Practice. Churchill Livingstone, New York, 1988.
- Bobyn JD, Pilliar RM, Cameron HU, Weatherly GC.** The Optimum Pore Size for the Fixation of Porous Surfaced Metal Surfaced Metal Implants by the Ingrowth of Bone. *Clinical Orthopaedics and Related Research* 1980; 150: 263-270.
- Bonfield W, Behiri JC, Charalambides B.** Orientation and Age Related Dependence of the Fracture Toughness of Cortical Bone. *Biomechanics: Current Interdisciplinary Research*. eds. Perren SM, Schneider E. Martinus Nijhoff, Dordrecht 1985: 185-189.
- Bonfield W, Datta PK.** Fracture Toughness of Compact Bone. *Journal of Biomechanics* 1976; 9: 131-134.
- Bonfield W, Datta PK.** Impact Fracture of Compact Bone in a Shock Tube. *Journal of Materials Science* 1974; 9: 1609-1614.
- Bonfield W, Grynpas MD, Young RJ.** Crack Velocity and the Fracture of Bone. *Journal of Biomechanics* 1978; 11: 473-479.
- Bonfield W, Grynpas MD.** Anisotropy of the Young's Modulus of Bone. *Nature* 1977; 270: 453-454.
- Bonfield W, Li CH.** Deformation and Fracture Bone. *Journal of Applied Physiology* 1966; 37: 869-875.
- Bos I, Fredebold D, Diebold J, Löhrs U.** Tissue Reactions to Cemented Hip Sockets Histologic and Morphometric Autopsy Study of 25 Acetabula. *Acta Orthopaedica Scandinavica* 1995; 66: 1-8.
- British Standard 5724 Section 1.1: 1992** Medical Electrical Equipment Part 1 General Requirements for Safety. British Standards Institute, 1992.
- Brown TD, Ferguson AB.** Mechanical Property Distribution in the Cancellous Bone of the Human Proximal Femur. *Acta Orthopaedica Scandinavica* 1980; 51: 429-437.
- Brunski JB, Aquilante FM, Pollack SR, Korostoff E, Trachtenburg DI.** The Influence of Functional Use of Endosseous Dental Implants on the Tissue Implant Interface I Histological Aspects. *Journal of Dental Research* 1979; 58: 1953-1969.

- Bugbee WD, Barrera DL, Lee AC, Convery FR.** Variation in Shear Strength of the Bone Cement Interface in the Proximal Femur. *Proceedings of 38th Annual Meeting Orthopaedic Research Society* 1992: 22
- Burke DW, Gates EI, Harris WH.** Centrifugation as a Method of Improving Tensile and Fatigue Properties of Acrylic Bone Cement. *Journal of Bone and Joint Surgery* 1984; 66-A: 1265-1273.
- Burke DW, Bragdon CR, O'Connor DO, Jasty M, Haire T, Harris WH.** Dynamic Measurements of Interface Mechanics *In Vivo* and the Effects of Micromotion on Bone Ingrowth into a Porous Surface Device Under Controlled Loads *In Vivo*. Transactions of the 37th Annual Meeting of the Orthopaedic Research Society, Anaheim, 1991, 103.
- Burstein AH, Reilly DT, Martens M.** Aging of Bone Tissue: Mechanical Properties. *Journal of Bone & Joint Surgery* 1976; 58-A: 82-86.
- Carlsson AF, Gentz CF.** Radiographic Versus Clinical Loosening of the Acetabular Component in Noninfected Total Hip Arthroplasty. *Clinical Orthopaedics and Related Research* 1984; 185: 145-150.
- Carlstedt CA, Nordin M.** Biomechanics of Tendons and Ligaments. In *Basic Biomechanics of the Musculoskeletal System 2nd Edition*, eds. Nordin M and Frankel VH. Lea and Febiger, Philadelphia, 1989.
- Carter DR, Caler WE, Spengler DM, Frankel VH.** Fatigue Behaviour of Adult Cortical Bone: The Influence of Mean Strain and Strain Range. *Acta Orthopaedica Scandinavica* 1981; 52: 481-485.
- Carter DR, Hayes WC.** Compact Bone Fatigue Damage: a Microscopic Examination. *Clinical Orthopaedics and Related Research* 1977a; 127: 265-274.
- Carter DR, Hayes WC.** The Compressive Behaviour of Bone as a Two Phase Porous Structure. *Journal of Bone and Joint Surgery* 1977b; 59-A: 954-962.
- Carter DR, Schwab GH, Spengler DM.** Tensile Fracture of Cancellous Bone. *Acta Orthopaedica Scandinavica* 1980; 51: 733-741.
- Carter DR, Spengler DM.** Mechanical Properties and Composition of Cortical Bone. *Clinical Orthopaedics and Related Research* 1978; 135: 192-217.
- Charnley J.** *Low Friction Arthroplasty of the Hip.* Springer-Verlag, Berlin, 1979.
- Chen SC, Lowe SA, Scales JT, Ansell RH.** An *In Vivo* Experiment to Determine the Efficiency of Fixation of the McKee-Farrar Acetabular Component in Relation to Torsional Force. *Acta Orthopaedica Scandinavica* 1974, 45; 429-435.
- Choi K, Kuhn JL, Ciarelli MJ, Goldstein SA.** The Elastic Moduli of Human Subchondral, Trabecular and Cortical Bone Tissue and the Size Dependency of Cortical Bone Modulus. *Journal of Biomechanics* 1990; 23: 1103-1113.
- Clarke HJ, Jinnah RH, Warden KE, Cox QGN, Curtis MJ.** Evaluation of Acetabular Stability in Uncemented Prostheses. *Journal of Arthroplasty* 1991; 6: 335-340.
- Cook SD, Thomas KA, Kay JF.** Experimental Coating Defects in Hydroxylapatite Coated Implants. *Clinical Orthopaedics and Related Research* 1991; 265: 280-290.

- Corondan G, Haworth WL.** A Fractographic Study of Human Long Bone. *Journal of Biomechanics* 1986; 19: 207-218.
- Crowninshield RD, Brand RA.** A Physiologically Based Criterion of Muscle Force Prediction in Locomotion. *Journal of Biomechanics* 1981; 14; 793-801.
- Cunningham's Textbook of Anatomy 11th Edition.** ed Romanes GJ. Oxford University Press, Oxford, 1972.
- Currey J.** The Mechanical Adaptions of Bones. Princeton University Press, Princeton, 1984.
- Currey JD.** The Effect of Porosity and Mineral Content on the Young's Modulus of Elasticity of Compact Bone. *Journal of Biomechanics* 1988; 21: 131-139.
- Currey JD, Butler G.** The Mechanical Properties of Bone Tissue in Children. *Journal of Bone and Joint Surgery* 1975; 57A: 810-814.
- Curtis MJ, Jinnah RH, Wilson VD, Hungerford DS.** The Initial Stability of Uncemented Acetabular Components. *Journal of Bone and Joint Surgery* 1992; 74-B: 372-376.
- Dalstra M, Huiskes R, van Erning L.** Development and Validation of a Three Dimensional Finite Element Model of the Pelvic Bone. *Journal of Biomechanical Engineering* 1995; 117: 272-278.
- Dalstra M, Huiskes R.** Load Transfer Across the Pelvic Bone. *Journal of Biomechanics* 1995; 28: 715-724.
- Dalstra M.** Biomechanical Aspects of the Pelvic Bone and Design Criteria for Acetabular Prostheses. Ph.D. Thesis, University of Nijmegen, The Netherlands, 1993.
- Davies JP, Burke DW, O'Connor DO, Harris WH.** Comparison of the Fatigue Characteristics of Centrifuged and Uncentrifuged Simplex P Bone Cement. *Journal of Orthopaedic Research* 1987; 5: 366-371.
- Davies JP, Harris WH.** *In Vitro* and *In Vivo* Studies of Pressurization of Femoral Cement in Total Hip Arthroplasty. *Journal of Arthroplasty* 1993; 8: 585-591.
- Davies JP, Jasty M, O'Connor DO, Burke DW, Harrigan TP, Harris WH.** The Effect of Centrifuging Bone Cement *Journal of Bone and Joint Surgery* 1989; 71-B: 39-42.
- Davy DT, Kotzar GM, Brown RH, Heiple KG, Goldberg VM, Heiple Jr KG, Berilla J, Burstein AH.** Telemetric Force Measurements across the Hip after Total Arthroplasty. *Journal of Bone and Joint Surgery* 1988; 70-A: 45-50.
- Dieter GE.** Mechanical Metallurgy SI Metric Edition. Macraw-Hill, New York, 1988.
- Deligianni DD, Missirlis YF, Tanner KE, Bonfield W.** Mechanical Behaviour of Trabecular Bone of the Human Femoral Head in Females. *Journal of Materials Science: Materials in Medicine* 1991; 2: 168-175.
- Delesse MA.** Procédé Mécanique pour Déterminer la Composition des Roches. *C. r. hebdomadaire des séances Acad Sci., Paris* 1847; 25: 544.
- Dempster WT, Coleman RF.** Tensile Strength of Bone Along and Across the Grain. *Journal of Applied Physiology* 1960; 16: 355.

- Dempster WT, Liddicoat RT.** Compact Bone as a Non Isotropic Material. *American Journal of Anatomy* 1952; 91: 331-362.
- DiPisa JA, Sih GS, Berman AT.** The Temperature Problem at the Bone-Acrylic Cement Interface of the Total Hip Replacement. *Clinical Orthopaedics and Related Research* 1976; 121: 95-98.
- Dorr LD, Lindberg JP, Claude-Faugere X, Malluche HH.** Factors Influencing the Intrusion of Methylmethacrylate into Human Tibiae. *Clinical Orthopaedics and Related Research* 1984; 183: 147-152.
- Dostal WF, Andrews JG.** A Three Dimensional Biomechanical Model of Hip Musculature. *Journal of Biomechanics* 1981; 14: 803-812.
- Draenert K.** Modern Cementing Techniques - An Experimental Study of Vacuum Insertion of Bone Cement. *Acta Othopaedica Belgica* 1989; 55: 273-293.
- Durst F, Haas R, Interthal W.** The Nature of Flows Through Porous Media. *Journal of Non-Newtonian Fluid Mechanics* 1987; 22: 169-189.
- Eftekhar NS, Nercessian O.** Incidence and Mechanism of Failure of Cemented Acetabular Components in Total Hip Arthroplasty. *Orthopedic Clinics of North America* 1988; 19: 557-566.
- Eriksson AR, Albreksson T.** Temperature Threshold Levels for Heat Induced Bone Tissue Injury: A Vital Microscopic Study in the Rabbit. *Journal of Prosthetic Dentistry* 1983: 101-107.
- Evans FG.** Mechanical Properties of Bone. Charles C Thomas, Springfield, 1973
- Evans FG, King AL.** Regional Differences in Some Physical Properties of Human Spongy Bone. in *Biomechanical Studies of the Musculo-Skeletal System*, ed. Evans FG, Charles C Thomas, Springfield, 1961.
- Feith R.** Side Effects of Acrylic Cement Implanted into Bone. *Acta Orthopaedica Scandinavica* 1975; 46: Sup. 161
- Fowler JL, Gie GA, Lee AJC, Ling RSM.** Experience with the Exeter Total Hip Replacement Since 1970. *Orthopaedic Clinics of North America* 1988; 19: 477-489.
- Freeman MAR, Plante-Bordeneuve P.** Early Migration and Late Aseptic Failure of Proximal Femoral Prosheses. *Journal of Bone and Joint Surgery* 1994; 76-B: 432-438.
- Frost HM.** Perspectives - Bone's Mechanical Usage Windows. *Bone and Mineral* 1992; 19: 257-271.
- Galante JO.** The Biological Basis to Bone Ingrowth in Titanium Fibre Composites. in *Advanced Concepts in Total Hip Replacement*. ed Harris WH. SLACK Incorporated, Thorofare, 1985.
- Galante J, Rostoker W, Ray RD.** Physical Properties of Trabecular Bone. *Calcified Tissue Research* 1970; 5: 236-246.
- Gardner ER, Wilkinson R, Stother IG.** The Effect of Lavage During Total Hip Arthroplasty on the Mechanical Properties of Bone Cement. *Proceedings of 7th International Conference on Biomedical Engineering, Singapore, 1992: 163-164*
- Geesink RGT, de Groot K, Klein CPAT.** Chemical Implant Fixation Using Hydroxyl-Apatite Coatings - the Development of a Human Total Hip Prosthesis for

- Chemical Fixation to Bone Using Hydroxyl-Apatite Coatings on Titanium Substrates. *Clinical Orthopaedics and Related Research* 1987; 225: 147-170.
- Gibson LJ.** The Mechanical Behaviour of Cancellous Bone. *Journal of Biomechanics* 1985; 18: 317-328.
- Gibson LJ, Ashby MF.** Cellular Solids: Structure and Properties. Pergamon Press, Oxford, 1988.
- Gluck T.** Referat über die durch das moderne chirurgische Experiment gewonnenen positiven Resultate, betreffend die Nacht und den Ersatz von Defecten höherer Gewebe, sowie über die Verwerthung resorbirbarer und lebendiger Tampons in der Chirurgie, *Archiv für klinische Chirurgie* 1891; 41: 186-239.
- Goldstein SA.** The Mechanical Properties of Trabecular Bone: Dependence on Anatomic Location and Function. *Journal of Biomechanics* 1987; 20: 1055-1061.
- González O, Smith RL, Goodman SB.** Effects of PMMA Particles of Various Sizes and Concentrations on Human Macrophages *In Vitro*. Proceedings of 41st Annual Meeting Orthopaedic Research Society 1995: 167.
- Gordon JE.** The New Science of Strong Materials or Why You Don't Fall Through the Floor 2nd Edition. Penguin Books, London, 1976.
- Gray's Anatomy 36th Edition.** eds. Williams PL, Warwick R. Churchill Livingstone, Edinburgh, 1980.
- Grennan DM.** Rheumatology. Baillière Tindall, London, 1984.
- Grewal R, Rimmer MG, Freeman MAR.** Early Migration of Prostheses Related to Long Term Survivorship Comparison of Tibial Components in Knee Replacement. *Journal of Bone and Joint Surgery* 1992; 74B: 239-242.
- Grynblas MD, Alpert B, Katz I, Lieberman I, Pritzker KP.** Subchondral Bone in Osteoarthritis. *Calcified Tissue International* 1991; 49: 20-26.
- Haas SS, Brauer GM, Dickson GA.** Characterisation of Polymethylmethacrylate Bone Cement. *Journal of Bone and Joint Surgery* 1975; 57-A: 380-391.
- Halawa M, Lee AJC, Ling RSM, Vangala SS** The Shear Strength of Trabecular Bone from the Femur and Some Factors Affecting the Shear Strength of the Cement-Bone Interface. *Archives of Orthopaedic and Traumatic Surgery* 1978; 92: 19-30.
- Harris WH.** Is it Advantageous to Strengthen the Cement Metal Interface and use a Collar for Cemented Femoral Components of Total Hip Replacements ? *Clinical Orthopaedics and Related Research* 1992a; 285: 67-72.
- Harris WH.** The First 32 Years of Total Hip Arthroplasty - One Surgeon's Perspective. *Clinical Orthopaedics and Related Research* 1992b; 274: 6-11.
- Hodgkinson JP, Maskell AP, Paul A, Wroblewski BM.** Flanged Acetabular Components in Cemented Charnley Hip Arthroplasty - Ten Year Follow Up of 350 Patients. *Journal of Bone and Joint Surgery* 1993; 75B: 464-467.
- Hodgkinson JP, Shelley P, Wroblewski BM.** The Correlation Between the Roentgenographic Appearance and Operative Findings at the Bone Cement Junction of the Socket in Charnley Low Friction Arthroplasties. *Clinical Orthopaedics and Related Research* 1988; 228: 105-109.

- Hodgkinson R, Currey JD.** Young's Modulus, Density and Material Properties in Cancellous Bone Over A Large Density Range. *Journal of Materials Science: Materials in Medicine* 1992; 3: 377-381.
- Hodgkinson R, Currey JD.** Effects of Structural Variation on Young's Modulus of Non-Human Cancellous Bone. *Proceedings of the Institute of Mechanical Engineers Part H: Engineering in Medicine* 1990; 204: 43-52.
- Hoffman O.** The Brittle Strength of Orthotropic Materials. *Journal of Composite Materials* 1967; 1; 200-206.
- Hollister, SJ, Guldberg, RE, Kuelske, CL, Caldwell, NJ, Richards, M, Goldstein, SA.** Effects of Healing and Mechanical Stimulus on Bone Adaption to Porous Coated Implants at Five Weeks. Proceedings of 41st Annual Meeting Orthopaedic Research Society 1995: 556.
- Holm, NJ.** The Internal Stress Pattern of the Os Coxae. *Acta Orthopaedica Scandinavica* 1980; 51: 421-428.
- Howorth H.** The Evolution and Development of Clean Air Systems for Surgery. *Health Estate Journal* 1993; 47:
- Huiskes R, Sloof TJ.** Thermal Injury of Cancellous Bone Following Pressurised Penetration of Acrylic Cement. *Transactions of the Orthopedic Research Society* 1981; 6: 134.
- Huiskes R.** Finite Element Analysis of Acetabular Reconstruction. *Acta Orthopaedica Scandinavica* 1987; 58: 620-625.
- Huiskes R.** Some Fundamental Aspects of Human Joint Replacement. *Acta Orthopaedica Scandinavica* 1980; Suppl 185.
- Huiskes R.** The Current State and Future of Cemented and Non-Cemented Total Hip Replacement. Post Graduate Lectures ed Duparc J. 1st European Congress of Orthopaedic Surgery 1993.
- Jacob HAC, Huggler AH, Dietschi C, Schreiber A.** Mechanical Function of Subchondral Bone as Experimentally Determined on the Acetabulum of the Human Pelvis. *Journal of Biomechanics* 1976; 9: 625-627.
- Juliussen R, Arve J, Ryd L.** Cementation Pressure in Arthroplasty: *In Vitro* Study of Cement Penetration into Femoral Heads. *Acta Orthopaedica Scandinavica* 1994; 65: 131-134.
- Juliussen R, Flivik G, Nilsson J, Ryd L, Önnarfält R.** Circulating Blood Diminishes Cement Penetration into Cancellous Bone - *In vivo* Studies of 21 Arthrotic Femoral Heads. *Acta Orthopaedica Scandinavica* 1995; 66: 234-238.
- Kaplan EL, Meier P.** Non Parametric Estimation from Incomplete Observations. *American Statistics Association Journal* 1958: 457-481.
- Kaplan SJ, Hayes WC, Stone JL, Beaupré GS.** Tensile Strength of Bovine Trabecular Bone. *Journal of Biomechanics* 1985; 18: 723-727.
- Kärrholm J, Borssén B, Löwenhielm G, Snorrason F.** Does Early Micromotion of Femoral Stem Prostheses Matter ? *Journal of Bone and Joint Surgery* 1994; 76-B: 912-917.

Kay JM, Neddeman RM. An Introduction to Fluid Mechanics and Heat Transfer 3rd Edition, Cambridge, 1974.

Kawanabe K, Yamamuro T, Nakamura T, Kokubo T, Yoshihara S, Shibuya T. A New Bioactive Bone Cement Consisting of BIS-GMA Resin and Bioactive Glass Powder. in *Bioceramics Vol 5*. eds. Yamamuro T, Kokubo T, Nakamura T. Kobunshi Kankokai, Kyoto, 1992.

Keaveny TM, Borchers RE, Gibson LJ, Hayes WC. Trabecular Bone Modulus and Strength can Depend on Specimen Geometry. *Journal of Biomechanics* 1993; 26: 991-1000.

Keaveny TM, Guo XE, Wachtel EF, McMahon TA, Hayes WC. Trabecular Bone Exhibits Fully Linear Elastic Behaviour and Yields at Low Strains. *Journal of Biomechanics* 1994a; 27: 1127-1136.

Keaveny TM, Wachtel EF, Ford CM, Hayes WC. Differences Between the Tensile and Compressive Strengths of Bovine Tibial Trabecular Bone Depend on Modulus. *Journal of Biomechanics* 1994b; 27: 1137-1146.

Kershaw CJ, Atkins RM, Dodd CAF, Bulstrode CJK. Revision Total Hip Arthroplasty for Aseptic Failure: A Review of 276 Cases. *Journal of Bone and Joint Surgery* 1991; 73-B: 564-568.

Kim YS, Callaghan JJ, Ahn PB, Brown TD. Acetabular Fracture During Oversize Component Insertion. Proceedings of 41st Annual Meeting Orthopaedic Research Society 1995: 245

Kloss M. Hip simulator and Interface to Materials Testing Machine. Report on project carried out during placement at the Unit for Joint Reconstruction, 1996.

Krause WR, Krug W, Miller J. Strength of the Cement-Bone Interface. *Clinical Orthopaedics and Related Research* 1982a; 163: 290-299.

Krause WR, Miller J, Ng P. The Viscosity of Acrylic Bone Cements. *Journal of Biomedical Materials Research* 1982b; 16: 219-243.

Kuiper JH. Numerical Optimization of Artificial Hip Joint Designs. Ph D Thesis, University of Nijmegen, The Netherlands, 1993

Kuivila TE, Geiger JM, Berry JL, Udovic NA. Use of Negative Pressure During Acetabular Cement Application for Enhanced Bone-Cement Interface Strength. *Transactions of the Orthopaedic Research Society* 1989; 14: 390

Kurrat, HJ, Oberländer, W. The Thickness of the Cartilage in the Hip Joint. *Journal of Anatomy* 1978; 126: 145-155.

Lanyon LE. Osteocytes, Strain Detection, Bone Modelling and Remodelling. *Calcified Tissue International* 1993; 53: Sup 1, 102-107.

Lautenschlager EP, Stupp SI, Keller JC. Structure and Properties of Acrylic Bone Cement. In *Fundamental Behaviour of Orthopaedic Materials Vol II Applications*. CRC Series in Structure/Property Relationships of Biomaterials; 87-117, 1987.

Lavernia CJ, Reindel ES, Gomez ES, Compton P, Woo SL-Y, Convery FR. The Effects of Sustained Pressurisation on the Bone-Cement Interface Mechanics *Transactions of the Orthopaedic Research Society* 1988; 13: 356.

Lawrence, JS. Osteoarthritis. In *Rheumatism in Populations*. Heinemann, London, 1977: 98-155.

- Lee AJC, Ling RSM.** A Device to Improve the Extrusion of Bone Cement into the Bone of the Acetabulum in the Replacement of the Hip Joint. *Biomedical Engineering* 1974; 522-524.
- Lee AJC, Ling RSM.** Loosening. in *Complications of Total Hip Replacement*. ed Ling RSM. Churchill Livingstone 1984.
- Lee AJC, Ling RSM, Vangala SS.** The Mechanical Properties of Bone Cements. *Journal of Medical Engineering and Technology* 1977; 137-140
- Linder, L.** Reaction of Bone to the Acute Chemical Trauma of Bone Cement. *Journal of Bone and Joint Surgery* 1977; 59-A: 82-87.
- Ling RSM.** Observations on the Fixation of Implants to the Bony Skeleton. *Clinical Orthopaedics and Related Research* 1986; 210: 80-95.
- Ling RSM.** The Use of a Collar and Precoating on Cemented Femoral Stems is Unnecessary and Detrimental. *Clinical Orthopaedics and Related Research* 1992; 285: 73-83.
- Luklinska ZB, Bonfield W.** Ultrastructure of Bone-Composite Interface by High Resolution Transmission Electron Microscopy. in *Bone-Bonding Biomaterials*. eds Ducheyne P, Kokubo T, van Blitterswijk. Reed Healthcare Communications 1992.
- Lundskog J.** Heat and Bone Tissue, An Experimental Investigation of the Thermal Properties of Bone and Threshold Levels for Thermal Injury. *Scandinavian Journal of Plastic and Reconstructive Surgery* 1972; Sup 91.
- Majkowski RS, Bannister GC, Miles AW.** The Effect of Bleeding on the Cement-Bone Interface - an Experimental Study. *Clinical Orthopaedics and Related Research* 1994; 299: 293-297.
- Malchau H, Herberts P.** Prognosis of Total Hip Replacement Surgical and Cementing Technique in THR: A Revision Risk Study of 134,056 Primary Operations. 63rd Annual Meeting of the AAOS, February 1996.
- Malchau H, Herberts P, Ahnfelt L.** Prognosis of Total Hip Replacement in Sweden. Follow-up of 92,675 Operations Performed 1978-1990. *Acta Orthopaedica Scandinavica* 1993; 64: 497-506.
- Mann KA, Ayers DC, Werner FW, Nicoletta RJ, Fortino MD.** Tensile Strength of the Cement-Bone Interface Depends on the Amount of Bone Interdigitated with PMMA Cement. *Journal of Biomechanics* 1997; 30: 339-346.
- Martens M, van Audekercke R, Delpont P, de Meester P, Muelier JC.** The Mechanical Characteristics of Cancellous Bone at the Upper Femoral Region. *Journal of Biomechanics* 1983; 16: 971-983.
- Massin P, Landjerit B, Roy-Camille R, Thourot M, Jacquard-Simon N.** Deformation of the Acetabulum on Bearing Weight Before and After Prosthetic Implantation. *Journal of Orthopaedic Surgery* 1993; 7: 181-190.
- McElhaney JH, Fogle JL, Melvin JW, Haynes RR, Roberts VL, Alem NM.** Mechanical Properties of Cranial Bone. *Journal of Biomechanics* 1970; 3: 495-511.
- McKellop H, Lu Z, Ebramzadeh E, Sarmiento A.** Variation of Stress in the Cement Mantle of Total Hip Replacements as a Result of Creep. Proceedings of 40th Annual Meeting Orthopaedic Research Society 1994: 798.

- McKenzie JR, Callaghan JJ, Pederson DR, Brown TD.** Areas of Contact and Extent of Gaps with Implantation of Oversized Acetabular Components in Total Hip Arthroplasty. *Clinical Orthopaedics and Related Research* 1994; 298: 127-136.
- McLeish RD, Charnley J.** Abduction Forces in the One-Legged Stance. *Journal of Biomechanics* 1970; 3: 191-209.
- Melvin JW, Evans FG.** Crack Propagation in Bone. Biomaterials Symposium AMD 2. eds. Fung YC, Brighton JA. American Society of Mechanical Engineers, New York, 1973
- Merchant KK, Rohr WL, Lintner WP, Bhambri SK.** Orthopaedic Implant Surface Debris. Proceedings of 41st Annual Meeting Orthopaedic Research Society 1995: 164.
- Meyer JR, Lautenschlager EP, Moore EK.** On the Setting Properties of Acrylic Bone Cement, *Journal of Bone and Joint Surgery* 1973; 55A: 149-156.
- Michel MC, Guo X-DE, Gibson LJ, McMahan TA, Hayes WC.** Compressive Fatigue Behaviour of Bovine Trabecular Bone. *Journal of Biomechanics* 1993, 26: 453-463.
- Moritz AR, Henriques FC Jr.** The Relative Importance of Time and Surface Temperature in the Causation of Cutaneous Burns. *American Journal of Pathology* 1947; 23: 695.
- Morscher EW.** Current Status of Acetabular Fixation in Primary Total Hip Arthroplasty. *Clinical Orthopaedics and Related Research* 1992; 274: 172-193.
- Mulroy RD, Harris WH.** The Effect of Improved Cementing Techniques on Component Loosening in Total Hip Replacement. *Journal of Bone and Joint Surgery* 1990; 72-B: 757-760.
- Natali AN, Meroi EA.** A Review of the Biomechanical Properties of Bone as a Material. *Journal of Biomedical Engineering* 1989; 11: 266-276.
- New AMR, Northmore-Ball MD, Tanner KE.** *In Vitro* Evaluation of Two New Designs of Acetabular Cement Pressuriser. Poster at the BOA Spring Meeting, Llandudno, April 1996.
- Nishimura N, Yamamuro T, Nakamura T, Taguchi Y, Kokubo T, Yoshihara S.** A Novel Bioactive Bone Cement Based on CaO-SiO₂-P₂O₅-CaF₂ Glass. in Bioceramics Vol 4. eds Bonfield W, Hastings GW, Tanner KE. Butterworth Heinemann, Oxford, 1991.
- Noble PC, Swarts E.** Penetration of Acrylic Bone Cements into Cancellous Bone. *Acta Orthopaedica Scandinavica* 1983; 54: 566-573.
- Norman TL, Vashishth D, Burr DB.** Fracture Toughness of Human Bone Under Tension. *Journal of Biomechanics* 1995; 28: 309-320.
- Northmore-Ball MD.** Osteotomy, Arthrodesis and Arthroplasty. in Cash's Textbook of Orthopaedics and Rheumatology for Physiotherapists 2nd Edition. ed Tidswell ME. Mosby Year Book Europe, London, 1992.
- Ober NS, Lavernia CJ, Reindel ES, Woo SL-Y, Convery FR.** Sustained Pressurisation of Polymethylmethacrylate (PMMA) a Biomechanical Study of the Bone-Cement Interface: an *In Vitro* and *In Vivo* Comparison. *Transactions of the Orthopaedic Research Society* 1989; 14: 395.

- O'Connor JJ.** Standard Handbook of Lubrication Engineering. McGraw-Hill New York, 1968, 1-24.
- Oh I, Sander TW, Treharne RW.** Total Hip Acetabular Cup Flange Design and its Effect on Cement Fixation. *Clinical Orthopaedics and Related Research* 1985; 195: 304-309.
- Oh I.** A Comprehensive Analysis of the Factors Affecting Acetabular Cup Fixation and Design in Total Hip Replacement Arthroplasty: A Series of Experimental and Clinical Studies. Proceedings of the 11th Open Scientific Meeting Hip Society 1983: 129-177.
- Ohlin A, Balkfors B.** Stability of Cemented Sockets after 3-14 Years. *Journal of Arthroplasty* 1992; 7: 87-92.
- Önsten I, Bengnér U, Besjakov J.** Socket Migration after Charnley Arthroplasty in Rheumatoid Arthritis and Osteoarthritis: A Röntgen Stereophotogrammetric Study. *Journal of Bone and Joint Surgery* 1993; 75-B: 677-680.
- Overgaard S, Søballe K, Hansen ES, Josephson K, Bünger C.** Implant Loading Accelerates Resorption of Hydroxyapatite Coating. Proceedings of 41st Annual Meeting Orthopaedic Research Society 1995: 187.
- Pal S, Saha S.** Stress Relaxation and Creep Behaviour of Normal and Carbon Fibre Reinforced Acrylic Bone Cement. *Biomaterials* 1982; 3: 93-96.
- Paul JP.** Approaches to Design - Force Actions Transmitted by Joints in the Human Body. *Proceedings of the Royal Society of London B* 1976; 192: 163-172.
- Pedersen DR, Callaghan JJ, Olejniczak JP, Jonston RC.** Polyethylene Wear Rates for Five Different *In Vivo* Acetabular Components Used Over a Five to Twenty Two Year Period. Proceedings of 41st Annual Meeting Orthopaedic Research Society 1995: 115.
- Pereira DS, Ricci JL, Scott D, Casar RS, Jaffe W, Hawkins M, Oh YH, Alexander, H.** Comprehensive Testing of Experimental Coatings Using an Implantable Chamber Model. Proceedings of 41st Annual Meeting Orthopaedic Research Society 1995: 557.
- Perona PG, Lawrence J, Paprosky WG, Patwardhan AG, Sartori M.** Acetabular Micromotion as a Measure of Initial Implant Stability in Primary Hip Arthroplasty. *Journal of Arthroplasty* 1992; 7: 537-547.
- Petty W, Miller GJ, Piotrowski G.** *In Vitro* Evaluation of the Effect of Acetabular Prosthesis Implantation on Human Cadaver Pelves. *Bulletin of Prosthetics Research* 1980; 17: 82-89.
- Pilliar RM, Lee JM, Maniopoulos C.** Observation on the Effect of Movement on Bone Ingrowth into Porous Surfaced Implants. *Clinical Orthopaedics and Related Research* 1986; 208: 108-113.
- Platzer W.** Sesam Atlas van de Anatomie. Bosch & Keuning NV, Baarn, 1981.
- Prendergast PJ, Taylor D.** Prediction of Bone Adaption Using Damage Accumulation. *Journal of Biomechanics* 1994; 27: 1067-1076.
- Rapperport DJ, Carter DR, Schurman DJ.** Contact Finite Element Analysis of the Hip Joint. *Journal of Orthopaedic Research* 1985; 3: 435-446.

- Reilly DT, Burstein AH.** The Elastic and Ultimate Properties of Compact Bone Tissue. *Journal of Biomechanics* 1975; 8: 393-405.
- Revell PA, Al-Saffar N, Kobayashi A.** Biological Reaction to Debris in Relation to Joint Prostheses. *Proceedings of the Institute of Mechanical Engineers Part H: Engineering in Medicine* 1997; 211: 187-197.
- Revie IC, Wallace ME, Orr JF.** The Effect of PMMA Thickness on Thermal Bone Necrosis Around Acetabular Sockets. *Proceedings of the Institute of Mechanical Engineers Part H: Engineering in Medicine* 1994; 204: 45-51.
- Rey RM, Paiement GD, McGann WM, Jasty M, Harrigan TP, Burke DW, Harris WH.** A Study of Intrusion Characteristics of Low Viscosity Cement, Simplex-P and Palacos Cements in a Bovine Cancellous Bone Model. *Clinical Orthopaedics and Related Research* 1987; 215: 272-278.
- Rice JC, Cowin SC, Bowman JA.** On the Dependence of the Elasticity and Strength of Cancellous Bone on Apparent Density. *Journal of Biomechanics* 1988; 21: 155-168.
- Richardson JB.** Personal Communication, 1995
- Ries M, Pugh J, Au JC, Gurtowski J, Dee R.** Cortical Pelvic Strains with Varying Size Hemiarthroplasty *In Vitro*. *Journal of Biomechanics* 1989; 22: 775-780.
- Ritter MA, Keating EM, Faris PM, Brugo G.** Metal-backed Acetabular Cups in Total Hip Arthroplasty. *Journal of Bone and Joint Surgery* 1990; 72-A: 672-677.
- Røhl L; Larsen E; Linde F; Odgaard A; Jørgensen J.** Tensile and Compressive Mechanical Properties of Cancellous Bone. *Journal of Biomechanics* 1991; 24: 1143-1149.
- Rubeinstein J, Kellam J, Mcgonigal D.** Cross Sectional Anatomy of the Adult Bony Acetabulum, *Journal of the Canadian Association of Radiologists* 1982; 33: 137-138.
- Rydell NW.** Forces Acting on the Femoral Head Prosthesis. *Acta Orthopaedica Scandinavica* 1966: Sup. 88.
- Sandborn PM, Cook SD, Anderson RC, Spires WP, Kester MA.** Tissue Response to Porous Coated Implants Lacking Initial Bone Apposition. *Journal of Arthroplasty* 1988; 3: 337-346.
- Schaffler MB, Burr DR.** Stiffness of Compact Bone: Effects of Porosity and Density. *Journal of Biomechanics* 1988; 21: 13-16.
- Schmalzried TP, Kwong LM, Jasty M, Sedlacek RC, Haire TC, O'Connor DA, Bragdon CR, Kabo JM, Malcolm AJ, Harris WH.** The Mechanism of Loosening of Cemented Acetabular Components in Total Hip Arthroplasty - Analysis of Specimens Retrieved at Autopsy. *Clinical Orthopaedics and Related Research* 1992; 274: 60-78.
- Schreurs BW, Spierings PTJ, Huiskes R, Sloof TJJH.** Effects of Preparation Techniques on the Porosity of Acrylic Bone Cements. *Acta Orthopaedica Scandinavica* 1988; 59: 403-409.
- Schurman DJ, Bloch DA, Segal MR, Tanner CM.** Conventional Cemented Total Hip Arthroplasty, Assessment of Clinical Factors Associated with Revision for Mechanical Failure. *Clinical Orthopaedics and Related Research* 1989; 240: 173-180.

- Selvik G.** Roentgen Stereophotogrammetry: A Method for the Study of the Kinematics of the Skeletal System. *Acta Orthopaedica Scandinavica* 1989; Sup. 232: 1-51.
- Sharp DJ.** Subchondral Bone of the Normal and Osteoarthrotic Human Femoral Head. M.D. Thesis, Queen Mary College/Royal Postgraduate Medical School, London, 1988.
- Shelley P, Wroblewski BM.** Socket Design and Cement Pressurisation in the Charnley Low-Friction Arthroplasty. *Journal of Bone and Joint Surgery* 1988; 70-B: 358-363.
- Shulte KR, Callaghan JJ, Kelley SS, Johnston RC.** The Outcome of Charnley Total Hip Arthroplasty with Cement after a Minimum Twenty Year Follow-Up - The Results of One Surgeon. *Journal of Bone and Joint Surgery* 1993; 75-A: 961-975.
- Snorrason F, Kärrholm J, Holmgren C.** Fixation of Cemented Acetabular Prostheses: The Influence of Pre-Operative Diagnosis. *Journal of Arthroplasty* 1993; 8: 83-90.
- Søballe K, Hansen ES, Rasmussen HB, Jorgensen PH, Bünger C.** Tissue Ingrowth into Titanium and Hydroxyapatite-Coated Implants During Stable and Unstable Mechanical Conditions. *Journal of Orthopaedic Research* 1992; 10: 285-299.
- Somville JM, Moldanaers PF, Mulier JC, Mewis J.** *In vitro* Experiments with an Injection Technique for Cup Fixation. *Archives of Orthopaedic and Traumatic Surgery* 1987; 106: 173-178.
- Spierings PTJ.** Review of Pressurisation and Penetration of Bone Cement. Lecture Notes, University of Nijmegen, The Netherlands, 1993.
- Stephenson PK, Freeman MAR, Revell PA, Germain J, Tuke M, Pirie CJ.** The Effect of Coating on Ingrowth of Bone into Cavities in an Implant. *Journal of Arthroplasty* 1991; 6: 51-58.
- Stocks GW, Freeman MAR, Evans SJW.** Acetabular Cup Migration: Prediction of Aseptic Loosening. *Journal of Bone and Joint Surgery* 1995; 77-B: 853-861.
- Stone JL, Beaupré GS, Hayes WC.** Multiaxial Strength Characteristics of Trabecular Bone. *Journal of Biomechanics* 1983; 16: 743-752.
- Strömberg CN, Herberts P, Palmertz B, Garellick G.** Radiographic risk signs for loosening after cemented THA: 61 loose stems and 23 loose sockets compared with 42 controls. *Acta Orthopaedica Scandinavica* 1996; 67: 43-48.
- Sumner DR, Jasty M, Jacobs JJ, Urban RM, Bragdon CR, Harris WH, Galante JO.** Histology of Porous Coated Acetabular Components 25 Cementless Cups Retrieved after Arthroplasty. *Acta Orthopaedica Scandinavica* 1993; 64: 619-626.
- Swanson SAV.** Mechanical Aspects of Fixation. in *The Scientific Basis of Joint Replacement*. eds Swanson SAV, Freeman MAR. Pitman Medical, Tunbridge Wells, 1977.
- Tadmor Z, Gogos CG.** Principles of Polymer Processing, John Wiley and Sons, New York, 1979.

- Tanner KE, Reed PE, Bonfield W, Rasmussen GL, Freeman MAR.** A System for Modelling Forces on the Hip Joint in One-Legged Stance. *Journal of Biomedical Engineering* 1988; 10: 289-290.
- Tanner KE.** Mechanical Assessment of the Interface. Bio-active Materials in Orthopaedics. The Welding Institute, Cambridge, UK, 1994.
- Taylor M, Tanner KE.** Fatigue Failure of Cancellous Bone: A Possible Cause of Implant Migration and Loosening *Journal of Bone and Joint Surgery* 1997; 79B: 181-182.
- Taylor M, Tanner KE, Freeman MAR, Yettram AL.** Finite Element Modelling - Predictor of Implant Survival ? *Journal of Materials Science Materials in Medicine* 1995; 6: 808-812.
- Taylor M, Tanner KE, Yettram AL, Freeman MAR.** The Effect of Muscle Forces on the Stress and Strain Distribution Within the Intact Femur. Transactions of the European Orthopaedic Research Society 1994; 4: 78.
- te Nuyt D and Vossebeld M.** Report on project carried out during placement at the Unit for Joint Reconstruction, 1996.
- Thanner J, Freij-Larsson C, Kärrholm J, Malchau H, Wesslén B.** Evaluation of Boneloc: Chemical and Mechanical Properties, and a Randomized Clinical Study of 30 Total Hip Arthroplasties. *Acta Orthopaedica Scandinavica* 1995; 66: 207-214.
- Thomas KA, Kay JF, Cook SD, Jarcho M.** Influence of Surface Macrotecture and Hydroxyapatite Coating on the Mechanical Strength and Histological Profiles of Titanium Implant Materials. *Journal of Biomedical Materials Research* 1987; 21: 1395-1414.
- Thunnissen J.** Muscle Force Prediction During Human Gait (PhD Thesis). University of Enschede, The Netherlands, 1993
- Verdonschot N, Huiskes R.** Dynamic Creep Behaviour of Acrylic Bone Cement. Proceedings of 40th Annual Meeting Orthopaedic Research Society 1994: 590.
- Volz RG, Wilson RJ.** Factors Affecting the Mechanical Stability of the Cemented Acetabular Component in Total Hip Arthroplasty. *Journal of Bone and Joint Surgery* 1977; 59A: 501-504.
- Walker PS, Soudry M, Ewald FC, McVickar H.** Control of Cement Penetration in Total Knee Arthroplasty. *Clinical. Orthopaedics and Related Research.* 185, 155-164, 1984.
- Weightman B, Freeman MAR, Revell PA, Braden M, Albrektsson BEJ, Carlson LV.** The Mechanical Properties of Cement and Loosening of the Femoral Components of Hip Replacements. *Journal of Bone and Joint Surgery* 1987; 69-B: 558-564.
- Weinans H, Huiskes R, Grootenboer HJ.** Trends of Mechanical Consequences and Modelling of a Fibrous Membrane Around Femoral Hip Prostheses. *Journal of Biomechanics* 1990; 23: 991-1000.
- Weinans H, Huiskes R, Grootenboer HJ.** Quantitative Analysis of Bone Reactions to Relative Motions at Implant-Bone Interfaces. *Journal of Biomechanics* 1993; 26: 1271-1281.

- Wenda K, Scheuermann H, Weitzel E, Rudiger J.** Pharmacokinetics of Methylmethacrylate Monomer During Total Hip Replacement in Man. *Archives of Orthopaedic and Traumatic Surgery* 1988; 107: 316-321.
- Whitehouse, W.J.** The Quantitative Morphology of Anisotropic Trabecular Bone. *Journal of Microscopy* 1974; 101: 153-168.
- Willert H-G, Puls P.** Die Reaction des Knochens auf Knochenzement bei der Allo-Arthroplastik der Hüfte. *Archiv für Orthopädische und Unfall-Chirurgie* 1972; 72: 33-71.
- Wright TM, Hayes WC.** Fracture Mechanics Parameters for Compact Bone - Effects of Density and Specimen Thickness. *Journal of Biomechanics* 1977; 10: 419-430
- Wright TM, Hayes WC.** Tensile Testing of Bone Over a Wide Range of Strain Rates: Effects of Strain Rate, Microstructure and Density. *Medical and Biological Engineering* 1976, 14; 671-680.
- Wright TM, Robinson RP.** Fatigue Crack Propagation in Polymethylmethacrylate Bone Cement. *Journal of Materials Science* 1982; 17: 2463-2468.
- Wroblewski BM.** 15-21 Year Results of the Charnley Low Friction Arthroplasty. *Clinical Orthopaedics and Related Research* 1986; 211: 30-35.
- Wroblewski BM.** Direction and Rate of Socket Wear in Charnley Low Friction Arthroplasty. *Journal of Bone & Joint Surgery* 1985; 67-B: 757-761.
- Yamada H.** 1970, cited in Evans (1973).
- Yao J, Glant TT, Kuettner KE, Galante JO.** Particle Debris Suppress Collagen Gene Expression in Osteoblast-Like Cells *In Vitro*. Proceedings of 41st Annual Meeting Orthopaedic Research Society 1995: 166.
- Yoshioka Y, Shiba R.** A Study on the Stress Analysis of the Pelvis by Means of the Three-Dimensional Photoelastic Experiments. *Journal of the Japanese Orthopaedic Association* 1981; 55: 63-76.

Appendix A Shear Rates in Oscillating Plate-on-Plate Rheometry

Consider two circular plates separated by a distance H , one fixed and one driven so as to oscillate sinusoidally about an axis through the plate centres (Figure A-1)

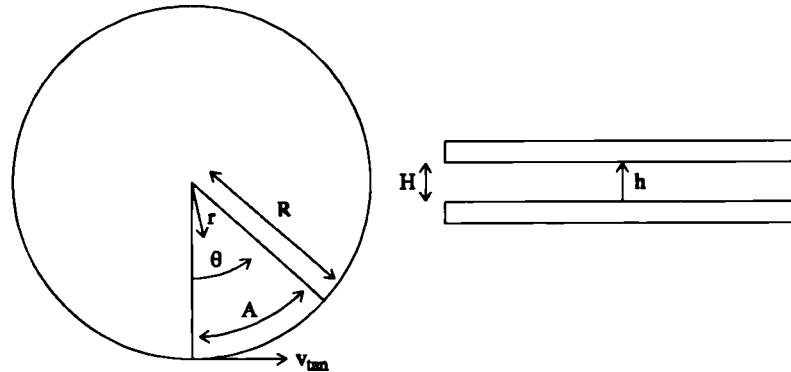


Figure A-1: Diagram and nomenclature for oscillating parallel plate problem.

where r , θ and h are the radial, angular and axial co-ordinate directions respectively, R the plate radius, A and f the amplitude and frequency of the oscillation, v_{ang} the angular velocity of the driven plate, v_{tan} the tangential velocity of a point on the driven plate and t is time.

The angular velocity of the driven plate at time t is given by:-

$$v_{ang}(t) = A \cos 2\pi ft \quad \text{Equation A-1}$$

The tangential velocity of any point on the plate is then given by:-

$$v_{tan}(t, r) = rA \cos 2\pi ft \quad \text{Equation A-2}$$

The shear rate is therefore given by:-

$$\frac{d}{dh} v_{tan}(t, r) = \frac{r}{H} A \cos 2\pi ft \quad \text{Equation A-3}$$

Shear rates as a function of r for the tests of section 4.1.1 are shown in Figure A-2.

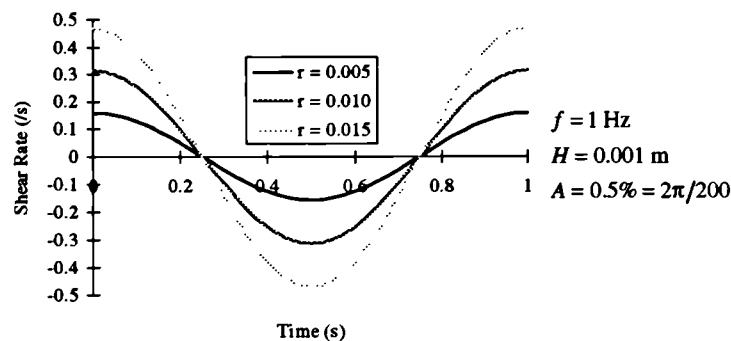


Figure A-2: Shear strain rates in rheometer tests as a function of r (m).

Appendix B Errors in Image Processing of Bone Microstructures

A number of possible sources of error exist in the processing of images to obtain the permeability of a porous material as described in section 4.1.2. The most important of these are loss of image resolution in the digitisation process due to the finite extent of a digital picture element (pixel), which depends on magnification of the object, and errors associated with conversion to a binary image (thresholding). To assess the magnitude of these two errors, the method used by Berryman (1985) was employed.

Consider an arbitrary two phase composite material. Define a two point spatial correlation function $S_2(x)$ such that $S_2(x)$ is the probability that two points a specified distance x apart are in the same phase of the material. For an isotropic material the value of $S_2(x)$ evaluated at $x = 0$ is equal to the porosity ϕ and the derivative of $S_2(x)$ evaluated at $x = 0$ is proportional to the specific surface area (internal area per unit volume), s , viz:-

$$S_2(0) = \phi \quad \text{Equation B- 1}$$

$$\frac{dS_2(0)}{dx} = -\frac{s}{4} \quad \text{Equation B- 2}$$

The penetrable sphere model for a two phase composite assumes that the material can be modelled by an array of spheres of fixed radius R whose centres are distributed randomly in space. The spheres defined in this way may overlap if the density and/or the sphere radius is high enough. The analytical solution for the two point spatial correlation function of this model is given by:-

$$S_2(x) = \exp(-\rho V_2) \quad \text{Equation B- 3}$$

Where ρ is the number density of spheres and V_2 is the union volume of two spheres of fixed radius R and centres x apart, given by:-

$$V_2 = \begin{cases} \frac{4\pi R^3}{3} \left(1 + \frac{3x}{4R} - \frac{x^3}{16R^3} \right) & \text{for } x \leq 2R \\ \frac{8\pi R^3}{3} & \text{for } x \geq 2R \end{cases} \quad \text{Equation B- 4}$$

$$\begin{aligned} \frac{dS_2(0)}{dx} &= \frac{d}{dx} \exp\left(-\rho \frac{4\pi R^3}{3} \left(1 + \frac{3x}{4R} - \frac{x^3}{16R^3}\right)\right) \\ &= \frac{1}{4} \rho \pi (x^2 - 4R^2) \exp\left(\frac{1}{12} \rho \pi (x - 4R)(x + 2R)^2\right) \end{aligned} \quad \text{Equation B-5}$$

Computer generated images of a penetrable sphere material, with qualitatively similar microstructure to the cancellous bone specimens (Figure 4-3), were produced by a specially written computer program. Examples of images created in this way are shown in Figure B-1. Note that in this situation the porosity is equivalent to the trabeculae in the cancellous bone images. This has no effect on the surface area to volume ratio calculated, and simply involves the substitution of bone volume fraction for porosity.

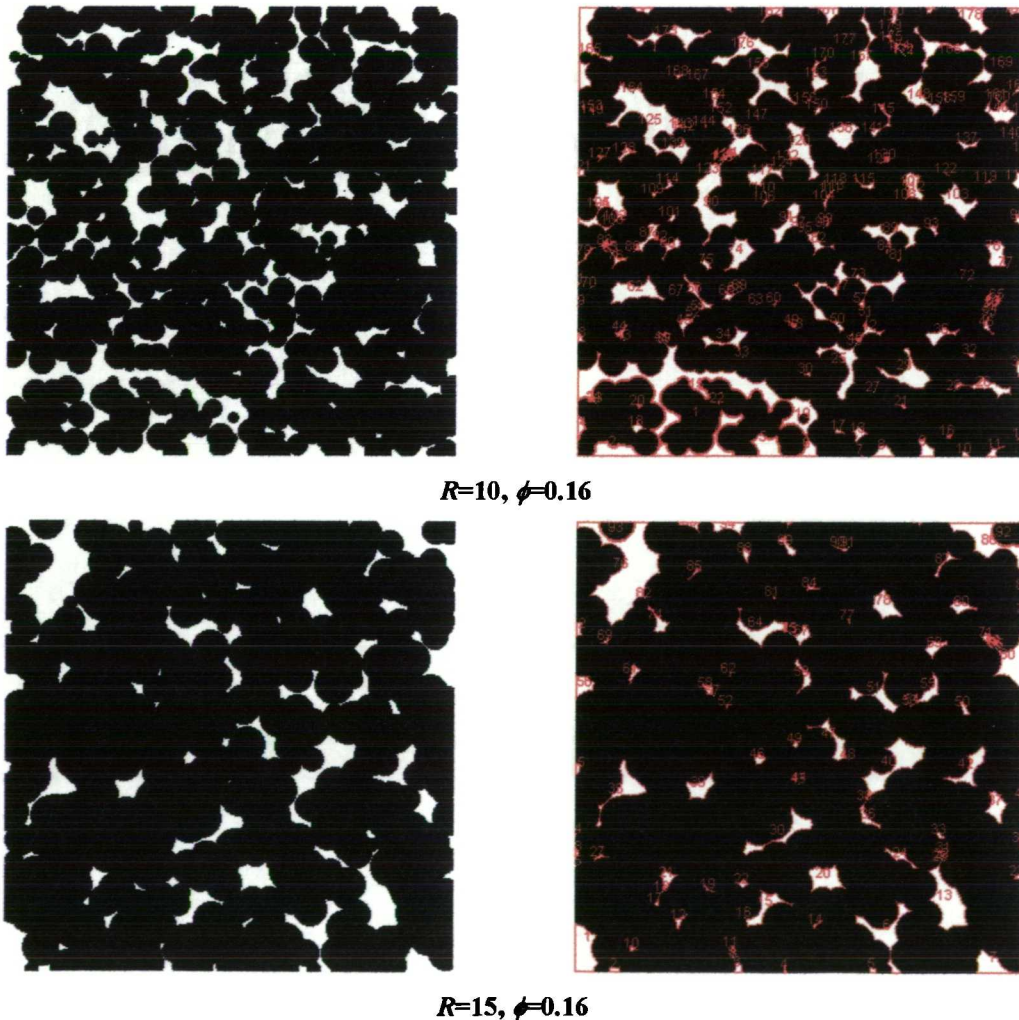


Figure B-1 : Computer generated images of penetrable sphere material. Images before (left) and after (right) edge detection and perimeter measurement.

Analysis on the computer generated images was performed on an IBM compatible PC running Microsoft Windows 95 using the program described in section 4.1.2. This

program measures the perimeter of objects directly by measuring the length of the boundary lines shown in Figure B-1. Figure B-2 shows the relationship between the theoretical and measured surface area to volume ratio for the computer generated images.

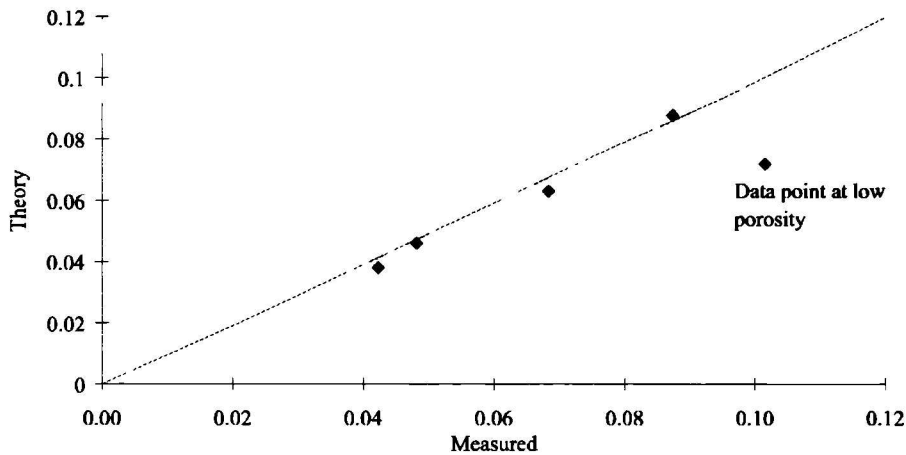
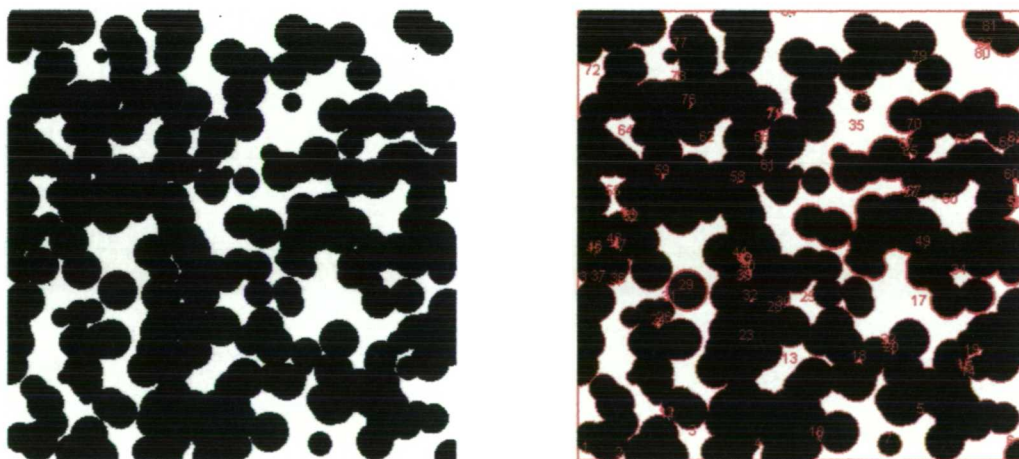


Figure B-2: Surface area to volume ratio for the computer generated images. The dashed line represents the 1:1 relationship. Units are pixel²/pixel³.

The direct measurement of object boundaries fails when the void spaces and the particles are of similar size. This causes the object detection algorithm to count some boundaries twice, as belonging to both a particle of void and a particle of solid material (see Figure B-3 for an example). This however occurs only under conditions of high porosity (for the penetrable sphere model) or high density of trabeculae (for cancellous bone), where objects tend towards spanning the entire image field.



$R=15, \phi=0.3$

Figure B-3: Example of the breakdown of the object boundary measurement.

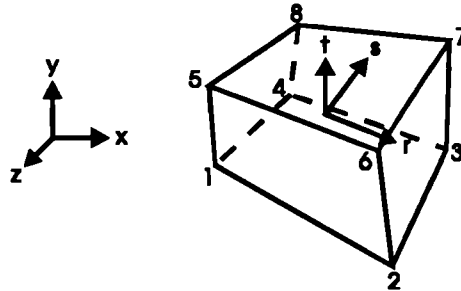
Thus, for the images of cancellous bone, where the surface area to volume ratio for a typical image was of the order of 0.08 pixel²/pixel³, the digital image processing method for determining morphological parameters appears to perform satisfactorily.

Appendix C Calculation of Strain Rate in Fluid Flow Analysis

Typical finite element formulations for fluid flow assume the variation of velocity across an element to be described by simple polynomials (in this case linear polynomials) - the element shape functions. In the isoparametric formulation, the same set of shape functions are used for the co-ordinate transformation from the global Cartesian co-ordinate system (x, y, z) to the element natural co-ordinate system (r, s, t) and to describe the variation of degree of freedom values (velocity) across the element. The relevant element shape functions N_i for 8 node isoparametric brick elements are:-

$$\begin{aligned}
 N_1 &= \frac{1}{8}(1-r)(1-s)(1-t) & N_5 &= \frac{1}{8}(1-r)(1-s)(1+t) \\
 N_2 &= \frac{1}{8}(1+r)(1-s)(1-t) & N_6 &= \frac{1}{8}(1+r)(1-s)(1+t) \\
 N_3 &= \frac{1}{8}(1+r)(1+s)(1-t) & N_7 &= \frac{1}{8}(1+r)(1+s)(1+t) \\
 N_4 &= \frac{1}{8}(1-r)(1+s)(1-t) & N_8 &= \frac{1}{8}(1-r)(1+s)(1+t)
 \end{aligned}$$

Equation C- 1



**Figure C-1: Eight node isoparametric brick element.
Node numbering and element natural co-ordinate system.**

The derivatives of the shape functions with respect to the element natural co-ordinates are given by:-

$$\begin{aligned}
\frac{\partial N_1}{\partial r} &= -\frac{1}{8}(1-s)(1-t) \\
\frac{\partial N_1}{\partial s} &= -\frac{1}{8}(1-r)(1-t) \\
\frac{\partial N_1}{\partial t} &= -\frac{1}{8}(1-r)(1-s) \\
\frac{\partial N_2}{\partial r} &= \frac{1}{8}(1-s)(1-t) \quad \text{etc.} \\
\frac{\partial N_2}{\partial s} &= -\frac{1}{8}(1+r)(1-t) \\
\frac{\partial N_2}{\partial t} &= -\frac{1}{8}(1+r)(1-s)
\end{aligned}
\tag{Equation C- 2}$$

The relationship between strain rate $\dot{\gamma}$ and velocity is given by:-

$$\{\dot{\gamma}\} = [C]\{v\} \tag{Equation C- 3}$$

where $[C]$ is the strain rate-velocity matrix, based on the element shape functions and evaluated at the element integration points, and $\{v\}$ is the vector of nodal velocities.

The submatrix c_i associated with node i of the finite element has the form:-

$$c_i = \begin{bmatrix} \frac{\partial N_i}{\partial x} & 0 & 0 \\ 0 & \frac{\partial N_i}{\partial y} & 0 \\ 0 & 0 & \frac{\partial N_i}{\partial z} \\ \frac{\partial N_i}{\partial y} & \frac{\partial N_i}{\partial x} & 0 \\ 0 & \frac{\partial N_i}{\partial z} & \frac{\partial N_i}{\partial y} \\ \frac{\partial N_i}{\partial z} & 0 & \frac{\partial N_i}{\partial x} \end{bmatrix}, i = 1 \dots n \tag{Equation C- 4}$$

where n is the number of nodes per element. The matrix C is formed by summing the submatrices c_i .

The derivatives of the shape functions with respect to the x, y, z axes are related to the derivatives with respect to the r, s, t axes by:-

$$\begin{bmatrix} \frac{\partial N_i}{\partial x} \\ \frac{\partial N_i}{\partial y} \\ \frac{\partial N_i}{\partial z} \end{bmatrix} = J^{-1} \begin{bmatrix} \frac{\partial N_i}{\partial r} \\ \frac{\partial N_i}{\partial s} \\ \frac{\partial N_i}{\partial t} \end{bmatrix}, i = 1 \dots n \quad \text{Equation C- 5}$$

where J^{-1} is the inverse of the Jacobian matrix J :-

$$J = \sum_{i=1}^n \begin{bmatrix} \frac{\partial N_i}{\partial r} x_i & \frac{\partial N_i}{\partial r} y_i & \frac{\partial N_i}{\partial r} z_i \\ \frac{\partial N_i}{\partial s} x_i & \frac{\partial N_i}{\partial s} y_i & \frac{\partial N_i}{\partial s} z_i \\ \frac{\partial N_i}{\partial t} x_i & \frac{\partial N_i}{\partial t} y_i & \frac{\partial N_i}{\partial t} z_i \end{bmatrix} \quad \text{Equation C- 6}$$

and x_i, y_i, z_i are the nodal co-ordinates in the global Cartesian system.

To derive the strain rate tensor from the nodal degree of freedom values (velocity), an ANSYS macro was written to calculate the strain rate tensor at the element centroid, for which $r = s = t = 0$.

The macro was tested in two ways:

1. Against the built in algorithm for calculating strain in a linear elastic stress analysis, since strain in this case is analogous to strain rate in a fluid flow analysis. The macro gave identical results to the built in algorithm.
2. In a test case for which an analytical solution for the strain rate is available.

The test case was the laminar incompressible isothermal flow of a viscous fluid in a long straight pipe. The velocity gradient (rate of strain) as a function of radial co-ordinate q in a pipe in which flows a fluid of viscosity μ is given by (Kay and Nedderman, 1985):-

$$\frac{dv}{dq} = -\frac{\Delta P}{2\mu L} q \quad \text{Equation C- 7}$$

where $\Delta P/L$ is the pressure gradient in the fully developed flow region.

The finite element mesh and boundary conditions for the finite element solution to the problem are shown in Figure C-2.

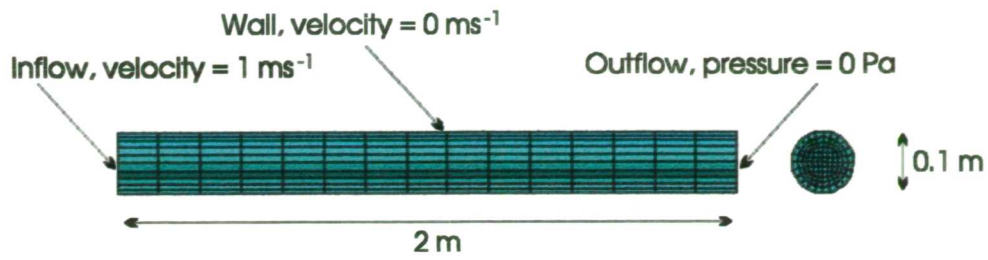


Figure C-2: Finite element mesh and boundary conditions

The consequent calculation of strain rate with the macro produced the results shown in Figure C-3. Figure C-4 compares this result with the analytical solution.

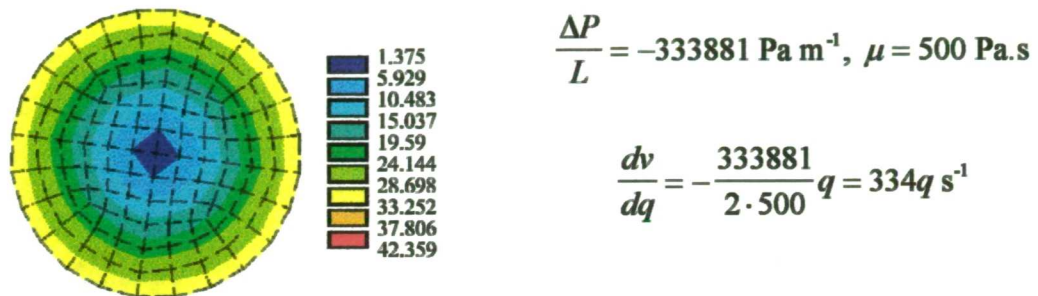


Figure C-3: Variation in strain rate across pipe section.

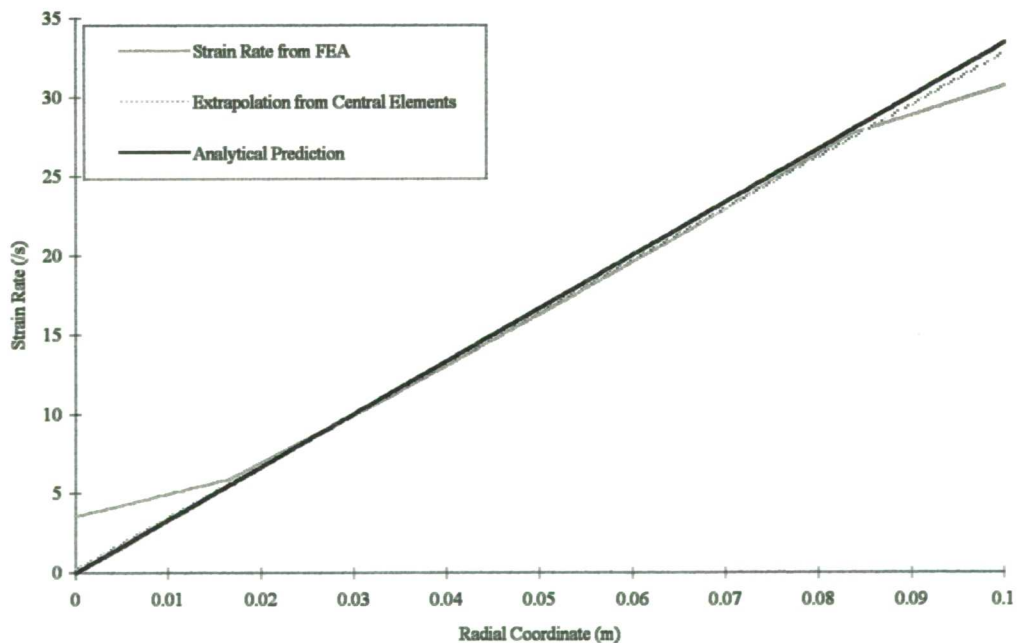


Figure C-4: Comparison of analytical and finite element results.

It can be seen that in general the macro performs well, except at the boundaries of the fluid domain where the effects of averaging of strain rate across the element become apparent. Given the parametric nature of the simulations performed in section 4.4, the performance of the macro is deemed to be adequate.

Appendix D Publications and Abstracts

Bernoski, F.P., Scott, R.A., New, A.M.R.

An improved acetabular cement pressuriser

Poster presented at the 62nd Annual Meeting of the American Academy of Orthopaedic Surgeons, Orlando, Florida, February 16-21, 1995

New, A.M.R., Northmore-Ball, M.D., Tanner, K.E.

In vitro evaluation of two new designs of acetabular cement pressuriser

Poster presented at the British Orthopaedic Association Spring Meeting, Llandudno, April 16-18, 1996

New, A.M.R., Northmore-Ball, M.D., Tanner, K.E.

Cancellous Bone Stresses in Normal and Reconstructed Acetabula

Poster presented at the 1996 Symposium of the International Society of Technology in Arthroplasty, Amsterdam, August 20-21, 1996

New, A.M.R., Northmore-Ball, M.D., Tanner, K.E., Cheah, S.K.

Per-operative Measurement of Acetabular Cement Pressurisation

Presented at the British Hip Society Meeting, Wrightington, March 1, 1997

New, A.M.R., Northmore-Ball, M.D., Tanner, K.E., Cheah, S.K.

Measurement of Acetabular Cement Pressurisation During Total Hip Replacement

Presented at the British Orthopaedic Research Society Meeting, Leeds, March 3-4, 1997

New, A.M.R., Northmore-Ball, M.D., Tanner, K.E.

Finite Element Modelling of Bone Cement Flow During Component Insertion in Hip Replacement

Presented at the Third International Symposium on Computer Methods in Biomechanics and & Biomedical Engineering, Barcelona, May 7-10, 1997

Bernoski, F.P., New, A.M.R., Scott, R.A., Northmore-Ball, M.D.

An In Vitro Study of a New Design of Acetabular Cement Pressuriser

The Journal of Arthroplasty (Accepted)

New, A.M.R., Kloss, M., Northmore-Ball, M.D., Tanner, K.E., Veldkamp, E., Kuiper, J.H.

Dynamic Mechanical Testing of Prosthetic Acetabular Components for Total Hip Replacement

Accepted for 11th International Conference on Experimental Mechanics, Oxford, August 24-28, 1998.

An Improved Acetabular Cement Pressuriser

Dr. F.P. Bernoski
R.A. Scott
A. New

Den Haag, NETHERLANDS
New Milton, ENGLAND
Oswestry, ENGLAND

Aseptic loosening of the acetabular component in total hip arthroplasty remains one of the limiting factors in prosthesis longevity. Acetabular cement pressurisation has been shown to improve fixation in the acetabulum. However, pressure must be sustained and uniformly distributed to be effective; this requires the acetabulum to be sealed while pressure is applied. A pressuriser has been designed which not only seals around the rim of the acetabulum, but also covers the transverse ligament notch.

In Vitro Evaluation of Two New Designs of Acetabular Cement Pressuriser

A M R New ^{***}, M D Northmore-Ball ^{*}, K.E. Tanner ^{**}

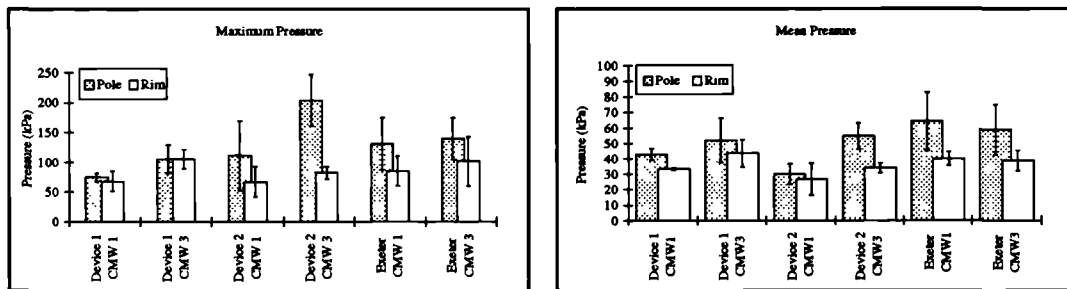
^{*} Unit for Joint Reconstruction, The Robert Jones and Agnes Hunt Orthopaedic Hospital, Oswestry, Shropshire SY10 7AG

^{**} IRC Biomedical Materials, Queen Mary and Westfield College, London E1 4NS

The purpose of this study was to evaluate acetabular cement pressurisation *in vitro* with two new designs of pressuriser and to compare the results with those of an established device, the Exeter pressuriser¹. The first new device (Device 1) aims to create a closed, cement filled space within the acetabulum by means of a compliant silicone rubber seal. The second (Device 2) attaches to a standard cement gun to allow cement to be pressure-injected into the acetabulum.

A "Sawbones" hemi-pelvis was mounted securely on a workbench in a position simulating a lateral approach with the patient supine. The acetabulum was fitted with two pressure transducers connected to a PC for data logging, one at the pole of the acetabulum and the second in the ilium approximately 10 mm from the acetabular rim. Each pressuriser was tested three times with both CMW1 and CMW3 bone cement, mixed using a standardised method. Use of the pressuriser was started at 2 minutes after mixing for CMW1 and 4 minutes for CMW3.

Maximum pressures and mean pressures averaged for the three tests with each device / cement combination are shown in the figures below (error bars represent one standard deviation).



All three devices were able to produce sustained cement pressurisation at both the pole and the rim of the acetabulum. Mean pressure was comparable for all except Device 2 with CMW1 cement. The highest peak pressure was obtained with Device 2 and CMW3 cement. Common to all devices was consistently lower rim pressure, reflecting slight leakage of the cement and loss of hydrostatic pressure. Overall, Device 1 with CMW1 cement and Device 2 with CMW3 cement showed the least variation between tests.

In view of its simplicity and ease of use, Device 1 would appear to offer the most reliable method of acetabular cement pressurisation.

¹ Lee AJC, Ling RSM. A Device to Improve the Extrusion of Bone Cement into the Bone of the Acetabulum in the Replacement of the Hip Joint. *Biomedical Engineering* 1974, 522-524

CANCELLOUS BONE STRESSES IN NORMAL AND RECONSTRUCTED ACETABULA

A.M.R.New*, M.D. Northmore-Ball*, K.E. Tanner*

*The Robert Jones and Agnes Hunt Orthopaedic Hospital, Oswestry, Shropshire SY10 7AG

*IRC in Biomedical Materials, Queen Mary and Westfield College, London E1 4NS

Recent studies of reconstructed femora in various configurations have indicated that peak cancellous bone stresses can be an appreciable fraction of and may exceed the strength of the bone and also that these stresses correlate with early migration¹. Based on these observations it has been suggested that migration is caused by the collapse and remodelling of cancellous bone. In view of this hypothesis, the cancellous bone stresses in the normal and reconstructed acetabulum were compared with the bone strength.

A three dimensional finite element model of the pelvis, constructed from CT scans², was used to analyse the normal acetabulum and an acetabulum reconstructed with a cemented all-polyethylene prosthesis. The CT density data provided Young's modulus and tensile, compressive and shear strength data on an element by element basis. The results of the stress analysis were used in conjunction with the strength data to define a Hoffman failure index for each cancellous bone element.

In both the normal and reconstructed acetabulum the maximum value of the Hoffman index in the region of the acetabulum was less than 0.2 (values greater than 1 represent failure). More significantly, the introduction of a prosthesis increased the peak cancellous bone stresses (and thence the Hoffman index) only slightly. Varying the cement thickness also produced minimal changes. We conclude that collapse and remodelling of cancellous bone is less likely to be a significant failure mechanism in the acetabulum than in the femur, agreeing with RSA studies indicating that acetabular component migration is less than femoral component migration in the first years post operation.

Acknowledgement: The authors would like to thank Professor Rik Huiskes and Dr. Michel Dalstra for the finite element mesh data.

¹ Taylor M., Tanner K.E., Freeman M.A.R., Yettram A.L.; Finite element modelling - predictor of implant survival?; *Journal of Materials Science: Materials in Medicine* **6**, 1995, 808-812.

² Dalstra M., Huiskes R., van Erning L.; Development and validation of a three dimensional finite element model of the pelvic bone.; *Journal of Biomechanical Engineering* **117**, 1995, 272-278.

Per-operative Measurement of Acetabular Cement Pressurisation

New, A.M.R.^{†*}, Northmore-Ball, M.D.[†], Tanner, K.E.^{*}, Cheah, S.K.[†]

[†]The Robert Jones and Agnes Hunt Orthopaedic Hospital, Oswestry, Shropshire SY10 7AG

^{*}IRC in Biomedical Materials, Queen Mary and Westfield College, London E1 4NS

Cement pressurisation in the acetabulum has been shown to improve the longevity of hip replacements¹. However, the pressures that are required for optimal fixation in the acetabulum and the pressures that are achieved in practice are uncertain. Using an instrumented pressuriser, we have measured the cement pressurisation in the acetabulum during 16 primary hip replacement operations performed by 2 experienced surgeons.

The pressuriser (figure 1) consists of a domed silicone rubber pressuriser head mounted on a support attached to a positioning handle, with a separate pusher to apply pressurisation force. A pressure transducer (Entran EPX series) was mounted in the support and fitted into a sized hole drilled through the centre of the silicone head such that the sensing diaphragm remained approximately 1 mm interior to the surface. Per-operatively, the pressure transducer was connected to a standard IBM compatible portable computer via a power supply/amplifier unit and an analogue to digital converter (PICO ADC-11) for data collection and display. By using battery powered equipment the electrical hazard to the patient was minimised.

A typical pressure recording is shown in figure 2. Figure 3 shows mean and peak pressures (calculated as indicated in figure 2) for the two surgeons. The differences between the surgeons were not significant at the 0.05 level (one tailed t-test assuming unequal variances).

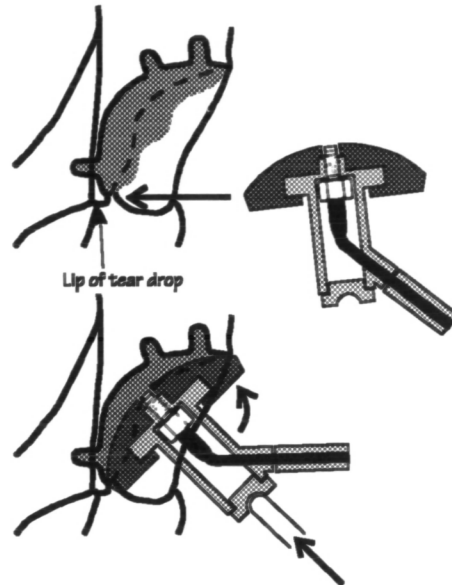


Figure 1: Use of the instrumented pressuriser.

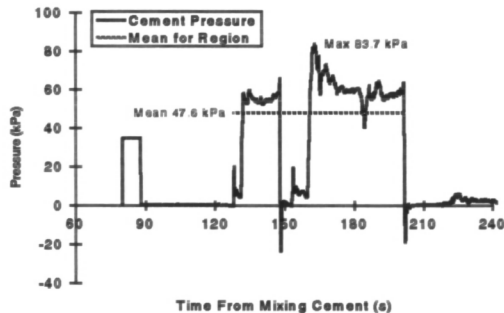


Figure 2

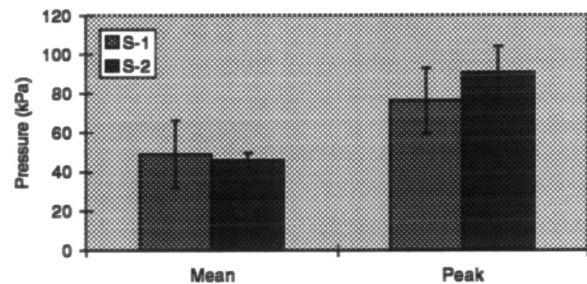


Figure 3

The pressurisation required for optimal cement penetration into low density cancellous bone is reported to be of the order of 35-50 kPa for 30-60 seconds². The present data show that this is practically achievable *in vivo* using a simple and inexpensive device. In the short term the measurements have proved useful in validating laboratory models of cement pressurisation³, with which we have found excellent agreement. In the long term we hope to perform cement pressure measurements as a fairly routine part of hip replacement operations and to establish the relationships between cement pressure, radiographic appearance and the development of aseptic loosening.

¹ Malchau, H., Herberts, P. Prognosis of Total Hip Replacement Surgical and Cementing Technique in THR: A Revision Risk Study of 134,056 Primary Operations. 63rd Annual Meeting AAOS, February 1996.

² Noble, P.C., Swarts, E. Penetration of Acrylic Bone Cements into Cancellous Bone. *Acta. Orthop. Scan.* 54, 566-573, 1983.

³ New, A.M.R., Northmore-Ball, M.D., Tanner, K.E. *In Vitro* Evaluation of Two New Designs of Acetabular Cement Pressuriser. Poster at the BOA Spring Meeting, Llandudno, April 1996.

Measurement of Acetabular Cement Pressurisation During Total Hip Replacement

New, A.M.R.^{†*}, Northmore-Ball, M.D.[†], Tanner, K.E.^{*}, Cheah, S.K.[†]

[†]The Robert Jones and Agnes Hunt Orthopaedic Hospital, Oswestry, Shropshire SY10 7AG

^{*}IRC in Biomedical Materials, Queen Mary and Westfield College, London E1 4NS

Cement pressurisation in the acetabulum has been shown to improve the longevity of hip replacements¹. However, the pressures that are required for optimal fixation in the acetabulum and the pressures that are achieved in practice are uncertain. Using an instrumented pressuriser, we have measured the cement pressurisation in the acetabulum during 16 primary hip replacement operations performed by 2 experienced surgeons.

The pressuriser (figure 1) consists of a domed silicone rubber pressuriser head mounted on a support attached to a positioning handle, with a separate pusher to apply pressurisation force. A pressure transducer (Entran EPX series) was mounted in the support and fitted into a sized hole drilled through the centre of the silicone head such that the sensing diaphragm remained approximately 1 mm interior to the surface. Perioperatively, the pressure transducer was connected to a standard IBM compatible portable computer via a power supply/amplifier unit and an analogue to digital converter (PICO ADC-11) for data collection and display. Exclusive use of battery powered equipment minimised the electrical hazard to the patient.

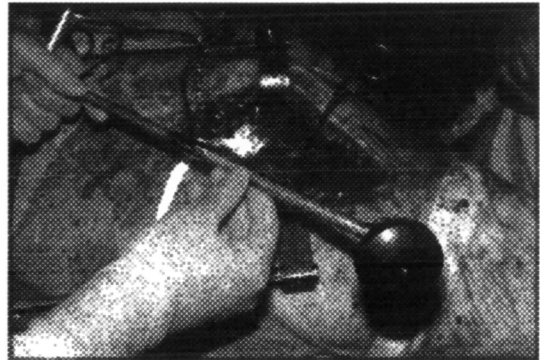


Figure 1: The instrumented pressuriser.

A typical pressure recording is shown in figure 2. Figure 3 shows mean and peak pressures (calculated as indicated in figure 2) for the two surgeons. The differences between the surgeons were not significant at the 0.05 level (one tailed t-test assuming unequal variances).

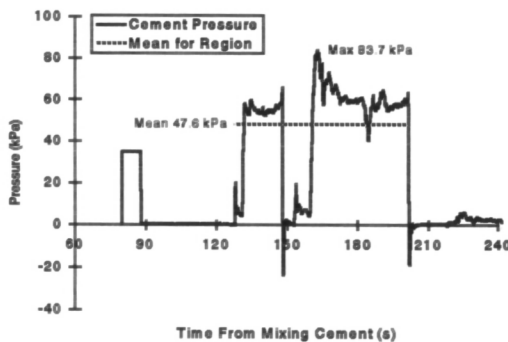


Figure 2

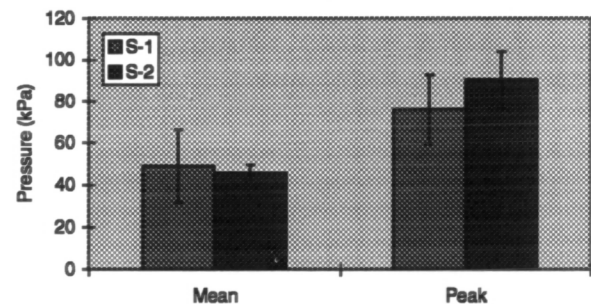


Figure 3

The pressurisation required for optimal cement penetration into low density cancellous bone is reported to be of the order of 35-50 kPa for 30-60 seconds². The present data show that this can be attained *in vivo* using a simple and inexpensive device. In the short term the measurements have proved useful in validating laboratory models of cement pressurisation³, with which we have found excellent agreement. In the long term we hope to perform cement pressure measurements as a fairly routine part of hip replacement operations and to establish the relationships between cement pressure, radiographic appearance and the development of aseptic loosening.

¹ Malchau, H., Herberts, P. Prognosis of Total Hip Replacement Surgical and Cementing Technique in THR: A Revision Risk Study of 134,056 Primary Operations. 63rd Annual Meeting AAOS, February 1996.

² Noble, P.C., Swarts, E. Penetration of Acrylic Bone Cements into Cancellous Bone. Acta. Orthop. Scan. 54, 566-573, 1983.

³ New, A.M.R., Northmore-Ball, M.D., Tanner, K.E. *In Vitro* Evaluation of Two New Designs of Acetabular Cement Pressuriser. Poster at the BOA Spring Meeting, Llandudno, April 1996.

Finite Element Modelling of Bone Cement Flow During Component Insertion in Hip Replacement

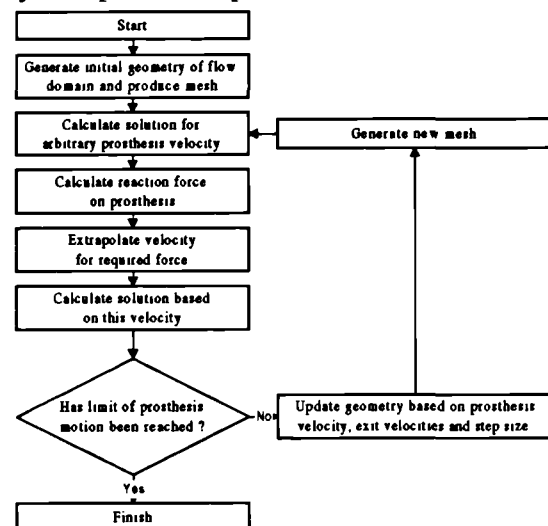
New, A.M.R.^{†*}, Northmore-Ball, M.D.[†], Tanner, K.E.^{*}

[†]The Robert Jones and Agnes Hunt Orthopaedic Hospital, Oswestry, Shropshire SY10 7AG

^{*}IRC in Biomedical Materials, Queen Mary and Westfield College, London E1 4NS

Aseptic loosening is the most common cause of late failure of total hip replacement. Analysis of the Swedish Arthroplasty Register¹ has demonstrated a relationship between modern surgical techniques and improved survivorship. The enhanced initial fixation brought about by thorough cleaning and cement pressurisation is considered to be the source of the improvement. In this study the finite element method has been used to predict the pressurisation of bone cement and subsequent penetration into cancellous bone during component insertion in joint replacement operations.

The method used is summarised in the flow chart. Prosthesis insertion was simulated by applying a constant velocity at all the boundary nodes associated with the exterior prosthesis surface. By calculating the steady state velocity and pressure solution of the Navier-Stokes equations and integrating the pressure over the same set of nodes, a linear relationship was established for insertion force vs. insertion velocity, which allowed the development of cement penetration based on a constant applied force, a more realistic simulation of a surgeon. A new solution was then calculated and the bone cement domain modified based on the velocity of the prosthesis and the exit velocity of the bone cement through the porous cancellous bone. Bone cement was assumed to



behave as a linear viscous liquid. Since cement penetration typically occurs within a short time of commencing prosthesis insertion, no attempt was made to model the increase in viscosity with time for the curing cement. Cancellous bone was modelled as an isotropic porous material. The penetration of fluid through such a material can be described by Darcy's law which assumes a linear relationship between volumetric flow rate and pressure gradient, the constant of proportionality being the permeability. All analyses was carried out using ANSYS 5.3/FLOTRAN running under Windows 95 on an IBM compatible PC.

Results for a flanged 25 mm diameter acetabular cup inserted into a 30 mm diameter acetabulum are shown in figure 1. The development of cement penetration is shown for a constant insertion force of 150 N as the gap between prosthesis and bone narrows from 5 to 0.5 mm.

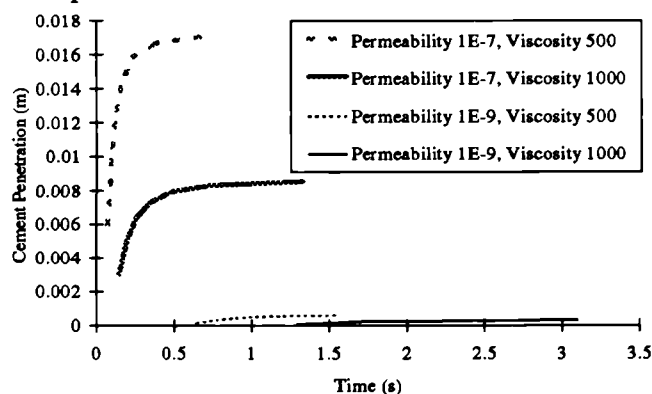


Figure 1: Development of cement penetration for flanged acetabular cup.

Parametric studies show that lower cement viscosity cement permits greater cement penetration regardless of prosthesis design. Occlusion of cement outflows by prosthesis design features further enhances penetration, but only if the occlusive features, such as flanges on cups, are well fitting.

¹ Malchau, H., Herberts, P. Prognosis of Total Hip Replacement Surgical and Cementing Technique in THR: A Revision Risk Study of 134,056 Primary Operations. 63rd Annual Meeting AAOS, February 1996.

An *In Vitro* Study of a New Design of Acetabular Cement Pressuriser

Frans P. Bernoski ^{1*} MD PhD

Andrew M.R. New ² BEng

Robert A.Scott ³ MA

Martin D. Northmore-Ball ⁴ MA FRCS

ABSTRACT

Aseptic loosening of the acetabular component remains one of the limiting factors in the long term success of total hip arthroplasty. Cement pressurisation has been shown to improve fixation. A new pressuriser has been designed which seals around the rim of the acetabulum and covers the transverse ligament notch with a flap. The results of *in vitro* testing of this device are presented and compared with pressure generated by insertion of an acetabular cup. The pressuriser allowed sustained, uniform cement pressurisation. Peak pressures with the new pressuriser were 180 kPa at both the iliac region of the rim and the pole of an instrumented model acetabulum, compared with 55 kPa at the rim and 120 kPa at the pole on cup insertion. Pressures were maintained in the 80-90 kPa range. The flap was effective in preventing cement leakage from the notch, and pressures were higher than when the flap was absent. Cup insertion alone gave only transient pressurisation, substantially less near the rim of the acetabulum than at the pole. Peripheral pressurisation may be significant in producing secure local fixation at the rim of the acetabulum, in particular in the region of the ilium (Charnley zone 1) where radiolucencies are most commonly observed and where stresses in the implanted acetabulum are highest. Improved rim fixation may also play a role in preventing the ingress of wear debris.

¹ Westeinde Ziekenhuis, Postbox 432, 2501 CK The Hague, The Netherlands. Tel: +31 70 3302056. Fax: +31 70 3809459.

² The Unit for Joint Reconstruction, The Robert Jones and Agnes Hunt Orthopaedic Hospital, Oswestry, Shropshire, U.K. & IRC in Biomedical Materials, Queen Mary and Westfield College, London, U.K.

³ Johnson & Johnson Orthopaedics, New Milton, Hampshire, U.K.

⁴ The Unit for Joint Reconstruction, The Robert Jones and Agnes Hunt Orthopaedic Hospital, Oswestry, Shropshire, U.K.

* Author to whom reprint requests and correspondence should be sent.

Dynamic Mechanical Testing of Prosthetic Acetabular Components for Total Hip Replacement

New, A.M.R.^{1,2}, Kloss, M.^{1,3}, Northmore-Ball, M.D.¹, Tanner, K.E.², Veldkamp, E.^{1,4}, Kuiper, J.H.¹

¹ The Robert Jones and Agnes Hunt Orthopaedic Hospital, Oswestry, Shropshire SY10 7AG, UK.

² IRC in Biomedical Materials, Queen Mary and Westfield College, London E1 4NS, UK.

³ Fachhochschul Studiengaenge Vorarlberg, 6850 Dornbirn, Austria.

⁴ Hogeschool Enschede, P.O. 70000, 7500 KB Enschede, The Netherlands.

The mechanics of cemented acetabular reconstruction remain little studied, particularly with respect to the dynamic aspects of hip joint loading during activity, where both the magnitude and the direction of the hip joint force vary significantly with respect to the anatomical axes of the pelvis. A simulator has been designed to reproduce the forces acting on reconstructed joints when used in conjunction with a servo-hydraulic materials testing machine. This device has been used to investigate the relationship between cementing technique and acetabular component fixation in bovine calf acetabula. There were measurable differences in the stability of cups defined qualitatively by radiological examination as "well fixed" or "poorly fixed". "Micromotion" between prosthesis and bone, measured by a displacement transducer at the anterior-superior margin of the acetabulum, was found, even in "well fixed" cases, to be far greater than that which could be attributed to elastic deformation of the intervening material. Thus it is reasonable to assume that "perfect" bonding was never achieved even under laboratory conditions and that relatively large micromotion was possible in specimens that appeared radiologically well fixed with no apparent radiolucent lines. These results suggest that rim fixation against the edge of the pelvic cortex may not be achievable even with the best current cementing techniques and thus finite element models which assume complete bonding of the cement bone interface may be unrealistic.

Keywords: Biomechanics, Dynamic Failure Mechanics

